Dipole representation of composite fermions in graphene quantum Hall systems

Sonja Predin [*]

Scientific Computing Laboratory, Center for the Study of Complex Systems, Institute of Physics Belgrade,
University of Belgrade, Pregrevica 118, 11080 Belgrade, Serbia

The even denominator fractional quantum Hall effect has been experimentally observed in graphene in the fourth Landau level ($\mathcal{N} = 3$). This paper is motivated by recent studies regarding the possibility of pairing and the nature of the ground state in this system. By extending the dipole representation of composite fermions, we adapt this framework to the context of graphene's quantum Hall systems, with a focus on half-filled Landau levels. We derive an effective Hamiltonian that incorporates the key symmetry of half-filled Landau levels, particularly particle-hole symmetry. At the Fermi level, the energetic instability of the dipole state is influenced by the interplay between topology and symmetry, driving the system toward a critical state. We explore the possibility that this critical state stabilizes into one of the paired states with well-defined pairing solutions. However, our results demonstrate that the regularized state which satisfies boost invariance at the Fermi level and lacks well-defined pairing instabilities emerges as energetically more favorable. Therefore, we find no well-defined pairing instabilities of composite fermions in the dipole representation in the half-filled fourth Landau level ($\mathcal{N} = 3$) of electrons in graphene. Although the theory of composite fermions has its limitations, further research is required to investigate other possible configurations. We discuss the consistency of our results with experimental and numerical studies and their relevance for future research efforts.

I. INTRODUCTION

The discovery of the fractional quantum Hall effect (FQHE) [1] represents a significant breakthrough in the study of topological states of matter, introducing a rich landscape of quantum phases driven by electron correlations in two-dimensional electron systems (2DESs) [2]. Among the most intriguing manifestations of the FQHE is the observation of a quantized Hall plateau at the filling factor $\nu = 5/2$ [3], indicating the FQHE at the half-filled second Landau level ($n = 1$). The observation of even-denominator FQHE states is astonishing, considering that the fermionic statistics of electrons suggest the denominator of the fraction should be an odd number. These significant discoveries have inspired intensive theoretical and experimental efforts to decode the underlying physics and implications of these states.

The concept of composite fermions (CFs), introduced by Jain [4,5], has provided an insightful framework for comprehending various aspects of quantum Hall phenomena, primarily for the half-filled second LL ($n = 1$). CFs are quasiparticles formed by attaching an even number of quantized vortices to electrons.

In recent years, advancements in noncommutative field theory in high-energy physics inspired Dong and Senthil [6] to revisit longstanding problems in quantum Hall physics. In particular, this includes the problem of the LL at $\nu = 1$ for bosons, initially formulated by Pasquier and Haldane [7] and further developed by Read [8]. This problem involves an additional degree of freedom, namely, the vortex degree of freedom, where each boson is associated with a single flux of the magnetic field, and since vortices are fermionic and the resulting composite quasiparticles are neutral, resembles CFs. Furthermore, CFs experience a zero average effective magnetic field, similar to electrons at $\nu = 1/2$. Unlike previous approaches that relied on an averaged field energy, Dong and Senthil [6] introduced the concept of intrinsic dipole energy. The application of noncommutative field theory to quantum Hall systems has since led to significant advancements, with recent studies extending these concepts to various quantum Hall states [9–14].

Moreover, fractional quantum Hall (FQH) states with additional half-integer filling factors have been observed in various materials, including graphene—a monolayer of carbon atoms arranged in a hexagonal lattice. Graphene's unique electronic and topological properties make it an ideal platform for studying exotic quantum phenomena, including the FQHE. Notably, a recent experimental study by Kim *et al.* [15] identified FQHE states at half filling in the fourth Landau level ($\mathcal{N} = 3$) of monolayer graphene.

Additionally, research by Sharma *et al.* [16] investigated CF pairing in monolayer graphene, using alternative pairing functions and numerical simulations on a torus within the Bardeen-Cooper-Schrieffer (BCS) framework. The microscopic CF-BCS theory has been highly successful in capturing many known pairing instabilities, particularly in 2DESs such as GaAs at filling factors $\nu = 1/2$ and $\nu = 5/2$ [17]. Remarkably, the CF-BCS approach has also effectively described instabilities in wide quantum wells at filling factors $\nu = 1/2$ and $\nu = 1/4$ [18]. In the case of graphene, the authors in Ref. [16] concluded that the BCS variational state for CFs reveals an f-wave pairing instability in the $\mathcal{N} = 3$

---
[*]Contact author: sonja@ipb.ac.rs

LL. Furthermore, they suggested the possibility of a *p*-wave instability for the $\mathcal{N} = 2$ LL, where FQHE has not been experimentally observed. However, these findings are in contrast with numerical studies on the sphere, which have not observed such pairing instabilities [15]. The disparity between these results highlights the need for further investigation. In addition, topological pairing, particularly *p* wave and *f* wave, is crucial for quantum computing applications due to its non-Abelian statistics, which enable robust qubits and fault-tolerant quantum operations [19].

The dipole representation of FQHE states, introduced in Ref. [10], is particularly relevant to this paper. In this representation, dipoles are neutral composite objects formed by an electron and its correlation hole. These dipoles possess moments proportional to their momentum in an external magnetic field. This effective theory has proven to be robust, capturing the microscopic description of several problems and aligning with previous experimental and numerical studies. In particular, it yielded results consistent with numerical and experimental studies of 2DESs, where the Pomeranchuk instability is observed in higher half-filled LLs. A recent study [20] even provided an explanation for the mechanism of *p*-wave pairing of CFs at half filling in the second LL ($n = 1$) of electrons in 2DESs and in the fully filled first LL ($n = 0$) of bosons, further underscoring the importance of this representation.

In this paper, we aim to explore the potential for CF pairing in monolayer graphene using the BCS framework, also utilizing the dipole representation. The half-filled LL system possesses an additional feature, the particle-hole (PH) symmetry [10], which implies that the density of holes corresponds to the density of composite holes. Consequently, this state is energetically unstable with respect to repulsive interactions, leading to a critical state. Through analytical studies, we demonstrate that in the fourth LL ($\mathcal{N} = 3$) of a graphene monolayer, this critical state is not stabilized by selecting one of the two possible symmetry-broken paired states; instead, it stabilizes into a regularized nonpaired state, which cannot support gapped pairing solutions due to the absence of mass. Our findings are consistent with numerical studies conducted on spherical geometries [15].

This paper is organized as follows: In Sec. II, we introduce the necessary formalism and key concepts of the dipole representation and apply them to the half-filled LLs of electrons in graphene. In particular, we discuss the model, and the effective Hamiltonian in the dipole representation. Section III explores the possibility and mechanism of paired states within the context of the dipole representation and analyzes their stability. Finally, in Sec. IV, we conclude with a discussion of our findings and their implications for future research.

II. IMPLEMENTING BOOST INVARIANCE AND STATE REGULARIZATION IN GRAPHENE'S LANDAU LEVELS

A. The model

Graphene exhibits unique electronic properties, including a relativistic quantum Hall effect due to its charge carriers, which behave as massless Dirac fermions [21,22]. In graphene, electrons are arranged in a honeycomb lattice

composed of two sublattices, *A* and *B*, and their behavior can be described by a two-dimensional Dirac equation [23]. In a tight-binding model, we consider only the nearest-neighbor hopping parameter *t* between sites *A* and *B*. The low-energy properties of graphene are captured by a two-band model labeled as $\lambda = \pm$, where the dispersion is linear. The valence band $\lambda = +$ and the conduction band $\lambda = -$ touch each other at the two inequivalent corners K_+ and K_- (referred to as valleys) of the Brillouin zone [23,24].

When an external magnetic field is applied, the Hamiltonian for low-energy states around the K_+ valley is given by [25,26]

$$H = v \begin{pmatrix} 0 & \pi^\dagger \\ \pi & 0 \end{pmatrix}, \tag{1}$$

where $v = \frac{\sqrt{3}}{2} \frac{at}{\hbar}$ is the velocity, and the operators $\pi^\dagger$ and π, in the Landau gauge, coincide with the LL creation and annihilation operators, respectively [26].

Here we focus on spinless electrons confined to the $\mathcal{N}$th LL, where only intra-LL excitations are considered.

The spinor states in the $\lambda-$band, obtained from the two-dimensional Dirac equation, can be expressed as

$$\psi^\xi_{\lambda\mathcal{N},m} = \frac{1}{\sqrt{2}} \begin{pmatrix} |\mathcal{N}-1, m\rangle \\ \lambda|\mathcal{N}, m\rangle \end{pmatrix} \tag{2}$$

for $\mathcal{N} \neq 0$, and

$$\psi^\xi_{\mathcal{N}=0,m} = \begin{pmatrix} 0 \\ |0, m\rangle \end{pmatrix} \tag{3}$$

for $\mathcal{N} = 0$, in terms of the harmonic oscillator states $|\mathcal{N}, m\rangle$ and the guiding-center quantum number *m*. These spinors describe states within the $\mathcal{N}$th LL in the band λ. The first component of the spinor represents the amplitude on the *A* sublattice at the point K_+ ($\xi = +$) and the amplitude on the *B* sublattice at point K_- ($\xi = -$).

B. The Pasquier-Haldane-Read construction for half-filled LL of electrons in graphene

In this section, we extend the traditional Pasquier-Haldane-Read (PHR) construction [7,8] to describe the complex excitations in half-filled LLs of electrons in graphene. The Pasquier-Haldane approach reformulates the theory by using an expanded Hilbert space of composite fermions, rather than the original Hilbert space of bosons, to represent the GMP algebra. Unlike the original model, which was formulated for fully filled LLs of bosons, our approach adapts the PHR construction to systems where LLs are half-filled of electrons. In this paper, we employ an expansion of the Hilbert space by incorporating correlation holes, which are positive charges that pair with electrons to form neutral dipoles. This representation is crucial for describing systems with PH symmetry, a key characteristic of half-filled LLs, and for maintaining the topological properties of the quantum Hall states.

We begin by representing the basis states in a LL as

$$\{|o_1\rangle, |o_2\rangle, \ldots, |o_{N_\phi/2}\rangle, |m_1\rangle, |m_2\rangle, \ldots, |m_{N_\phi/2}\rangle\}, \tag{4}$$

where $|o_i\rangle$ and $|m_i\rangle$ represent the states, which form the foundation for describing the system in our enlarged Hilbert

space, which accommodates both electrons and correlation holes [10]. Here, N_ϕ represents the number of orbitals.

In this expanded space, we define creation and annihilation operators that satisfy the algebra:

$$\{c_{mo}, c^\dagger_{o'm'}\} = \delta_{mm'}\delta_{oo'}, \quad \{c_{mo}, c_{o'm'}\} = 0,$$
$$\{c^\dagger_{mo}, c^\dagger_{o'm'}\} = 0. \tag{5}$$

CFs operators c_{mo} and $c^\dagger_{mo}$ in the LL have double indices, where m and n label physical electrons and correlation holes, respectively. Using these operators, we define the Fourier components of the physical (left) and unphysical (right) densities in the $\mathcal{N}$th LL, incorporating the form factor $F_\mathcal{N}(|\vec{q}|)$:

$$\rho^L_\mathcal{N}(\vec{q}) = F_\mathcal{N}(|\vec{q}|) \sum_{o,o'} \sum_m \langle o|\tau_{-\vec{q}}|o'\rangle c^\dagger_{mo}c_{o'm}, \tag{6}$$

$$\rho^R_\mathcal{N}(\vec{q}) = F_\mathcal{N}(|\vec{q}|) \sum_{m,m'} \sum_o \langle m|\tau_{-\vec{q}}|m'\rangle c^\dagger_{mo}c_{om'}. \tag{7}$$

Here, $\tau_{\vec{q}} = e^{i\vec{q}\vec{R}}$ is the translation operator, where $\vec{R} = (X, Y)$ represents the guiding center coordinates of a CF [27–29] in the external magnetic field $\vec{B} = -B\vec{e}_z$, with components obeying the commutation relation:

$$[X, Y] = il_B^2. \tag{8}$$

Here, l_B is the magnetic length. In what follows, we will set $l_B \equiv 1$. This framework ensures that the neutral CFs are accurately described within the context of the LL dynamics.

The Fourier components of the form factor in the $\mathcal{N}$th LL are given in terms of Laguerre polynomials $L_\mathcal{N}$ in the following way:

$$F^{(\mathcal{N})}(q) = \begin{cases} 1 & \text{if } \mathcal{N} = 0 \\ \frac{1}{2}\left[L_{\mathcal{N}-1}\left(\frac{q^2}{2}\right) + L_\mathcal{N}\left(\frac{q^2}{2}\right)\right] & \text{if } \mathcal{N} \neq 0. \end{cases} \tag{9}$$

For $\mathcal{N} = 0$, the form factor for graphene coincides with that of a 2DES, such as GaAs. However, for higher $\mathcal{N}$ it can be viewed as an average of the two form factors of those for 2DES [30].

Furthermore, the annihilation operator can be written in relation to its momentum space representation in the following way:

$$c_{mo} = \int \frac{d\vec{k}}{(2\pi)^2} \langle m|\tau_{\vec{k}}|o\rangle c_{\vec{k}}. \tag{10}$$

By substituting Eq. (10) into the equations for the left and right density operators, Eqs. (6) and (7), we obtain

$$\rho^L_\mathcal{N}(\vec{q}) = F_\mathcal{N}(\vec{q}) \int \frac{d^2\vec{k}}{(2\pi)^2} e^{\frac{i}{2}\vec{k}\times\vec{q}} c^\dagger_{\vec{k}-\vec{q}}c_{\vec{k}}, \tag{11}$$

$$\rho^R_\mathcal{N}(\vec{q}) = F_\mathcal{N}(\vec{q}) \int \frac{d^2\vec{k}}{(2\pi)^2} e^{-\frac{i}{2}\vec{k}\times\vec{q}} c^\dagger_{\vec{k}-\vec{q}}c_{\vec{k}}. \tag{12}$$

Using the relations Eq. (5), it is easy to show that these densities obey the Girvin-MacDonald-Platzman (GMP)

algebra [31]:

$$\left[\rho^L_0(\vec{q}), \rho^L_0(\vec{q}')\right] = 2i\sin\left(\frac{\vec{q}\times\vec{q}'}{2}\right)\rho^L_0(\vec{q}+\vec{q}'),$$

$$\left[\rho^R_0(\vec{q}), \rho^R_0(\vec{q}')\right] = -2i\sin\left(\frac{\vec{q}\times\vec{q}'}{2}\right)\rho^R_0(\vec{q}+\vec{q}'),$$

$$\left[\rho^L_0(\vec{q}), \rho^R_0(\vec{q}')\right] = 0. \tag{13}$$

This is induced by the commutation relation Eq. (8) and restriction to the single LL. The realization of the GMP algebra using the canonical CF variables facilitates the application of mean-field methods [8].

C. The effective Hamiltonian in dipole representation in graphene

To accurately describe the system within the dipole representation, it is essential to impose a specific constraint. These constraints serve several purposes. First, the constraint ensures that the number of degrees of freedom in the effective model aligns with the microscopic description of the physical problem. Furthermore, the constraint also defines the physical subspace within the enlarged Hilbert space, which includes additional degrees of freedom such as correlation holes. Second, the imposed constraint must preserve the PH symmetry, a fundamental characteristic of the half-filled LL, ensuring that the model accurately reflects the physical properties of the system.

We introduce the following constraint:

$$\rho^L_{\mathcal{NN}} + \rho^R_{\mathcal{NN}} = 1. \tag{14}$$

This constraint acts as a null operator in momentum space:

$$\rho^L_{\vec{q}} + \rho^R_{\vec{q}} = 0. \tag{15}$$

It is important to highlight that this constraint incorporates both physical and unphysical quantities, treating them as mutually dependent. Since the right degrees of freedom (additional degrees of freedom) represent correlation holes in the enlarged space, this constraint effectively ensures, in the long-distance limit, that the density of correlation holes equals the density of real holes.

Furthermore, when defining the problem in the enlarged space, operators, including the Hamiltonian, may map physical states into superpositions of physical and unphysical states. To ensure that physical states remain within the physical subspace, the Hamiltonian must commute with the constraint.

The effective Hamiltonian in this framework must reflect the dipole representation within $\mathcal{N}$th LL. Additionally, it must preserve PH symmetry, meaning it remains invariant under the exchange of particles and holes. The Hamiltonian is carefully constructed to satisfy these conditions, and we impose a constraint that ensures the resulting Hamiltonian has a PH symmetric form [10]:

$$\mathcal{H}_{\text{eff}} = \frac{1}{8} \int \frac{d^2\vec{q}}{(2\pi)^2} V^{(\mathcal{N})}(\vec{q})\left(\rho^L_0(\vec{q}) - \rho^R_0(\vec{q})\right)\left(\rho^L_0(-\vec{q}) - \rho^R_0(-\vec{q})\right). \tag{16}$$

Here, $V^{(\mathcal{N})}(\vec{q}) = \frac{2\pi e^2}{\epsilon|\vec{q}|} e^{-q^2/2} (F^{(\mathcal{N})})^2$ represents the effective interaction, which takes into account states within the $\mathcal{N}$th LL. The form factor mimics the LL characteristics. Moreover, it should be noted that $\upsilon(\vec{q}) = \frac{2\pi e^2}{\epsilon|\vec{q}|}$ defines the Fourier transform of the Coulomb interaction potential.

Using mean-field approximation and Hartree-Fock (HF) calculations, one easily finds that dispersion relation for graphene for the $\mathcal{N}$th LL has the following form:

$$\varepsilon^{(\mathcal{N})}(\vec{k}) = \varepsilon_0^{(\mathcal{N})}(\vec{k}) + \varepsilon_{HF}^{(\mathcal{N})}(\vec{k}), \tag{17}$$

where

$$\varepsilon_0^{(\mathcal{N})}(\vec{k}) = \frac{1}{2} \int \frac{d^2\vec{q}}{(2\pi)^2} V^{(\mathcal{N})}(|\vec{q}|) \sin^2\left(\frac{\vec{k} \times \vec{q}}{2}\right) \tag{18}$$

represents single-particle energy and

$$\varepsilon_{HF}^{(\mathcal{N})}(\vec{k}) = -\int \frac{d^2\vec{q}}{(2\pi)^2} V^{(\mathcal{N})}(|\vec{k} - \vec{q}|) \sin^2\left(\frac{\vec{k} \times \vec{q}}{2}\right) n_q \tag{19}$$

represents the HF contributions. Here, n_q is the Fermi (step) function with $n_q = 1$ for q inside a circular Fermi surface of radius q_F, and zero otherwise. This result aligns with Ref. [32], with the difference that here $V(|\vec{q}|)$ represents the Coulomb interaction in the graphene system in the $\mathcal{N}$th LL, and includes an additional factor of $1/4$ that reduces the strength of the Coulomb interaction. Furthermore, the single-particle energy $\varepsilon_0^{(\mathcal{N})}$ can be obtained in a closed analytical fashion as detailed in Appendix A. Moreover, in Appendix A we also give the complete data of the corresponding energies for the lowest fourth LL ($\mathcal{N} = 0, 1, 2, 3$). On the other hand, we obtained the energy of interaction of this particles $\varepsilon_{HF}^{(\mathcal{N})}$ via numerical integration.

The interaction of electrons within a single LL can be fully described by its Haldane pseudopotentials V_m [33], which quantify the interaction energies of two electrons with relative angular momentum m. For the nth Landau level, the Haldane pseudopotentials are expressed as

$$V_m^{(n)} = \int \frac{d^2\vec{q}}{(2\pi)^2} F^{(n)}(q) e^{-q^2} L_m(q^2), \tag{20}$$

where $F^{(n)}(q)$ is the form factor associated with the nth LL. In this paper, we focus on two approximate effective interactions, V_{Toke} and V_{Park} [34,35], which are defined in real space as

$$V_{\text{Toke}}(r) = \frac{1}{r} + \sum_{i=0}^{6} c_i \, r^i \, e^{-r}, \tag{21}$$

$$V_{\text{Park}}(r) = \frac{1}{r} + a_1 \, e^{-\alpha_1 r^2} + a_2 \, r^2 \, e^{-\alpha_2 r^2}, \tag{22}$$

respectively. It can be concluded that the effective interaction can be represented as the Coulomb interaction $1/r$ combined with short-range functions to account for deviations at short distances. Thus, in addition to the Coulomb interaction, we will also utilize the Toke and Park interactions in the subsequent analysis. The coefficients c_i ($i = 0, 1, 2, 3, 4, 5, 6$) for V_{Toke} and $a_1, a_2, \alpha_1, \alpha_2$ for V_{Park} are determined by matching the effective interactions $V_{\text{Toke}}(q)$ and $V_{\text{Park}}(q)$, operating in the the lowest LL (LLL), to the first seven ($m = 0, 1, 2, 3, 4, 5, 6$) and four ($m = 0, 1, 2, 3$) pseudopotentials of the Coulomb

TABLE I. Values of coefficients c_i, a_i, α_i of the effective interactions for $n = 1$, and $n = 3$ LL in graphene.

Coefficient	$n = 1$	$n = 3$
c_0	−6.631	492.524
c_1	13.298	−976.021
c_2	−8.997	692.713
c_3	2.934	−235.342
c_4	−0.499	41.446
c_5	0.0426	−3.645
c_6	−0.00143	0.126
a_1	0.0107017	11.8887
a_2	0.109467	−9.64883
α_1	0.038443	0.247147
α_2	0.446909	0.479972

interaction $V_{2m-1}^{(n)}$, respectively, in the second LL ($n = 1$) and the fourth LL ($n = 3$). The Fourier transforms of the effective interactions are obtained as

$$V_{\text{eff}}(q) = \int d^2\vec{r} \, V_{\text{eff}}(r) e^{-i\vec{q}\cdot\vec{r}}. \tag{23}$$

The coefficients obtained through the symbolic solution of the corresponding system of equations for both interactions are listed in Table I.

D. Boost invariance and state regularization in graphene

In this section, we derive the Hamiltonian from the constraint previously established, ensuring that our effective theory maintains a valid microscopic description, at least at the Fermi level. As we noted above, the FQHE systems at half filling in LLL exhibit the emergence of a Fermi liquid (FL) state of composite quasiparticles (CFs, for example). The Hamiltonian described in Eq. (16), which governs the dipole representation, incorporates a finite (bare) mass for single-particle energies as a consequence of the dipole structure. To achieve a well-defined FL state description within the LL framework [10], it is essential for the Hamiltonian to exhibit boost invariance, which imposes a condition on the (bare) mass at the Fermi level.

To begin, we introduce an interaction term that is null within the physical space:

$$\mathcal{H}_0 = \mathcal{C}_{\mathcal{N}} \int \frac{d^2\vec{q}}{(2\pi)^2} V^{(\mathcal{N})}(\vec{q}) \big(\rho_0^L(\vec{q}) + \rho_0^R(\vec{q})\big) \big(\rho_0^L(-\vec{q})$$
$$+ \rho_0^R(-\vec{q})\big). \tag{24}$$

Therefore, the resulting Hamiltonian has the following form:

$$\mathcal{H}_{\text{res}} = \mathcal{H}_{\text{eff}} + \mathcal{H}_0. \tag{25}$$

Furthermore, we denote the constant $\mathcal{C}_{\mathcal{N}}$ such that the energy ε_1 denoting the single energy of the resulting Hamiltonian in Eq. (25) fulfills the condition

$$\frac{1}{m^*} = \frac{\partial^2 \varepsilon_0(\vec{k})}{\partial k^2}\bigg|_{k=k_F} = 0, \tag{26}$$

where m^* is the effective mass. Therefore, the resulting Hamiltonian in Eq. (25) has no terms $\frac{k^2}{m^*}$, which contribute to

the kinetic energy. The regularized state represents a FL-like (FLL) state, as is the case in the half-filled LLL of electrons.

III. DIPOLE REPRESENTATION OF COMPOSITE FERMIONS IN GRAPHENE

As discussed earlier, a key feature of the Hamiltonian in the dipole representation of CFs is its inherent symmetry, particularly PH symmetry. This symmetry means that the system remains unchanged when particles are exchanged with real holes or when the densities $\rho_L(\vec{q})$ and $\rho_R(\vec{q})$ are swapped, where $\rho_R(\vec{q})$ corresponds to the density of correlation holes.

In the context of the Coulomb interaction, it is energetically favorable for these correlation holes to move away from the electrons, allowing real holes to surround the electrons instead. We have previously shown that the density of these correlation holes is equal to the density of real holes, and that the size of the resulting dipoles is determined by a translation operator. As a result, at the Fermi level $k = k_F$, the electrons are positioned far from the holes, making this FLL state energetically unstable and prone to become a critical FLL state [20].

Breaking the symmetry between the left (L) and right (R) components of the system is equivalent to breaking the symmetry between particles and real holes. Therefore, states that break this symmetry are likely to be more energetically favorable. It is worth noting that at half filling, most of the paired states that emerge (such as the Moore-Read Pfaffian, anti-Pfaffian, and f-wave states) spontaneously break this symmetry.

Motivated by the aim to explore a well-defined state of CFs within the dipole representation that stabilizes the critical state, we derive an effective Hamiltonian. This is achieved by revisiting the Hamiltonian in Eq. (16) and subsequently subtracting (or adding) the following term:

$$\mathcal{H}_1 = \frac{1}{8} \int \frac{d^2\vec{q}}{(2\pi)^2} V^{(\mathcal{N})}(\vec{q}) \big(\rho_0^R(-q) + \rho_0^L(-q)\big)\big(\rho_0^R(\vec{q}) - \rho_0^L(\vec{q})\big), \tag{27}$$

which effectively represents zero in the physical space. Consequently, the resulting effective Hamiltonians take the following forms:

$$\mathcal{H}_{\text{res}}^{(1)} = \frac{1}{4} \int \frac{d^2\vec{q}}{(2\pi)^2} V^{(\mathcal{N})}(\vec{q}) \rho_0^R(-q)\big(\rho_0^R(\vec{q}) - \rho_0^L(\vec{q})\big) \tag{28}$$

and

$$\mathcal{H}_{\text{res}}^{(2)} = \frac{1}{4} \int \frac{d^2\vec{q}}{(2\pi)^2} V^{(\mathcal{N})}(\vec{q}) \rho_0^L(-q)\big(\rho_0^L(\vec{q}) - \rho_0^R(\vec{q})\big). \tag{29}$$

The dipole representation of these Hamiltonians plays a crucial role in defining a single energy, which is essential for obtaining paired solutions. Additionally, they can also be interpreted as symmetry-breaking modifications of the Hamiltonian in Eq. (16), stabilizing the system into one of two paired states [20].

To explore potential paired solutions, we apply the HF approach to the relevant part of the Hamiltonian in Eq. (28), yielding

$$\mathcal{H}_{HF}^{(\mathcal{N})} = \int \frac{d^2\vec{k}}{(2\pi)^2} \xi_{\mathcal{N}}(\vec{k}) c_{\vec{k}}^\dagger c_{\vec{k}} + \frac{1}{4} \int \frac{d^2\vec{q}}{(2\pi)^2} \int \frac{d^2\vec{k}_1}{(2\pi)^2} \int \frac{d^2\vec{k}_2}{(2\pi)^2} \upsilon(|\vec{q}|) F_{\mathcal{N}}^2(|\vec{q}|)(1 - e^{i\vec{k} \times \vec{q}})$$
$$\cdot \big(\langle c_{\vec{k}_1+\vec{q}}^\dagger c_{\vec{k}_2-\vec{q}}^\dagger \rangle c_{\vec{k}_1} c_{\vec{k}_2} + c_{\vec{k}_1+\vec{q}}^\dagger c_{\vec{k}_2-\vec{q}}^\dagger \langle c_{\vec{k}_1} c_{\vec{k}_2} \rangle - \langle c_{\vec{k}_1+\vec{q}}^\dagger c_{\vec{k}_2-\vec{q}}^\dagger \rangle \langle c_{\vec{k}_1} c_{\vec{k}_2} \rangle\big), \tag{30}$$

where $\xi_{\mathcal{N}}(\vec{k}) = \varepsilon_{\mathcal{N}}(\vec{k}) - \varepsilon_{\mathcal{N}}(\vec{k}_F)$, with $\epsilon_{\mathcal{N}}(\vec{k})$ representing the dispersion relation given by

$$\varepsilon_{\mathcal{N}}(\vec{k}) = \frac{1}{4} \int \frac{d^2\vec{q}}{(2\pi)^2} \upsilon(|\vec{q}|) F_{\mathcal{N}}^2(|\vec{q}|)(1 - e^{i\vec{k} \times \vec{q}}) - \frac{1}{2} \int \frac{d^2\vec{q}}{(2\pi)^2} \upsilon(|\vec{k} - \vec{q}|) F_{\mathcal{N}}^2(|\vec{k} - \vec{q}|)(1 - e^{i\vec{k} \times \vec{q}}). \tag{31}$$

Furthermore, we define

$$\Delta_{\mathcal{N}}(\vec{k}) = -\frac{1}{4} \int \frac{d^2\vec{q}}{(2\pi)^2} \upsilon(|\vec{k} - \vec{q}|) F_{\mathcal{N}}^2(|\vec{k} - \vec{q}|)(1 - e^{-i\vec{k} \times \vec{q}}) \cdot \langle c_{\vec{k}_1} c_{\vec{k}_2} \rangle \tag{32}$$

Finally, using standard BCS transformations to diagonalize the Hamiltonian in Eq. (28), we obtain the total energy,

$$E_{\text{paired}}^{(\mathcal{N})} = \int \frac{d^2\vec{k}}{(2\pi)^2} (\xi_{\mathcal{N}}(\vec{k}) - E_{\mathcal{N}}(\vec{k})) + \int \frac{d^2\vec{k}}{(2\pi)^2} \frac{|\Delta_{\mathcal{N}}(\vec{k})|^2}{2E_{\mathcal{N}}(\vec{k})}, \tag{33}$$

where the Bogoliubov quasiparticle energy is given by $E_{\mathcal{N}}(\vec{k}) = \sqrt{\xi_{\mathcal{N}}^2(\vec{k}) + |\Delta_{\mathcal{N}}(\vec{k})|^2}$. In the BCS treatment, we obtain the pairing instability is described by the order parameter $\Delta(\vec{k})$ self-consistently:

$$\big|\Delta_{\mathcal{N}}^{(l)}(\vec{k})\big| = \frac{1}{4} \int \frac{d^2\vec{q}}{(2\pi)^2} \upsilon(|\vec{k} - \vec{q}|) F_{\mathcal{N}}^2(|\vec{k} - \vec{q}|)(1 - e^{-i\vec{k} \times \vec{q}}) \frac{\Delta_{\mathcal{N}}^{(l)}(\vec{q})}{2E_{\mathcal{N}}(\vec{q})}. \tag{34}$$

Here, the gap function takes the following form: $\Delta^{(l)}(\vec{k}) = e^{il\theta_l}|\Delta(\vec{k})|$, where θ is the angular coordinate of k, with $l = 0, \pm 1, \pm 3$ representing different pairing channels. Details regarding the numerical solutions of the self-consistent equation in Eq. (34) are provided in Appendix B. We note that we

obtain the same solutions for $l = 1$ in Hamiltonian Eq. (29) as we do for $l = -1$ in Hamiltonian Eq. (28).

In the previous section, we regularized the state of the Hamiltonian in Eq. (25) by eliminating the quadratic term, which contributes to the kinetic energy. Consequently, the regularized state cannot support gapped pairing solutions due
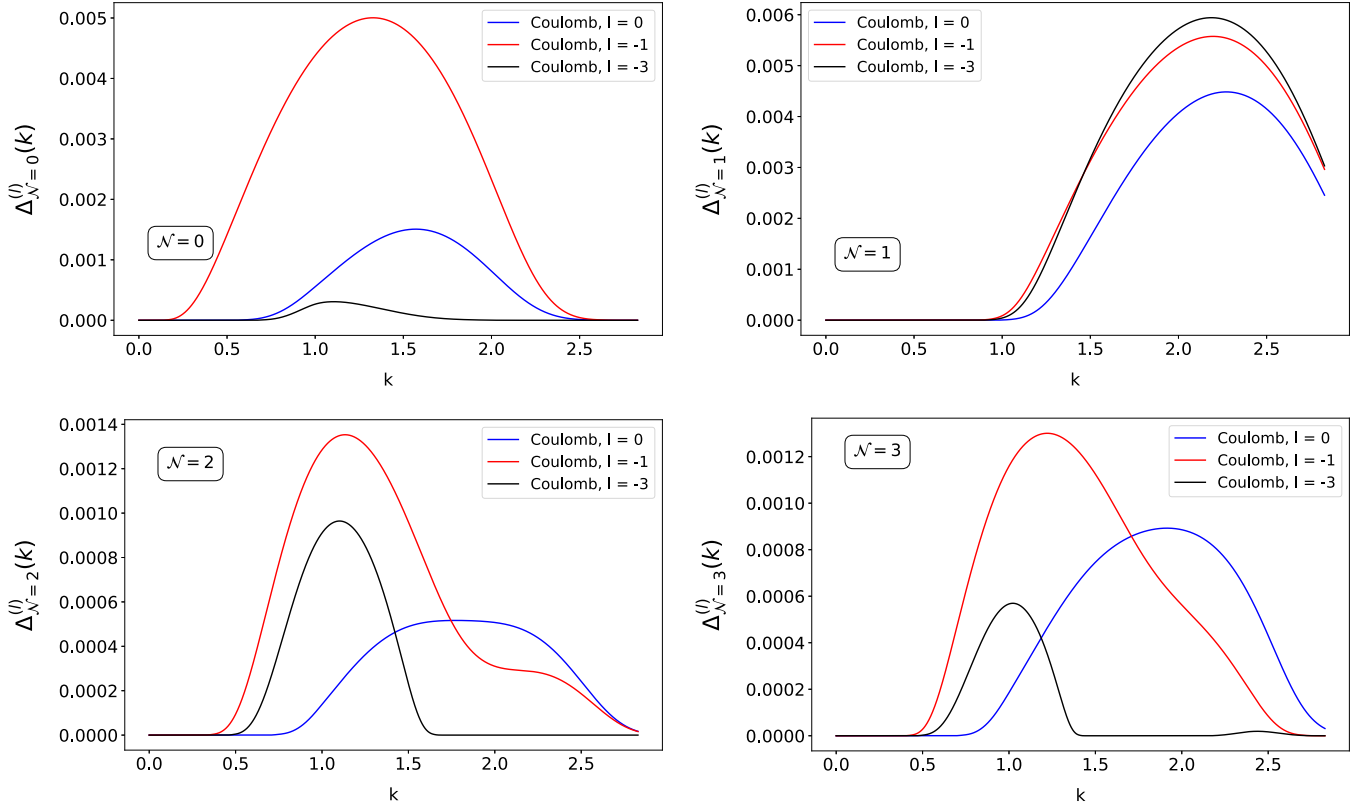
FIG. 1. The solutions for $\Delta(\vec{k})$ calculated self-consistently using Eq. (34) for different pairing channels l in the lowest four LLs ($\mathcal{N} = 0, 1, 2, 3$) for the Coulomb interaction.

to the absence of (bare) mass. While the critical state can be stabilized among the paired states, it can also be stabilized within the regularized state. To investigate in which of these states the critical state is stabilized, we define the energy of the regularized state of CFs in the dipole representation using a mean-field approach as follows:

$$E_{\text{FLL}}^{(\mathcal{N})} = \int \frac{d^2\vec{k}}{(2\pi)^2} \left(\varepsilon_0^{(\mathcal{N})}(\vec{k}) + \frac{1}{2}\varepsilon_{\text{HF}}^{(\mathcal{N})}(\vec{k}) \right). \quad (35)$$

In calculating the total energy, we apply a cutoff when necessary, using the radius of a circle in momentum space $Q = \sqrt{2}\,k_F$, which denotes the volume of available states in the LL. Furthermore, the only viable cutoff value for the regularized FLL state being k_F, as it is designed to accurately describe the physics at the Fermi surface k_F. We have carefully used the cutoff $Q = \sqrt{2}\,k_F$ for the paired state, but we have also ensured that our findings do not depend on the choice of the cutoff value. In spherical coordinates, this corresponds to $Q = \sqrt{2}\,k_F$.

We illustrate in Fig. 1 the self-consistently obtained mean-field parameter $\Delta(\vec{k})$ in the fourth LL $\mathcal{N} = 0, 1, 2, 3$ for the Coulomb potential, and Fig. 2 for the Toke and Park potentials. Here, it can be noticed that nonzero pairing solutions also appear in the LLL, which might suggest that pairing could persist in the thermodynamic limit. However, this stands in contrast to numerical studies, which consistently find the FLL state to be the most stable configuration. The definitive confirmation about the presence or absence of pairing lies in direct comparison of the total energies between a paired state and a

regularized FLL state. Additionally, we plotted in Fig. 3 the total energy E_{paired} of the different pairing solutions compared to the normal state energy to determine the energetically most favorable l in the case of Coulomb and Haldane potentials. In Fig. 4, we compare the results for E_{FLL} and E_{paired} in the case of graphene for the four lowest LLs ($\mathcal{N} = 0, 1, 2, 3$) for the Coulomb, Toke, and Park interactions to investigate the possibility of pairing instability. We would like to note that here we calculated E_{paired} to compare the energy for the self-consistent solution that minimizes the energy value. We find that the critical state is stabilized within the regularized state, which is energetically more favorable than the paired states. In the following sections, we will discuss these findings in more detail for each of the four lowest LLs ($\mathcal{N} = 0, 1, 2, 3$), emphasizing how our results align with previous experiments and numerical studies.

In the lowest LL ($\mathcal{N} = 0$), considering the short-range, repulsive Coulomb interaction $\mathcal{V}(|\vec{q}|) = q^2$, which describes a two-body interaction between dipoles, the three-body Hamiltonian can be derived using the Chern-Simons approach [36,37] as follows:

$$\mathcal{H}_{\text{eff}}^{(e)} = \sum_{\langle ijk \rangle} \nabla_i^2 \delta^2(\vec{x}_i - \vec{x}_j)\delta^2(\vec{x}_i - \vec{x}_k), \quad (36)$$

which aligns with the commonly used interaction model for the Pfaffian [38]. In the lowest LL ($\mathcal{N} = 0$), the effective interaction between CFs (and therefore the physics in general) in monolayer graphene is the same as in a 2DES, such as GaAs quantum wells with zero width. Here, numerical experiments
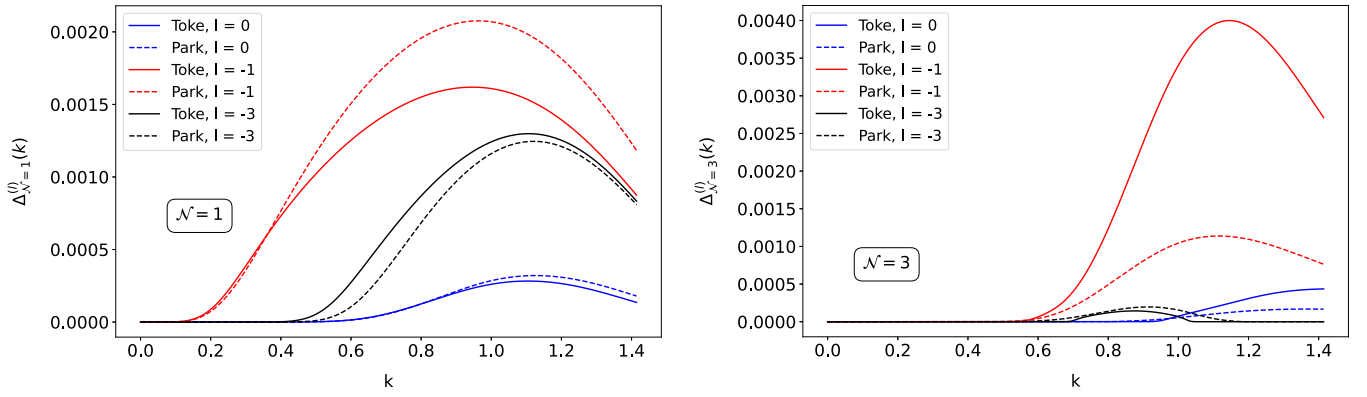
FIG. 2. Self-consistently calculated solutions for $\Delta(\vec{k})$ for different pairing channels l in the second ($\mathcal{N} = 1$) (left) and fourth ($\mathcal{N} = 3$) (right) Landau levels (LLs). These results correspond to the Toke and Park interactions.

indicate that the Fermi-liquid-like state is the most stable in the half-filled first LL ($\mathcal{N} = 0$).

In the half-filled second LL ($n = 1$), nontrivial topology is identified via Majorana edge states in the case of a 2DES. In this LL, well-defined p-wave solutions in the 2DES are present, particularly $l = 1$ ($l = -1$) wave pairing in the Hamiltonian as described in Eq. (29) [Eq. (28)], but with form factors characteristic of the 2DES [20]. This corresponds

to the Pfaffian topological order [38]. The PH conjugate of the Pfaffian, the anti-Pfaffian, can be obtained by switching the sign of the particles [39,40]. We would like to point out here that a well-defined paired state can only exist if the effective dipole physics at the Fermi level, driven by the
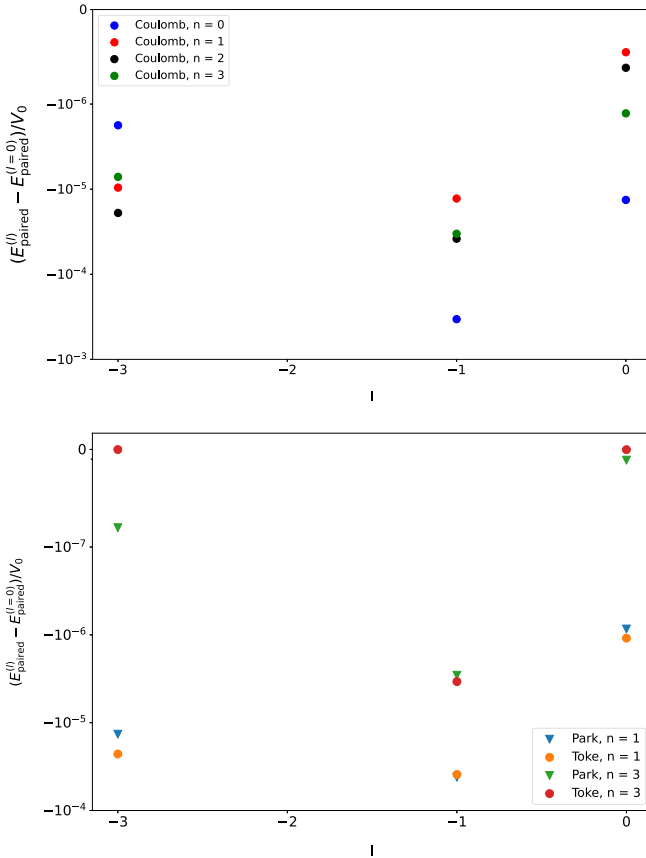

FIG. 3. Comparison of the total energy for various pairing solutions, expressed as $E_{\text{paired}}(l) - E_{\text{paired}}(l = 0)$ for Coulomb interactions (upper), Toke, and Park interactions (lower). The interaction strength is given by $V_0 = 2\pi e^2/l_B$.
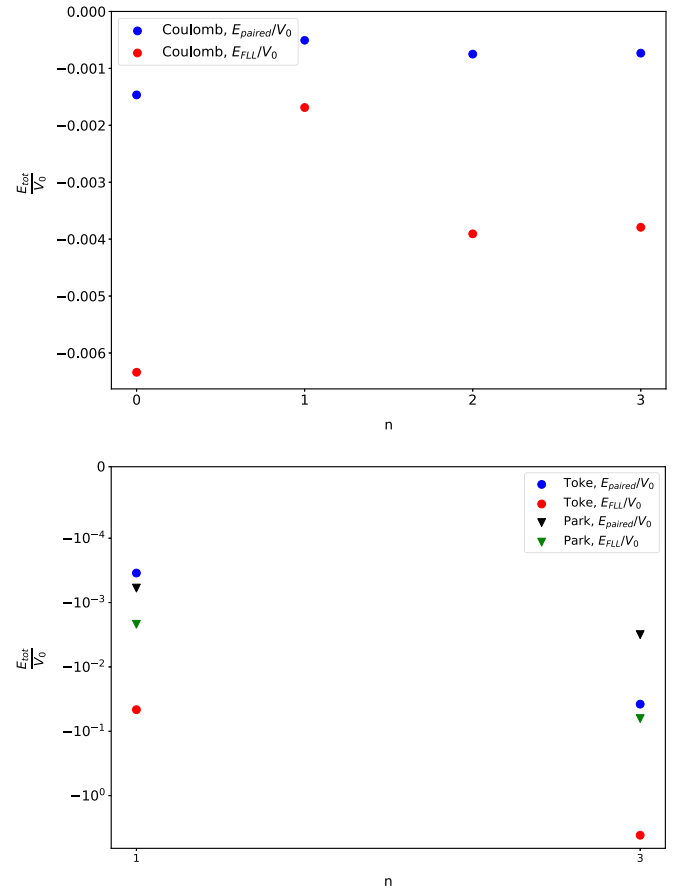

FIG. 4. Comparing total energies of the pairing solutions E_{paired} and the regularized state E_{FLL} in the four lowest LLs in the case of Coulomb interactions (upper), Toke, and Park interactions (lower). Here, we calculated E_{paired} for $l = -1$, which minimizes the energy value and is therefore the most energetically favorable. The interaction strength is defined by $V_0 = 4\pi e^2/l_B$.

nontrivial topology of the LL, is present. However, in mono-layer graphene, in the second LL ($\mathcal{N} = 1$) the regularized state dominates over the paired state, which is consistent with earlier studies indicating that the lowest energy state is a Fermi sea of CFs with no pairing instabilities [41].

In the half-filled third LL ($\mathcal{N} = 2$) of graphene, the FQHE has not been observed [42,43]. However, in numerical experiments on a torus using a BCS variational state for CFs, the authors in Ref. [17] identified the presence of pairing instability, which most likely corresponds to p-wave pairing. This may result in the observation of pairing solutions in the thermodynamic limit, which is well represented in numerical experiments on a torus. In contrast with this numerical study constructed on a torus, we propose that the regularized state is energetically more favorable, which does not exhibit well-defined pairing solutions.

Finally, in a previously mentioned study [17], it was proposed that the Fermi sea of CFs may be unstable to f-wave pairing in the half-filled fourth LL ($\mathcal{N} = 3$) of graphene. This particular LL is significant due to the experimental observation of the FQHE [15]. However, numerical studies conducted on a spherical geometry reveal that neither the anti-Pfaffian nor the PH symmetric Pfaffian [44] states exhibit a strong overlap with the exact ground state near the pure Coulomb interaction point. Additionally, various spin and valley singlet states were examined, yet none showed significant overlap with the ground state in the $\mathcal{N} = 3$ LL. Although the 221-parton state [45] demonstrates a notable similarity to the pure Coulomb interaction across a wide parameter range, its validation still requires further theoretical and experimental studies. Our findings suggest that the critical state in the fourth LL ($\mathcal{N} = 3$) is not stabilized among the paired states, such as the Pfaffian. Instead, the regularized state, which lacks well-defined pairing instabilities, emerges as energetically more favorable. This suggests the absence of well-defined pairing instabilities within the dipole representation of CFs in this context. Therefore, our results are consistent with numerical studies conducted on spherical geometry. To conclusively validate the nature of the ground state and fully elucidate the pairing mechanism, particularly in higher LLs, additional theoretical and experimental research extending beyond the framework of CFs is essential. Strong short-range repulsive interaction is crucial for defining CFs in lower LLs, where the effects of this interaction are dominant [see Eq. (36)].

IV. CONCLUSIONS

In this paper, we have derived the dipole representation of CFs in graphene's quantum Hall systems, focusing particularly on the half-filled LLs. Our investigation extended the Pasquier-Haldane-Read construction to describe the excitations in half-filled LLs of electrons in graphene, and we derived an effective Hamiltonian within the dipole framework that respects the key symmetry of these systems, including PH symmetry. We demonstrated that this symmetry, inherent in the effective Hamiltonian, can be broken and stabilized either in the phase of paired states or in a regularized state without bare mass at the Fermi level.

We discussed the relationship of paired states to the Pfaffian state. Furthermore, our analysis of the pairing mechanism shows that the regularized state, which lacks well-defined pairing instabilities, emerges as the energetically favored state over the paired states with p-wave and f-wave pairing. This finding suggests that, within the dipole representation, the ground state in the half-filled fourth LL ($\mathcal{N} = 3$) of graphene is not characterized by pairing instabilities.

We also discussed the consistency of our results with experimental and numerical studies. Furthermore, we highlighted the limitations of the dipole representation framework. Additionally, going beyond the mean-field theory and including fluctuations might be crucial in accurately describing the true nature of the ground state.

We hope this paper will inspire further investigations of these states, including the pairing mechanism and the origin of the ground state. Notably, the experimental observation of FQHE in bilayer graphene systems [46] suggests that similar approaches could be applied to understand these phenomena in other layered or structured graphene systems.

APPENDIX A: ANALYTICAL DERIVATION OF SINGLE-PARTICLE ENERGIES FOR THE LOWEST FOUR LANDAU LEVELS

The Hamiltonian in the dipole representation, as described by Eq. (16), is given by

$$\mathcal{H}_{\text{eff}} = \frac{1}{8} \int \frac{d^2\vec{q}}{(2\pi)^2} V^{(n)}(\vec{q})(\rho_L(\vec{q}) - \rho_R(\vec{q}))(\rho_L(-\vec{q}) - \rho_R(-\vec{q})). \tag{A1}$$

The energy dispersion relation for graphene in the nth LL is expressed as

$$\varepsilon(\vec{k}) = \varepsilon_0(\vec{k}) + \varepsilon_{\text{HF}}(\vec{k}), \tag{A2}$$

where

$$\varepsilon_0^{(n)}(\vec{k}) = \frac{1}{2} \int \frac{d^2\vec{q}}{(2\pi)^2} V^{(n)}(|\vec{q}|) \sin^2\left(\frac{\vec{k} \times \vec{q}}{2}\right) \tag{A3}$$

represents the single-particle energy and

$$\varepsilon_{\mathrm{HF}}^{(n)}(\vec{k}) = -\int \frac{d^2\vec{q}}{(2\pi)^2} V^{(n)}(|\vec{k}-\vec{q}|) \sin^2\left(\frac{\vec{k}\times\vec{q}}{2}\right) n \tag{A4}$$

represents the HF contributions.

In this Appendix, we analytically derive the single-particle energies for the first four Landau levels. We begin by utilizing the identity $\cos(a) = \frac{1}{2}(e^{ia} + e^{-ia})$, which allows us to express the single-particle energy as

$$\varepsilon_0^{(0)}(k) = \int_0^\infty \frac{dq}{8\pi} e^{-\frac{q^2}{2}} - \int_0^\infty \int_0^{2\pi} \frac{dq\,d\phi}{32\pi^2} e^{-\frac{q^2}{2}} (e^{ikq\sin(\phi)} + e^{-ikq\sin(\phi)}). \tag{A5}$$

The equality $\mathrm{erf}(x) = \frac{2}{\sqrt{\pi}}\int_0^x e^{-t^2}dt$ motivates us to introduce the substitution $u = \frac{q}{\sqrt{2}}$, which transforms the expression into

$$\varepsilon_0^{(0)}(k) = \int_0^\infty \frac{du}{8\sqrt{2}\sqrt{\pi}} \frac{2}{\sqrt{\pi}} e^{-u^2} - \int_0^\infty \int_0^{2\pi} \frac{dq\,d\phi}{32\pi^2} e^{-\frac{1}{2}k^2\sin^2(\phi)} \left(e^{-\frac{1}{2}(q-ik\sin(\phi))^2} + e^{-\frac{1}{2}(q+ik\sin(\phi))^2}\right). \tag{A6}$$

Next, by introducing the substitutions $v_1 = \frac{1}{\sqrt{2}}(q - ik\sin(\phi))$ and $v_2 = \frac{1}{\sqrt{2}}(q + ik\sin(\phi))$, we obtain

$$\epsilon_0^{(0)}(k) = \frac{1}{8\sqrt{2}\sqrt{\pi}} - \int_0^{2\pi} \frac{d\phi}{16\sqrt{2\pi}\sqrt{\pi}} e^{-\frac{1}{2}k^2\sin^2(\phi)}. \tag{A7}$$

Finally, utilizing the identity $\sin^2(\phi) = 1 - \cos^2(\phi)$, we derive the final expression for the single-particle energy,

$$\epsilon_0^{(0)}(k) = \frac{1}{8\sqrt{2}\sqrt{\pi}}\left(1 - e^{-\frac{1}{4}k^2} I_0\left(\frac{k^2}{4}\right)\right), \tag{A8}$$

where $I_0(k)$ is the modified Bessel function of the first kind.

Analogously, we obtain the single-particle energies for the other LLs:

$$\varepsilon_0^{(1)}(k) = \frac{1}{256\sqrt{2\pi}}\left(22 - e^{-\frac{k^2}{4}}\left((22 + 2k^2 + k^4)I_0\left(\frac{k^2}{4}\right) - k^2(4 + k^2)I_1\left(\frac{k^2}{4}\right)\right)\right), \tag{A9}$$

$$\varepsilon_0^{(2)}(k) = \frac{1}{4096\sqrt{2\pi}}\left(290 - e^{-\frac{k^2}{4}}\left((290 - 12k^2 + 28k^4 - 2k^6 + k^8)I_0\left(\frac{k^2}{4}\right) + k^2(56 + 30k^2 + k^6)I_1\left(\frac{k^2}{4}\right)\right)\right), \tag{A10}$$

$$\varepsilon_0^{(3)}(k) = \frac{1}{147456\sqrt{2\pi}}\left(9270 - e^{-\frac{k^2}{4}}(9270 - 1458k^2 + 1809k^4 - 360k^6 + 114k^8 - 14k^{10} + k^{12})I_0\left(\frac{k^2}{4}\right)\right.$$
$$\left. + e^{-\frac{k^2}{4}} k^2(1836 + 1563k^2 - 192k^4 + 92k^6 - 12k^8 + k^{10})I_1\left(\frac{k^2}{4}\right)\right). \tag{A11}$$

APPENDIX B: NUMERICAL METHODS

In this Appendix, we describe the numerical methods used to solve the self-consistent equation [Eq. (34)] using the trapezoidal rule algorithm. The integral on the right-hand side of Eq. (34) is computed by discretizing the momentum space using a uniform grid. For each grid point, the integral is approximated by summing the contributions from neighboring points, weighted by the trapezoidal rule. The integration is performed iteratively, starting with an initial guess for the mean-field parameter $\Delta(\vec{k})$ (for example, $\Delta(\vec{k}) = 10^{-5}$ for all k) and updating it until the convergence criterion is satisfied. The criterion for convergence is set as

$$\frac{\max_k |\Delta_k^{\mathrm{new}} - \Delta_k^{\mathrm{old}}|}{\max_k |\Delta_k^{\mathrm{new}}|} < 10^{-3}. \tag{B1}$$

It typically takes between 11 and 70 iterations to meet the convergence criterion.

We perform the integration on the right-hand side of Eq. (34) using the trapezoidal rule. The trapezoidal rule for a two-dimensional integral over a grid can be expressed as

$$\int_a^b \int_c^d f(x, y)\,dx\,dy$$
$$\approx \sum_{i=1}^{N_x-1} \sum_{j=1}^{N_y-1} \frac{\Delta x \,\Delta y}{4}[f(x_i, y_j) + f(x_{i+1}, y_j)$$
$$+ f(x_i, y_{j+1}) + f(x_{i+1}, y_{j+1})], \tag{B2}$$

where Δx and Δy are the grid spacings in the x and y directions, respectively, and N_x and N_y are the number of grid points in each direction.

This numerical approach ensures that the results are accurate and independent of the specific choice of numerical parameters, providing a robust solution to the self-consistent equation.

[1] D. C. Tsui, H. L. Stormer, and A. C. Gossard, Two-dimensional magnetotransport in the extreme quantum limit, Phys. Rev. Lett. **48**, 1559 (1982).

[2] S. M. Girvin and K. Yang, *Modern Condensed Matter Physics*, (Cambridge University Press, Cambridge, UK, 2019).

[3] R. Willett, J. P. Eisenstein, H. L. Störmer, D. C. Tsui, A. C. Gossard, and J. H. English, Observation of an even-denominator quantum number in the fractional quantum Hall effect, Phys. Rev. Lett. **59**, 1776 (1987).

[4] J. K. Jain, Composite-fermion approach for the fractional quantum Hall effect, Phys. Rev. Lett. **63**, 199 (1989).

[5] J. K. Jain, *Composite Fermions* (Cambridge University Press, Cambridge, UK, 2007).

[6] Z. Dong and T. Senthil, Noncommutative field theory and composite Fermi liquids in some quantum Hall systems, Phys. Rev. B **102**, 205126 (2020).

[7] V. Pasquier and F. D. M. Haldane, A dipole interpretation of the $\nu = 12$ state, Nucl. Phys. B **516**, 719 (1998).

[8] N. Read, Lowest-Landau-level theory of the quantum Hall effect: The Fermi-liquid-like state of bosons at filling factor one, Phys. Rev. B **58**, 16262 (1998).

[9] H. Goldman and T. Senthil, Lowest Landau level theory of the bosonic Jain states, Phys. Rev. B **105**, 075130 (2022).

[10] S. Predin, A. Knežević, and M. V. Milovanović, Dipole representation of half-filled Landau level, Phys. Rev. B **107**, 155132 (2023).

[11] S. Predin and M. V. Milovanović, Quantum Hall bilayer in dipole representation, Phys. Rev. B **108**, 155129 (2023).

[12] D. Gočanin, S. Predin, M. D. Ćirić, V. Radovanović, and M. Milovanović, Microscopic derivation of Dirac composite fermion theory: Aspects of noncommutativity and pairing instabilities, Phys. Rev. B **104**, 115150 (2021).

[13] K. K. W. Ma and K. Yang, Quantitative theory of composite fermions in Bose-Fermi mixtures at $\nu = 1$, Phys. Rev. B **105**, 035132 (2022).

[14] Z. Dong and T. Senthil, Evolution between quantum Hall and conducting phases: Simple models and some results, Phys. Rev. B **105**, 085301 (2022).

[15] Y. Kim, A. C. Balram, T. Taniguchi, K. Watanabe, J. K. Jain, and J. H. Smet, Even denominator fractional quantum Hall states in higher Landau levels of graphene, Nat. Phys. **15**, 154 (2019).

[16] A. Sharma, S. Pu, A. C. Balram, and J. K. Jain, Fractional quantum Hall effect with unconventional pairing in monolayer graphene, Phys. Rev. Lett. **130**, 126201 (2023).

[17] A. Sharma, S. Pu, and J. K. Jain, Bardeen-Cooper-Schrieffer pairing of composite fermions, Phys. Rev. B **104**, 205303 (2021).

[18] A. Sharma, A. C. Balram, and J. K. Jain, Composite-fermion pairing at half-filled and quarter-filled lowest Landau level, Phys. Rev. B **109**, 035306 (2024).

[19] A. Kitaev, Fault-tolerant quantum computation by anyons, Ann. Phys. **303**, 2 (2003).

[20] N. Nešković, I. Vasić, and M. V. Milovanović, Topological pairing of composite fermions via criticality, Phys. Rev. B **110**, 125107 (2024).

[21] K. S. Novoselov, A. K. Geim, S. V. Morozov, D. Jiang, M. I. Katsnelson, I. V. Grigorieva, S. V. Dubonos, and A. A. Firsov, Two-dimensional gas of massless Dirac fermions in graphene, Nature (London) **438**, 197 (2005).

[22] Y. Zhang, Y.-W. Tan, H. Horst, L. Stormer, and P. Kim, Experimental observation of the quantum Hall effect and Berry's phase in graphene, Nature (London) **438**, 201 (2005).

[23] A. H. Castro Neto, F. Guinea, N. M. R. Peres, K. S. Novoselov, and A. K. Geim, The electronic properties of graphene, Rev. Mod. Phys. **81**, 109 (2009).

[24] S. Predin, P. Wenk, and J. Schliemann, Trigonal warping in bilayer graphene: Energy versus entanglement spectrum, Phys. Rev. B **93**, 115106 (2016).

[25] D. P. DiVincenzo and E. J. Mele, Self-consistent effective-mass theory for intralayer screening in graphite intercalation compounds, Phys. Rev. B **29**, 1685 (1984).

[26] E. McCann, V. I. Fal'ko, Landau level degeneracy and quantum Hall effect in a graphite bilayer, Phys. Rev. Lett. **96**, 086805 (2006).

[27] R. E. Prange and S. M. Girvin, *The Quantum Hall Effect*, (Springer-Verlag New York, NY, 1987).

[28] M. O. Goerbig and N. Regnault, Theoretical aspects of the fractional quantum Hall effect in graphene, Phys. Scr. **T146**, 014017 (2012).

[29] R. Shankar, Hamiltonian theory of gaps, masses, and polarization in quantum Hall states, Phys. Rev. B **63**, 085322 (2001).

[30] M. O. Goerbig, P. Lederer, and C. M. Smith, Competition between quantum-liquid and electron-solid phases in intermediate Landau levels, Phys. Rev. B **69**, 115327 (2004).

[31] S. M. Girvin, A. H. MacDonald, and P. M. Platzman, Magneto-roton theory of collective excitations in the fractional quantum Hall effect, Phys. Rev. B **33**, 2481 (1986).

[32] G. Murthy and R. Shankar, Hamiltonian theories of the fractional quantum Hall effect, Rev. Mod. Phys. **75**, 1101 (2003).

[33] F. D. M. Haldane, Fractional quantization of the Hall effect: A hierarchy of incompressible quantum fluid states, Phys. Rev. Lett. **51**, 605 (1983).

[34] C. Töke, M. R. Peterson, G. S. Jeon, and J. K. Jain, Fractional quantum Hall effect in the second Landau level: The importance of inter-composite-fermion interaction, Phys. Rev. B **72**, 125315 (2005).

[35] K. Park, V. Melik-Alaverdian, N. E. Bonesteel, and J. K. Jain, Possibility of p-wave pairing of composite fermions at $\nu = 1/2$, Phys. Rev. B **58**, R10167 (1998).

[36] M. Greiter, X. G. Wen, and F. Wilczek, Paired Hall states, Nucl. Phys. B **374**, 567 (1992).

[37] M. Greiter, X. G. Wen, and F. Wilczek, Paired Hall states in double-layer electron systems, Phys. Rev. B **46**, 9586 (1992).

[38] G. Moore and N. Read, Nonabelions in the fractional quantum Hall effect, Nucl. Phys. B **360**, 362 (1991).

[39] M. Levin, B. I. Halperin, and B. Rosenow, Particle-hole symmetry and the Pfaffian state, Phys. Rev. Lett. **99**, 236806 (2007).

[40] S.-S. Lee, S. Ryu, C. Nayak, and M. P. A. Fisher, Particle-hole symmetry and the $\nu = \frac{5}{2}$ quantum Hall state, Phys. Rev. Lett. **99**, 236807 (2007).

[41] A. C. Balram, C. Töke, A. Wójs, and J. K. Jain, Spontaneous polarization of composite fermions in the $n = 1$ Landau level of graphene, Phys. Rev. B **92**, 205120 (2015).

[42] G. Diankov, C.-T. Liang, F. Amet, P. Gallagher, M. Lee, A. J. Bestwick, K. Tharratt, W. Coniglio, J. Jaroszynski, K. Watanabe, T. Taniguchi, and D. Goldhaber-Gordon, Robust fractional quantum Hall effect in the $n = 2$ Landau level in bilayer graphene, Nat. Commun. **7**, 13908 (2016).

[43] S. Chen, R. Ribeiro-Palau, K. Yang, K. Watanabe, T. Taniguchi, J. Hone, M. O. Goerbig, and C. R. Dean, Competing fractional quantum Hall and electron solid phases in graphene, Phys. Rev. Lett. **122**, 026802 (2019).

[44] R. V. Mishmash, D. F. Mross, J. Alicea, and O. I. Motrunich, Numerical exploration of trial wave functions for the particle-hole-symmetric Pfaffian, Phys. Rev. B **98**, 081107(R) (2018).

[45] J. K. Jain, Incompressible quantum Hall states, Phys. Rev. B **40**, 8079(R) (1989).

[46] Y. Hu, Y.-C. Tsui, M. He, U. Kamber, T. Wang, A. S. Mohammadi, K. Watanabe, T. Taniguchi, Z. Papic, M. P. Zaletel, and A. Yazdani, High-resolution tunneling spectroscopy of fractional quantum Hall states, arXiv:2308.05789.

Quantum Hall bilayer in dipole representation

S. Predin and M. V. Milovanović

Scientific Computing Laboratory, Center for the Study of Complex Systems, Institute of Physics Belgrade,
University of Belgrade, 11080 Belgrade, Serbia

The Quantum Hall Bilayers (QHB) at filling factor $\nu = 1$ represents a competition between Bose-Einstein condensation (BEC) at small distances between layers and fermionic condensation, whose influence grows with distance and results in two separate Fermi liquid states for the underlying quasiparticles at very large (or infinite) distances. The question that can be raised is whether, at intermediate distances between layers, a distinct phase exists or if a singular transition occurs, with the possibility that this happens at infinite distances. Here, using a dipole representation for fermionic quasiparticles, we find support for the latter scenario: Within a large and relevant range of distances, BEC condensation, identified as Cooper s-wave pairing of dipole quasiparticles, prevails over both Cooper p-wave pairing and s-wave excitonic pairing of the same quasiparticles.

I. INTRODUCTION

The QHB [1,2] is a fractional quantum Hall effect (FQHE) system with an additional layer degree of freedom: Two layers of two-dimensional electron gases at distance d from each other are pierced by a strong magnetic field, B, perpendicular to the layers. The total density of the system, n_T, matches the density of available states in the (lowest) Landau level (LL), $(eB)/h$, in which electrons live. Thus the total filling factor is $\nu_T = n_T(2\pi l_B^2) = 1$, with the characteristic length of the system, $l_B = \sqrt{\hbar/(cB)}$, the magnetic length.

Therefore, each layer is half-filled, i.e., it represents a system of electrons that occupy half of the available states in the lowest LL (LLL), and thus $\nu_T = \nu_\uparrow + \nu_\downarrow$, $\nu_\sigma = 1/2$, $\sigma = \uparrow, \downarrow$, where the up and down signs refer to a specific layer. At long distances, $d \gg l_B$, the layers are almost independent, at least much less intertwined, and at $d \lesssim l_B$, they are strongly coupled and an excitonic binding between a hole in one layer and a particle in the opposite one dominates. Thus, a distance, $\bar{d} \sim l_B$, may represent a characteristic distance for the transition from a strong-coupling to a weak-coupling regime for the system of two layers, and a question can be raised: What happens at these intermediate, $d \sim l_B$ distances? A new intermediate phase, a single transition between two phases (connected with two extremes, small and large distances), or a crossover with no phase transition? Various scenarios appeared in the literature and in this work we will address this question using a special formalism.

The first proposals for multicomponent FQHE systems and studies of the QHB in Refs. [3–6] were followed by experiments [7,8] that confirmed the integer QHE for small distances between the layers in the case of the QHB. Further development of the theoretical understanding of the system at $d \lesssim l_B$, as an excitonic condensate or an ordered state of the pseudospin of electrons [9–12], was followed by experiments [13,14] that revealed the new ordered state and phase at small distances. On the other hand, there is an expectation that at large distances $(d \gg l_B)$, we have well-separated layers, each in a compresssible state [15] of a single layer at filling factor 1/2 [16,17].

Many theoretical, analytical, and numerical studies have been done [9–12,18–51] in order to understand the evolution of the QHB with distance; in particular with the assumption of the projection of the physics into the LLL in the absence of disorder. The modeling and understanding of the FQHE is based on the composite excitations—particles which are often identified as composite fermions (CFs) [52–54].

In the case of the single-layer at filling factor 1/2, and under assumption that all electrons are in the LLL, composite fermion can be viewed as a composite of electron and its correlation hole, which represents a unit of a positive charge. Thus CF is an overall neutral fermionic object which can make a Fermi sea of CFs (and we may expect a compressible behavior of the system). If we apply a classical analogy, such an overall neutral composite, in an external magnetic field, B, then it must have its momentum proportional to its dipole moment, and at and near Fermi surface we have dipoles [55–57]. This dipole picture is a direct consequence of the projection into a LL [55–57].

Nevertheless, there is an additional feature of the system of electrons that fill half of available states in a LL: The physics should be invariant under exchange of particles and holes, i.e., we have a particle-hole (PH) symmetry and, together with CFs, we should also consider and incorporate composite holes (CHs) in our description to have the PH symmetry manifestly represented. To include the PH symmetry, a two component Dirac-type description was introduced in Ref. [58] for the description of half-filled LL. But, to describe, in a Fermi-liquid (FL) framework, a half-filled LL of electrons, we may also consider a variant of the dipole construction in a one-component fermion formalism, as introduced in Ref. [59]. This construction is a generalization of the dipole, i.e., CF representation in the case of bosons at filling factor $\nu = 1$ in

the LLL [60,61], and it is applicable in the low-energy limit (of the effective FL description).

In this work, we applied the variant of the dipole representation that we developed [59], in order to understand the evolution of the QHB with distance. We identified, at all distances between layers, the presence of a single phase that can be described as an *s*-wave Cooper pairing of dipole quasiparticles. The underlying physics of this pairing is the excitonic attraction between electrons in one layer and holes in the opposite layer, and thus the phase that is well understood at small distances continues to exist at large distances. This scenario was proposed in Ref. [49], on the basis of the Dirac description [58] of the physics in each layer, and was numerically supported in a recent work [50] by modeling the system on a sphere. This work modeled the underlying physics as an attraction (Cooper pairing) between CF in one layer and CH in the other, opposite layer. In our study, using the formalism of Ref. [59], the nature of the dominant phase is further elucidated, as is the competition among other candidates for the ground state of the system as the distance *d* is varied. The *s*-wave Cooper pairing of dipoles prevails over a Cooper *p*-wave pairing and *s*-wave excitonic pairing of dipole quasiparticles. The excitonic pairing would represent a topological, incompressible phase inside an LLL. Our formalism and the BCS treatment of its setup are more accurate in the weak-coupling regime, and the confirmation at intermediate and large distances of the same phase (that is dominant in the strong-coupling regime at small distances) is, in this sense, reliable and supports the extension to all *d*'s.

In the dipole formalism that we applied, in the case of bilayer, the dipole quasiparticles [which are neither CFs nor CHs but are symmetric objects that are consistent with the PH symmetry] enable a representation that has manifest symmetry under the exchange of particles and holes is done simultaneously in both layers. The dipole representation has additional, artificial degrees of freedom - correlation holes, which are identified with holes in the electron system(s). This unusual constraint, which we have to incorporate into the description, comes from the projection into a single LL of the states of fermionic quasiparticles that reside near the Fermi level (and most significantly influence the physics). To incorporate the constraint and use the mean-field method, we need to deal with effective Hamiltonians which are adapted to the use of the method by explicit inclusion of the constraint (as null operators) in their description. We focus (narrow possibilities) on small number of effective Hamiltonians which explicitly represent, in their forms, physics of potential phases. We solve them (in the mean-field approximation) and compare the energies of different Hamiltonians to find the most stable solution at distance *d*.

The paper is organized as follows. Section II provides a review of the dipole representation in a single layer. We discuss the key concepts and principles underlying the dipole representation and its relevance to our study. In Sec. III, we investigate the implications of the dipole representation in the QHB case and present results on the competition among phases and the resulting phase diagram. Finally, in Sec. IV, we summarize our findings and provide concluding remarks.

II. DIPOLE REPRESENTATION FOR HALF-FILLED LL

The dipole representation for half-filled LL is an extension of the formalism introduced for the description of the CF quasiparticles for a system of bosons at a filling factor $\nu = 1$ in an isolated LL [60,61]. In an enlarged space the CF annihilation operator, c_{mn}, is introduced as an operator with double indices, where each index corresponds to a state in a LL, $n, m = 1, 2, \ldots, N_\phi$, the left ($L$, physical) index is associated with a state of an elementary boson, and the right (R, artificial) index is associated with the state of the corresponding correlation hole. In the context of FQHE the correlation hole can be defined by a (local) insertion of flux quanta in the system and represents a well-defined object with charge and statistics. In the system of bosons, the many-body hole is fermionic, and the resulting composite object is a fermion, i.e., boson + correlation hole = CF. We may introduce the physical and artificial (of additional degrees of freedom) densities,

$$\rho_{nn'}^L = \sum_m c_{mn}^\dagger c_{n'm}, \tag{1}$$

and

$$\rho_{mm'}^R = \sum_n c_{mn}^\dagger c_{nm'}, \tag{2}$$

and their forms in the inverse space,

$$\rho_q^L = \int \frac{d\boldsymbol{k}}{(2\pi)^2} c_{\boldsymbol{k}-\boldsymbol{q}}^\dagger c_{\boldsymbol{k}} \exp\left(i\frac{\boldsymbol{k} \times \boldsymbol{q}}{2}\right), \tag{3}$$

and

$$\rho_q^R = \int \frac{d\boldsymbol{k}}{(2\pi)^2} c_{\boldsymbol{k}-\boldsymbol{q}}^\dagger c_{\boldsymbol{k}} \exp\left(-i\frac{\boldsymbol{k} \times \boldsymbol{q}}{2}\right), \tag{4}$$

which have the same form as the projected densities of systems of elementary particles into a single LL; they are nonlocal and obey the Girvin-MacDonald-Platzmann algebra. The collapse from the two-particle to a single-particle index $\boldsymbol{k}$ is physically enabled by the existence of the well-defined dipole object (CF) which momentum ($\boldsymbol{k}$) in the (external) magnetic field is proportional to its dipole moment.

To complete the description of the system we need to impose constraints in order to have as many degrees of freedom as required by the definition of the problem. It is not hard to see (due to the fact that the total number of CFs is equal to the number of bosons and due to their fermionic statistics) that we need to have $\rho_{nn}^R = 1$ for each n, or $\rho_q^R = 0$ when $\boldsymbol{q} \neq 0$, in inverse space. In the case of the half-filled LL of electrons, details can be found in Ref. [59], we may formally proceed with the same constructions as in the previous case, but now the correlation holes have bosonic statistics. To have a well-defined description we need to impose $\rho_{nn}^L + \rho_{nn}^R = 1$ for each n or $\rho_q^L + \rho_q^R = 0$ when $\boldsymbol{q} \neq 0$ (which requires that correlation holes are hard-core bosons). But these constraints include the densities of the physical sector and thus have nontrivial influence on the physical degrees of freedom: The correlation holes are on the positions of the real (fermionic) holes. This is an unexpected constraint that opposes the usual interpretation of the correlation hole as a potential well for an elementary particle. Nevertheless, the constraint corresponds to the physics of the CFs near the Fermi level, i.e., to the most

important, effective physics of the problem: The magnitude of the momentum of these CFs is $|\mathbf{k}| \sim k_F = 1/l_B$ (l_B is the magnetic length), and due to the projection to a fixed LL [55–57], this implies that the correlation hole is shifted, distanced from the electron for the same amount, $|\mathbf{k}|l_B^2 \sim l_B$. Furthermore, we consider the Hamiltonian of the problem in a PH symmetric form, one that is symmetric under exchange of particles and holes, i.e., L and R densities,

$$H = \frac{1}{2} \int \frac{d\mathbf{q}}{(2\pi)^2} \tilde{V}(|\mathbf{q}|) \frac{[\rho^L(-\mathbf{q}) - \rho^R(-\mathbf{q})]}{2} \frac{[\rho^L(\mathbf{q}) - \rho^R(\mathbf{q})]}{2}. \quad (5)$$

Because of the constraint and the implied PH symmetry, we may refer to the composite object not as a CF but simply as a dipole, i.e., a symmetric object which is neither CF nor CH.

III. THE QUANTUM HALL BILAYER IN DIPOLE REPRESENTATION

We begin with the Hamiltonian for the QHB in the second quantization, with electron density operators, $\rho_\sigma(\mathbf{q})$, $\sigma = \uparrow, \downarrow$ ($\uparrow$ and $\downarrow$ refer to the two different layers):

$$\mathcal{H}_e = \int \frac{d\mathbf{q}}{(2\pi)^2} \left\{ \sum_\sigma \frac{1}{2} V(|\mathbf{q}|) : \rho_\sigma(\mathbf{q}) \rho_\sigma(-\mathbf{q}) : \right.$$
$$\left. + V_{\uparrow\downarrow}(|\mathbf{q}|) \rho_\uparrow(\mathbf{q}) \rho_\downarrow(-\mathbf{q}) \right\}. \quad (6)$$

In the enlarged space formalism, the bilinears $\rho_\sigma(\mathbf{q})$ become

$$\rho_\sigma^L(\mathbf{q}) = \int \frac{d\mathbf{k}}{(2\pi)^2} c_\sigma^\dagger(\mathbf{k} - \mathbf{q}) c_\sigma(\mathbf{k}) \exp\left(i \frac{\mathbf{k} \times \mathbf{q}}{2} \right), \quad (7)$$

where formally we have, instead of electron annihilation and creation operators, the quasiparticle operators, $c_\sigma(\mathbf{k})$ and $c_\sigma^\dagger(\mathbf{k})$. Quasiparticles in the long-distance approximation can be interpreted as fermionic dipoles. In the Hamiltonian we recognize the intrainteraction terms with $V(|\mathbf{q}|) = (1/|\mathbf{q}|) \exp(-|\mathbf{q}|^2/2)$ and the interinteraction term with $V_{\uparrow\downarrow}(|\mathbf{q}|) = V(|\mathbf{q}|) \exp(-d|\mathbf{q}|)$, where d denotes the distance between the layers. We then proceed by using the dipole representation, which we find optimal for exploring the influence of the fermionic quasiparticles and physics that grows with distance. This representation allows the inclusion of the PH symmetry of the system (under exchange of all electrons, irrespective of index, and holes) in a manifestly invariant way in the Hamiltonian. We then proceed to utilize the dipole representation, which we find optimal for exploring the influence of the fermionic quasiparticles and the physics that evolves with distance.

By imposing the constraints,

$$\rho_\sigma^L(\mathbf{k}) + \rho_\sigma^R(\mathbf{k}) = 0 \quad \sigma = \uparrow, \downarrow, \quad (8)$$

that define the dipole representation in each layer, we place correlation holes where holes are, and thus the PH exchange is followed by the density exchange:

$$\rho_\sigma^L(\mathbf{k}) \leftrightarrow \rho_\sigma^R(-\mathbf{k}) \quad \sigma = \uparrow, \downarrow. \quad (9)$$

Therefore, the Hamiltonian can be written (by using the constraints) in an explicitly invariant form under this exchange:

$$\mathcal{H}_0 = \int \frac{d\mathbf{q}}{(2\pi)^2} \left\{ \sum_\sigma \frac{1}{8} V(|\mathbf{q}|) [\rho_\sigma^L(-\mathbf{q}) - \rho_\sigma^R(-\mathbf{q})] \right.$$
$$\times [\rho_\sigma^L(\mathbf{q}) - \rho_\sigma^R(\mathbf{q})] + \frac{V_{\uparrow\downarrow}(|\mathbf{q}|)}{4} [\rho_\uparrow^L(-\mathbf{q}) - \rho_\uparrow^R(-\mathbf{q})]$$
$$\left. \times [\rho_\downarrow^L(\mathbf{q}) - \rho_\downarrow^R(\mathbf{q})] \right\}. \quad (10)$$

Note the absence of normal ordering due to the requirement that the constraints commute with the Hamiltonian in the physical space. This induces single particle terms (beside purely interacting) with effective mass M (due to the intralayer interaction) [62,63]. By treating the constraints as null operators (in the physical space), which we can include in the Hamiltonian, we reach forms of the Hamiltonian that are adapted to the mean-field approach, as they offer obvious interpretation which phase in the mean-field approach they support.

In the QHB case we can add and subtract (product of) constraints and define the following (effective) Hamiltonians:

$$\mathcal{H}_1 = \int \frac{d\mathbf{q}}{(2\pi)^2} \left\{ \sum_\sigma \frac{1}{8} V(|\mathbf{q}|) [\rho_\sigma^L(-\mathbf{q}) - \rho_\sigma^R(-\mathbf{q})] \right.$$
$$\times [\rho_\sigma^L(\mathbf{q}) - \rho_\sigma^R(\mathbf{q})] + \frac{V_{\uparrow\downarrow}(|\mathbf{q}|)}{2}$$
$$\left. \times [-\rho_\uparrow^L(-\mathbf{q})\rho_\downarrow^R(\mathbf{q}) - \rho_\uparrow^R(-\mathbf{q})\rho_\downarrow^L(\mathbf{q})] \right\}, \quad (11)$$

and

$$\mathcal{H}_2 = \int \frac{d\mathbf{q}}{(2\pi)^2} \left\{ \sum_\sigma \frac{1}{8} V(|\mathbf{q}|) [\rho_\sigma^L(-\mathbf{q}) - \rho_\sigma^R(-\mathbf{q})] \right.$$
$$\times [\rho_\sigma^L(\mathbf{q}) - \rho_\sigma^R(\mathbf{q})] + \frac{V_{\uparrow\downarrow}(|\mathbf{q}|)}{2}$$
$$\left. \times [\rho_\uparrow^L(-\mathbf{q})\rho_\downarrow^L(\mathbf{q}) + \rho_\uparrow^R(-\mathbf{q})\rho_\downarrow^R(\mathbf{q})] \right\}. \quad (12)$$

The form of $\mathcal{H}_1$ emphasizes the excitonic attraction between densities from opposite layers (electron-hole attraction), which we expect to dominate physics at small distances. On the level of effective dipoles - composite particles (c's) this will translate to a strong instability to a Cooper pair formation between c's from different layers. On the other hand, the form of $\mathcal{H}_2$ is suggestive of excitonic pairing between c's from opposite layers. Indeed, in a mean-field treatment of $\mathcal{H}_1$ and $\mathcal{H}_2$, these instabilities can be identified as shown in Fig. 1. Details of the mean-field treatment are provided in the Appendix. For all distances considered, the s-wave ($l = 0$) Cooper pairing between layers has lower energy than the p-wave ($l = 1$) Cooper pairing and s-wave ($l = 0$) excitonic pairing. The s-wave excitonic phase of quasiparticles is similar to the one proposed in Ref. [45], which describes an interlayer correlated CF liquid (ICCFL). However, in our work, we operate within an LL, and the quasiparticles involved are (neutral) dipoles.
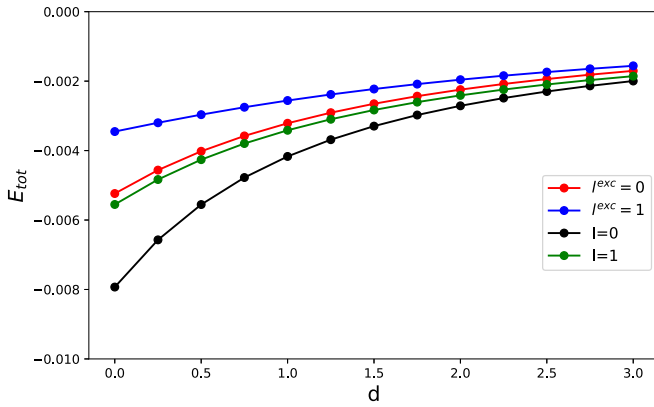
FIG. 1. The total energies of the ground states of effective Hamiltonians H_1 and H_2 as functions of the distance between layers; s-wave Cooper pairing of H_1 in black, p-wave Cooper pairing of H_1 in green, s-wave exciton pairing of H_2 in red, and p-wave exciton pairing of H_2 in blue.

In calculating total energies we applied a short-distance "cutoff" if necessary (if we encountered divergences). Though consistently defined on the whole $\boldsymbol{k}$ plane [61], the enlarged space description must be supplied with a natural "cutoff" (due to an intrinsic "lattice constant" l_B for this system): radius $k = \sqrt{2}/l_B$ of a circle in the $\boldsymbol{k}$ space, i.e., a volume of the available states in a single LL. In most cases the presence of Gaussians allows the extension of the integration over the whole space.

The exciton instability in the plotted range $d \in [0, 3l_B]$ can be described as an occupation of a single, lower band that is associated with the symmetric superposition: $[c_{\uparrow}(\boldsymbol{k}) + c_{\downarrow}(\boldsymbol{k})]/\sqrt{2}$. Thus a single, large Fermi sea exists in this range according to the mean-field calculation. Related to this is the excitonic binding of c's implied by $\mathcal{H}_0$ (with a dipole-dipole interaction that screens the bare Coulomb interaction) with the gap parameter, $\Delta_{\boldsymbol{k}} \sim |\boldsymbol{k}|^2$ (not a constant as in the case of $\mathcal{H}_2$). The total energy of this solution is negligible and may be relevant only for very large d when a transition to two decoupled Fermi seas takes place, i.e., for an equal population of symmetric and antisymmetric bands.

We applied the mean-field approach to the effective Hamiltonians and thus we may expect that our results are more reliable for larger d, i.e., weak coupling between layers. The weak-coupling assumption is completely justified for $d \sim 3l_B$ [see Fig. 1, weak attraction (pairing amplitudes), i.e., weak coupling can be recognized in small differences in total energies with respect to the asymptotic value, i.e., the free-fermion limit], and we may ask whether (at all, because of the strong coupling for $d \lesssim l_B$) a conclusion for the state of the system at any d can be drawn. But the nature of the predicted phase for $d \lesssim l_B$ (in the strong-coupling regime) in our formalism is the same as the one that is firmly confirmed in many calculations and approaches, a binding of the density of electrons with the density of holes in the opposite layers (opposite charge binding), and given that this phase (in our formalism) persists to large d (weak-coupling regime where the approach is fully reliable), we can conclude (assuming continuity, i.e., that a reentrant scenario is unlikely) that one and the same phase is present for all relevant distances including $d \gg l_B$.

In our approach, the binding of charges from opposite layers is described (effectively) as s-wave binding of dipoles of momenta $\boldsymbol{k}$ and $-\boldsymbol{k}$ and thus involves opposite dipole moments from opposite layers. This is similar to the binding described in Ref. [50], where a CF in one layer binds to a CH in the other one. The underlying physics of pairing is the same, and the descriptions should correspond to the same phase [64].

We did not include a requirement for the boost invariance (K invariance [63,65]) as in the single-layer case [59], because in this case, a real increase of the energy of the system is possible due to a relative motion between layers. In the mean field, the dispersion of the Goldstone mode is $\omega_{\boldsymbol{k}} \sim \sqrt{\Delta_s/M}$, where Δ_s is the BCS gap and M is the mass of quasiparticles due to the Coulomb interaction between the same layer particles. The boost invariance should be ensured in the limiting cases, $d = 0$ and $d = \infty$, but at intermediate distances, we may rely on the mean-field estimates.

IV. DISCUSSION AND CONCLUSIONS

Thus, we may conclude that within the scope of dipole representation and mean-field method, there is no transition in the QHB at finite distance between layers; the excitonic phase of electrons (or Cooper s-wave pairing of fermionic quasiparticles and dipoles in the long-distance approximation) dominates the physics at relevant distances. On the other hand, the suppressed yet competing, s-wave excitonic phase of quasiparticle inside LLL can be described as a large Fermi sea of quasiparticles (with no layer index, i.e., with symmetric superpositions). An intermediate state in the QHB has been identified and described by exact diagonalization on a torus in Ref. [46]. In our description the Fermi sea of (neutral) dipoles, in the absence of the boost invariance (or K invariance), leads to the incompressibility in the charge channel [63,65] of the competing phase, and that is consistent with findings of Ref. [46] (and distinct from the ICCFL phase of Ref. [45]). The exciton condensation induces a gapped, topological behavior in the neutral channel, just as in the case of the ICCFL phase (of Ref. [45]) and consistent with findings of Ref. [46].

Based on previous analyses [47,48], one may expect that the inclusion of LL mixing will lead to the formation of the p-wave pairing state of CFs (from opposite layers, i.e., interpairing). This state can be found in an unprojected (to a fixed LL) Chern-Simons field-theoretical description. A Dirac type of the gauge theory leads to the conclusion that the p-wave Cooper pairing of CFs from opposite layers describes the system at any distance between layers [49] (except at $d = \infty$). The no-transition scenario continues to exist under LL mixing [51]. The results of our work, within the LLL, and the results of Ref. [51], with no projection in a Chern-Simons treatment, are in correspondence. This continuous (one and only for all distances) phase can be simulated by selecting an appropriate shift (i.e., bias) in the spherical geometry, inside the LLL, as described in Ref. [50].

In short, we have demonstrated the usefulness of the dipole representation in the case of the long-standing problem of the QHB, with potential to be used for half-filled problems of general Chern bands. Inside an LLL, the QHB physics is dominated by a single phase: the Cooper s-wave pairing of effective dipoles. While for the system of electrons in a

single layer that occupy half of the available states in a LL a compressible behavior is only possible [69], here we find that a nontrivial double, a nontrivial superposition of two such systems with incompressible, topological behavior based on the noncommutative nature of projection(s) inside LL(s) is in a competition with a compressible phase, but again the compressible (in the neutral channel) phase is realized.

APPENDIX: MEAN-FIELD APPROACH TO EFFECTIVE HAMILTONIANS

In this Appendix, we give a brief account of the mean-field treatment of the Hamiltonians, $\mathcal{H}_1$, (11), and $\mathcal{H}_2$, (12). Due to the attractive nature of the effective interaction in $\mathcal{H}_1$, and the repulsive nature of the effective interaction in $\mathcal{H}_2$, we introduce a mean-field reduction of the Hamiltonians, assuming the pairing in the Cooper channel of $\mathcal{H}_1$, i.e., $\langle c_{k,\uparrow}^\dagger c_{-k,\downarrow}^\dagger \rangle = \Delta_k^{\text{bcs}} \neq 0$, and the excitonic pairing of $\mathcal{H}_2$, i.e., $\langle c_{k,\uparrow}^\dagger c_{k,\downarrow} \rangle = \Delta_k^{\text{exc}} \neq 0$.

In the BCS case, we need to solve self-consistently the following equation, for the order parameter Δ_q^{bcs}:

$$\Delta_k^{\text{bcs}} = \int \frac{d\boldsymbol{q}}{(2\pi)^2} V_{\uparrow\downarrow}(|\boldsymbol{q}-\boldsymbol{k}|) \frac{\Delta_q^{\text{bcs}}}{2E_q}, \quad \text{(A1)}$$

where $E_q = \sqrt{\xi_q^2 + |\Delta_q^{\text{bcs}}|^2}$ and $\xi_q = \epsilon_q - \epsilon_{q_F}$, with $\boldsymbol{q}_F = 1$ (a half-filled condition for each layer). Also ϵ_q represents

the single-particle energy of quasiparticles in each layer that is calculated using the Hartree-Fock method, applied to the single-layer part of the Hamiltonian that describes the intralayer interaction. See below an explicit formula in (A5). The (total) ground-state energy of the system is

$$E_0^{\text{bcs}} = \int \frac{d\boldsymbol{q}}{(2\pi)^2}(\xi_q - E_q) + \int \frac{d\boldsymbol{q}}{(2\pi)^2}\frac{|\Delta_q^{\text{bcs}}|^2}{2E_q}. \quad \text{(A2)}$$

In the excitonic case, we need to self-consistently solve the following equation, for the order parameter Δ_q^{exc}:

$$\Delta_k^{\text{exc}} = \int \frac{d\boldsymbol{q}}{(2\pi)^2} V_{\uparrow\downarrow}(|\boldsymbol{q}-\boldsymbol{k}|) \frac{\Delta_q^{\text{exc}}}{2|\Delta_q^{\text{exc}}|}[n_\alpha(\boldsymbol{q}) - n_\beta(\boldsymbol{q})], \quad \text{(A3)}$$

where $n_\alpha(\boldsymbol{q})$ and $n_\beta(\boldsymbol{q})$ denote the occupations of the states with momentum $\boldsymbol{q}$, in the band with energies $\mathcal{E}_\alpha(\boldsymbol{q}) = \epsilon_q - |\Delta_q^{\text{exc}}|$, and in the band with energy $\mathcal{E}_\beta(\boldsymbol{q}) = \epsilon_q + |\Delta_q^{\text{exc}}|$, respectively. In solving (A3), we have to keep the density of the system constant, i.e., the occupation of the lower and upper band, described by appropriate Fermi momenta, q_+^F and q_-^F, should satisfy the following equation: $(q_+^F)^2 + (q_-^F)^2 = 2$.

The (total) ground-state energy of the system is

$$\begin{aligned} E_0^{\text{exc}} = \int \frac{d\boldsymbol{q}}{(2\pi)^2}\big[&(\xi_q - |\Delta_q^{\text{exc}}|/2)n_\alpha(\boldsymbol{q}) \\ &+ (\xi_q + |\Delta_q^{\text{exc}}|/2)n_\beta(\boldsymbol{q})\big], \end{aligned} \quad \text{(A4)}$$

where, as before, $\xi_q = \epsilon_q - \epsilon_{q_F}$, with $\boldsymbol{q}_F = 1$ (a half-filled condition for each layer).

The following equation describes the single-particle energy obtained after the application of the (Hartree-)Fock procedure to the intralayer part of the Hamiltonian:

$$\begin{aligned} \epsilon_k = \frac{1}{2}\int \frac{d\boldsymbol{q}}{(2\pi)^2}\tilde{V}(|\boldsymbol{q}|)\left[\sin\left(i\frac{\boldsymbol{k}\times\boldsymbol{q}}{2}\right)\right]^2 \\ - \int \frac{d\boldsymbol{q}}{(2\pi)^2}\tilde{V}(|\boldsymbol{q}-\boldsymbol{k}|)\left[\sin\left(i\frac{\boldsymbol{k}\times\boldsymbol{q}}{2}\right)\right]^2 n(\boldsymbol{q}). \end{aligned} \quad \text{(A5)}$$

The occupation $n(\boldsymbol{q})$ describes the filled Fermi sphere with radius $q_F = 1$. The first contribution comes from the normal ordering of the density-density form of the intralayer term and may represent the self-energy of a dipole [62], and the second term represents a Fock contribution.

[1] J. P. Eisenstein and A. H. MacDonald, Bose-Einstein condensation of excitons in bilayer electron systems, Nature (Lond.) **432**, 691 (2004).

[2] J. P. Eisenstein, Exciton condensation in bilayer auantum Hall systems, Annu. Rev. Condens. Matter Phys. **5**, 159 (2014).

[3] B. I. Halperin, Theory of quantized Hall conductance, Helv. Phys. Acta **56**, 75 (1983).

[4] R. B. Laughlin, Anomalous quantum Hall effect: An incompressible quantum fluid with fractionally charged excitations, Phys. Rev. Lett. **50**, 1395 (1983).

[5] F. D. M. Haldane and E. H. Rezayi, Fractional quantum Hall effect at even denominator filling factors in multi-layer systems, Bull. Am. Phys. Soc. **32**, 892 (1987).

[6] T. Chakraborty and P. Pietilainen, Fractional quantum Hall effect at half-filled Landau level in a multiple-layer electron system, Phys. Rev. Lett. **59**, 2784 (1987).

[7] Y. W. Suen, L. W. Engel, M. B. Santos, M. Shayegan, and D. C. Tsui, Observation of a $\nu = 1/2$ fractional quantum Hall state in a double-layer electron system, Phys. Rev. Lett. **68**, 1379 (1992).

[8] J. P. Eisenstein, G. S. Boebinger, L. N Pfeiffer, K. W. West, and S. He, New fractional quantum Hall state in double-layer two-dimensional electron systems, Phys. Rev. Lett. **68**, 1383 (1992).

[9] H. A. Fertig, Energy spectrum of a layered system in a strong magnetic field, Phys. Rev. B **40**, 1087 (1989).

[10] X. G. Wen and A. Zee, Neutral superfluid modes and "magnetic" monopoles in multilayered quantum Hall systems, Phys. Rev. Lett. **69**, 1811 (1992).

[11] K. Yang, K. Moon, L. Zheng, A. H. MacDonald, S. M. Girvin, D. Yoshioka, and S. C. Zhang, Quantum ferromagnetism and phase transitions in double-layer quantum Hall systems, Phys. Rev. Lett. **72**, 732 (1994).

[12] K. Moon, H. Mori, K. Yang, S. M. Girvin, A. H. MacDonald, L. Zheng, D. Yoshioka, and S. C. Zhang, Spontaneous interlayer coherence in double-layer quantum Hall systems: Charged vortices and Kosterlitz-Thouless phase transitions, Phys. Rev. B **51**, 5138 (1995).

[13] I. B. Spielman, J. P. Eisenstein, L. N. Pfeiffer, and K. W. West, Resonantly enhanced tunneling in a double layer quantum Hall ferromagnet, Phys. Rev. Lett. **84**, 5808 (2000).

[14] M. Kellogg, J. P. Eisenstein, L. N. Pfeiffer, and K. W. West, Vanishing Hall resistance at high magnetic field in a double-layer two-dimensional electron system, Phys. Rev. Lett. **93**, 036801 (2004).

[15] B. I. Halperin, P. A. Lee, and N. Read, Theory of the half-filled Landau level, Phys. Rev. B **47**, 7312 (1993).

[16] A. H. MacDonald, P. M. Platzman, and G. S. Boebinger, Collapse of integer Hall gaps in a double-quantum-well system, Phys. Rev. Lett. **65**, 775 (1990).

[17] M. Kellogg, J. P. Eisenstein, L. N. Pfeiffer, and K. W. West, Bilayer quantum Hall systems at $\nu_T = 1$: Coulomb drag and the transition from weak to strong interlayer coupling, Phys. Rev. Lett. **90**, 246801 (2003).

[18] N. E. Bonesteel, I. A. McDonald, and C. Nayak, Gauge fields and pairing in double-layer composite fermion metals, Phys. Rev. Lett. **77**, 3009 (1996).

[19] H. Isobe and L. Fu, Interlayer pairing symmetry of composite fermions in quantum Hall bilayers Phys. Rev. Lett. **118**, 166401 (2017).

[20] T. Morinari, Composite-fermion pairing in bilayer quantum Hall systems, Phys. Rev. B **59**, 7320 (1999).

[21] Z. F. Ezawa and G. Tsitsishvili, Quantum Hall ferromagnets, Rep. Prog. Phys. **72**, 086502 (2009).

[22] B. Lian and S.-C. Zhang, Wave function and emergent SU(2) symmetry in the $\nu_T = 1$ quantum Hall bilayer, Phys. Rev. Lett. **120**, 077601 (2018).

[23] Y. B. Kim, C. Nayak, E. Demler, N. Read, and S. Das Sarma, Bilayer paired quantum Hall states and Coulomb drag, Phys. Rev. B **63**, 205315 (2001).

[24] Y. N. Joglekar and A. H. MacDonald, Microscopic functional integral theory of quantum fluctuations in double-layer quantum Hall ferromagnets, Phys. Rev. B **64**, 155315 (2001).

[25] K. Yang, Dipolar excitons, spontaneous phase coherence, and superfluid-insulator transition in bilayer quantum Hall systems at $\nu = 1$, Phys. Rev. Lett. **87**, 196802 (2001).

[26] Y. N. Joglekar and A. H. MacDonald, Bias-voltage-induced phase transition in bilayer quantum Hall ferromagnets, Phys. Rev. B **65**, 235319 (2002).

[27] R. Côté, L. Brey, and A. H. MacDonald, Broken-symmetry ground states for the two-dimensional electron gas in a double-quantum-well system, Phys. Rev. B **46**, 10239 (1992).

[28] K. Nomura and D. Yoshioka, Evolution of $\nu = 1$ bilayer quantum Hall ferromagnet, Phys. Rev. B **66**, 153310 (2002).

[29] J. Schliemann, S. M. Girvin, and A. H. MacDonald, Strong correlation to weak correlation phase transition in bilayer quantum Hall systems, Phys. Rev. Lett. **86**, 1849 (2001).

[30] N. Shibata and D. Yoshioka, Fractional quantum Hall effects in graphene and its bilayer, J. Phys. Soc. Jpn. **75**, 043712 (2006).

[31] K. Park, Spontaneous pseudospin spiral order in bilayer quantum Hall systems, Phys. Rev. B **69**, 045319 (2004).

[32] K. Park and S. Das Sarma, Coherent tunneling in exciton condensates of bilayer quantum Hall systems, Phys. Rev. B **74**, 035338 (2006).

[33] G. Möller, S. H. Simon, and E. H. Rezayi, Trial wave functions for $\nu = \frac{1}{2} + \frac{1}{2}$ quantum Hall bilayers, Phys. Rev. B **79**, 125106 (2009).

[34] G. Möller, S. H. Simon, and E. H. Rezayi, Paired composite fermion phase of quantum Hall bilayers at $\nu = \frac{1}{2} + \frac{1}{2}$, Phys. Rev. Lett. **101**, 176803 (2008).

[35] S. H. Simon, E. H. Rezayi, and M. V. Milovanovic, Coexistence of composite bosons and composite fermions in $\nu = \frac{1}{2} + \frac{1}{2}$ quantum Hall bilayers, Phys. Rev. Lett. **91**, 046803 (2003).

[36] M. V. Milovanovic, E. Dobardzic, and Z. Papic, Meron deconfinement in the quantum Hall bilayer at intermediate distances, Phys. Rev. B **92**, 195311 (2015).

[37] J. Ye, Fractional charges and quantum phase transitions in imbalanced bilayer quantum Hall systems, Phys. Rev. Lett. **97**, 236803 (2006).

[38] J. Ye and L. Jiang, Quantum phase transitions in bilayer quantum Hall systems at a total filling factor $\nu_T = 1$, Phys. Rev. Lett. **98**, 236802 (2007).

[39] R. L. Doretto, C. Morais Smith, and A. O. Caldeira, Finite-momentum condensate of magnetic excitons in a bilayer quantum Hall system, Phys. Rev. B **86**, 035326 (2012).

[40] R. L. Doretto, A. O. Caldeira, and C. M. Smith, Bosonization approach for bilayer quantum Hall systems at $\nu_T = 1$, Phys. Rev. Lett. **97**, 186401 (2006).

[41] B. I. Halperin, in *Fractional Quantum Hall Effects: New Developments*, edited by B. I. Halperin and J. K. Jain (World Scientific, Singapore, 2020), pp. 79–132.

[42] Z. Papic and M. V. Milovanovic, Quantum disordering of the 111 state and the compressible-incompressible transition in quantum Hall bilayer systems, Phys. Rev. B **75**, 195304 (2007).

[43] M. V. Milovanovic and Z. Papic, Nonperturbative approach to the quantum Hall bilayer, Phys. Rev. B **79**, 115319 (2009).

[44] M. V. Milovanovic, Paired states in half-filled Landau levels, Phys. Rev. B **95**, 235304 (2017).

[45] J. Alicea, O. I. Motrunich, G. Refael, and M. P. A. Fisher, Interlayer coherent composite Fermi liquid phase in quantum Hall bilayers, Phys. Rev. Lett. **103**, 256403 (2009).

[46] Y. Zhu, L. Fu, and D. N. Sheng, Numerical study of quantum Hall bilayers at total filling $\nu_T = 1$: A new phase at intermediate layer distances, Phys. Rev. Lett. **119**, 177601 (2017).

[47] N. E. Bonesteel, Compressible phase of a double-layer electron system with total Landau-level filling factor 1/2, Phys. Rev. B **48**, 11484(R) (1993).

[48] R. Cipri and N. E. Bonesteel, Gauge fluctuations and interlayer coherence in bilayer composite fermion metals, Phys. Rev. B **89**, 085109 (2014).

[49] I. Sodemann, I. Kimchi, C. Wang, and T. Senthil, Composite fermion duality for half-filled multicomponent Landau levels, Phys. Rev. B **95**, 085135 (2017).

[50] G. Wagner, D. X. Nguyen, S. H. Simon, and B. I. Halperin, s-Wave paired electron and Hole composite fermion trial state for quantum hall bilayers with $\nu = 1$, Phys. Rev. Lett. **127**, 246803 (2021).

[51] L. Rüegg, G. Chaudhary, and R.-J. Slager, Pairing of composite-electrons and composite-holes in $\nu_T = 1$ quantum Hall bilayers, arXiv:2303.10212.

[52] J. K. Jain, Composite-fermion approach for the fractional quantum Hall effect, Phys. Rev. Lett. **63**, 199 (1989).

[53] J. K. Jain, *Composite Fermions* (Cambridge University Press, Cambridge, UK, 2007).

[54] O. Heinonen, ed., *Composite Fermions: A Unified View of the Quantum Hall Regime* (World Scientific, Singapore, 1998).

[55] N. Read, Theory of the half-filled Landau level, Semicond. Sci. Technol. **9**, 1859 (1994).

[56] N. Read, Recent progress in the theory of composite fermions near even-denominator filling factors, Surf. Sci. **361-362**, 7 (1996).

[57] E. Rezayi and N. Read, Fermi-liquid-like state in a half-filled Landau level, Phys. Rev. Lett. **72**, 900 (1994).

[58] D. T. Son, Is the composite fermion a Dirac particle? Phys. Rev. X **5**, 031027 (2015).

[59] S. Predin, A. Knežević, and M. V. Milovanović, Dipole representation of half-filled Landau level, Phys. Rev. B **107**, 155132 (2023).

[60] V. Pasquier and F. D. M. Haldane, A dipole interpretation of the $\nu = 1/2$ state, Nucl. Phys. B **516**, 719 (1998).

[61] N. Read, Lowest-Landau-level theory of the quantum Hall effect: The Fermi-liquid-like state of bosons at filling factor one, Phys. Rev. B **58**, 16262 (1998).

[62] Z. Dong and T. Senthil, Noncommutative field theory and composite Fermi liquids in some quantum Hall systems, Phys. Rev. B **102**, 205126 (2020).

[63] G. Murthy and R. Shankar, Hamiltonian theories of the fractional quantum Hall effect, Rev. Mod. Phys. **75**, 1101 (2003).

[64] For example, the wave function of the phase in Ref. [50] has the characteristic topological number shift equal to one. If we relate CFs and CHs to the components of the Dirac PH symmetric description of the layers, as argued in Ref. [66], then the *s*-wave pairing of CFs and CHs of Ref. [50], on the level of of the Dirac's eigenstates corresponds to the *p*-wave pairing (of opposite chirality with respect to the one given by the external field) of effective, low-energy fermions of two layers [44], and thus we expect such a shift. Similarly, in our picture, the intralayer description is related to an effective Majorana fermion theory [67] that leads to *p*-wave pairing as in the previous case. (Our dipoles are made of charges with a half unit of electron charge, and have a Dirac structure built in Ref. [68], but are one-component and thus Majorana fermions.) Therefore we expect the same shift.

[65] S. Simon, The Chern-Simons Fermi liquid description of fractional quantum Hall states, in *Composite Fermions: A Unified View of the Quantum Hall Regime*, edited by O. Heinonen (World Scientific, Singapore, 1998).

[66] D. Gočanin, S. Predin, M. D. Ćirić, V. Radovanović, and M. Milovanović, Microscopic derivation of Dirac composite fermion theory: Aspects of noncommutativity and pairing instabilities, Phys. Rev. B **104**, 115150 (2021).

[67] M. V. Milovanović (unpublished).

[68] C. Wang and T. Senthil, Half-filled Landau level, topological insulator surfaces, and three-dimensional quantum spin liquids, Phys. Rev. B **93**, 085110 (2016).

[69] F. D. M. Haldane, Incompressible quantum Hall fluids as electric quadrupole fluids, arXiv:2302.12472.

Dipole representation of half-filled Landau level

S. Predin,[1] A. Knežević,[2] and M. V. Milovanović[1]

[1]*Scientific Computing Laboratory, Center for the Study of Complex Systems, Institute of Physics Belgrade,*
University of Belgrade, Pregrevica 118, 11080 Belgrade, Serbia
[2]*Faculty of Physics, University of Belgrade, Studentski Trg 12-16, 11000 Belgrade, Serbia*

We introduce a variant of a dipole representation for composite fermions in a half-filled Landau level, taking into account the symmetry under an exchange of particles and holes. This is implemented by a special constraint on a composite fermion and a composite hole degree of freedom (of an enlarged space), which makes the resulting composite particle (dipole) a symmetric object. We study an effective Hamiltonian that commutes with the constraint on the physical space and fulfills the requirement for boost invariance on the Fermi level. The calculated Fermi liquid parameter F_2 is in good agreement with numerical investigations in Phys. Rev. Lett. **121**, 147601 (2018).

I. INTRODUCTION

The fractional quantum Hall effect (FQHE) is a phenomenon of strongly correlated electrons that is amenable to quasiparticle pictures and modeling. The presence of a strong magnetic field very often leads to dominance of the physics inside a Landau level (LL) (a subspace of the Hilbert space of the half-filled LL problem), and it justifies approaches that assume that the description of the problem can be confined to an isolated LL. The half-filled LL problem (relevant for systems at half-filling factors) is very interesting because it contains an additional symmetry that is not present in experiments or any other fillings of LLs, namely the symmetry of the exchange of particles (electrons) and holes, i.e., particle-hole (PH) symmetry. On the other hand, systems at half-filling contain physics that are specific for the FQHE, including the formation of a Fermi-liquid state of composite quasiparticles (fermions) that reside in the lowest LL (LLL) [1,2], and the incompressible half-integer filling factor, 5/2, for electrons in the second LL [3]. Moreover, it is widely believed that the physics at 5/2 is connected with a Cooper pairing of underlying quasiparticles that form so-called Pfaffian states [4]. The LL mixing (the influence of other LLs on the effective physics in the base LL) is very important for the physics of Pfaffian states because it selects and stabilizes a unique Pfaffian state among three possibilities: Pfaffian, anti-Pfaffian, and PH Pfaffian. On the other hand, the LL mixing is not that important for the physics of electrons in the LLL. Moreover, we are interested to know what will happen to the PH symmetry that is present if we assume that the Hilbert space of the system is an isolated LL. The state in the experiments may correspond to the spontaneous PH symmetry breaking state of a Hamiltonian that contains PH symmetry.

Even if we confine our description to the isolated LL, the problem at half-filling is still a strongly correlated one. Our hope is that by selecting appropriate quasiparticles, and by applying approximate methods (usually mean-field methods), we can arrive at an effective description of the system that is consistent with numerical and real experiments.

The Fermi liquid (FL) concept for the physics of composite quasiparticles, i.e., composite fermions, was introduced in the seminal work of Halperin, Lee, and Read (HLR) [1] on the basis of the Chern-Simons field-theoretical description, which does not include a projection to the LLL. To achieve a detailed description and understanding of the Fermi-liquid state inside the LLL, Pasquier and Haldane [5], and later Read [6], analyzed a related system of bosons at filling factor 1, with an exact representation of the composite fermion (CF) quasiparticles in an enlarged space of the half-filled LL problem. On the other hand, Shankar and Murthy [7] advanced a field-theoretical description of the dipole-CF representation of the problem [8]. In recent years, the concept of a Dirac, i.e., a two-component quasiparticle, was introduced by Son [9] for the description of the half-filled LL, i.e., a system that features PH symmetry. In Ref. [10], a microscopic derivation of such a theory was given in which the two components were connected to the two possibilities for quasiparticles, i.e., CFs and CHs (composite holes).

Here we propose an extension of the quasiparticle view of the physics inside an isolated LL based on a one-component fermion, namely a dipole. Our description does not distinguish between CFs and CHs. We employ the enlarged-space formalism [5–7], but with a special constraint that incorporates PH symmetry, in the system of electrons that fill half of an isolated LL. The special constraint and demand for the boost invariance defines an effective Hamiltonian and FL description, in agreement with numerical experiments [11].

The paper is organized as follows. In Sec. II, the enlarged-space formalism for the system of bosons at filling factor 1 is reviewed before the exposition of our proposal in the same section. At the end of the section, we discuss the FL description based on that proposal. In Sec. III, in order to further understand the nature of the introduced quasiparticles, the problem of the bilayer, i.e., two half-filled LLLs, is analyzed in the new representation. In Sec. IV, we discuss an additional implementation of our approach, i.e., a quantum Boltzmann equation based on the dipole picture that incorporates the

boost invariance and PH symmetry, and we end with conclusions. In Appendix A, the invariance under the change of basis, i.e., the SU(N) invariance for the proposed formalism, is described, and in Appendix B we provide details concerning the derivation of the quantum Boltzmann equation.

II. DIPOLE REPRESENTATION IN AN ISOLATED LANDAU LEVEL

We study an extension of the formalism for CFs that was developed in [5,6] for the case of bosons at filling factor 1 to the case of electrons in an isolated LL that is half-filled. Although an extension of the CF formalism to the case of half-filled LL of electrons has to incorporate *bosonic* correlation holes (i.e., artificial degrees of freedom in the setup), we will show that with a hard-core constraint in an enlarged space, we can delineate a physical subspace and reach a faithful description. In the following, we will review the basic formalism for the system of bosons at filling factor 1.

A. Bosons at filling factor $\nu = 1$

1. Review of the CF formalism for bosons at filling factor $\nu = 1$

In this section, we will briefly review the CF formalism that was introduced in [5] and further developed in [6] for bosons at filling factor $\nu = 1$. The CF is a composite quasiparticle of an underlying system of bosons (or electrons) that consists of a boson (an electron) and its (associated) correlation hole in the incompressible or weakly compressible (like the FL state of CFs) FQHE states. For the case of bosons at filling factor $\nu = 1$, we have one boson on average per state Ψ_n in an isolated LL, $n = 1, \ldots, N_\phi$. N_ϕ denotes the number of flux quanta through the system. Thus n enumerates states in a chosen basis of the relevant LL.

The Laughlin solution of the FQHE at $\nu = 1/3$ of electrons—an excellent description of the ground-state wave function, which incorporates basic correlations among particles that are solely interaction-driven in an isolated LL, motivates the introduction of the composite quasiparticles. In the regime of the FQHE, we can easily envision a structure of a neutral quasiparticle: an underlying boson (or an electron) and its associated correlation hole, which we can express and regard as (Laughlin) quasihole excitation (eigenstate) of the system with quantized charge and statistics [or nearly quantized and localized, almost an eigenstate in a weakly compressible systems (like the FL state of CFs)].

In the case of bosons at filling factor $\nu = 1$ of an isolated LL, and by following the Laughlin ansatz, we can easily find out that the most natural assignment for the statistics of the correlation hole is fermionic (so that the statistics of CFs is fermionic and counterbalances the Vandermonde determinant fermionic correlations, and produces overall bosonic correlations and wave functions), and that it represents a deficiency of a unit of charge (a hole). Thus we are inclined to consider a composite fermionic object (CF) and associate an annihilation operator with two indices m and n, c_{nm}, where n and m refer to two states of a chosen basis in a LL: the left index, n, describes the state of an (underlying, elementary) boson, and the right index, m, describes the state of its correlation hole—an artificial (additional) degree of freedom. In this way, we

are enlarging the space that we associate with the system's description; we introduce also creation operators, $c_{mn}^\dagger$, so that

$$\{c_{nm}, c_{m'n'}^\dagger\} = \delta_{n,n'}\delta_{m,m'}, \tag{1}$$

and we consider states in the enlarged space,

$$c_{mn}^\dagger \cdots c_{pq}^\dagger |0\rangle. \tag{2}$$

The physical subspace of this enlarged space can be delineated by projecting out artificial, nonphysical degrees of freedom, i.e., "vortices" (correlation holes), that possess fermionic statistics:

$$|n_1, \ldots, n_N\rangle = \sum_{m_1, \ldots, m_N}^{N_\phi} \varepsilon^{m_1 \cdots m_N} c_{m_1 n_1}^\dagger \cdots c_{m_N n_N}^\dagger |0\rangle, \tag{3}$$

where $\varepsilon^{m_1 \cdots m_N}$ is the Levi-Civita symbol.

We may notice that this construction is invariant under an SU(N) transformation, i.e., a change of basis in the LL in the R sector only, i.e.,

$$c_{mn}^\dagger \rightarrow \sum_{m'}^{N_\phi} U_{mm'} c_{m'n}^\dagger, \tag{4}$$

where $U_{mm'}$ is an SU(N) matrix. (The physical states are spin-singlets under this transformation.)

In the CF representation, one can consider $\rho_{mm'}^L$ and $\rho_{mm'}^R$, density operators for physical (L) and unphysical (holelike, R) degrees of freedom:

$$\rho_{nn'}^L = \sum_m c_{mn}^\dagger c_{n'm} \tag{5}$$

and

$$\rho_{mm'}^R = \sum_n c_{mn}^\dagger c_{nm'}. \tag{6}$$

Also the following decomposition [of the basic state (n, m) of the composite object] can be considered:

$$c_{nm} = \int \frac{d\boldsymbol{k}}{(2\pi)^{\frac{3}{2}}} \langle n|\tau_k|m\rangle c_k, \tag{7}$$

with $\tau_k = \exp(i\boldsymbol{k} \cdot \boldsymbol{R})$, where $\boldsymbol{R}$ is a guiding-center coordinate of a single particle in the external magnetic field,

$$[R_x, R_y] = -i. \tag{8}$$

We took l_B (magnetic length) $= 1$, and $\{|n\rangle\}$ are single-particle states (orbitals) in a fixed LL.

The parameter $\boldsymbol{k}$ denotes the momentum of the composite object, i.e., a CF. Physically, the state of the CF with vortex orbital m and electron orbital n can be described by a superposition of the (commutative) momentum $\boldsymbol{k}$ states, the weights of which depend on the effective distance between orbitals (the size of the dipole), $|\boldsymbol{k}_{\text{eff}}|$, because $\tau_k = \exp(i\boldsymbol{k} \cdot \boldsymbol{R})$ is the translation operator.

The introduced decomposition implies the following expressions for the L and R densities in the inverse space:

$$\rho_{nn'}^L = \sum_m c_{mn}^\dagger c_{n'm} = \int \frac{d\boldsymbol{q}}{2\pi} \langle n'|\tau_q|n\rangle \rho_q^L, \tag{9}$$

where

$$\rho_{\boldsymbol{q}}^L = \int \frac{d\boldsymbol{k}}{(2\pi)^2} c_{\boldsymbol{k}-\boldsymbol{q}}^\dagger c_{\boldsymbol{k}} \exp\left(i\frac{\boldsymbol{k}\times\boldsymbol{q}}{2}\right). \tag{10}$$

Note the inverse order of indices, n and n', on the left- and right-hand sides of (9). Similarly,

$$\rho_{mm'}^R = \sum_n c_{mn}^\dagger c_{nm'} = \int \frac{d\boldsymbol{q}}{2\pi} \langle m|\tau_{\boldsymbol{q}}|m'\rangle \rho_{\boldsymbol{q}}^R, \tag{11}$$

where

$$\rho_{\boldsymbol{q}}^R = \int \frac{d\boldsymbol{k}}{(2\pi)^2} c_{\boldsymbol{k}-\boldsymbol{q}}^\dagger c_{\boldsymbol{k}} \exp\left(-i\frac{\boldsymbol{k}\times\boldsymbol{q}}{2}\right). \tag{12}$$

The density $\rho_{\boldsymbol{q}}^L$ satisfies the GMP algebra,

$$\left[\rho_{\boldsymbol{q}}^L, \rho_{\boldsymbol{q}'}^L\right] = 2i\sin\left(\frac{\boldsymbol{q}\times\boldsymbol{q}'}{2}\right)\rho_{\boldsymbol{q}+\boldsymbol{q}'}^L, \tag{13}$$

while $\rho_{\boldsymbol{q}}^R$, as a density of "holes,"

$$\left[\rho_{\boldsymbol{q}}^R, \rho_{\boldsymbol{q}'}^R\right] = -2i\sin\left(\frac{\boldsymbol{q}\times\boldsymbol{q}'}{2}\right)\rho_{\boldsymbol{q}+\boldsymbol{q}'}^R, \tag{14}$$

i.e., GMP algebra for particles with opposite electric charge.

Thus we can realize the basic algebra of the electron density projected to a LL as an algebra of the same density expressed via operators that represent overall neutral objects (dipoles), i.e., CFs. We expect that the CF representation will capture the basic physics of the problem, and already at the mean-field level will give meaningful results (stable FL if we apply Hartree-Fock [6]).

2. Hamiltonian and constraints

The basic Hamiltonian in the second-quantized notation,

$$\mathcal{H} = \frac{1}{2}\sum_{m_1,\dots,m_4} V_{m_1,m_2;m_3,m_4} a_{m_1}^\dagger a_{m_2}^\dagger a_{m_4} a_{m_3}, \tag{15}$$

can be represented by the following Hamiltonian in CF representation [6]:

$$\mathcal{H} = \frac{1}{2}\sum_{\substack{m_1,\dots,m_4 \\ n_1,n_2}} V_{m_1,m_2;m_3,m_4} c_{n_1 m_1}^\dagger c_{n_2 m_2}^\dagger c_{m_4 n_2} c_{m_3 n_1}. \tag{16}$$

That this is possible can be seen because by mapping bilinear $a_p^\dagger a_q$ into $\sum_k c_{kp}^\dagger c_{qk}$, we are preserving the basic algebra of fermionic (electron) bilinears, but what may happen is that new (in the enlarged space) operators (including the Hamiltonian) can map physical states into superpositions of physical and unphysical states. Thus we have to ensure that physical states are mapped into physical (sub)space: the Hamiltonian has to commute with the constraint(s) (that determine the physical subspace of the enlarged space). From (3) we see that in this case the constraint that defines the physical space is $\rho_{nn}^R = 1$ and $[\mathcal{H}, \rho_{nn}^R] = 0$. In the inverse space [6],

$$\mathcal{H} = \frac{1}{2}\int \frac{d\boldsymbol{q}}{(2\pi)^2} \tilde{V}(|\boldsymbol{q}|) : \rho^L(\boldsymbol{q})\rho^L(-\boldsymbol{q}) :, \tag{17}$$

we have $[\rho_{\boldsymbol{q}}^L, \rho_{\boldsymbol{q}'}^R] = 0$, and thus $[\mathcal{H}, \rho_{\boldsymbol{q}}^R] = 0$, as required for the constraint $\rho_{\boldsymbol{q}}^R = 0$. In the following section, where we study electron systems at half-fillings, the constraints will not

be so simple, and we have to ensure the commutation with $\mathcal{H}$ at least in the physical subspace (with the help of constraints).

B. Electron system of (an isolated) half-filled Landau level

1. Physical states

In the case of the electron system at half-filling, the correlation hole, i.e., the superposition of two Laughlin quasihole constructions, if considered as an independent and well-defined degree of freedom, should carry bosonic statistics. This is a departure from the simple introduction of the unphysical degrees of freedom in the case of the bosonic system at filling factor 1. These degrees of freedom, in that case, carry fermionic statistics and are entering the description via the simple constraint $\rho_{nn}^R = 1$ that ensures easy implementation of the SU(N) invariance; we can transform the basis only in the R sector, and the physical state will be invariant with respect to that particular transformation. Thus, as expected and required, if we are transforming a physical state, we have a usual, unitary implementation of SU(N), and only L degrees of freedom are affected.

We may wonder if it is possible at all to implement the SU(N) invariance if we have bosonic unphysical (additional) degrees of freedom that enter the CF description. If we do not consider CFs and CHs (to account for the PH symmetry in a half-filled Landau level) and a Dirac-type theory [10], we can attempt a description that is similar to that in the bosonic $\nu = 1$ case by considering only CFs, more precisely single-particle operators with two indexes, c_{mn}, but only of one kind, and the following associated physical states (Slater determinants) in the enlarged space:

$$|\Psi_{\text{phy}}\rangle = |n_1,\dots,n_{N_\phi/2}\rangle = \sideset{}{'}\sum_{\sigma\in S_{N_\phi/2}} c_{\sigma(m_1)n_1}^\dagger \cdots c_{\sigma(m_{N_\phi/2})n_{N_\phi/2}}^\dagger |0\rangle, \tag{18}$$

where the prime over the sum means that the sum is over permutations of distinct states, $m_1 \neq m_2 \neq \cdots \neq m_{N_\phi/2}$, i.e., indexes connected with a basis in a LL: $\{|n_1\rangle, |n_2\rangle, \dots, |n_{N_\phi/2}\rangle, |m_1\rangle, |m_2\rangle, \dots, |m_{N_\phi/2}\rangle\}$. In (18) we have electrons that occupy states from subspace $V = \{|n_1\rangle, |n_2\rangle, \dots, |n_{N_\phi/2}\rangle\}$, i.e., half of the available states in a LL. The second half, $V_\perp = \{|m_1\rangle, |m_2\rangle, \dots, |m_{N_\phi/2}\rangle\}$ (states from the orthogonal subspace), are occupied by "hard-core" bosonic correlation holes.

We may consider both bosonic correlation holes and real (associated with a Chern band, i.e., an LL) fermionic holes. When we talk about PH symmetry, we refer to fermionic holes. But due to the implied constraint, in Eq. (18), on the density and occupation by correlation holes, their densities (occupation numbers) are constrained to be equal, and in that sense the PH symmetry (active exchange of electrons and real holes) can be associated with the exchange of L and R (correlation hole) in the Hamiltonian and constraint(s) that are expressed via densities.

In Appendix A we discuss how the SU(N) invariance can be implemented if one consider simultaneous transformation(s) on L and R; a transformation on only one type of index is nontrivial (nonunitary). In an isolated half-filled LL

we have PH symmetry, and in that case we may expect that the change of basis affects both L (particle) and R (hole), because of the intertwined physics of particles and (real) holes. This is unavoidable, and it is the only option we have both in the Dirac (manifestly invariant PH symmetric with CFs and CHs) or CF-only representation and the description of the problem discussed here.

2. Hamiltonian and constraints

The realization of the SU(N) symmetry and the quasiparticle description relies on the requirement that

$$\rho_{nn}^L + \rho_{nn}^R = 1, \qquad (19)$$

i.e., the hard-core constraint that we introduced at the beginning of the subsection in the description of the basic physical states (18). The constraint is part of the formulation of the problem; it specifies the half-filling condition. What is special with respect to the previous introduction of the additional degrees of freedom that should represent correlation holes is that here correlation holes describe hole degrees of freedom of the half-filled problem. In that sense, our approach can be considered as only effective, not microscopic, considering how the quasiparticle description is introduced (with respect to the bosonic case at $\nu = 1$). But once the constraint is assumed, we can build our description, i.e., an effective Hamiltonian, by requiring that the Hamiltonian commutes with the constraint, as we will describe shortly. On the other hand, there are reasons why such a constraint is appropriate. First, it includes particle and hole degrees of freedom (CFs and CHs) in such a way that the PH symmetry is accounted for. Second, it leads to a PH symmetric form of the Hamiltonian, which is known as a dipole representation of the underlying quasiparticle physics introduced by Shankar and Murthy, but with an additional factor of 4 that reduces the strength of the Coulomb interaction. That factor is likely the one that was missing in the interpretation of surface acoustic wave experiments by the HLR theory and the dipole-based theory [8]. An additional and important reason for the form of the constraint, as we will show in the following, is that the constraint can be used to obtain a final form of the Hamiltonian that features the boost invariance. The boost invariance should characterize an effective description at least at the Fermi level as an invariance in the system that does not have (bare) mass (i.e., a kinetic term) in its microscopic description. As we will show, the calculated Fermi liquid parameter, F_2, on the basis of that Hamiltonian and constraint, is in very good agreement with the numerical experiment of Ref. [11].

To get the form of the Hamiltonian that satisfies these requirements, we start with the microscopic form of the Hamiltonian [the same as for bosons in (17)] where we abandon the requirement for normal ordering and make the following substitution:

$$\rho^L(\boldsymbol{q}) \to \frac{\rho^L(\boldsymbol{q}) - \rho^R(\boldsymbol{q})}{2}. \qquad (20)$$

Therefore,

$$H = \frac{1}{8} \int \frac{d\boldsymbol{q}}{(2\pi)^2} \tilde{V}(|\boldsymbol{q}|)[\rho^L(-\boldsymbol{q}) \\ - \rho^R(-\boldsymbol{q})][\rho^L(\boldsymbol{q}) - \rho^R(\boldsymbol{q})]. \quad (21)$$

Here $\tilde{V}(|\boldsymbol{q}|) = \frac{1}{|\boldsymbol{q}|} \exp(-\frac{|\boldsymbol{k}|^2}{2})[L_n(\frac{|\boldsymbol{k}|^2}{2})]^2$, where L_n represents the Laguerre polynomial for a fixed LL index n. Thus we modified the Hamiltonian in the particle representation to the one that features PH symmetry in such a way that the exchange $\rho^L(\boldsymbol{q}) \leftrightarrow \rho^R(\boldsymbol{q})$ does not change the form of the Hamiltonian. Also,

$$[H, [\rho^L(\boldsymbol{q}) + \rho^R(\boldsymbol{q})]]|_{[\rho^L(\boldsymbol{k}) + \rho^R(\boldsymbol{k})] = 0} = 0, \qquad (22)$$

i.e., the constraint commutes with the Hamiltonian in the physical space, as required.

The Hamiltonian in (21) possesses a single-particle term, H_1 [12],

$$H = H_1 + : H :, \qquad (23)$$

next to the purely interacting term, $: H :$. If we interpret the mass in H_1 at k_F as the effective mass, m^*, of a FL description, we need an additional interaction, a term next to the bare one, i.e., $: H :$ in order to achieve (a) the FL description of the system, and (b) the description that is also invariant under boosts, i.e., whose Hamiltonian is purely interacting at the Fermi level. We will come back to these requirements with more explanations below the final form of the Hamiltonian in Eq. (27).

To implement this, we may add a term that needs to represent an interaction, but at the same time be equal to zero in the physical space (not to add or spoil energetics encoded in H based on the bare, Coulomb interaction). In the inverse space, that term may be of the following form:

$$\int \frac{d\boldsymbol{q}}{(2\pi)^2} C(|\boldsymbol{q}|) \exp\left(-\frac{\boldsymbol{q}^2}{2}\right) \left[L_n\left(\frac{\boldsymbol{q}^2}{2}\right)\right]^2 \\ \times [\rho^L(-\boldsymbol{q}) + \rho^R(-\boldsymbol{q})][\rho^L(\boldsymbol{q}) + \rho^R(\boldsymbol{q})]. \quad (24)$$

On the other hand, in the space of the LL orbitals, we may consider the following term:

$$\sum_{n,n'} \delta_{n,n'} (\rho_{nn}^L + \rho_{nn}^R)(\rho_{n'n'}^L + \rho_{n'n'}^R), \qquad (25)$$

based on the constraint expressed on the space of orbitals $\{|n\rangle\}$, which is not zero but, due to the constraint, simply a constant in the physical space, i.e., a constant equal to the number of orbitals. By comparing two expressions that constrain the form of the required interaction term, we can conclude that $C(|\boldsymbol{q}|)$ in (24) should be a constant, independent of $\boldsymbol{q}$. Namely, if we regularize the expression in (25) in the thermodynamic limit by omitting the terms that do not conserve momentum in the inverse space, and may represent local single-particle potentials, we find that the remaining term that represents an interaction invariant under translation is

$$H_C = C \int \frac{d\boldsymbol{q}}{(2\pi)^2} \exp\left(-\frac{\boldsymbol{q}^2}{2}\right) \left[L_n\left(\frac{\boldsymbol{q}^2}{2}\right)\right]^2 \\ \times [\rho^L(-\boldsymbol{q}) + \rho^R(-\boldsymbol{q})][\rho^L(\boldsymbol{q}) + \rho^R(\boldsymbol{q})], \quad (26)$$

i.e., a δ-function interaction projected into an isolated LL. This term is equal to zero in the physical space.

The complete Hamiltonian that describes the low-energy physics at the Fermi level and incorporates the boost

invariance is

$$\mathcal{H}_C = H + H_C, \tag{27}$$

where the constant C is chosen such that the second derivative with respect to momentum of the total single-particle dispersion in the single-particle term of $\mathcal{H}_C$ at the Fermi level is equal to zero.

In short, the FL assumption and assertion is that the effective physics can be expressed via quasiparticle excitations near the Fermi surface with energy,

$$\tilde{\epsilon}(\boldsymbol{p}) = \frac{\boldsymbol{p}^2}{2m^*} + \int \frac{d\boldsymbol{p}'}{(2\pi)^2} f(\boldsymbol{p}, \boldsymbol{p}') n(\boldsymbol{p}'), \tag{28}$$

where m^* is the effective quasiparticle mass, f is the effective interaction among quasiparticles, and $n(\boldsymbol{p})$ is the occupation number at momentum $\boldsymbol{p}$ of quasiparticles. To identify f in the scope of our approximation, we will consider for f the interaction based on the Fock approximation and approach to $\mathcal{H}_C$ (which will coincide with the bare interaction). Furthermore, as usual in the FL description, we are concerned with excitations near the Fermi surface, and we assume that f is only a function of the directions of $\boldsymbol{p}$ and $\boldsymbol{p}'$. Thus we consider FL parameters,

$$F_l = \frac{m^* f_l}{2\pi}, \tag{29}$$

where

$$f_l = \frac{1}{2\pi} \int_0^{2\pi} d\theta \, f(\theta) \exp(il\theta). \tag{30}$$

The very important aspect of the FL description is the connection between the bare mass of underlying particles $m_b \equiv m_e$ and the quasiparticle description. We may use the Galilean invariance under boost by momentum $\boldsymbol{q}$, which induces the change in the energy density equal to $n_e \frac{|\boldsymbol{q}|^2}{2m_b}$, and we equate this energy to that implied by the FL description, to obtain (see, for example, [8])

$$\frac{1}{m_b} = \frac{1}{m^*} + \frac{f_1}{2\pi}. \tag{31}$$

Thus, in a FL description, to have a consistent theory, we need to have a special (additional) interaction defined by f_1 that will compensate for the renormalization of the mass by interaction (from m_b to m^*) in order to reach a quasiparticle picture. Furthermore, in our case, in the microscopic underlying (electron) description, there is no single-particle term (and bare mass m_b) in the solely interacting (microscopic) Hamiltonian defined inside a LL. To ensure the boost invariance in the purely interacting theory, we need

$$0 = \frac{1}{m^*} + \frac{f_1}{2\pi} \quad (\text{i.e., } F_1 = -1). \tag{32}$$

Thus the mass m^* is expressed and defined solely by the Landau interaction (parameter). Concretely, in our case, the introduced H_C is necessary to complete the effective FL description near the Fermi surface. It plays the role of f_1, an extra, necessary interaction. As already emphasized, it also (by a definite value of constant C) eliminates the (total) mass term at the Fermi level in the Fock approximation. Thus, in
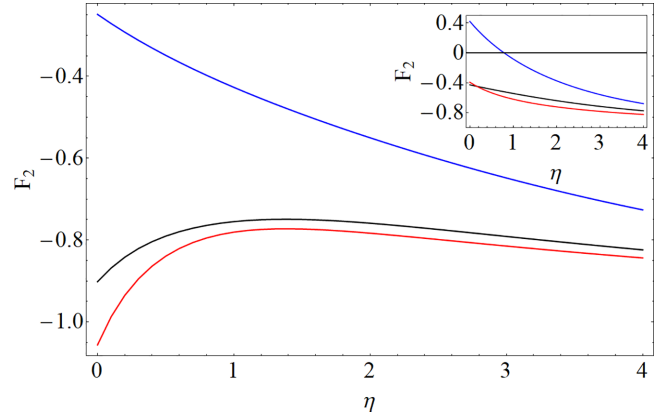

FIG. 1. Fermi liquid parameter F_2 as defined in Eq. (34) with (35), in the case of the LLL (blue), the second LL (black), and the third LL (red). The inset shows the calculated values for F_2 if the interaction with C_η is absent in (35).

our case, the Landau interaction f is given in the Fock approximation by the interaction defined by the normal ordering of $\mathcal{H}_C$ for the interacting particles at the Fermi level.

To probe the FL description implied by $\mathcal{H}_C$, we consider a generalized Coulomb interaction [11],

$$V_\eta(q) = \frac{1}{|\boldsymbol{q}|} \exp(-|\boldsymbol{q}|\eta), \tag{33}$$

which models the effect of the finite thickness of samples in experiments, but also stabilizes FL behavior [11]. The calculated F_2—the FL parameter at angular momentum $l = 2$—on the basis of the effective Hamiltonian $\mathcal{H}_C$ (in the Fock approximation) is given in Fig. 1. We calculated

$$F_2 = -\frac{\int d\theta \cos(2\theta) f(\theta)}{\int d\theta \cos(\theta) f(\theta)}, \tag{34}$$

where $f(\theta)$ is defined by the total interaction at $\boldsymbol{q} = \boldsymbol{p} - \boldsymbol{p}'$, for which $|\boldsymbol{p}| = |\boldsymbol{p}'| = k_F = 1$, $\boldsymbol{p}' = \hat{e}_x$, $\boldsymbol{p} \cdot \boldsymbol{p}' = \cos(\theta)$, and thus $|\boldsymbol{q}| = 2|\sin(\frac{\theta}{2})|$ with

$$f(\theta) = \left[V_\eta(|\boldsymbol{q}|) \sin^2\left(\frac{\sin(\theta)}{2}\right) + 8C_\eta \cos^2\left(\frac{\cos(\theta)}{2}\right) \right]$$
$$\times \exp\left(-\frac{\boldsymbol{q}^2}{2}\right) \left[L_n\left(\frac{\boldsymbol{q}^2}{2}\right) \right]^2, \tag{35}$$

where C_η is the value of C at a particular η necessary to eliminate the mass term at k_F. The calculated F_2 (Fig. 1) is in an agreement with the trends of the numerical experiment of Ref. [11]; it predicts the absence and presence of the Pomeranchuk instability in the LLL and third LL, respectively, for the pure Coulomb interaction, as in Ref. [11], but it does not predict one in the second LL, which exists according to the analysis in [11]. In the inset of Fig. 1, the values of F_2 are given for the usual Hamiltonian H in the dipole representation, in the absence of the single-particle term, i.e., for $:H:$. We can see that they differ considerably from the expectations based on $\mathcal{H}_C$ and the results of the numerical experiment in [11]; the inclusion of the C-interaction together with the requirement for boost invariance is essential to get an agreement with the
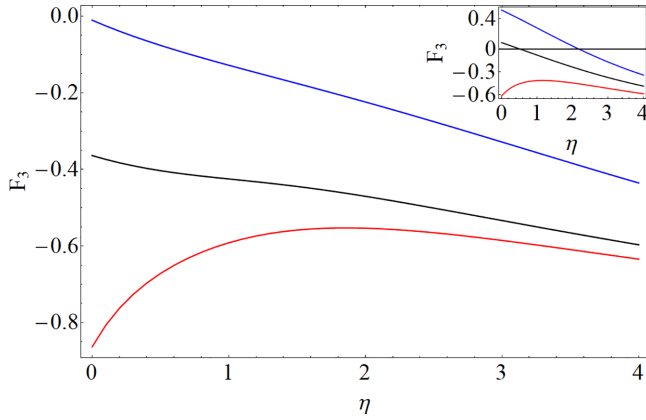
FIG. 2. Fermi liquid parameter F_3 as defined in Eq. (34) with (35), in the case of the LLL (blue), the second LL (black), and the third LL (red). The inset shows the calculated values for F_3 if the interaction with C_η is absent in (35).

results of Ref. [11]. In Figs. 2 and 3 we present the values of Fermi liquid parameters, F_3 and F_4.

III. THE BILAYER CASE: PAIRING BETWEEN TWO LLLs

To get a better understanding of the underlying quasiparticle—a dipole in the new representation—we consider the quantum bilayer problem, i.e., the problem with two half-filled LLLs. The bilayer consists of two layers. Each layer represents a half-filled LLL, but with no PH symmetry, because of the interlayer interaction. The two-component physics can be represented inside a single LLL by the following Hamiltonian with electron density operators, $\rho_\sigma(\boldsymbol{q})$, $\sigma = \uparrow, \downarrow$:

$$\mathcal{H}_e = \int \frac{d\boldsymbol{q}}{(2\pi)^2} \left\{ \sum_\sigma \frac{1}{2} V(|\boldsymbol{q}|) : \rho_\sigma(\boldsymbol{q}) \, \rho_\sigma(-\boldsymbol{q}) : \right.$$
$$\left. + V_{\uparrow\downarrow}(|\boldsymbol{q}|) \, \rho_\uparrow(\boldsymbol{q}) \, \rho_\downarrow(-\boldsymbol{q}) \right\}. \quad (36)$$
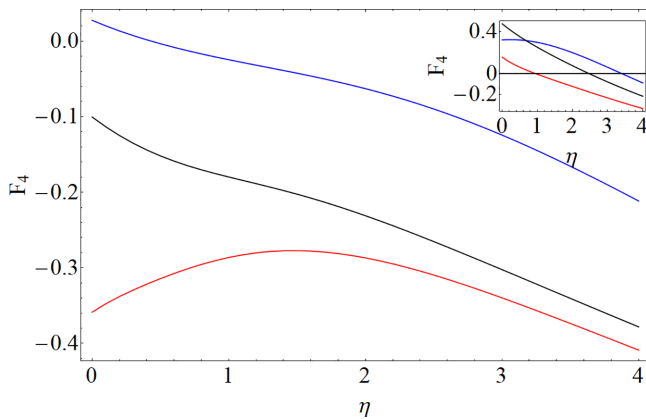

FIG. 3. Fermi liquid parameter F_4 as defined in Eq. (34) with (35), in the case of the LLL (blue), the second LL (black), and the third LL (red). The inset shows the calculated values for F_4 if the interaction with C_η is absent in (35).

We begin the description of the system in the new representation with the following Hamiltonian:

$$\mathcal{H} = \int \frac{d\boldsymbol{q}}{(2\pi)^2} \left\{ \sum_\sigma \frac{1}{8} V(|\boldsymbol{q}|) [\rho_\sigma^L(-\boldsymbol{q}) - \rho_\sigma^R(-\boldsymbol{q})] \right.$$
$$\times [\rho_\sigma^L(\boldsymbol{q}) - \rho_\sigma^R(\boldsymbol{q})]$$
$$\left. + \frac{V_{\uparrow\downarrow}(|\boldsymbol{q}|)}{4} [\rho_\uparrow^L(-\boldsymbol{q}) - \rho_\uparrow^R(-\boldsymbol{q})][\rho_\downarrow^L(\boldsymbol{q}) - \rho_\downarrow^R(\boldsymbol{q})] \right\},$$
$$(37)$$

with constraints $[\rho_\sigma^L(\boldsymbol{k}) + \rho_\sigma^R(\boldsymbol{k})] = 0; \sigma = \uparrow, \downarrow$.

We chose the form of the Hamiltonian as the one that will conform to the requirements, $[\mathcal{H}, [\rho_\sigma^L(\boldsymbol{q}) + \rho_\sigma^R(\boldsymbol{q})]] = 0; \sigma = \uparrow, \downarrow$, that hold if the constraints $[\rho_\sigma^L(\boldsymbol{k}) + \rho_\sigma^R(\boldsymbol{k})] = 0; \sigma = \uparrow, \downarrow$ are applied. The constraints define physical spaces in two layers, and they also constrain the form of the Hamiltonian in the description with enlarged space(s). Just as in the single-layer case, we can add the terms that are zero on the physical space of the form of H_C in each layer to ensure the boost invariance of the system at the Fermi level. Our main interest is the effect of the interlayer interaction. To get a transparent representation of the underlying physics, within the physical space, we can add effectively zero terms, and transform the operators that define the interlayer interaction in the following way:

$$[\rho_\uparrow^L(-\boldsymbol{q}) - \rho_\uparrow^R(-\boldsymbol{q})][\rho_\downarrow^L(\boldsymbol{q}) - \rho_\downarrow^R(\boldsymbol{q})]$$
$$- [\rho_\uparrow^L(-\boldsymbol{q}) + \rho_\uparrow^R(-\boldsymbol{q})][\rho_\downarrow^L(\boldsymbol{q}) + \rho_\downarrow^R(\boldsymbol{q})]$$
$$= -2[\rho_\uparrow^L(-\boldsymbol{q}) \, \rho_\downarrow^R(\boldsymbol{q}) + \rho_\uparrow^R(-\boldsymbol{q}) \, \rho_\downarrow^L(\boldsymbol{q})]. \quad (38)$$

Now the effective form of the interlayer interaction represents a view of the underlying physics: excitonic binding of electrons and holes, i.e., CFs and CHs as emphasized in the recent work in Ref. [13], which we know is a completely justified view of the physics at small distances. But here we have only one effectively neutral quasiparticle operator "c" which is CF and CH at the same time—a simple dipole; the excitonic pairing that is implied by (38) is effectively Cooper pairing of the underlying quasiparticles "c" from each layer. Indeed, in the BCS mean-field treatment, we have an obvious instability described by the order parameter $\Delta_{\boldsymbol{k}}$,

$$\Delta_{\boldsymbol{k}} = \int \frac{d\boldsymbol{q}}{(2\pi)^2} V_{\uparrow\downarrow}(|\boldsymbol{q} - \boldsymbol{k}|) \frac{\Delta_{\boldsymbol{q}}}{2E_{\boldsymbol{q}}}, \quad (39)$$

where

$$V_{\uparrow\downarrow}(q) = \frac{\exp(-qd)}{q} \exp\left(-\frac{q^2}{2}\right), \quad (40)$$

and $E_{\boldsymbol{q}}$ is the Bogoliubov quasiparticle energy, defined considering the complete Hamiltonian that contains the boost invariance, and d is the distance between the layers.

In Fig. 4, solutions for $\Delta_{\boldsymbol{k}}$ at $k = k_F$ for s, p, and d waves are plotted as a function of distance. For a large interval of d, the results are in qualitative agreement with the most recent numerical results of Ref. [13], done on the sphere, when we identify CF-CH (excitonic) pairing of the same reference with the s-wave Cooper pairing of dipoles in the representation that we presented here. Nevertheless, a question can be raised
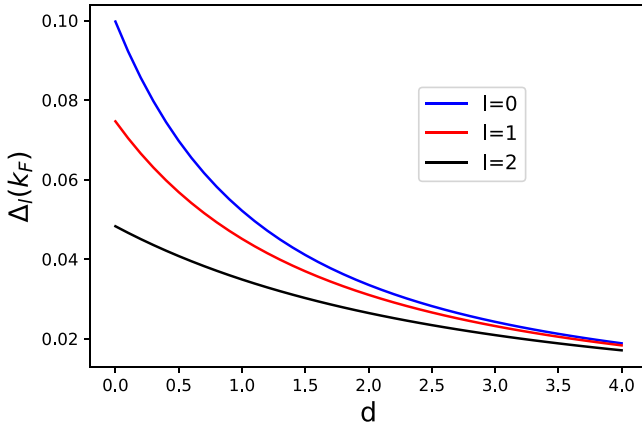
FIG. 4. The solutions for Δ_k calculated self-consistently using (39), in the case of s (blue), p (red), and d (black) wave at $k = k_F$.

whether for larger (or even intermediate, $d \sim l_B$) distances, an effective description given by the Hamiltonian in (37) is more appropriate, because at very large distances we expect two decoupled Fermi liquids, for which a dipole representation, with dipole densities $\rho_\sigma^L(\boldsymbol{q}) - \rho_\sigma^R(\boldsymbol{q})$, $\sigma = \uparrow, \downarrow$ that are interacting, seems quite appropriate (according to our reasoning and comments in Sec. II B). Then the mean-field solutions $\Delta_{\boldsymbol{k}}^s$ for the dominant s-wave excitonic instability, for this setup, will necessarily behave near $k = 0$ as $\Delta_{\boldsymbol{k}}^s \sim |\boldsymbol{k}|^2$, and thus they will exemplify an anomalous behavior and may lead to the prediction of a new (intermediate) phase detected in numerical experiments on a torus [14,15].

IV. DISCUSSION AND CONCLUSIONS

To further gauge the FL nature of our system (in the proposed formalism), we can consider the quantum Boltzmann equation for the Wigner function,

$$\nu(\boldsymbol{k}, \boldsymbol{r}) = \int d\boldsymbol{s} \exp{(i\boldsymbol{k}\boldsymbol{s})} \text{Tr}\left\{ \rho \Psi^\dagger \left(\boldsymbol{r} + \frac{\boldsymbol{s}}{2} \right) \Psi \left(\boldsymbol{r} - \frac{\boldsymbol{s}}{2} \right) \right\},$$
(41)

where ρ is the density matrix of the system, and Ψ, $\Psi^\dagger$ are second-quantized operators that are defined, in the long-distance approximation (in the usual way) on the space of commuting coordinates, as

$$\Psi(\boldsymbol{x}) = \int \frac{d\boldsymbol{k}}{(2\pi)^2} \exp{(i\boldsymbol{k}\boldsymbol{x})} c_k,$$

$$\Psi^\dagger(\boldsymbol{x}) = \int \frac{d\boldsymbol{k}}{(2\pi)^2} \exp{(-i\boldsymbol{k}\boldsymbol{x})} c_k^\dagger.$$
(42)

Applying $i\frac{\partial \rho}{\partial t} = [\mathcal{H}_C, \rho]$, i.e., the von Neumann equation, we arrive at the following equation for $\nu(\boldsymbol{k}, \boldsymbol{r})$:

$$i\frac{\partial \nu(\boldsymbol{k}, \boldsymbol{r})}{\partial t} = \int d\boldsymbol{s} \exp{(i\boldsymbol{k}\boldsymbol{s})} \text{Tr}\left\{ \rho \left[\Psi^\dagger \left(\boldsymbol{r} + \frac{\boldsymbol{s}}{2} \right) \Psi \right. \right.$$
$$\left. \left. \times \left(\boldsymbol{r} - \frac{\boldsymbol{s}}{2} \right), \mathcal{H}_C \right] \right\}.$$
(43)

By considering shifts in $\boldsymbol{r}$ in single-particle correlators to linear order, we can derive an effective expression presented in Appendix B. Only in the small-momentum limit, i.e., the

limit in which the change of momentum (that couples with the $\boldsymbol{r}$ coordinate) is small, does the expression take the form of the usual quantum Boltzmann equation for a description of a FL with a boost invariance,

$$\frac{\partial \nu}{\partial t} + \partial_r \nu \partial_k \epsilon - \partial_k \nu \partial_r \epsilon$$
$$= \text{additional (negligible insmall-momentum transfer)}$$
$$\text{terms.}$$
(44)

Here

$$\epsilon = -\int d\boldsymbol{q} \exp\left(-\frac{\boldsymbol{q}^2}{2} \right) \left(\frac{V(\boldsymbol{q})}{4} - 2C \right) (\boldsymbol{q} \times \boldsymbol{k})^2 \nu(\boldsymbol{k} + \boldsymbol{q}),$$
(45)

i.e., the Fock contribution to the quasiparticle dispersion that also includes the C-interaction contribution, i.e., the interaction defined in (26). The C-interaction ensured that no term with a finite mass $(= \frac{1}{M} \boldsymbol{k} \nabla_r \nu)$ appears in the quantum Boltzmann equation and on the Fermi level to the order that was considered. Overall, the description based on the dipole representation is in accordance with Ref. [16] and the quantum Boltzmann equation for CFs in the absence of the projection to a LL (based on the Chern-Simons field-theoretical approach), if we associate the processes behind smooth variations of the Fermi surface with small-momentum transfer variations in the dipole representation that lead to FL behavior. We leave a detailed comparison and analysis of the quantum Boltzmann equation for future work.

Thus the C-interaction ensures the boost invariance even if we go beyond the ordinary (Hartree)-Fock mean-field approach. Our description incorporates also the PH symmetry, and it does not contain a potential bias to CFs like the use of the Rezayi-Read state [17] in [11]. Thus the discrepancy between our prediction for the absence of the Pomeranchuk instability in the second LL with respect to Ref. [11] may come from the explicit PH symmetry breaking in their analysis. The PH symmetry breaking can be associated with LL mixing, which may drive the Pomeranchuk instability and also stabilize p-wave at larger distances in the bilayer system.

Our proposal maintains the PH symmetry with the application of the constraint in (19). At the same time, it places correlation holes in the place of real holes, which seems to be an unusual circumstance—correlation holes should bind to particles (or vice versa). But this is a reflection of the effective physics at the Fermi level where particles are shifted from their correlation holes by an amount proportional to $k_F l_B^2 = l_B$, i.e., on the order of the average distance between LL orbitals. This is an important consequence of the projection to a fixed LL of the Fermi sea correlations among quasiparticles [17].

Therefore, our proposal takes into account the requirements for the boost invariance and PH symmetry in the theory that captures the effective physics at the Fermi level of dipole quasiparticles.

APPENDIX A: THE SU(N) INVARIANCE IN THE HALF-FILLED CASE

In this Appendix, we will discuss the action of the SU(N) symmetry in the theory for the half-filled LL. The symmetry must exist, but, as we will describe, not as an independent transformation on L and R indexes. An arbitrary, fixed SU(N) transformation on one type of index only is not unitary. However, we show that, in principle, we can complete a transformation, defined by the same SU(N) matrix on the other index, and after a projection to the physical space we can reach a unitary realization of the SU(N) symmetry. In describing this action, we want to show how the transformations on both sectors, i.e., the indexes, are intertwined, and we provide a description of the unitary realization of the SU(N) symmetry on the physical space described by Eq. (A9). On the other hand, we can regard (A9) as an expected, natural (unitary) realization of the SU(N) symmetry on the space defined by Eq. (18), in which only one set of indexes (L or R) is independent and defines the other.

We may ask, "How can the SU(N) invariance be implemented on the states defined in Eq. (18)?" First, let us consider an artificial but instructive problem of electrons at $\nu = 1$ in a CF representation. The unique physical state can be defined in an enlarged space by a trace on bosonic, artificial degrees of freedom,

$$|\Psi_{\text{phy}}\rangle^{\nu=1} = \sum_{\sigma \in S_{N_\phi}}' c^\dagger_{\sigma(m_1)n_1} \cdots c^\dagger_{\sigma(m_{N_\phi})n_{N_\phi}} |0\rangle, \qquad \text{(A1)}$$

and $m_1 \neq m_2 \neq \cdots \neq m_{N_\phi}$. Thus bosonic (artificial) degrees of freedom enter as hard-core bosons into the description. The requirement is a necessary condition for the implementation of the SU(N) invariance, and it reflects a physical expectation that correlation holes for a fermionic system should not overlap. Namely, by introducing

$$c^\dagger_{mn} \rightarrow \sum_{m'} U_{mm'} c^\dagger_{m'n}, \qquad \text{(A2)}$$

we may notice that under the hard-core constraint, the SU(N) transformation in the R sector will act locally, i.e., it will induce the permanent number of the SU(N) matrix that will be multiplied by the same state:

$$\hat{g}^R |\Psi_{\text{phy}}\rangle^{\nu=1} = \Lambda(g)|\Psi_{\text{phy}}\rangle^{\nu=1}. \qquad \text{(A3)}$$

The SU(N) invariance exists if its action is unitary under simultaneous transformations in the R and L sectors. Thus by allowing a nonunitary (in general) action on L degrees of freedom,

$$\hat{g}^L |\Psi_{\text{phy}}\rangle^{\nu=1} = \frac{1}{\Lambda(g)}|\Psi_{\text{phy}}\rangle^{\nu=1}, \qquad \text{(A4)}$$

we can reach the invariance:

$$\hat{g}_{\text{SU}(N)}|\Psi_{\text{phy}}\rangle^{\nu=1} = \hat{g}^L \hat{g}^R |\Psi_{\text{phy}}\rangle^{\nu=1} = |\Psi_{\text{phy}}\rangle^{\nu=1}. \qquad \text{(A5)}$$

The previous case is artificial and of no physical importance, but it suggests how the SU(N) invariance can be accommodated in the system of interest, namely a half-filled LL of electrons (if we first apply an independent transformation on the indexes on one of the sectors). We may begin with the usual transformation on R indexes as in (A2). As a result of the hard-core constraint among holes, we have

$$|\Psi_{\text{phy}}\rangle^R = \sum_{\{m'_1 \neq m'_2 \neq \cdots \neq m'_{N_\phi/2}\}} \sum_{\sigma \in S_{N_\phi/2}}$$
$$\times \left[\sum_{p \in S_{N_\phi/2}}' U^{p(m_1)\sigma(m'_1)} \cdots U^{p(m_{N_\phi/2})\sigma(m'_{N_\phi/2})} \right]$$
$$\times c^\dagger_{\sigma(m'_1)n_1} \cdots c^\dagger_{\sigma(m'_{N_\phi/2})n_{N_\phi/2}} |0\rangle, \qquad \text{(A6)}$$

where the first sum is over all possible distinct collections of $N_\phi/2$ numbers, i.e., basis vectors. We can denote the number in square brackets by $[\cdots] = \Lambda(\{m'_i\}) = K(\{n'_i\})$, where $\{n'_i\}$ denote basis states from the subspace orthogonal to the one spanned by $\{m'_i\}$. ($|\Psi_{\text{phy}}\rangle$ is defined by the set of $\{n_i\}$'s [or $\{m_i\}$'s; see Eq. (18)] and they fix Λ's.) The number $\Lambda(\{m'_i\})$ is symmetric under permutations of $\{m'_i\}$ and can be pulled out of the sum over σ permutations. Thus

$$\hat{g}^R |\Psi_{\text{phy}}\rangle \equiv |\Psi_{\text{phy}}\rangle^R$$
$$= \sum_{\{m'_1 \neq m'_2 \neq \cdots \neq m'_{N_\phi/2}\}} \Lambda(\{m'_i\})$$
$$\times \sum_{\sigma \in S_{N_\phi/2}} c^\dagger_{\sigma(m'_1)n_1} \cdots c^\dagger_{\sigma(m'_{N_\phi/2})n_{N_\phi/2}} |0\rangle, \qquad \text{(A7)}$$

where the resulting state may not be in the physical space, which is spanned by vectors in Eq. (18). Now if we define an SU(N) transformation on the L indexes, in such a way that for each term $\{n_i\} \rightarrow \{n'_i\}$ in the generated expansion we divide by $K(\{n'_i\})$, i.e.,

$$\hat{g}^L |\Psi_{\text{phy}}\rangle \equiv |\Psi_{\text{phy}}\rangle^L$$
$$= \sum_{\{n'_1 \neq n'_2 \neq \cdots \neq n'_{N_\phi/2}\}} \frac{1}{K(\{n'_i\})} U^{n'_1 n_1} \cdots U^{n'_{N_\phi/2} n_{N_\phi/2}}$$
$$\times \sum_{\sigma \in S_{N_\phi/2}} c^\dagger_{\sigma(m_1)n'_1} \cdots c^\dagger_{\sigma(m_{N_\phi/2})n'_{N_\phi/2}} |0\rangle, \qquad \text{(A8)}$$

it follows, under application of all hard-core constraints that define the physical space in the enlarged space, which action we will denote by P_{hc}, that

$$\hat{g}_{\text{SU}(N)}|\Psi_{\text{phy}}\rangle = P_{\text{hc}}(\hat{g}^L \hat{g}^R |\Psi_{\text{phy}}\rangle)$$
$$= \sum_{\{n'_1 \neq n'_2 \neq \cdots \neq n'_{N_\phi/2}\}} U^{n'_1 n_1} \cdots U^{n'_{N_\phi/2} n_{N_\phi/2}}$$
$$\times \sum_{\sigma \in S_{N_\phi/2}} c^\dagger_{\sigma(m'_1)n'_1} \cdots c^\dagger_{\sigma(m'_{N_\phi/2})n'_{N_\phi/2}} |0\rangle. \qquad \text{(A9)}$$

Any change of basis in enlarged space (that acts on R and L indices) is represented in physical states by the unitary implementation (A9), as required and expected. The implementation is unitary and represents an expected expansion on physical states, but it cannot be described as a simple action on L indices.

APPENDIX B: QUANTUM BOLTZMANN EQUATION

The explicit expression for the right-hand side of Eq. (43) to linear order in shifts in single-particle correlators is

$$
\begin{aligned}
i\frac{\partial \nu(\boldsymbol{k},\boldsymbol{r})}{\partial t} =& \int \frac{d\boldsymbol{q}}{(2\pi)^2}\frac{\tilde{V}(\boldsymbol{q})}{4}\{(\boldsymbol{q}\times\boldsymbol{k})(i\boldsymbol{q}\times\nabla_{\boldsymbol{r}})[\nu(\boldsymbol{k},\boldsymbol{r},t)\nu(\boldsymbol{k}+\boldsymbol{q},\boldsymbol{r},t)] - \frac{1}{4}[i\nabla_{\boldsymbol{k}}(i\boldsymbol{q}\times\nabla_{\boldsymbol{r}})\nu(\boldsymbol{k},\boldsymbol{r},t)][\nabla_{\boldsymbol{r}}(i\boldsymbol{q}\times\nabla_{\boldsymbol{r}}) \\
&\times \nu(\boldsymbol{k}+\boldsymbol{q},\boldsymbol{r},t)] + \frac{1}{4}[\nabla_{\boldsymbol{r}}(i\boldsymbol{q}\times\nabla_{\boldsymbol{r}})\nu(\boldsymbol{k},\boldsymbol{r},t)][i\nabla_{\boldsymbol{k}}(i\boldsymbol{q}\times\nabla_{\boldsymbol{r}})\nu(\boldsymbol{k}+\boldsymbol{q},\boldsymbol{r},t)] \\
&+ i(\boldsymbol{q}\times\boldsymbol{k})^2[\nabla_{\boldsymbol{r}}\nu(\boldsymbol{k},\boldsymbol{r},t)\nabla_{\boldsymbol{k}}\nu(\boldsymbol{k}+\boldsymbol{q},\boldsymbol{r},t) - \nabla_{\boldsymbol{k}}\nu(\boldsymbol{k},\boldsymbol{r},t)\nabla_{\boldsymbol{r}}\nu(\boldsymbol{k}+\boldsymbol{q},\boldsymbol{r},t)] \\
&+ (\boldsymbol{q}\times\boldsymbol{k})(i\boldsymbol{q}\times\boldsymbol{z})[\nu(\boldsymbol{k},\boldsymbol{r},t)\,\nabla_{\boldsymbol{r}}\nu(\boldsymbol{k}+\boldsymbol{q},\boldsymbol{r},t) - \nabla_{\boldsymbol{r}}\nu(\boldsymbol{k},\boldsymbol{r},t)\,\nu(\boldsymbol{k}+\boldsymbol{q},\boldsymbol{r},t)]\} \\
&\times \int \frac{d\boldsymbol{q}}{(2\pi)^2}(-2C)\{(\boldsymbol{q}\times\boldsymbol{k})(i\boldsymbol{q}\times\nabla_{\boldsymbol{r}})[\nu(\boldsymbol{k},\boldsymbol{r},t)\nu(\boldsymbol{k}+\boldsymbol{q},\boldsymbol{r},t)] + i(\boldsymbol{q}\times\boldsymbol{k})^2[\nabla_{\boldsymbol{r}}\nu(\boldsymbol{k},\boldsymbol{r},t)\nabla_{\boldsymbol{k}}\nu(\boldsymbol{k}+\boldsymbol{q},\boldsymbol{r},t) \\
&- \nabla_{\boldsymbol{k}}\nu(\boldsymbol{k},\boldsymbol{r},t)\nabla_{\boldsymbol{r}}\nu(\boldsymbol{k}+\boldsymbol{q},\boldsymbol{r},t)] - \frac{i}{8}[\nabla_{\boldsymbol{k}}\nu(\boldsymbol{k},\boldsymbol{r},t)\nabla_{\boldsymbol{r}}(\boldsymbol{q}\times\nabla_{\boldsymbol{r}})^2\nu(\boldsymbol{k}+\boldsymbol{q},\boldsymbol{r},t) + \nabla_{\boldsymbol{k}}(\boldsymbol{q}\times\nabla_{\boldsymbol{r}})^2\nu(\boldsymbol{k},\boldsymbol{r},t)\nabla_{\boldsymbol{r}}\nu(\boldsymbol{k}+\boldsymbol{q},\boldsymbol{r},t)] \\
&+ \frac{i}{8}[\nabla_{\boldsymbol{r}}\nu(\boldsymbol{k},\boldsymbol{r},t)\nabla_{\boldsymbol{k}}(\boldsymbol{q}\times\nabla_{\boldsymbol{r}})^2\nu(\boldsymbol{k}+\boldsymbol{q},\boldsymbol{r},t) + \nabla_{\boldsymbol{r}}(\boldsymbol{q}\times\nabla_{\boldsymbol{r}})^2\nu(\boldsymbol{k},\boldsymbol{r},t)\nabla_{\boldsymbol{k}}\nu(\boldsymbol{k}+\boldsymbol{q},\boldsymbol{r},t)] \\
&+ \frac{i}{4}[\nu(\boldsymbol{k}+\boldsymbol{q},\boldsymbol{r},t)(\boldsymbol{q}\times\boldsymbol{k})(\boldsymbol{q}\times\nabla_{\boldsymbol{r}})\nu(\boldsymbol{k},\boldsymbol{r},t) - \nu(\boldsymbol{k},\boldsymbol{r},t)(\boldsymbol{q}\times\boldsymbol{k})(\boldsymbol{q}\times\nabla_{\boldsymbol{r}})\nu(\boldsymbol{k}+\boldsymbol{q},\boldsymbol{r},t)]\}.
\end{aligned}
\tag{B1}
$$

If we neglect $(\boldsymbol{q}\times\nabla_{\boldsymbol{r}})$ with respect to $(\boldsymbol{q}\times\boldsymbol{k})$ and contributions higher in $\nabla_{\boldsymbol{r}}$, and also calculate the overall contribution to the mass term ($\sim \boldsymbol{k}\nabla_{\boldsymbol{r}}$) in the small-$\boldsymbol{q}$ limit, we arrive at the simple form in (44).

[1] B. I. Halperin, P. A. Lee, and N. Read, Theory of the half-filled Landau level, Phys. Rev. B **47**, 7312 (1993).

[2] R. L. Willett, R. R. Ruel, K. W. West, and L. N. Pfeiffer, Experimental Demonstration of a Fermi Surface at One-half Filling of the Lowest Landau Level, Phys. Rev. Lett. **71**, 3846 (1993).

[3] R. Willett, J. P. Eisenstein, H. L. Stormer, D. C. Tsui, A. C. Gossard, and J. H. English, Observation of an Even-denominator Quantum Number in the Fractional Quantum Hall Effect, Phys. Rev. Lett. **59**, 1776 (1987).

[4] G. Moore and N. Read, Nonabelions in the fractional quantum hall effect, Nucl. Phys. B **360**, 362 (1991).

[5] V. Pasquier and F. D. M. Haldane, Nonabelions in the fractional quantum hall effect, Nucl. Phys. B **516**, 719 (1998).

[6] N. Read, Lowest-Landau-level theory of the quantum Hall effect: The Fermi-liquid-like state of bosons at filling factor one, Phys. Rev. B **58**, 16262 (1998).

[7] G. Murthy and R. Shankar, Hamiltonian theories of the fractional quantum Hall effect, Rev. Mod. Phys. **75**, 1101 (2003).

[8] S. Simon, The Chern-Simons Fermi liquid description of fractional quantum Hall states, in *Composite Fermions*, edited by O. Heinonen (World Scientific, Singapore, 1998).

[9] D. T. Son, Is the Composite Fermion a Dirac Particle?, Phys. Rev. X **5**, 031027 (2015).

[10] D. Gočanin, S. Predin, M. D. Ćirić, V. Radovanović, and M. Milovanović, Microscopic derivation of Dirac composite fermion theory: Aspects of noncommutativity and pairing instabilities, Phys. Rev. B **104**, 115150 (2021).

[11] K. Lee, J. Shao, E.-A. Kim, F. D. M. Haldane, and E. H. Rezayi, Pomeranchuk Instability of Composite Fermi Liquids, Phys. Rev. Lett. **121**, 147601 (2018).

[12] Z. Dong and T. Senthil, Noncommutative field theory and composite Fermi liquids in some quantum Hall systems, Phys. Rev. B **102**, 205126 (2020).

[13] G. Wagner, D. X. Nguyen, S. H. Simon, and B. I. Halperin, s-Wave Paired Electron and Hole Composite Fermion Trial State for Quantum Hall Bilayers with $\nu = 1$, Phys. Rev. Lett. **127**, 246803 (2021).

[14] Y. Zhu, L. Fu, and D. N. Sheng, Numerical Study of Quantum Hall Bilayers at Total Filling $\nu_T = 1$: A New Phase at Intermediate Layer Distances, Phys. Rev. Lett. **119**, 177601 (2017).

[15] M. V. Milovanović, E. Dobardžić, and Z. Papić, Meron deconfinement in the quantum Hall bilayer at intermediate distances, Phys. Rev. B **92**, 195311 (2015).

[16] Y. B. Kim, P. A. Lee, and X. G. Wen, Quantum Boltzmann equation of composite fermions interacting with a gauge field, Phys. Rev. B **52**, 17275 (1995).

[17] E. Rezayi and N. Read, Fermi-Liquid-Like State in a Half-Filled Landau Level, Phys. Rev. Lett. **72**, 900 (1994).

Charge fluctuations, hydrodynamics, and transport in the square-lattice Hubbard model

J. Vučičević,[1] S. Predin,[1] and M. Ferrero[2,3]

[1]*Scientific Computing Laboratory, Center for the Study of Complex Systems, Institute of Physics Belgrade,*
University of Belgrade, Pregrevica 118, 11080 Belgrade, Serbia
[2]*CPHT, CNRS, Ecole Polytechnique, Institut Polytechnique de Paris, Route de Saclay, 91128 Palaiseau, France*
[3]*Collège de France, 11 place Marcelin Berthelot, 75005 Paris, France*

Recent experimental results suggest that a particular hydrodynamic theory describes charge fluctuations at long wavelengths in the square-lattice Hubbard model. Due to the continuity equation, the correlation functions for the charge and the current are directly connected: the parameters of the effective hydrodynamic model thus determine the optical conductivity. Here we investigate the validity of the proposed hydrodynamic theory in the full range of parameters of the Hubbard model. In the noninteracting case, there is no effective hydrodynamics, and the charge fluctuations present a rich variety of nonuniversal behaviors. At weak coupling, the optical conductivity is consistent with the hydrodynamic theory: at low frequency one observes a Lorentzian-shaped Drude peak, but the high-frequency asymptotics is necessarily different; the high-temperature limit for the product of the two hydrodynamic model parameters is also in agreement with numerical data. At strong coupling, we find that a generalization of the proposed hydrodynamic law is consistent with our quantum Monte Carlo, as well as the finite-temperature Lanczos results from literature. Most importantly, the temperature dependence of the hydrodynamic parameters as well as the dc resistivity are found to be very similar in the weak- and the strong-coupling regimes.

I. INTRODUCTION

Strange metallic behavior is one of the central subjects for the theory of strong electronic correlations [1]. It appears to be a universal phenomenon, observed in many different systems, often in close proximity to a superconducting phase [2–5], or quantum critical points [6–8]. In this regime, the dc resistivity is linear in temperature, in a very broad range of temperature. The origin of this behavior is unclear, but numerical investigations converge to the conclusion that the Hubbard model captures the underlying mechanisms [9–15]. Very recently, a variational solution of the semiclassical Boltzmann equation revealed a T-linear dc resistivity regime at high temperature, extending towards zero temperature as half-filling is approached [16]. This finding of Kiely and Mueller bares an important implication that strange metallicity is not necessarily a strong correlation phenomenon, even in cases when it extends to very low temperature (see also Ref. [17] highlighting the role of van Hove singularities at the Fermi level).

In the high-temperature limit, a simple and quite universal understanding of the linear resistivity was proposed in terms of the effective hydrodynamics that is expected to arise at long wavelengths in interacting systems. Diffusive transport should under very general circumstances lead to $\sigma_{\mathrm{dc}} = \chi_c D$, where σ_{dc} is the dc conductivity, χ_c is the charge compressibility, and D is the diffusion constant. In Refs. [11,12], it was argued that, at high temperature, D approaches a constant, while quite generally $\chi_c \sim 1/T$, which thus leads to $\rho_{\mathrm{dc}} \sim T$. In a subsequent optical lattice simulation of the Hubbard model by Brown *et al.* [18], the assumption of hydrodynamic behavior was exploited to extract values for the dc resistivity and the width of the Drude peak. In almost quantitative agreement

with the best available numerical method (finite-temperature Lanczos, FTLM [19,20]), the experiment found linear resistivity in a broad range of temperature. However, the width of the Drude peak Γ was greatly overestimated in the experiment, which brings into question the quality of the ρ_{dc} estimates and the underlying assumptions. The interpretation of experimental results relied on a specific hydrodynamic ansatz for the charge-charge correlation function, proposed to be valid in the long-wavelength limit. On the other hand, the fits to the direct measurement data were performed at relatively short wavelengths: Any discrepancy between the ansatz and the actual behavior at these wavelengths (and correspondingly higher frequencies) could have led to the apparent bias in the estimates of Γ, but perhaps even in the estimates of ρ_{dc}.

In this paper we investigate the validity of the hydrodynamic theory proposed in Ref. [18]. We first discuss its analytical properties and find that the high-frequency asymptotics is manifestly nonphysical. We propose a modified hydrodynamic law, which corrects the high-frequency behavior, and ultimately allows for a comparison with Matsubara-axis data we obtain from quantum Monte Carlo. We derive the equation of motion for the current, which must present a microscopic basis for the hydrodynamic theory. We are unable to rigorously connect the hydrodynamic parameters to Hubbard model parameters, but we find evidence that $D\Gamma \approx 2t^2$ (here t is the hopping amplitude), which is consistent with numerical results at both weak and strong coupling. Moreover, at weak coupling, $D\Gamma = 2t^2$ can be derived rigorously as the high-temperature limit of the hydrodynamic theory, only based on the knowledge of the exact asymptotics of the charge-charge correlation function.

We perform numerical calculations for the square-lattice Hubbard model and cover a wide range of parameters. We start with the noninteracting limit where the hydrodynamic theory is not expected to hold and find multiple interesting examples of charge-fluctuation spectra. At weak coupling we use second-order perturbation theory for the self-energy, and compute optical conductivity and the charge-charge correlation function from the bubble approximation. We confirm the recent findings of Kiely and Mueller [16] that the dc resistivity is linear at half-filling and, more generally, at high temperature. At stronger couplings, we use the numerically exact continuous-time quantum Monte Carlo (CTINT [21,22]) on a finite 10×10 lattice, and control for the lattice size. We show that a modified hydrodynamic law is consistent with the Matsubara-axis results for the charge-charge and current-current correlation functions, as well as with the FTLM result for optical conductivity. The hydrodynamic model parameters extracted from FTLM at strong coupling display strikingly similar behavior to what we find from the bubble approximation at weak coupling.

The paper is organized as follows. In Sec. II we introduce the two-dimensional (2D) Hubbard model and the hydrodynamic theory proposed to govern its charge and current fluctuations at long wavelengths. In Sec. III we show our numerical results, separated in three subsections based on the coupling strength. In Sec. IV we discuss our findings in the context of existing literature and give concluding remarks in Sec. V. In Appendixes A–E we give detailed derivations of equations used in this paper, and outline the fast algorithm we used for computing the second-order self-energy. In Appendix F we show and discuss static charge susceptibility data in the noninteracting limit.

II. MODELS

A. Square-lattice Hubbard model

We solve the Hubbard model given by the Hamiltonian

$$H = -t \sum_{\sigma,\langle i,j \rangle} c^\dagger_{\sigma,i} c_{\sigma,j} + U \sum_i n_{\uparrow,i} n_{\downarrow,i} - \mu \sum_{\sigma,i} n_{\sigma,i}, \quad (1)$$

where $\sigma \in \{\uparrow, \downarrow\}$, i, j enumerate lattice sites, t is the hopping amplitude between the nearest-neighbor sites $\langle i, j \rangle$, U is the onsite coupling constant, and μ is the chemical potential. We absorb the chemical potential in the bare dispersion, which is thus given by

$$\varepsilon_{\mathbf{k}} = -2t(\cos k_x + \cos k_y) - \mu. \quad (2)$$

We will switch between the site notation and real-space notation whenever convenient ($A_i \equiv A_{\mathbf{r}}$, with $\mathbf{r} = \mathbf{r}_i$, which is the real-space position of the site i). The density operator is denoted $n_{\sigma,i} = c^\dagger_{\sigma,i} c_{\sigma,i}$. Throughout the paper we use the half-bandwidth $4t$ as the unit of energy. We only consider paramagnetic solutions. In equilibrium we assume full lattice symmetry.

B. Hydrodynamic model

In Ref. [18] it was proposed that a hydrodynamic model describes the fluctuations of current and charge at long wave-

lengths in the Hubbard model. The hydrodynamic model reads as

$$\partial_t n = -\nabla \cdot \mathbf{j}, \quad (3)$$

$$\partial_t \mathbf{j} = -\Gamma(D\nabla n + \mathbf{j}), \quad (4)$$

where n and $\mathbf{j}$ are scalar and vector fields, respectively, dependent on time and space. The parameters of the model are the momentum-relaxation rate Γ and the diffusion constant D.

The first equation [Eq. (3)] is the continuity equation, and it is certainly valid in the Hubbard model for the time-dependent operators in the Heisenberg picture. However, on the square lattice, the spatial derivatives must be discretized, and the actual continuity equation reads as

$$\partial_t n_{\mathbf{r}} = -\sum_{\eta \in \{x,y\}} (j^\eta_{\mathbf{r}} - j^\eta_{\mathbf{r}-\mathbf{e}_\eta}) \quad (5)$$

which simply means that any increase in the particle density at a site $\mathbf{r}$ must be due to a disbalance between the currents entering and exiting the given site. The current operator is given by

$$j^\eta_{\mathbf{r}} = it \sum_{\sigma} (c^\dagger_{\mathbf{r}+\mathbf{e}_\eta,\sigma} c_{\mathbf{r},\sigma} - c^\dagger_{\mathbf{r},\sigma} c_{\mathbf{r}+\mathbf{e}_\eta,\sigma}), \quad (6)$$

where $\mathbf{e}_\eta$ denotes the lattice vector in the direction η. A derivation of Eq. (5) is presented in Appendix A, but can be found elsewhere [23]. Since the operators are connected instantaneously, the charge and current fluctuate synchronously. The corresponding charge-charge and current-current correlation functions must be connected directly, as well. Following the derivation presented in Appendix B, one obtains in the entire complex plane

$$z^2 \chi_{\mathbf{q}}(z) = \sum_{\eta \in \{x,y\}} \sum_{\mathbf{k}} \Phi^\eta_{\mathbf{k},\mathbf{q}} (\langle n_{\mathbf{k}+\mathbf{q}} \rangle - \langle n_{\mathbf{k}} \rangle)$$
$$+ \sum_{\eta,\eta' \in \{x,y\}} (1 - e^{iq_\eta} - e^{-iq_{\eta'}} + e^{i(q_\eta - q_{\eta'})}) \Lambda^{\eta,\eta'}_{\mathbf{q}}(z), \quad (7)$$

where $\Phi^\eta_{\mathbf{k},\mathbf{q}} = -2t[\cos(k_\eta + q_\eta) - \cos k_\eta]$, and $n_{\mathbf{k}} = \sum_\sigma c^\dagger_{\sigma,\mathbf{k}} c_{\sigma,\mathbf{k}}$. We define in imaginary time and site space

$$\chi_{ij}(\tau) = \langle n_i(\tau) n_j(0) \rangle - \langle n \rangle^2 \quad (8)$$

and

$$\Lambda^{\eta\eta'}_{ij}(\tau) = \langle j^\eta_i(\tau) j^{\eta'}_j(0) \rangle \quad (9)$$

the charge-charge and current-current correlation functions, respectively, calculated in thermodynamic equilibrium. The standard Fourier transform to Matsubara frequencies gives $\chi(z)$ and $\Lambda(z)$ at a discrete set of points along the imaginary axis; a spatial Fourier transform gives the corresponding quantities in reciprocal space. We are ultimately interested in retarded quantities which correspond to taking $z = \nu + i0^+$ and we denote them as $\chi_{\mathbf{q}}(\nu)$ and $\Lambda^{\eta\eta'}_{\mathbf{q}}(\nu)$. Here, ν is real frequency and $\mathbf{q}$ is momentum. We have checked numerically that Eq. (7) holds in the noninteracting limit, for any $\mathbf{q}$ and in any parameter regime of the model (data not shown). In general, the transversal components $\Lambda^{\eta,\eta' \neq \eta}$ play a role in Eq. (7). However, the expression greatly simplifies for the

imaginary part on the real axis at small $\mathbf{q}$ in the x direction,

$$\lim_{q \to 0} \text{Im} \chi_{\mathbf{q}=(q,0)}(\nu) = \frac{q^2}{\nu^2} \text{Im} \Lambda_{\mathbf{q}=(q,0)}^{xx}(\nu), \qquad (10)$$

which is the same expression one obtains in the continuum limit, directly from Eq. (3).

The second equation [Eq. (4)] is the so-called constitutive equation [24] of a hydrodynamic theory, needed to close the system of equations, as the continuity equation itself does not fully fix n and $\mathbf{j}$. In the stationary regime, Eq. (4) reduces to Fick's law of diffusion $\mathbf{j} = -D\nabla n$. Equation (4) is not nec-

essarily satisfied in the Hubbard model, and is an underlying assumption of the work presented in Ref. [18]. It is precisely the aim of this work to investigate whether the hydrodynamics encoded in Eq. (4) truly emerges in the Hubbard model at the longest wavelengths and. if yes, under which conditions.

1. Microscopic constitutive equation for the hydrodynamics in the Hubbard model

We start by deriving a microscopic expression for the time derivative of the current operator. The derivation presented in Appendix C yields

$$\partial_t j_{\mathbf{r}}^{\eta} = -t^2 \sum_{\sigma} \left\{ 2n_{\sigma,\mathbf{r}+\mathbf{e}_{\eta}} - 2n_{\sigma,\mathbf{r}} + \sum_{\mathbf{u}\in\{-\mathbf{e}_{\eta},\mathbf{e}_{\bar{\eta}},-\mathbf{e}_{\bar{\eta}}\}} (c_{\sigma,\mathbf{r}+\mathbf{u}}^{\dagger} c_{\sigma,\mathbf{r}+\mathbf{e}_{\eta}} - c_{\sigma,\mathbf{r}}^{\dagger} c_{\sigma,\mathbf{r}+\mathbf{e}_{\eta}-\mathbf{u}} + \text{H.c.}) \right\}$$
$$- tU \sum_{\sigma} (n_{\bar{\sigma},\mathbf{r}+\mathbf{e}_{\eta}} - n_{\bar{\sigma},\mathbf{r}})(c_{\sigma,\mathbf{r}}^{\dagger} c_{\sigma,\mathbf{r}+\mathbf{e}_{\eta}} + c_{\sigma,\mathbf{r}+\mathbf{e}_{\eta}}^{\dagger} c_{\sigma,\mathbf{r}}), \qquad (11)$$

where we used $\bar{\sigma} = \uparrow$ if $\sigma = \downarrow$, and vice versa; similarly $\bar{\eta} = y$ if $\eta = x$, etc. We immediately recognize the lattice version of the local gradient of charge in the direction of the current $n_{\sigma,\mathbf{r}+\mathbf{e}_{\eta}} - n_{\sigma,\mathbf{r}}$. If we are interested in the time-dependent averages, we can split the terms in the second row in the disconnected and connected parts $\langle nc^{\dagger}c \rangle = \langle n \rangle \langle c^{\dagger}c \rangle + \langle nc^{\dagger}c \rangle^{\text{conn}}$. Assuming that we are close to and approaching equilibrium, one can further split the averages in the equilibrium value and the time-dependent part. Taking into account the lattice symmetries satisfied in equilibrium, the constant appearing in front of the gradient of charge has the terms $2t^2 + 2tU \langle c_{\sigma,\mathbf{r}+\mathbf{e}_{\eta}}^{\dagger} c_{\sigma,\mathbf{r}} \rangle_{\text{eq}}$, and will therefore decay towards $2t^2$ as $T \to \infty$ or $U \to 0$. Identifying this with the term $D\Gamma\nabla n$ in the hydrodynamic theory [Eq. (4)], one could expect that at high temperature $D\Gamma \approx 2t^2$. In Sec. III B, we analyze numerical data and indeed find such behavior. However, in Eq. (11) there are also time-dependent factors that multiply the gradient of charge, and other terms which correspond to neither ∇n or $\mathbf{j}$. It is unclear under which conditions the remaining terms conspire to give rise to the effective Eq. (4), even if only in the long-wavelength, low-frequency, and linear-response limit. In Appendix C, we present Eq. (11) also in momentum space, but find no clear simplifications in the $\mathbf{q} \to 0$ limit (the Fourier transform to the frequency domain would be analogous).

2. Experimental quench setup and CDW amplitude evolution: The ballistic and diffusive regimes

One can combine Eqs. (3) and (4) to obtain a differential equation governing the time evolution of the amplitude of a charge density wave $n_{\mathbf{q}}$ (on the lattice, this field corresponds to the operator $n_{\mathbf{q}} = \sum_{\sigma,\mathbf{k}} c_{\sigma,\mathbf{k}+\mathbf{q}}^{\dagger} c_{\mathbf{k}} + \text{H.c.}$):

$$\partial_t^2 n_{\mathbf{q}} + \Gamma \partial_t n_{\mathbf{q}} + \Gamma D q^2 n_{\mathbf{q}} = 0. \qquad (12)$$

Consider a setup where a charge density wave was first thermalized by applying an external density-modulating field V $[H \to H + V \int d\mathbf{r} \sin x n(\mathbf{r})]$ for a long time, and was then let to evolve after abruptly switching off V. This time evolu-

tion is the solution of Eq. (12) with the boundary condition $\partial_t n_{\mathbf{q}}(t = 0) = 0$, $n_{\mathbf{q}}(t = 0) = n_0$. If n_0 is small, this behavior should also be described by the linear-response theory

$$n_{\mathbf{q}}(t) = \int_{-\infty}^{t} \chi_{\mathbf{q}}(t - t')\theta(-t')dt'$$
$$= \int_{t}^{\infty} \chi_{\mathbf{q}}(t')dt', \qquad (13)$$

assuming the knowledge of the charge-charge correlation function in real time, obtained as the Fourier transform from the retarded $\chi_{\mathbf{q}}(\nu)$ as $\chi_{\mathbf{q}}(t) = \int d\nu \, e^{-it\nu} \chi_{\mathbf{q}}(\nu)$. One can show [18] that the solution of Eq. (12) is equal to Eq. (13) with the retarded charge-charge correlation function of the form

$$\chi_{\mathbf{q}}(\nu) = \frac{\chi_{\text{c}}}{1 - \frac{i\nu}{q^2 D} - \frac{\nu^2}{q^2 D\Gamma}}, \qquad (14)$$

where χ_{c} is the charge compressibility, which connects n_0 with the strength of the density modulating field at $t < 0$, but does not affect the dynamics of Eq. (12). This correlation function has the important property $\chi_{q\to 0}(\nu \neq 0) = 0$. This indicates the conservation of the total number of particles, which is a prerequisite for the continuity equation. This is easy to understand as $n_{\mathbf{q}=0}$ equals the total number of particles N_{tot}, and therefore $\text{Im} \chi_{q\to 0}(\nu)$ describes the fluctuations of N_{tot}.

At any given $\mathbf{q}$, one can rewrite the frequency-dependent part of Eq. (14) in a more revealing way. In the upper half-plane, the dynamic charge susceptibility (14) can be represented as a sum of two poles in the lower half-plane:

$$\chi^{\text{tp}}(z^+) = A \left[\frac{1}{z^+ - z_1} - \frac{1}{z^+ - z_2} \right] \qquad (15)$$

with $A = -\chi_{\text{c}}/r$, $r = \sqrt{4b - a^2}$, $a = \frac{1}{q^2 D}$, $b = \frac{1}{q^2 D\Gamma}$, $z_1 = \frac{r - ia}{2b}$, $z_2 = \frac{-r - ia}{2b}$. It is clear that there are two distinct regimes: one where r is purely real, hence the two poles appear at $\text{Re} z_1 = -\text{Re} z_2$ and $\text{Im} z_1 = \text{Im} z_2 = -a$; the other one is when r is purely imaginary, and the two poles appear at $\text{Re} z_1 = \text{Re} z_2 = 0$, $\text{Im} z_1 = \text{Im} z_2 + 2 \text{Im} r$. The latter is the "diffusive

regime," which is realized whenever $4b < a^2$, i.e.,

$$q < q_D \equiv \sqrt{\frac{\Gamma}{4D}}. \tag{16}$$

To understand why $4b < a^2$ represents the diffusive behavior, and $4b > a^2$ ballistic behavior, we investigate the corresponding solutions of Eq. (12). The linear-response theory (13) can be solved analytically in the case when $\chi = \chi^{tp}$. One has

$$\chi^{tp}(t) \sim e^{-itz_1} - e^{-itz_2} \tag{17}$$

and, therefore, under the assumption that neither z_1 or z_2 are purely real, one gets

$$n_{\mathbf{q}}(t) \sim \frac{e^{-itz_1}}{z_1} - \frac{e^{-itz_2}}{z_2}. \tag{18}$$

We see that $n_{\mathbf{q}}(t)$ will be zero whenever

$$\frac{z_2}{z_1} = e^{-it(z_2 - z_1)}. \tag{19}$$

In the ballistic regime, $z_1 = E - i\eta$ and $z_2 = -E - i\eta$, and the condition (19) means

$$t = \frac{1}{2iE} \ln\left(\frac{-E - i\eta}{E - i\eta}\right). \tag{20}$$

At a fixed η and a finite E, there are infinitely many solutions to the above equation: the amplitude of the CDW presents damped oscillations after turning off the external field V. In the other case ($4b < a^2$), the poles are placed along the imaginary axis, say $z_1 = -i\eta_1$, and $z_2 = -i\eta_2$, $\eta_2 > \eta_1$ and r is purely imaginary. One thus has $n_{\mathbf{q}}(t) \sim \frac{e^{-t\eta_1}}{\eta_1} - \frac{e^{-t\eta_2}}{\eta_2}$ which can never be zero if $\eta_1 \neq \eta_2$. This means that the amplitude of the CDW will "crawl" towards zero, signaling an overdamped, or diffusive, regime. The correlator $\chi_{\mathbf{q}}(\nu)$ [Eq. (14)] and the corresponding solutions for $n_{\mathbf{q}}(t)$ [Eq. (12) or, equivalently, Eq. (13)] are illustrated in Fig. 1.

3. Asymptotic behavior and the connection between hydrodynamics and transport

The hydrodynamic form for the charge-charge correlation function [Eq. (14)] directly implies the form of the current-current correlation function. Inverting Eq. (10) (which is a direct consequence of the continuity equation) one obtains

$$\text{Im}\Lambda^{xx}_{\mathbf{q}=(q,0)}(\nu) = \frac{\chi_c D}{\frac{q^4 D^2}{\nu^3} + \frac{1}{\nu}\left(1 - 2q^2 \frac{D}{\Gamma}\right) + \frac{\nu}{\Gamma^2}}. \tag{21}$$

At any finite q, the behavior at small ν goes as $\sim \nu^3$. At precisely $q = 0$ one gets

$$\text{Im}\Lambda^{xx}_{\mathbf{q}=0}(\nu) = \frac{\chi_c D}{\frac{1}{\nu} + \frac{\nu}{\Gamma^2}} \tag{22}$$

which at small ν goes as $\sim \nu$. Having in mind that the conductivity is obtained as [14,25]

$$\sigma^{\eta\eta'}_{\mathbf{q}}(\nu) = \frac{1}{\nu}\text{Im}\Lambda^{\eta\eta'}_{\mathbf{q}}(\nu), \tag{23}$$

this model clearly predicts that $\sigma^{xx}_{dc,\mathbf{q}} = 0$ for any finite $\mathbf{q}$ in the x direction, which is precisely what is expected on physical

$$\text{Im}\chi^{hyd}_{\mathbf{q}}(\nu) = \text{Im}[1 - i\nu/(q^2 D) - \nu^2/(q^2 D\Gamma)]^{-1}$$
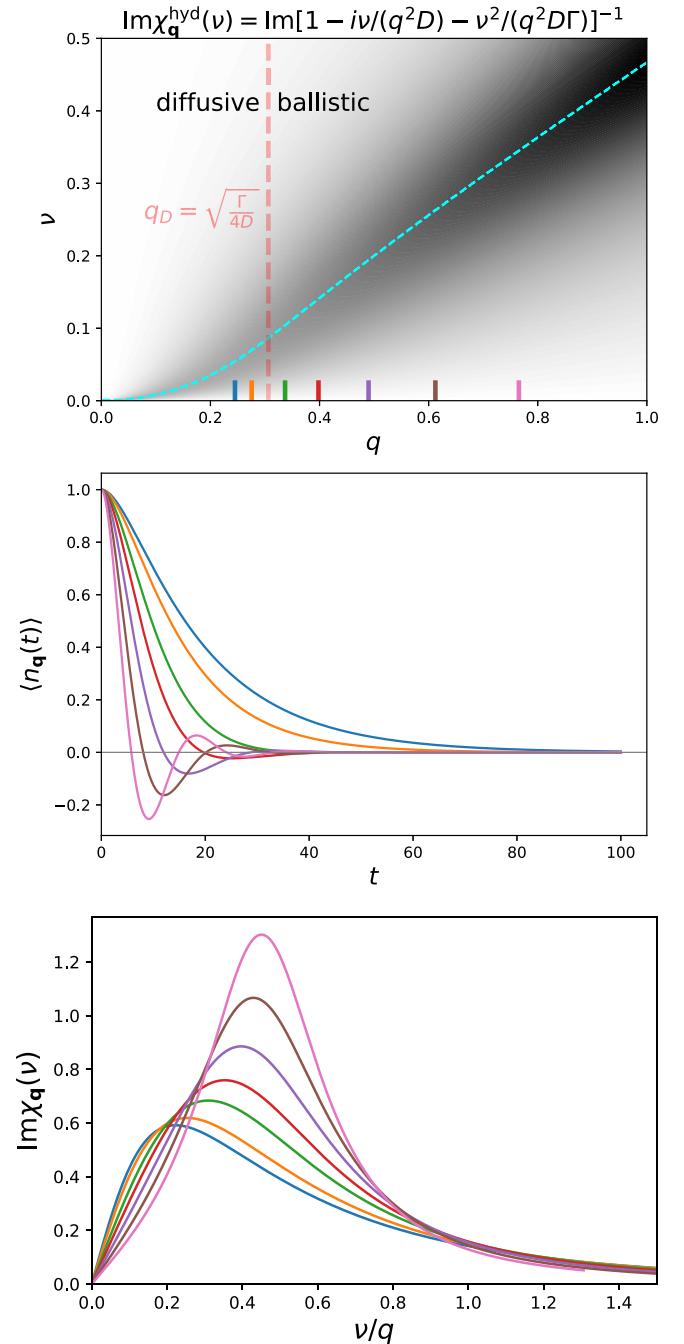
FIG. 1. Illustration of the hydrodynamic theory from Ref. [18], defined by Eqs. (3) and (4), with parameters taken to be $D = 0.8$, $\Gamma = 0.3$, $\chi_c = 1$. Top: the imaginary part of the charge-charge correlation function as a function of momentum and frequency [Eq. (14)]. Middle: the time evolution of relaxing charge density waves at wave vectors denoted by matching-color x ticks in the top panel; $\langle n_{\mathbf{q}}(t)\rangle$ [computed through Eq. (18)] is normalized to the initial amplitude $\langle n_{\mathbf{q}}(t = 0)\rangle$. Bottom: frequency dependence of the imaginary part of the charge-charge correlation function at the same wave vectors.

grounds. At $\mathbf{q} = 0$, which is the most relevant case, one gets a Lorentzian-shaped Drude peak

$$\sigma^{xx}_{\mathbf{q}=0}(\nu) = \frac{\chi_c D}{1 + \left(\frac{\nu}{\Gamma}\right)^2} \tag{24}$$

indicating $\sigma_{\mathrm{dc},\mathbf{q}=0}^{xx} \equiv \sigma_{\mathbf{q}=0}^{xx}(\nu=0) = \chi_c D$, which is the well-known Nernst-Einstein equation.

It is important to note that, *a priori*, the forms (21), (22) and (24) of Λ and σ are unphysical. The scaling with high frequency

$$\mathrm{Im}\Lambda_{\mathbf{q}=0}(\nu \to \infty) \sim \frac{1}{\nu} \tag{25}$$

cannot be obtained from a correlation function in imaginary time $\Lambda_{\mathbf{q}=0}(\tau)$ that has the correct symmetries. The Lorentzian Drude peak $\sigma \sim \frac{1}{\nu^2}$ must be restricted to some finite frequency. In general, one expects that at high-frequency, $\mathrm{Im}\chi(\nu)$ and $\mathrm{Im}\Lambda(\nu)$ decay exponentially. In the noninteracting case, there is even a sharp cutoff: both charge and current fluctuations are bounded in frequency from above, with a bound that depends on $\mathbf{q}$ (see Sec. III A). In any case, on the Matsubara axis one must have $\chi(i\nu \to i\infty) \sim 1/\nu^2$ and $\Lambda(i\nu \to i\infty) \sim 1/\nu^2$. The hydrodynamic ansatz for the charge fluctuations [Eq. (14)] does not violate this, as on the upper half of the Matsubara axis

$$\chi_{\mathbf{q}}(i\nu) = \frac{\chi_c}{1 + \frac{\nu}{q^2 D} + \frac{\nu^2}{q^2 D\Gamma}}, \tag{26}$$

but, through the continuity equation, it does imply a nonphysical asymptotic behavior $\Lambda_{\mathbf{q}=0}(i\nu \to i\infty) \sim \frac{1}{\nu}$. To be able to compare the hydrodynamic theory with Matsubara-frequency results for the charge-charge and current-current correlation functions, we thus propose a modified hydrodynamic form. The details are given in Sec. III C.

The imaginary-axis form (26) may still be useful in the $U \to 0$ limit. The high-frequency asymptotics on the imaginary axis is determined by the entirety of the function on the real axis. As the coupling constant is decreased, the weight of the function $\chi_{\mathbf{q} \to 0}$ on the real axis will be contained in an increasingly small range of low frequencies. If we assume that the hydrodynamic theory holds in some low-frequency range, say $|\omega| < |\omega_{\max}|$, and that $\omega_{\max}$ saturates to a finite constant as $U \to 0$, then we can conclude that the imaginary-axis asymptotics of $\chi_{\mathbf{q} \to 0}$ will tend to Eq. (26) as $U \to 0$. Clearly, nonuniversal features at high real frequencies will still be there, but they will not contribute significantly to the imaginary-axis asymptotics. Other scenarios are also possible, but in the following we work out the consequences of our expectation that the hydrodynamic law holds in a *finite* range of frequency in the $U \to 0$ limit. We start with Eq. (7), which implies the long-wavelength asymptotics of the charge-charge correlation function of the form (see Appendix B for details)

$$\mathrm{Re}\chi_{\mathbf{q} \to 0}(i\nu \to i\infty) = -\frac{2t}{\nu^2} \sum_{\eta=\{x,y\}} \sum_{\mathbf{k}} q_\eta \sin k_\eta \mathbf{q} \cdot \boldsymbol{\nabla}\langle n_{\mathbf{k}}\rangle. \tag{27}$$

This form is not necessarily isotropic. Nevertheless, one can take $\mathbf{q} = (q, 0)$ and, then, assuming a finite $\omega_{\max}$ and $U \to 0$, equate the right-hand side of Eq. (27) with the $i\nu \to i\infty$ limit of Eq. (26) to obtain

$$D\Gamma = -\frac{1}{\chi_c} \sum_{\mathbf{k}} v_{\mathbf{k}}^x \partial_{k_x}\langle n_{\mathbf{k}}\rangle \tag{28}$$

with $v_{\mathbf{k}}^x = 2t \sin k_x$. Under the current assumption of the weak-coupling limit, we can write further

$$D\Gamma = -\frac{1}{\chi_c} \sum_{\mathbf{k}} (v_{\mathbf{k}}^x)^2 [2n_{\mathrm{F}}'(\varepsilon_{\mathbf{k}})]. \tag{29}$$

At high temperature $T = 1/\beta \to \infty$, the first derivative of the Fermi distribution $n_{\mathrm{F}}'(\omega) \sim -\beta/4$, and $\chi_c = \frac{\partial \langle n \rangle}{\partial \mu} = -\int d\varepsilon\, \rho(\varepsilon) 2n_{\mathrm{F}}'(\varepsilon) \sim \frac{2\beta}{4} \int d\varepsilon\, \rho(\varepsilon) = \beta/2$. We also have $\frac{1}{(2\pi)^2} \int d\mathbf{k}\, \sin k_x = \frac{1}{2}$. We conclude that in the weak-coupling limit and high temperature, the effective hydrodynamic theory formulated by Eqs. (3) and (4) for the square-lattice Hubbard model [Eq. (1)], if valid in a finite range of real frequency, must satisfy

$$\lim_{\substack{U \to 0 \\ T \to \infty}} D\Gamma = 2t^2. \tag{30}$$

Thus, the equation of motion (11) provides some microscopic support for the effective hydrodynamic theory. As already mentioned, Eq. (30) indeed coincides with numerical results, and is roughly satisfied in a broad range of temperatures, even at strong coupling (see Sec. III B). Finally, we note that the imaginary-axis asymptotics [Eq. (27)] combined with $\sigma_{\mathrm{dc}} = \chi_c D$ [Eq. (24)] reveals that the hydrodynamic theory [Eq. (26)], taken to be valid at any frequency, is consistent with the Boltzmann expression for the dc conductivity

$$\sigma_{\mathrm{dc}} = -\frac{1}{\Gamma} \sum_{\mathbf{k}} v_{\mathbf{k}}^x \partial_{k_x}\langle n_{\mathbf{k}}\rangle. \tag{31}$$

III. RESULTS

A. Noninteracting limit

We are interested in calculating two-particle correlation functions, in particular for the charge and current. In the noninteracting limit, these can be obtained numerically exactly, to a high accuracy, from the general (Kubo) bubble formula

$$Q_{\mathbf{q}}[\varphi, \phi](\tau) = 2 \sum_{\mathbf{k}} \varphi_{\mathbf{k},\mathbf{q}} G_{0,\mathbf{k}}(\tau) G_{0,\mathbf{k}+\mathbf{q}}(-\tau) \phi_{\mathbf{k}+\mathbf{q},-\mathbf{q}}. \tag{32}$$

The factor 2 in front is due to summation over σ. We denote G_0 the bare propagator, which is, at a finite temperature $T = \frac{1}{\beta}$, defined in the imaginary-time window $\tau \in [-\beta, \beta]$ as

$$G_{0,\mathbf{k}}(\tau) = -\mathrm{sign}(\tau) e^{-\varepsilon_{\mathbf{k}}\tau} n_{\mathrm{F}}[-\mathrm{sign}(\tau)\varepsilon_{\mathbf{k}}] \tag{33}$$

with $n_{\mathrm{F}}(\omega) = \frac{1}{e^{\beta\omega}+1}$ the Fermi-Dirac distribution function.

The "vertex factors" φ and ϕ correspond to the operators for which the correlation function is calculated (in general, $\mathcal{O}_{\mathbf{q}} = \sum_{\sigma,\mathbf{k}} \varphi_{\mathbf{k},\mathbf{q}} c_{\sigma,\mathbf{k}+\mathbf{q}}^\dagger c_{\sigma,\mathbf{k}}$). We then simply have $\chi_{\mathbf{q}} = Q_{\mathbf{q}}[\varphi = 1, \phi = 1]$, and $\Lambda_{\mathbf{q}}^{\eta,\eta'} = Q_{\mathbf{q}}[\varphi = v^\eta, \phi = v^{\eta'}]$, with $v_{\mathbf{k},\mathbf{q}}^\eta = it(e^{-i(k_\eta+q_\eta)} - e^{ik_\eta})$. In the entire complex frequency plane, one can then write

$$Q_{\mathbf{q}}[\varphi, \phi](z) = 2 \sum_{\mathbf{k}} \varphi_{\mathbf{k},\mathbf{q}} \phi_{\mathbf{k}+\mathbf{q},-\mathbf{q}} \frac{n_{\mathrm{F}}(\varepsilon_{\mathbf{k}+\mathbf{q}}) - n_{\mathrm{F}}(\varepsilon_{\mathbf{k}})}{z - (\varepsilon_{\mathbf{k}} - \varepsilon_{\mathbf{k}+\mathbf{q}})}. \tag{34}$$

We now consider the long-wavelength limit for the charge-charge correlation function χ. At small enough $\mathbf{q}$, one can write further: $\varepsilon_{\mathbf{k}+\mathbf{q}} = \varepsilon_{\mathbf{k}} + \mathbf{q} \cdot \boldsymbol{\nabla}\varepsilon_{\mathbf{k}}$ and $n_{\mathrm{F}}(\varepsilon_{\mathbf{k}+\mathbf{q}}) = n_{\mathrm{F}}(\varepsilon_{\mathbf{k}}) +$
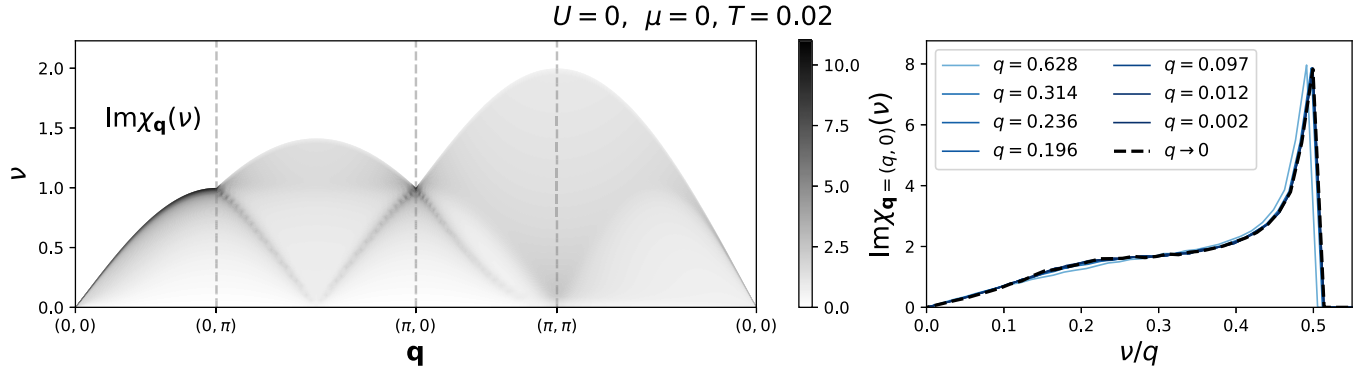
$$U = 0, \quad \mu = 0, \quad T = 0.02$$

FIG. 2. Noninteracting case, half-filling. Left: imaginary part of the charge-charge correlation function along a high-symmetry path in the BZ. Right: frequency dependence in the long-wavelength limit, for waves in the x direction. The spectral weight drops off abruptly at $\nu/q = \frac{1}{2}$; the apparent finite slope comes from the finite-frequency resolution in our numerics.

$(\mathbf{q} \cdot \nabla \varepsilon_{\mathbf{k}}) n'_{\mathrm{F}}(\varepsilon_{\mathbf{k}})$. These yield

$$\chi_{\mathbf{q}\to 0}(z) = 2 \sum_{\mathbf{k}} \frac{(\mathbf{q} \cdot \nabla \varepsilon_{\mathbf{k}}) n'_{\mathrm{F}}(\varepsilon_{\mathbf{k}})}{z + \mathbf{q} \cdot \nabla \varepsilon_{\mathbf{k}}}. \tag{35}$$

We see that at small $q \equiv |\mathbf{q}|$, the frequency dependence no longer depends on q. In the denominator, q multiplies the number which determines the position of a pole on the energy axis. Therefore, q sets the energy scale, which means that with a proper rescaling of the ν axis, χ results for different small $\mathbf{q}$ along a given direction can be collapsed onto a single curve. In the special case $\mathbf{q} = (q, 0)$, the gradient of the dispersion will simply yield the velocity $v^x_{\mathbf{k}} \equiv v^x_{\mathbf{k},\mathbf{q}=0} = 2t \sin k_x$, and one arrives at

$$\lim_{q\to 0} \chi_{\mathbf{q}=(q,0)}(z) = 2 \sum_{\mathbf{k}} \frac{v^x_{\mathbf{k}} n'_{\mathrm{F}}(\varepsilon_{\mathbf{k}})}{z/q + v^x_{\mathbf{k}}}. \tag{36}$$

On the most general physical grounds, it is not expected that in the noninteracting limit an effective hydrodynamics governs the charge fluctuations at however long the wavelengths. The diffusive motion of carriers at length scales $\lambda > 2\pi/q_D$ ultimately comes from a finite-lasting memory the electrons have of momentum; in the noninteracting case, the momentum eigenstates are infinitely long lived. It is clear that no identification between Eqs. (36) and (14) is possible. In fact, the noninteracting case presents strongly nonuniversal, parameter-dependent, and even anisotropic behavior that we illustrate in the following.

We obtain the $\chi_{\mathbf{q}}(\nu)$ along a high-symmetry path in the Brillouin zone (BZ) using a 6000×6000 site lattice, and adaptive frequency grids to ensure sufficient frequency resolution at all $\mathbf{q}$ vectors. We color plot $\mathrm{Im}\chi_{\mathbf{q}}(\nu)$ and show the frequency-dependent part at small $\mathbf{q}$ in Figs. 2–5.

In Fig. 2 we show results for the half-filled case $\mu = 0$, $T = 0.02$. In the long-wavelength limit, we observe a sharp peak at the edge of the spectrum, at $\nu \sim q$. The peak is highly asymmetric, as the spectral weight drops off abruptly on the higher-frequency side. The single-peak structure at $\nu \sim q$ is the expected linear zero-sound mode [23].

As the system is doped away from half-filling, we start to observe a two-peak structure at long wavelengths (Fig. 3). This can be understood by analyzing Eq. (36). In Fig. 3 we illustrate how the contributions to $\mathrm{Im}\chi_{\mathbf{q}=(q,0)}(\nu)$ at a given

energy ν comes from a line in the Brillouin zone (BZ) where $-v^x_{\mathbf{k}} = \nu/q$. The amplitude of a contribution at a given $\mathbf{k}$ is given by $v^x_{\mathbf{k}} n'_{\mathrm{F}}(\varepsilon_{\mathbf{k}})$, which roughly selects the Fermi surface. Therefore, one gets a peak at frequencies where $v^x_{\mathbf{k}}$ is maximal, but also where the Fermi surface is parallel to the k_y axis. This calculation resembles a histogram of a one-dimensional (1D) function, and thus the spectrum resembles a typical density of states of a 1D tight-binding chain.

On Fig. 4 we illustrate the great level of anisotropy, by comparing the $q \to 0$ limit for $\mathbf{q} = (q, 0)$ and $\mathbf{q} = \frac{1}{\sqrt{2}}(q, q)$. It is interesting that, as the temperature is increased, the anisotropy at low frequency becomes somewhat reduced.

Doping all the way to the near-empty limit, one observes a completely different behavior (see Fig. 5). The charge fluctuation spectrum closely resembles the electron dispersion. This indicates that in the single-particle limit, due to the irrelevance of the Fermi-Dirac statistics, the charge and the electron become the same.

1. CDW amplitude evolution

It is of interest to understand these $\chi_{\mathbf{q}}(\nu)$ results in the context of the quench setup studied in Ref. [18] and already mentioned in Sec. II B. Namely, we wish to investigate the time evolution of the amplitude of a relaxing charge density wave (CDW). If the initial CDW is weak, we can work within the linear-response theory, which can be solved numerically, by plugging Eq. (34) with $\varphi, \phi = 1$ in Eq. (13). The Fourier transform needed for this step is performed analogously to Eq. (17). Then, to perform the integral in Eq. (13) analytically, it is necessary to regularize the integrand function, first. As is always done when working with retarded quantities, we take that the poles are located slightly below the real axis. We obtain

$$\langle n_{\mathbf{q}}(t) \rangle \sim \sum_{\mathbf{k}} \frac{n_{\mathrm{F}}(\varepsilon_{\mathbf{k}+\mathbf{q}}) - n_{\mathrm{F}}(\varepsilon_{\mathbf{k}})}{\varepsilon_{\mathbf{k}} - \varepsilon_{\mathbf{k}+\mathbf{q}}} e^{-it(\varepsilon_{\mathbf{k}} - \varepsilon_{\mathbf{k}+\mathbf{q}})}. \tag{37}$$

We show several examples of this calculation in Fig. 6. We find numerous categories of solutions, and we illustrate some of them on the panels of Fig. 6, left to right:

(i) power-law damped oscillations,

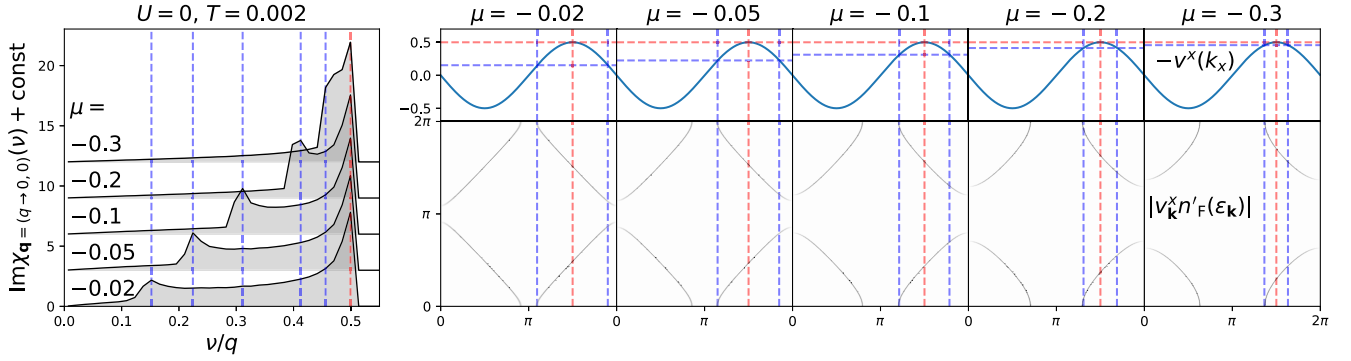(ii) power-law damped oscillations with a breathing amplitude,

FIG. 3. Noninteracting case, various moderate dopings. Left: frequency dependence of the imaginary part of the charge-charge correlation function in the long-wavelength limit, for waves in the x direction. Vertical blue and red dashed lines denote frequencies of two apparent peaks. Right: explanation for the appearance of two peaks. Top row: the electron velocity. Blue and red dashed lines denote the momenta where $v_{\mathbf{k}}^x = -\nu/q$, where ν is the frequency of the two peaks in the spectra on the left. Bottom row: the intensity plots (black and white scale) of the amplitude of the contribution to the charge-charge correlation function coming from different $\mathbf{k}$ vectors in the BZ. The blue and red dashed lines denote the contributions to the two peaks in the spectra on the left.

(iii) power-law damped oscillations with a decaying nonoscillatory component,

(iv) power-law decaying nonoscillatory behavior.

The behavior at $\mathbf{q} = (\pi, \pi)$ is drastically different from the behavior at long wavelengths. At (π, π) there is no clear peak in the spectrum, i.e., no characteristic frequency to produce oscillatory behavior. In particular, as $T \to 0$, the

charge-charge correlation function (which is in the noninteracting limit equal to the spin-spin correlation function) approaches the form of a second-order pole $\sim 1/z^2$, which signals the instability towards order. One therefore finds only a nonoscillatory decay of the initial CDW amplitude, somewhat reminiscent of the diffusive regime of the hydrodynamic theory.

2. Beyond linear response

To cross-check these results and to be able to access the regime beyond the linear response (corresponding to initial density wave of a bigger amplitude) we perform the corresponding Kadanoff-Baym three-piece contour calculation [26].

The external field couples to the density wave at the wave vector $\mathbf{q} = (q, 0)$,

$$H[V] = H_0 - V \sum_{\sigma, \mathbf{r}} \cos(\mathbf{q} \cdot \mathbf{r}) n_{\sigma, \mathbf{r}}$$

$$= H_0 - \frac{V}{2} \sum_{\sigma, \mathbf{k}} (c_{\sigma, \mathbf{k}+\mathbf{q}}^\dagger c_{\sigma, \mathbf{k}} + \text{H.c.}) \quad (38)$$

$$= H_0 - \frac{V}{2} (n_\mathbf{q} + n_{-\mathbf{q}}), \quad (39)$$

where V is the strength of the field. We assume the field was turned on slowly at $t = -\infty$, and that by the time $t = 0$, the system is already thermalized. Then, at $t = 0$, the field is turned off abruptly. Therefore,

$$H(t < 0) = H[V], \quad H(t > 0) = H_0. \quad (40)$$

In general, the expectation value of an operator $\mathcal{O}$ at time t following the quench of the field V is given by

$$\langle \mathcal{O}(t) \rangle = \frac{\text{Tr}[e^{-\beta H[V]} e^{iH_0 t} \mathcal{O} e^{-iH_0 t}]}{\text{Tr}[e^{-\beta H[V]}]}. \quad (41)$$

After the quench, the Hamiltonian has the diagonal form

$$H_0 = \sum_{\mathbf{k}\sigma} \varepsilon_\mathbf{k} c_{\sigma, \mathbf{k}}^\dagger c_{\sigma, \mathbf{k}}, \quad (42)$$
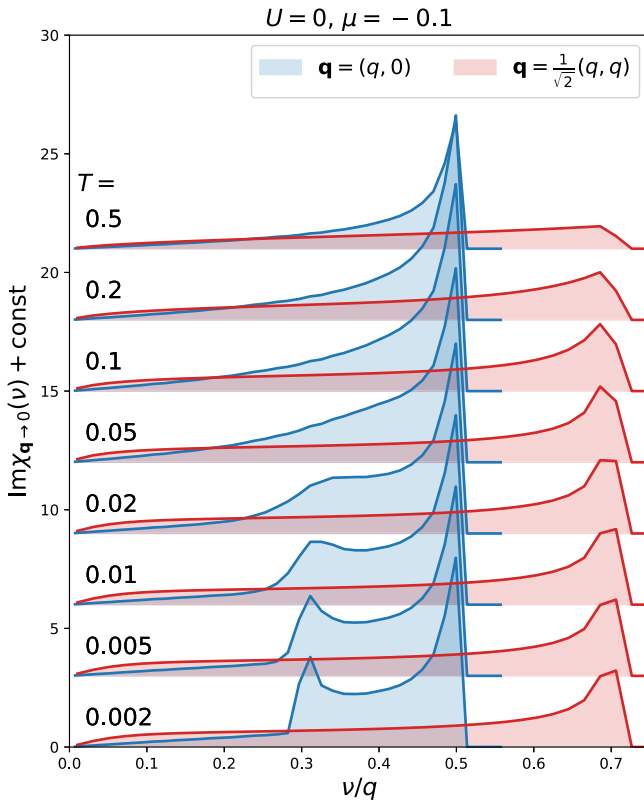

FIG. 4. Noninteracting case, moderate doping, various temperatures. Blue and red curves correspond to the long-wavelength limit of the imaginary part of the charge-charge correlation function for waves in the x and $x = y$ directions.
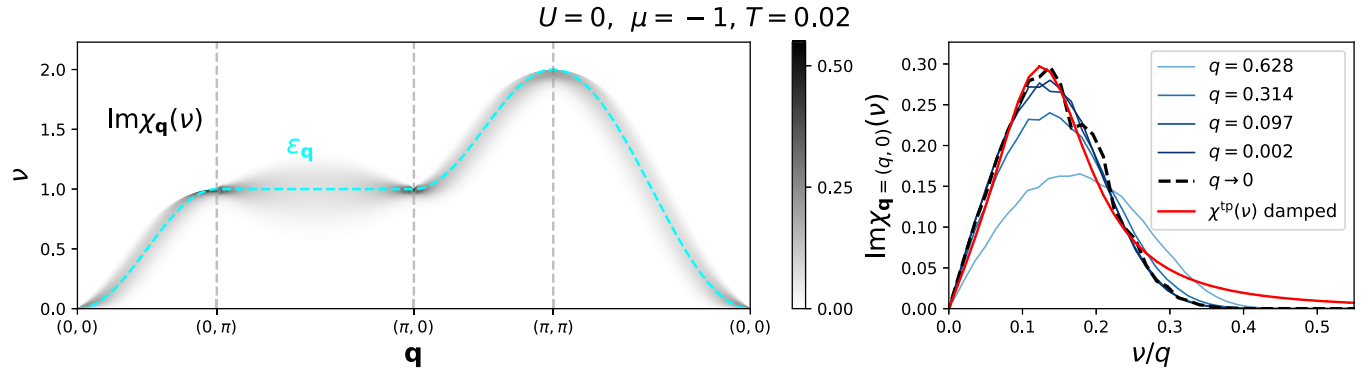
FIG. 5. Noninteracting case, nearly empty limit. Left and right: same as Fig. 2. Cyan line on the left: electron dispersion. Red line on the right: fit to the frequency-dependent part of the hydrodynamic theory χ^{tp} as defined in Eq. (15); best fit corresponds to the damped oscillations (or ballistic) regime (r purely real).

whereas before the quench, the diagonal form is

$$H[V] = \sum_{\tilde{k}_x \mathcal{V} k_y} \sum_{\sigma} \varepsilon_{(\tilde{k}_x \mathcal{V} k_y)\sigma} c^{\dagger}_{(\tilde{k}\mathcal{V} k_y)\sigma} c_{(\tilde{k}\mathcal{V} k_y)\sigma}. \qquad (43)$$

Because of the symmetry-breaking field, there is a reduction of the Brillouin zone, i.e., $\tilde{k}_x \in [0, 2\pi/\lambda)$, where $\lambda = 2\pi/q$ is the wavelength, or the number of sites in the unit cell; the additional quantum number arising due to the reduction of the BZ is $\mathcal{V}$.

The time evolution of density at a given point in space $\mathbf{r} = (x, 0)$ [the translational symmetry is not broken along the y axis: nothing changes if we take a more general $\mathbf{r} = (x, y)$] is given by

$$\langle n_{\mathbf{r}}(t) \rangle \equiv \left\langle \sum_{\sigma} c^{\dagger}_{\mathbf{r}\sigma}(t) c_{\mathbf{r}\sigma}(t) \right\rangle$$

$$= \frac{2}{N} \sum_{\tilde{k}_x, k_y \in \mathrm{RBZ}} \sum_{c,c' \in [0,\lambda)} \sum_{\mathcal{V}} e^{ix(c-c')q} e^{-i(\epsilon_{\mathbf{k}} - \epsilon_{\mathbf{k}'})t}$$

$$\times \langle \tilde{k}_x \mathcal{V} k_y | k'_x k_y \rangle \langle k_x k_y | \tilde{k}_x \mathcal{V} k_y \rangle n_{\mathrm{F}}(\varepsilon_{\tilde{k}_x \mathcal{V} k_y}), \qquad (44)$$

where we take $k_x = \tilde{k}_x + cq$, $k'_x = \tilde{k}_x + c'q$. The eigenstates of H_0 are denoted $|k_x k_y\rangle$, and the eigenstates of $H[V]$ are denoted $|\tilde{k}_x \mathcal{V} k_y\rangle$. The amplitude of the charge density wave $n_{\mathbf{q}}$ is given by the deviation of $n_{\mathbf{r}}$ from the lattice-averaged density, at the antinode of the wave, say $\mathbf{r} = (0, 0)$.

We find perfect agreement between the results of Eq. (44) with V taken small and Eq. (37) which is in the strict $V \to 0$ limit. The full Kadanoff-Baym calculation is clearly more computationally expensive, but it allows us to set V to stronger values and investigate the behavior starting from CDWs of finite amplitude. This is shown in Fig. 7. In the two panels on the right, we see that regular damped oscillations are replaced by a superposition of multiple waves as $V \to \infty$. This can
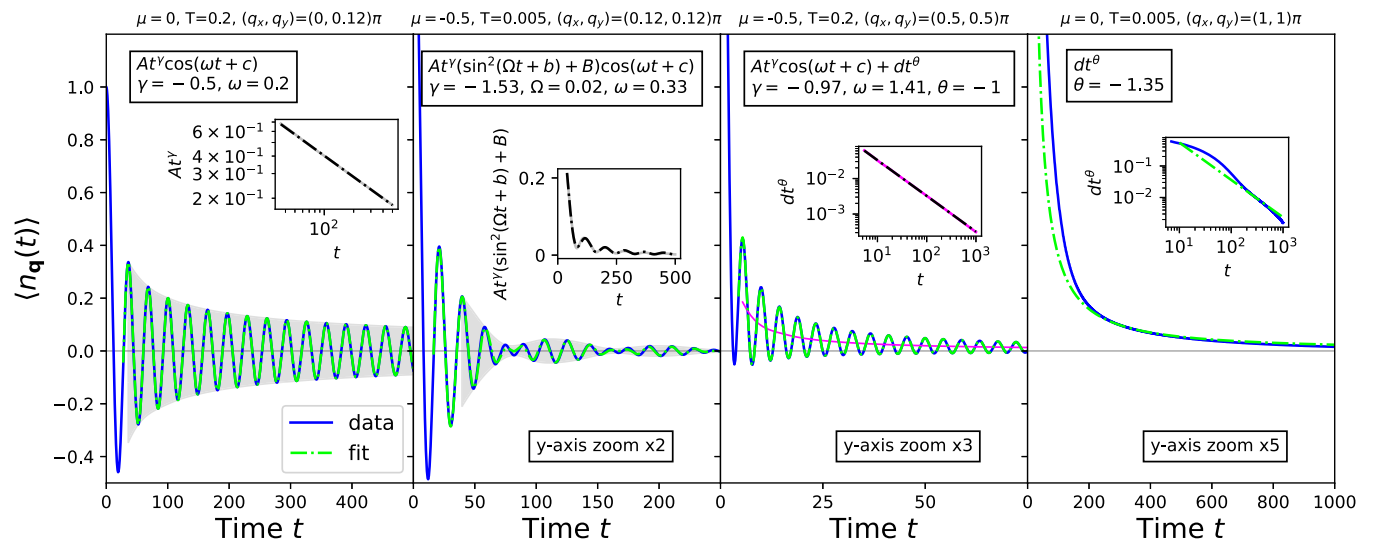

FIG. 6. Noninteracting case, various dopings, and temperatures. CDW amplitude vs time at various wave vectors, calculated within linear-response theory, normalized to the initial amplitude of the CDW. Text boxes show the fitting function and its main parameters. The insets in the two plots on the left show the amplitude of damped oscillations vs time, and the corresponding fit. The insets in the two plots on the right show the background, i.e., nonoscillatory components and the corresponding fits. Full lines are data, dotted-dashed lines are fits.
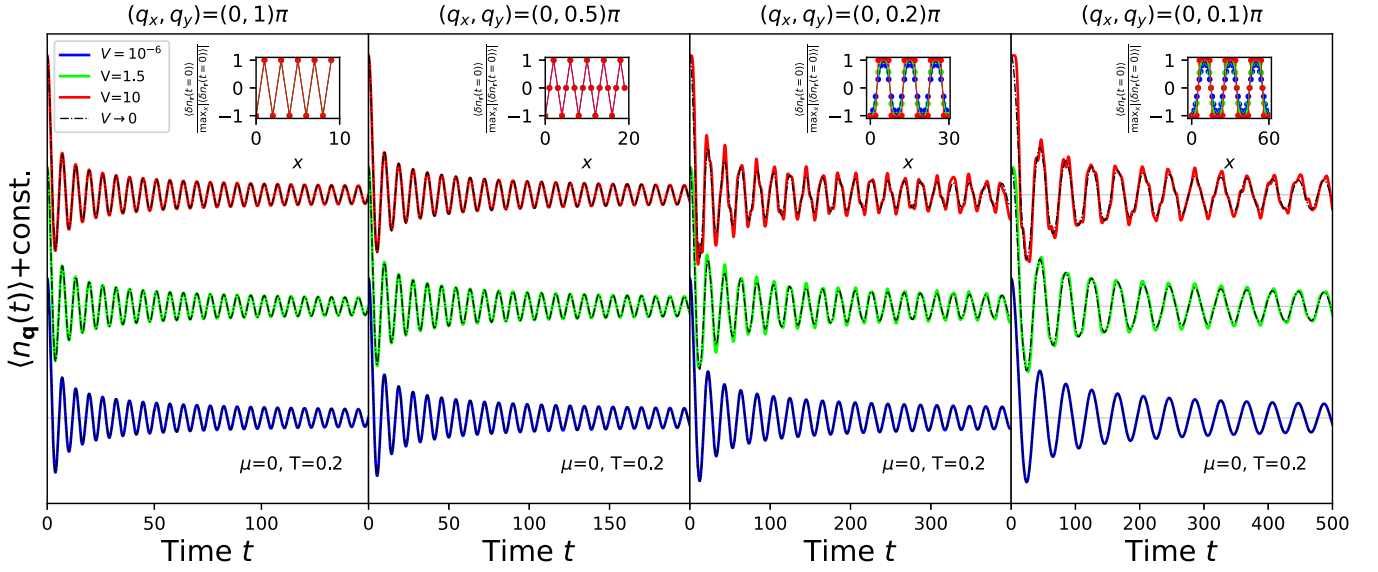
FIG. 7. Noninteracting case, half-filling, moderate temperature. CDW amplitude vs time at various wave vectors along the *x* axis, calculated within linear-response theory and from the full Kadanoff-Baym three-piece contour formalism, assuming different amplitudes of the density-modulating field *V* at $t < 0$. CDW amplitude is normalized to the initial amplitude of the CDW. Insets: density profile of the initial CDW at different strengths of the field *V*. See text for details.

be understood by looking at the density profile $n_{\mathbf{r}}$ at $t < 0$ (shown in the insets of Fig. 7). One cannot place more than two electrons on a single site, which means that at strong values of *V*, the CDW is no longer harmonic; as $V \to \infty$ it becomes similar to the step function. This density profile corresponds to having multiple CDWs at the same time, at *q*, $3q$, $5q$, etc. All these CDWs will oscillate at different frequencies, but one also expects interactions between the waves. It is not easy to explain the detailed structure of $n_{\mathbf{q}}(t)$ beyond the linear-response regime. However, in the long-wavelength limit, the characteristic frequency of CDWs is proportional to *q*, and we are able to roughly fit the resulting $\langle n_{\mathbf{q}}(t) \rangle$ to a superposition of waves $\sim \sum_{l=1,3,5,...} t^{a_l} \cos(l\omega t + C_l)$. This is shown in Fig. 8. However, the two panels on the left in Fig. 7

show that at shortest wavelengths, one observes no change in behavior as *V* is increased. This is because the density profile $n_{\mathbf{r}}(t < 0)$ cannot change: there are no shorter waves to be excited by the increasing field.

B. Weak-coupling theory

1. Self-energy

We start by calculating the self-energy up to the second order in the coupling constant:

$$\Sigma_{\mathbf{k}}(z) = U \langle n_{\bar{\sigma}} \rangle + U^2 \tilde{\Sigma}_{\mathbf{k}}(z), \qquad (45)$$

$$\tilde{\Sigma}_{\mathbf{k}}(z) = \sum_{\mathbf{k}',\mathbf{q}} \frac{\sum_{s=\pm 1} n_F(-s\varepsilon_{\mathbf{k}'}) n_F(s\varepsilon_{\mathbf{k}'+\mathbf{q}}) n_F(s\varepsilon_{\mathbf{k}-\mathbf{q}})}{z - \varepsilon_{\mathbf{k}-\mathbf{q}} - \varepsilon_{\mathbf{k}'+\mathbf{q}} + \varepsilon_{\mathbf{k}'}}. \qquad (46)$$

The first term is the instantaneous Hartree shift, and the second term is the dynamic part, described by the second-order Feynman diagram illustrated in Fig. 9. The calculation of $\tilde{\Sigma}$ is expensive. In Appendix E we describe a fast algorithm we used for this calculation, which allowed us to scan the phase diagram in considerable detail.
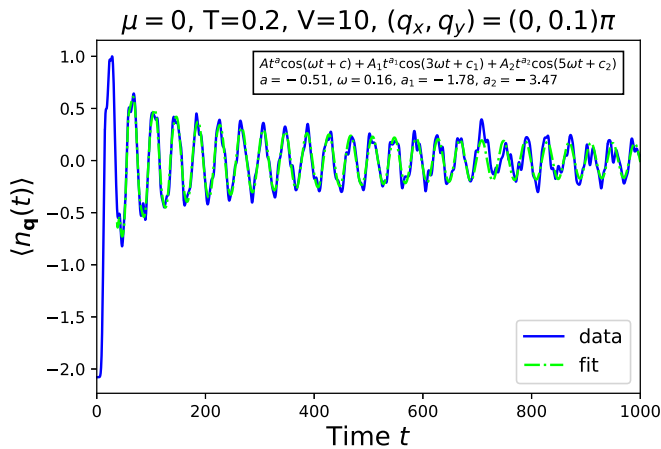

FIG. 8. Noninteracting case, half-filling, moderate temperature. Fit to the CDW amplitude vs time, starting from a saturated CDW with a short wave vector.
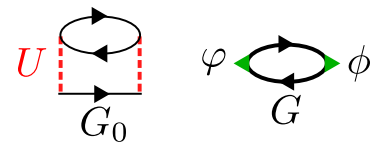

FIG. 9. Illustration of our weak-coupling theory. Left: second-order self-energy diagram comprising the dynamical part of the self-energy, formulated in terms of the bare fermionic propagator [Eq. (33)]. Right: generalized (Kubo) bubble approximation for two-particle correlation functions, formulated in terms of the "dressed" Green's function [Eq. (47)].
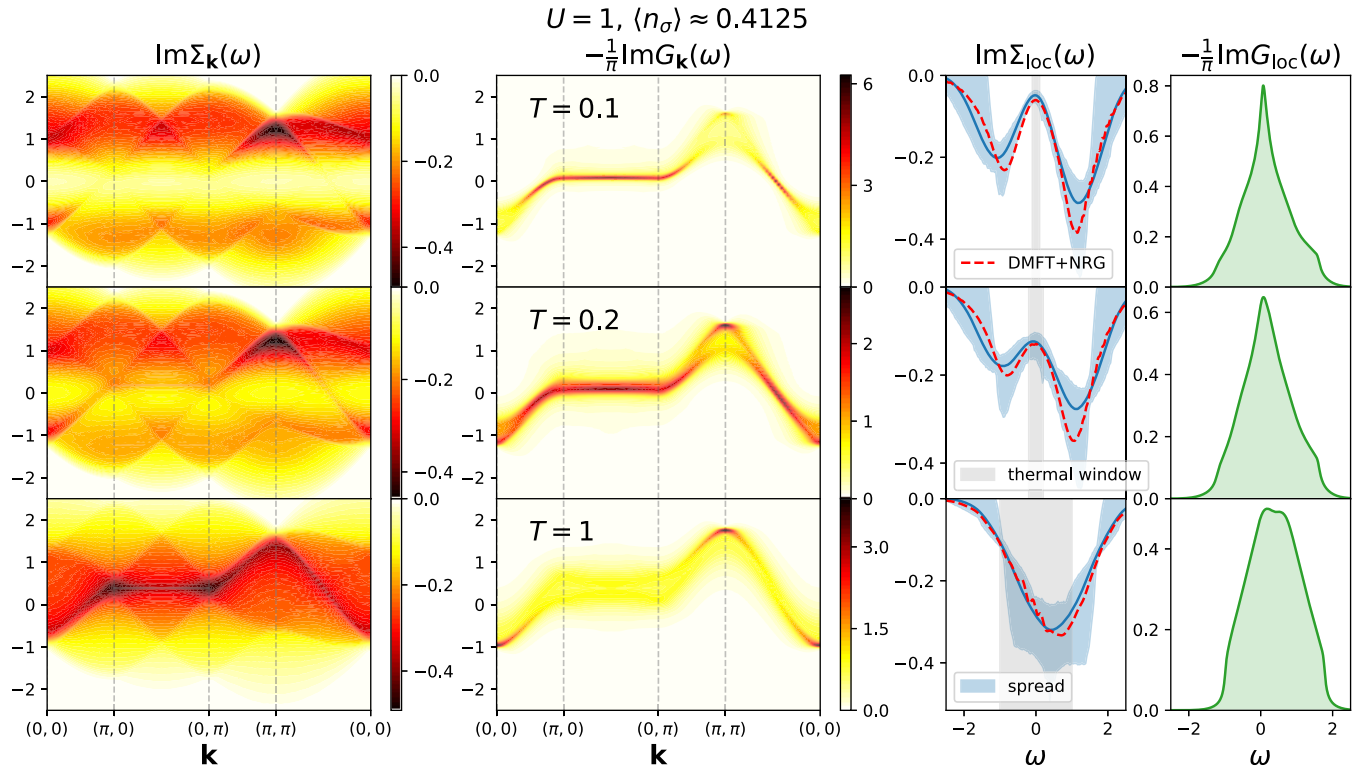
FIG. 10. Moderate coupling, moderate doping, various temperatures. Self-energy at the level of second-order perturbation theory, and the corresponding Green's functions. Third column: blue line is the local self-energy; blue shading is the **k** spread, i.e., the range of values of $\mathrm{Im}\Sigma_\mathbf{k}$ at the given real frequency ω; red line DMFT (NRG) result for local self-energy; gray shading is the thermal window, denoting $\omega \in [-T, T]$. Rightmost column: the local density of states.

As we will see, for the practical calculations of conductivity in the limit $U \to 0$, the Hartree shift vanishes. At a finite U, we absorb the Hartree shift in the chemical potential, i.e., $\mu \to \mu - U\langle n_\sigma \rangle$. This means that at a finite U, we compute the second-order self-energy diagram with Hartree-shifted propagators. Therefore, the frequency dependence of the dynamical part of the self-energy does not change with increasing U, if $\tilde{\mu} = \mu - U\langle n_\sigma \rangle$ is kept fixed. In practice, we compute the occupancy *a posteriori*, and infer μ from $U\langle n_\sigma \rangle$ and $\tilde{\mu}$. The other possibility is to compute the self-energy diagram using bare propagators. The difference between the two approaches disappears when higher-order diagrams are also computed (under the condition that both series converge), as well as in the $U \to 0$ limit.

We show examples of the self-energy results in Fig. 10. It is interesting that at low temperature, the frequency dependence of the self-energy generally features two peaks, while at high temperature, it features a single peak. At the highest temperatures, the peak follows the shape of the electron dispersion.

In Fig. 11 we zoom in on the low-frequency part, along a high-symmetry path in the BZ. We see that the scaling with ω around $\omega = 0$ takes different forms depending on **k** and parameters of the model. The most interesting is the half-filling case, where we see that $\mathbf{k} = (\pi, 0)$ and $\mathbf{k} = (\frac{\pi}{2}, \frac{\pi}{2})$ are special points where in the $T \to 0$ limit one approaches $\mathrm{Im}\tilde{\Sigma}(\omega \to 0) \sim |\omega|^\alpha$ with $\alpha \approx \frac{4}{5}$ and $\alpha = 1$, respectively. More precisely, the linear scaling $\alpha = 1$ is observed along the path connecting $(0, \pi)$ and $(\pi, 0)$, but is modified abruptly to $\alpha \approx \frac{4}{5}$ at those points. The linear scaling has been noted

before [27]. However, the apparent $T \to 0$ limit of our second-order self-energy should only apply in the strict $U \to 0$ limit. At any finite coupling and low enough temperature, higher perturbation orders will play a role, and produce an insulating state [28–31].

We also note a large number of kinks in the frequency dependence of $\mathrm{Im}\tilde{\Sigma}$. The prominent peaks that appear at high temperature are not smooth: at the maximum no derivatives appear to be well defined.

2. Green's function and compressibility

Once we have the self-energy, we can plug it in the expression for the Green's function

$$G_\mathbf{k}(\omega) = \frac{1}{\omega - \varepsilon_\mathbf{k} - \Sigma_\mathbf{k}(\omega)}. \tag{47}$$

Examples of the Green's function are shown in Fig. 10, as well as for the local density of states $-\frac{1}{\pi}\sum_\mathbf{k} \mathrm{Im}G_\mathbf{k}(\omega)$. We observe that the sharp structures in the self-energy at intermediate temperature lead to a splitting of the peak in the single-particle spectrum at $\mathbf{k} \approx (\pi, \pi)$.

Ultimately, from the Green's function we get the average density $\langle n \rangle = -\frac{2}{\pi}\int d\omega \sum_\mathbf{k} \mathrm{Im}G_\mathbf{k}(\omega)n_F(\omega)$, and from it, the charge compressibility $\chi_c = \frac{\partial \langle n \rangle}{\partial \mu}$, which will be needed to estimate the diffusion constant. At finite U, in practice, what enters the calculation is $\tilde{\mu} = \mu - U\langle n_\sigma \rangle$. It is then easiest to compute the quantity $\tilde{\chi}_c = \frac{\partial \langle n \rangle}{\partial \tilde{\mu}}$. To get to the physical charge compressibility, one uses $\chi_c = (\tilde{\chi}_c^{-1} + U/2)^{-1}$.
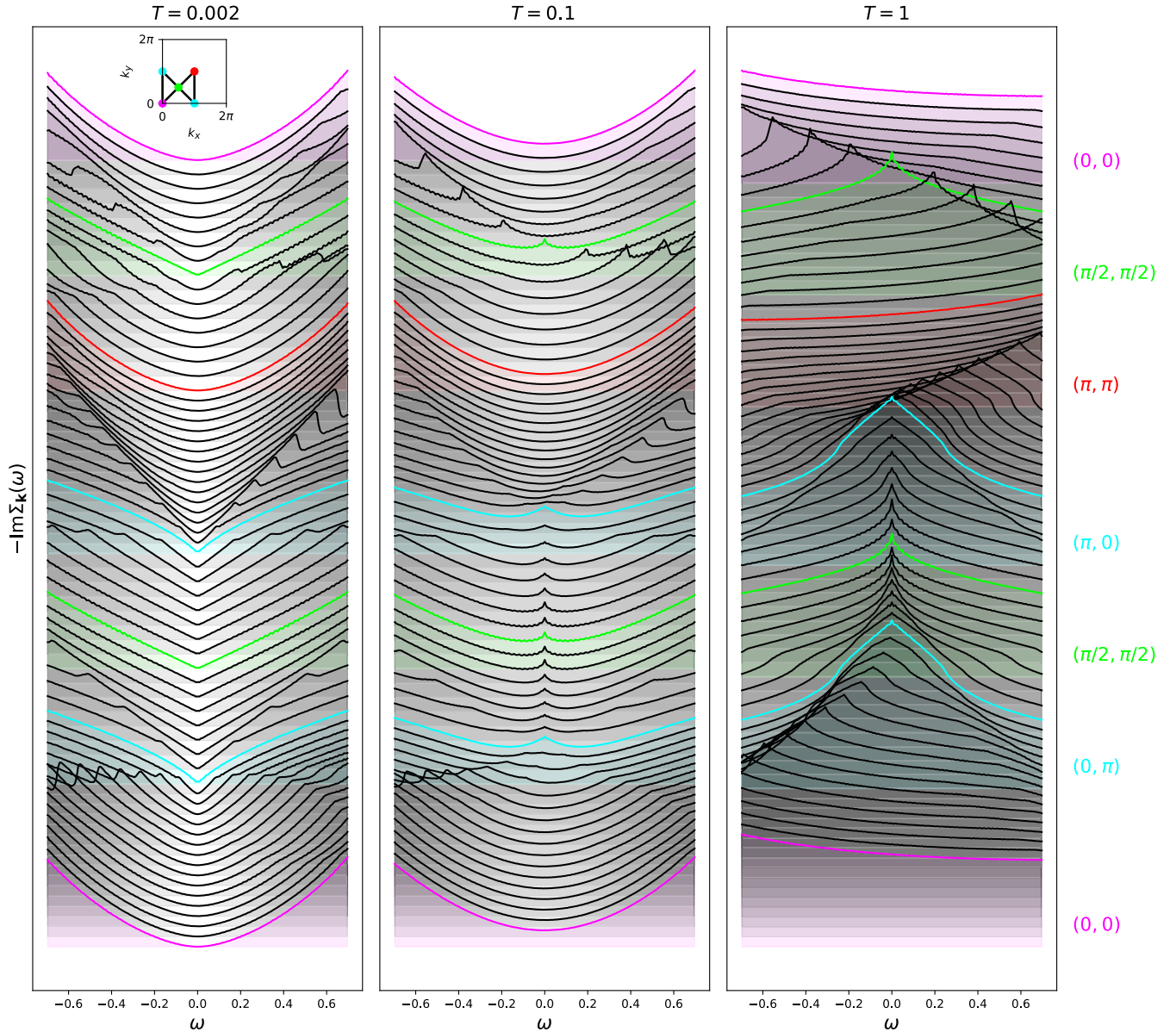
FIG. 11. Half-filling, various temperatures. Second-order self-energy along a high-symmetry path in the BZ; zoom in on low frequencies.

3. Bubble approximation for two-particle correlation functions

It is of great interest to see how the long-wavelength behavior of the charge-charge (or equivalently the current-current) correlation functions changes due to weak interactions. The simplest approach is to just calculate the bubble approximation for χ or Λ (illustrated in Fig. 9). The bubble expression is simply the real-frequency formulation of Eq. (34), with the replacement $G_0 \to G$. One obtains (under assumption that $\varphi_{\mathbf{k},\mathbf{q}}\phi_{\mathbf{k}+\mathbf{q},-\mathbf{q}}$ is purely real)

$$
\mathrm{Im}Q_{\mathbf{q}}[\varphi,\phi](\nu)
$$

$$
= \frac{2}{\pi}\sum_{\mathbf{k}}\varphi_{\mathbf{k},\mathbf{q}}\phi_{\mathbf{k}+\mathbf{q},-\mathbf{q}}\int d\omega
$$

$$
\times \mathrm{Im}G_{\mathbf{k}}(\omega)\mathrm{Im}G_{\mathbf{k}+\mathbf{q}}(\omega+\nu)[n_{\mathrm{F}}(\omega)-n_{\mathrm{F}}(\omega+\nu)], \quad (48)
$$

where 2 in front comes from the summation over spin, and $\frac{1}{\pi} = \frac{1}{\pi^2}\pi$ comes from the double Hilbert transform, and taking the delta-peak part of the integral (for detailed derivation in a more general case see Ref. [32]). We have implemented this calculation and show results below.

However, the bubble approximation is not sufficient to properly address the question of whether the hydrodynamic form for χ [Eq. (14)] or Λ [Eq. (21)] is valid at small $\mathbf{q}$. By construction, the bubble does *not* satisfy the continuity equation. The reason for this is simple: the bubble expression is *formally* an exact solution for a noninteracting system coupled to an external fermionic bath, the hybridization being the dynamical part of the self-energy. The bubble approximation for $\chi_{\mathbf{q}}(\nu)$ will therefore be manifestly wrong at $\mathbf{q} = 0$, as one will get $\chi_{\mathbf{q}=0}(\nu \neq 0) \neq 0$. Similarly, the bubble approximation for $\mathrm{Im}\Lambda_{\mathbf{q}}(\nu)$ will be manifestly wrong at $\mathbf{q} \neq 0$, $\nu \to 0$, as it will scale as $\sim \nu$, and thus signal a finite conductivity.

Clearly, if the system is open, a static wave of the electric field will scatter the incoming particles and maintain a current wave. The bubble approximations for χ and Λ do not satisfy Eq. (7), and are not connected in a simple way. To restore physical properties, one needs to include vertex corrections, even at tiny couplings.

On the other hand, the bubble approximation for $\mathrm{Im}\Lambda^{xx}_{\mathbf{q}=0}(\nu)$ will not be *a priori* unphysical, and can be considered a reasonable approximation for this object at low couplings. The parameters of the hydrodynamic model are encoded in $\mathrm{Im}\Lambda^{xx}_{\mathbf{q}=0}(\nu)$ or, equivalently, in $\sigma^{xx}_{\mathbf{q}=0}(\nu)$. One can check whether $\mathrm{Im}\Lambda^{xx}_{\mathbf{q}=0}(\nu)$ satisfies Eq. (22). However, one has to keep in mind that different theories may reduce to the same form of Λ^{xx} at $\mathbf{q}=0$. Even if $\mathrm{Im}\Lambda^{xx}_{\mathbf{q}=0}(\nu)$ satisfies Eq. (22) to a good degree, this cannot serve as proof that the hydrodynamic theory is valid. Nevertheless, assuming that the hydrodynamic theory is valid, one could use $\mathrm{Im}\Lambda^{xx}_{\mathbf{q}=0}(\nu)$ [or $\sigma^{xx}_{\mathbf{q}=0}(\nu)$] to extract the parameters for the hydrodynamic model, and investigate how they change with the microscopic parameters, which is what we will present in the following.

4. Optical conductivity in the weak-coupling limit

We distinguish here between the general weak-coupling regime (say $U < 1$) and the strict $U \to 0$ regime, i.e., the *weak-coupling limit*. To have a finite conductivity it is necessary to have scattering, so one cannot simply take $U = 0$, but must rather consider an infinitesimal U. In the weak-coupling limit, the bubble calculation for $\sigma^{xx}_{\mathbf{q}=0}(\nu)$ simplifies. In this way, one obtains the scaling of quantities in terms of U in the $U \to 0$ limit. In the following, we will distinguish between the simplified, *weak-coupling bubble*, and the *full bubble* calculations. The latter is computed for a finite U, using Eq. (48). The weak-coupling bubble is inexpensive and we use it to cover the entire phase diagram. We also perform some full bubble calculations at $U = 0.75$ and 1.0 and show results below.

The weak-coupling limit simplification of the bubble can be understood as follows. If U is sufficiently small, then the peaks in the spectral function start to resemble Lorentzians centered at $\omega = \varepsilon_{\mathbf{k}}$:

$$G_{\mathbf{k}}(\omega \approx \varepsilon_{\mathbf{k}}; U \to 0) = \frac{1}{\omega - \varepsilon_{\mathbf{k}} - i\,\mathrm{Im}\Sigma_{\mathbf{k}}(\varepsilon_{\mathbf{k}})}. \quad (49)$$

The shifts coming from $\mathrm{Re}\Sigma_{\mathbf{k}}(\omega)$ can be neglected, and $\mathrm{Im}\Sigma_{\mathbf{k}}(\omega)$ can be considered to be constant at the scale of the width of the peak. Away from $\omega \approx \varepsilon_{\mathbf{k}}$, $\mathrm{Im}G(\omega)$ can be considered zero. Furthermore, the optical conductivity is expected to be nonzero only at tiny frequencies, which also simplifies the Fermi-Dirac factor. We are ultimately able to employ the integral

$$\int dx\,\mathrm{Im}\frac{1}{x \pm iy}\mathrm{Im}\frac{1}{x \pm \Delta \pm iy} = \frac{\pi}{2y}\frac{1}{\left(\frac{\Delta}{2y}\right)^2 + 1} \quad (50)$$

which in the limit $\Delta = 0$ reduces to $\frac{\pi}{2y}$. In total we obtain

$$\sigma^{xx}_{\mathbf{q}=0}(\nu) = \sum_{\mathbf{k}} \frac{\left(v^x_{\mathbf{k}}\right)^2 n'_F(\varepsilon_{\mathbf{k}})}{\mathrm{Im}\Sigma_{\mathbf{k}}(\varepsilon_{\mathbf{k}})}\left[\left(\frac{\nu}{2\,\mathrm{Im}\Sigma_{\mathbf{k}}(\varepsilon_{\mathbf{k}})}\right)^2 + 1\right]^{-1}. \quad (51)$$

It is important to compare this expression to the Boltzmann expression for the dc conductivity (31). The two expressions do coincide, but only under the assumption that $\mathrm{Im}\Sigma_{\mathbf{k}}(\varepsilon_{\mathbf{k}})$ does *not* depend on $\mathbf{k}$, in which case one would have $\Gamma = -2\,\mathrm{Im}\Sigma_{\mathbf{k}}(\varepsilon_{\mathbf{k}})$. However, $\mathrm{Im}\Sigma_{\mathbf{k}}(\varepsilon_{\mathbf{k}})$ retains considerable $\mathbf{k}$ dependence even at infinite temperature as $\lim_{T\to\infty}\mathrm{Im}\tilde{\Sigma}_{\mathbf{k}}(\varepsilon_{\mathbf{k}}) = -\frac{\pi}{4}\sum_{\mathbf{k'q}}\delta(\varepsilon_{\mathbf{k}} - \varepsilon_{\mathbf{k+q}} - \varepsilon_{\mathbf{k'+q}} + \varepsilon_{\mathbf{k'}})$. The expression (51) presents a sum of Lorentzians of different heights and widths, and the end result might not fit well to the Lorentzian shape. Our weak-coupling theory does not *a priori* reduce to Eq. (31) or the hydrodynamic equation (24). At infinite temperature, the D and Γ we might extract from our results are *a priori* separate objects: their product $D\Gamma$ will depend on the precise form of the self-energy.

We now pull the U^2 factor out of the self-energy to obtain

$$\tilde{\sigma}^{xx}_{\mathbf{q}=0}(\tilde{\nu}) \equiv \sum_{\mathbf{k}} \frac{\left(v^x_{\mathbf{k}}\right)^2 n'_F(\varepsilon_{\mathbf{k}})}{\mathrm{Im}\tilde{\Sigma}_{\mathbf{k}}(\varepsilon_{\mathbf{k}})}\left[\left(\frac{\tilde{\nu}}{2\,\mathrm{Im}\tilde{\Sigma}_{\mathbf{k}}(\varepsilon_{\mathbf{k}})}\right)^2 + 1\right]^{-1} \quad (52)$$

with the definitions

$$\sigma(\nu = \tilde{\nu}U^2) = \frac{\tilde{\sigma}(\tilde{\nu})}{U^2}. \quad (53)$$

At low frequency, we can now equate the hydrodynamic form (24) with the above equation, to reach the following:

$$\tilde{D} = \frac{\tilde{\sigma}^{xx}_{\mathbf{q}=0}(\tilde{\nu}=0)}{\chi_c}\,, \quad D = \frac{\tilde{D}}{U^2}, \quad (54)$$

$$\tilde{\Gamma} = \delta\left(1 - \frac{\tilde{\sigma}^{xx}_{\mathbf{q}=0}(\tilde{\nu}=0)}{\tilde{\sigma}^{xx}_{\mathbf{q}=0}(\tilde{\nu}=\delta)}\right)^{-\frac{1}{2}}\,, \quad \Gamma = \tilde{\Gamma}U^2, \quad (55)$$

where we take δ small.

This result gives us the estimate of how Γ and D behave as functions of U^2, at low coupling. Additionally, one can conclude that the diffusive regime extends to shorter wavelengths as coupling is increased, i.e.,

$$q_D = \sqrt{\frac{\Gamma}{4D}} = U^2\sqrt{\frac{\tilde{\Gamma}}{4\tilde{D}}} \equiv U^2\tilde{q}_D. \quad (56)$$

The coefficients $\tilde{D}$ and $\tilde{\Gamma}$ depend on the microscopic parameters, and we extract them from $\tilde{\sigma}^{xx}_{\mathbf{q}=0}(\tilde{\nu})$, calculated by Eq. (52).

Even though $\tilde{\sigma}(\tilde{\nu})$ might not have the shape of a Lorentzian, the property $\tilde{\sigma}(\tilde{\nu} \to 0) \sim \tilde{\sigma}_{\mathrm{dc}}(1 - \tilde{\nu}^2)$ is guaranteed. Therefore, the form (24) is bound to hold at least at the lowest frequencies, and one can certainly extract the effective $\tilde{\Gamma}$ via Eq. (55). It is interesting to see in what range of frequencies will the hydrodynamic equation (24) be valid.

5. Results for dc resistivity

We first focus on the $\tilde{\rho}_{\mathrm{dc}} = 1/\tilde{\sigma}_{\mathrm{dc}}$ results. The color plot of $\tilde{\rho}_{\mathrm{dc}}$ as a function of doping and temperature is given in Fig. 12. We show the T dependence at different dopings in the upper part of Fig. 13. We see the following trends. At half-filling one observes $\tilde{\rho}_{\mathrm{dc}} \sim T$ in the full range of accessible temperatures. The high-temperature limit of Eq. (52) can be easily computed for the half-filled case based on the high-temperature asymptotic form of $\tilde{\Sigma}_{\mathbf{k}}(\varepsilon_{\mathbf{k}})$. One obtains $\tilde{\rho}_{\mathrm{dc}}(T) = 13.08T$. This appears to be the high-temperature asymptotic behavior at least at moderate dopings, as well. As one dopes away from
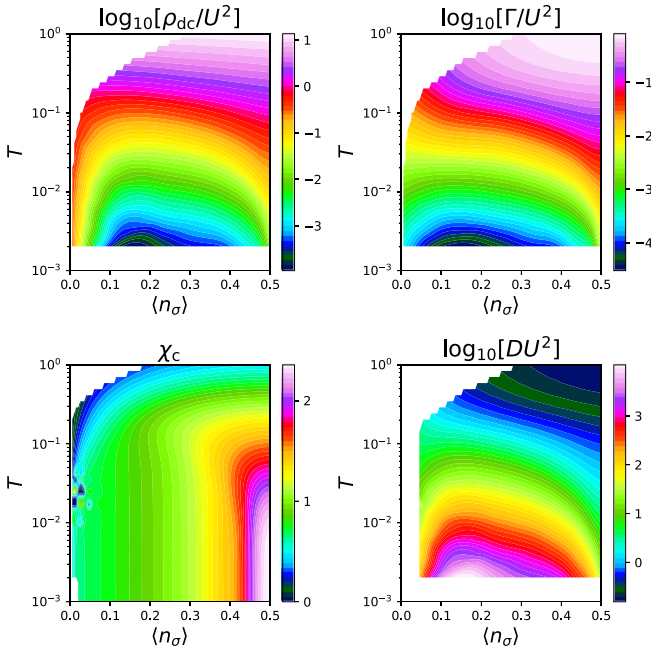
FIG. 12. Summary of weak-coupling results: doping-temperature phase diagram. Color plots of dc resistivity, diffusion constant, momentum-relaxation rate in the $U \to 0$ limit, extracted from the weak-coupling bubble calculation (52), and the corresponding noninteracting compressibility.

half-filling, a $\tilde{\rho}_{dc} \sim T^2$ (Fermi liquid, FL) regime emerges at ever higher temperatures, while the $\tilde{\rho}_{dc} \sim T$ is pushed to higher T. Starting from around $\langle n_\sigma \rangle = 0.3$, the low-$T$ regime transforms into $\tilde{\rho}_{dc} \sim T^{1.9}$. At $\langle n_\sigma \rangle = 0.15$ we no longer observe $\tilde{\rho}_{dc} \sim T$ in the accessible range of temperature, but further doping continuously reduces the exponent in the FL-like regime. At very low fillings, we again see $\tilde{\rho}_{dc} \sim T$ in the full range of T. The effective exponent α of the T dependence of resistivity can be obtained as $\alpha = \frac{\partial \ln \rho_{dc}(T)}{\partial \ln T}|_{\langle n \rangle}$ [33] and is color coded in the bottom part of Fig. 13.

It is interesting to inspect the case of fixed $\mu = -1$: this means that strictly $k_F = 0$ and all occupancy comes from thermal excitations. There we observe roughly $\tilde{\rho}_{dc} \to 0.4$ as $T \to 0$ (see Fig. 14). This can be understood as follows: at low temperature, the contribution will come from an increasingly small vicinity of $\mathbf{k} = 0$. We observe that $\text{Im}\Sigma_{\mathbf{k}=0}(\omega = 0) \sim T$. On the other hand, the velocity of electrons will decrease as temperature is lower. Ultimately, the amplitude of contributions will reduce to the integral $\int d\mathbf{k}\, k_x^2 e^{-\beta k^2} \sim \int_0^\infty dk\, k^3 e^{-\beta k^2} \sim T$. This means that the increased coherence of the electrons will be canceled exactly by their decreasing velocity, and the resistivity will converge to a constant as $T \to 0$. At μ slightly above -1 one expects the resistivity to go to 0, whereas for μ slightly below, one expects it to go to infinity.

6. Results for hydrodynamic parameters

The results for $\tilde{D}$ and $\tilde{\Gamma}$ are summarized on Fig. 12. It is apparent that roughly $\tilde{D} \sim 1/\tilde{\Gamma}$. This can be understood intuitively: the more coherent the quasiparticles, the bigger the
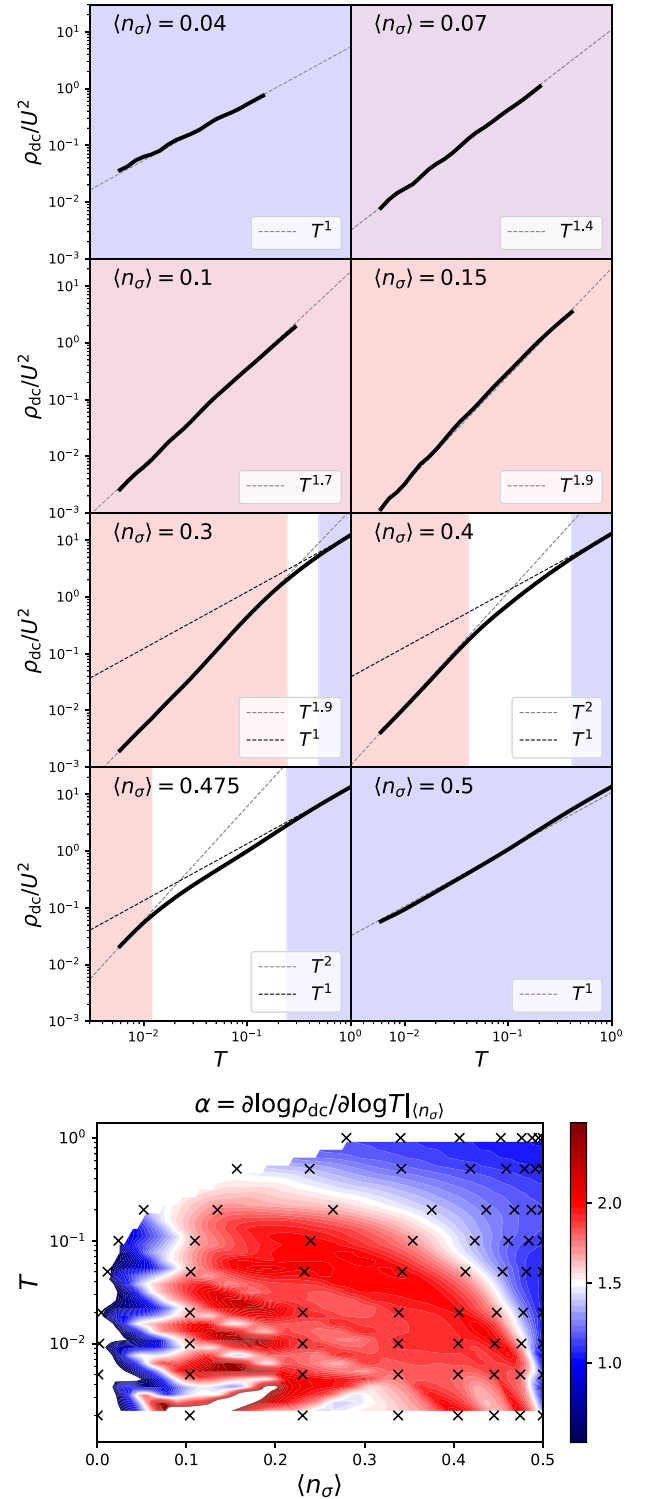

FIG. 13. Weak-coupling bubble dc resistivity results. Upper panels: temperature dependence at different dopings. Lower panel: effective exponent of the temperature dependence, color plotted in the doping-temperature plane; black crosses are actual data points: the rest are obtained by interpolation.

dc conductivity and the narrower the Drude peak. However, the inverse proportionality coefficient, i.e., $D\Gamma$ value is *a priori* unclear. We plot $D\Gamma$ in Fig. 15 and find that results approach $2t^2$ at high temperature. This is in agreement with
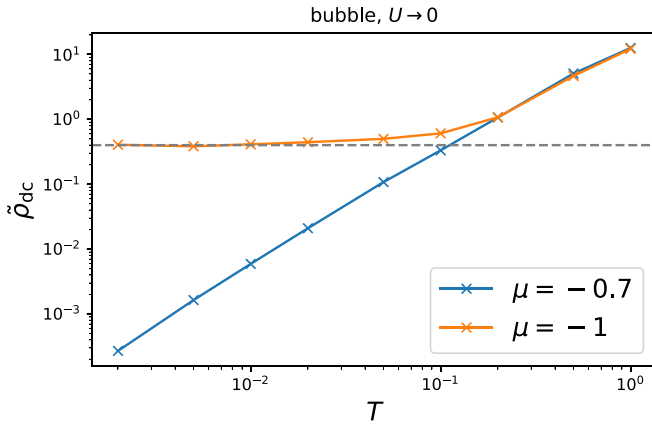
FIG. 14. Weak-coupling bubble ($U \to 0$ limit) dc resistivity results at a fixed chemical potential. Horizontal line denotes 0.4, which is the value $\rho_{\rm dc}$ apparently converges to at $\mu = -1$ and $T \to 0$.

the loose expectation based on Eq. (11), but also in agreement with the hydrodynamic theory [Eq. (30)]. We also plot the corresponding result from FTLM computed at a moderate and a strong value of coupling (strong-coupling data were reconstructed from Ref. [18]), and find a similar result. It is striking that $D\Gamma$ is within $\approx 20\%$ of $2t^2$ in a large range of temperature and even at strong coupling.

In Fig. 16 we cross-check our weak-coupling $\rho_{\rm dc}$ result based on Eq. (51) with the corresponding full bubble calculation [Eq. (48)] at $U = 1$. As expected, the agreement is better at lower temperature and lower coupling (for the latter, the data are not shown), i.e., in cases where scattering rates ${\rm Im}\tilde{\Sigma}_{\mathbf{k}}(\varepsilon_{\mathbf{k}})$ are smaller. We also compare our full bubble result to dynamical mean field theory (DMFT) [34] calculation at $U = 1$ (implemented with the numerical renormalization group, NRG, real-frequency impurity solver [14,15,32,35–38]) and surprisingly, find excellent agreement. Our second-order self-energy $\tilde{\Sigma}$ is clearly nonlocal (and remains nonlocal up to infinite temperature; see Fig. 10), yet the nonlocal part does not seem to play a big role in the value of dc resistivity. We check this explicitly by computing the bubble with only the local part of our self-energy: we find a very similar result. Moreover, the agreement with DMFT suggests that the local part of our second-order self-energy agrees well with DMFT. We confirm this in Fig. 10, especially in the thermal window $\omega \in [-T, T]$, which is the range of frequencies relevant for the conductivity calculation. We also compute the full bubble on a small 4×4 lattice. In the previous work of some of us [14], it was shown that finite-size effects subside at high temperature, and that the (4×4)-lattice FTLM calculation was correct at $T \gtrsim 0.3$. However, this was at the value of coupling $U = 2.5$; we now see similar lack of finite-size effects even at $U = 1$, which is somewhat unexpected (at a lower U the relevant correlation lengths should be greater, and the systematic errors due to finite system size more pronounced). Comparing our full bubble result for $\rho_{\rm dc}$ at $U = 1$ with the FTLM result at $U = 1.25$ we can conclude that the vertex corrections are still sizable, and affect the result in a similar fashion as at $U = 2.5$, i.e., the vertex corrections present a roughly constant shift towards lower resistivity.

We compare D and Γ obtained from the weak-coupling bubble at $U = 0.65$ [Eqs. (54) and (55)] to the FTLM result at $U = 1.875$ and 1.25 and find surprising similarity (see Fig. 17). As was already apparent from Refs. [14,18], the bubble approximation tends to overestimate $\rho_{\rm dc}$ (i.e., underestimate D) and overestimate Γ. This explains the apparent agreement between the weak-coupling bubble approximation and the numerically exact result at strong coupling. However, up to a prefactor, even our weak-coupling bubble results for $\tilde{D}(T)$ and $\tilde{\Gamma}(T)$ display a shape very similar to the FTLM result at $U = 1.875$. The behavior of the hydrodynamic parameters does not seem to change drastically going from weak to rather strong coupling. At a fixed temperature $T = 0.5$, the weak-coupling $\Gamma \sim U^2$ and $D \sim 1/U^2$ trends slow down at stronger coupling, so that the difference in Γ and D between $U = 1.25$ and 1.875 results is rather small. The full bubble computed at $U = 0.75$ improves the result of the weak-coupling bubble. It appears that in the strong-coupling limit, $D \to 2t$, and roughly $\Gamma \to t$, which is consistent with $\lim_{U \to \infty} D\Gamma \approx 2t^2$.

7. Deviations from the Lorentzian Drude peak

As for the frequency range of the validity of Eq. (24), i.e., the hydrodynamic form for the current-current correlation function (22): it strongly depends on the microscopic parameters. At high temperature the agreement is excellent up to the peak of ${\rm Im}\Lambda(\nu)$, but, as expected, the high-frequency tail has a different scaling. This is shown in Fig. 18 where we compare a fitted equation (22) with the result of the full bubble calculation (48).

8. Critical wavelength for diffusive behavior

Finally, we go back to the simple prediction (56) that the characteristic wavelength for diffusive behavior will become shorter with increasing coupling. We check this directly in our $\chi_{\mathbf{q}}(\nu)$ results. As already mentioned, the bubble approximation is unsuitable for the investigation of χ at very long wavelengths, but one might still want to inspect the results at somewhat bigger $\mathbf{q}$. In Fig. 19 we show the ${\rm Im}\chi_{\mathbf{q}}(\nu)$ results at a fixed $\mathbf{q} = (0.159, 0)\pi$, and vary the coupling. The corresponding $\langle n_{\mathbf{q}}(t) \rangle$ results calculated via Eq. (13) are presented on the panel on the right. For the occupancy $\langle n_\sigma \rangle \approx 0.4125$ and $T = 0.2$, our weak-coupling bubble calculation yields $\tilde{q}_D = \sqrt{\frac{\Gamma}{4\tilde{D}}} \approx 0.15\pi$, which means that the behavior should become diffusive at wave vector $\mathbf{q} \approx (0.15\pi, 0)$ at around $U = 1$. This is in excellent agreement with the result we obtain directly from the full bubble approximation for χ, as evidenced by Fig. 19, panel on the right. Here we have plugged the full bubble result for $\chi_{\mathbf{q}}(\nu)$ in the linear-response theory expression for the CDW amplitude $n_{\mathbf{q}}(t)$ [Eq. (13)].

C. Strong coupling

We focus now on quantum Monte Carlo (QMC) results for the charge-charge and current-current correlation functions. We make use of the continuous-time interaction-expansion QMC, CTINT [21]. This method is numerically exact for a given lattice size. We calculate the intersite $\chi_{ij}(i\nu)$ on the Matsubara frequency axis for a cyclic lattice of size $L \times L$ and
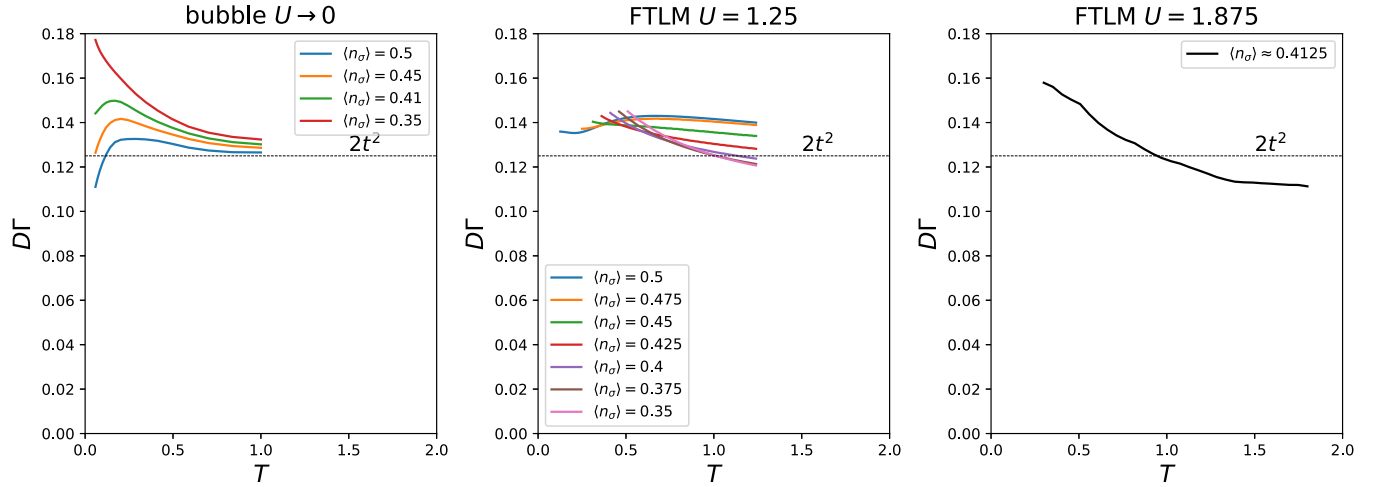
FIG. 15. Weak-coupling bubble ($U \to 0$ limit) in comparison with moderate and strong coupling. At weak coupling, D and Γ are computed using Eqs. (55) and (54) at various dopings. At moderate and strong coupling, FTLM result is the best available result. At strong coupling, data are reconstructed from Ref. [18], but only for a single doping.

then perform a periodization procedure, where we promote the intersite components to the real-space components of an infinite lattice, and thus obtain $\chi_\mathbf{r}(i\nu)$ of a finite range (components at $\mathbf{r} : r_\eta > L/2$ are considered 0). We then Fourier transform to obtain $\chi_\mathbf{q}(i\nu)$ with arbitrary resolution in the BZ. However, very short $\mathbf{q}$ vectors corresponding to wavelengths much greater than L remain inaccessible. Nevertheless, we are able to obtain solid results for wavelengths up to 20 lattice spacings and that way cover the range of wavelengths studied in the cold-atom experiment by Brown *et al.* [18]. We perform the exact same procedure for Λ^{xx} as well.
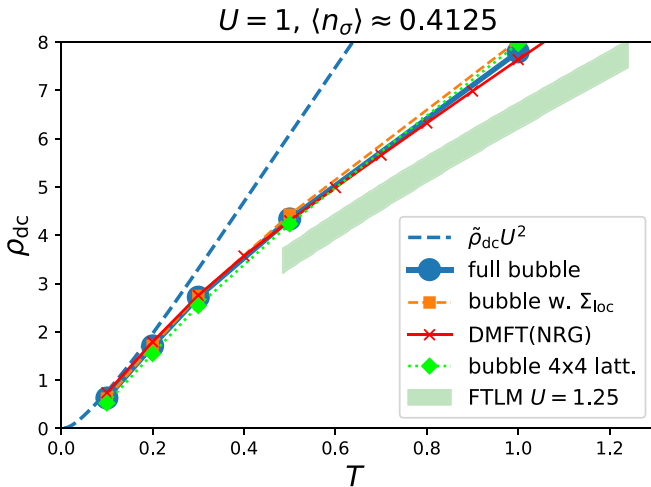

FIG. 16. Moderate coupling $U = 1$, moderate doping, results for dc resistivity. Dashed blue: weak coupling bubble. Blue line and dots: full bubble calculation. Orange dashed and squares: full bubble calculated with only the local component of self-energy. Red with crosses: full bubble with the local DMFT(NRG) self-energy result. Lime dotted with diamonds: full bubble computed on a 4×4 lattice with the full $\mathbf{k}$-dependent second-order self-energy. Green stripe: FTLM 4×4 result at a larger coupling $U = 1.25$ (including the vertex corrections).

We perform a finite-size scaling analysis and observe that no obvious trends with L are apparent in the results already between $L = 4$ and 10 (data not shown). This is consistent with the estimates from the recent Ref. [39] where it was shown in a thermodynamic limit DiagMC calculation that the charge correlations are short ranged, with values becoming very small already at distances of about 5 lattice spacings. In our calculations, we consider the statistical errors to be the leading uncertainty, and use the $L = 10$ results to perform analyses.

As already mentioned, it would make no sense to compare the hydrodynamic law to imaginary-axis data because the hydrodynamic law predicts an unphysical asymptotic behavior of the current-current correlation function. To be able to compare the hydrodynamic theory with our Matsubara-frequency results, we propose a modified hydrodynamic form

$$\mathrm{Im}\,\chi_\mathbf{q}^{\mathrm{mh}}(\nu) = \mathrm{Im}\,\chi_\mathbf{q}^{\mathrm{hyd}}(\nu)[1 + L(\nu; a, b, c)]n_\mathrm{F}(\nu - C; \beta_{\mathrm{art}}),$$

(57)

where χ^{hyd} denotes the form in Eq. (14), $L(\nu; a, b, c) = a \exp[-(\ln\nu - b)^2/c^2]$ is the log-normal distribution, and $n_\mathrm{F}(\omega; \beta) = \frac{1}{e^{\beta\omega}+1}$ is the Fermi-Dirac distribution function. The $1 + L$ part here is necessary to introduce high-frequency excitations to and from the upper Hubbard band, which are expected in the doped Mott insulator regime. The Fermi-Dirac distribution function facilitates the exponential cutoff at high frequency. This modified hydrodynamic form thus has five additional parameters: a, b, c are the amplitude, position, and width of the Hubbard peak, respectively, and C and β_{art} are the cutoff frequency and the artificial temperature determining the rate at which the spectral weight is exponentially suppressed at cutoff. We make sure that β_{art} is small enough so that $n_\mathrm{F}(-C, \beta_{\mathrm{art}}) \approx 1$. Our choice of $\mathrm{Im}\,\chi_\mathbf{q}^{\mathrm{mh}}(\nu)$ ensures $\sim 1/\nu^2$ Matsubara-axis asymptotic behavior for Λ^{xx}. The prefactor of the asymptotic behavior will in general depend on the parameters $a, b, c, C, \beta_{\mathrm{art}}$.

We now check whether the modified hydrodynamic form (57) is consistent with the available CTINT and FTLM data.
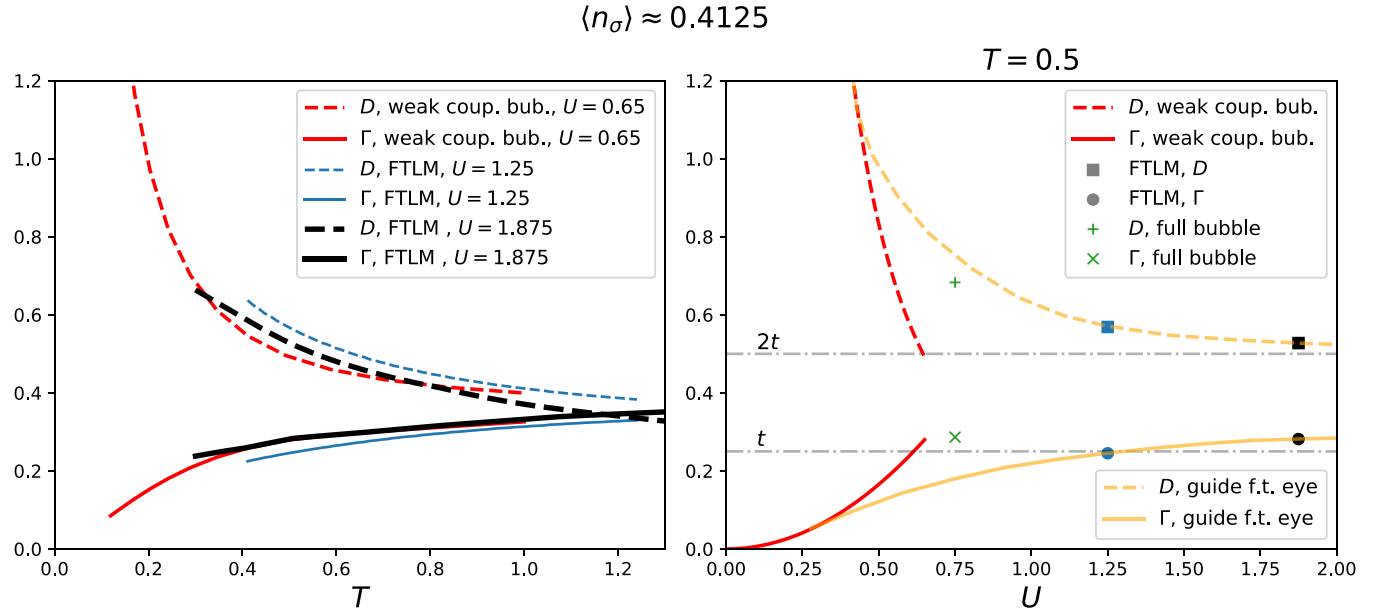
FIG. 17. Left panel: Temperature dependence of D and Γ in the weak-, moderate-, and strong-coupling regimes. Right panel: Coupling dependence of Γ and D, as obtained from the weak-coupling bubble, full bubble, and FTLM. The orange lines are guides for the eye, a possible scenario connecting results in the weak- and moderate- to strong-coupling regimes.

We first hand-pick the parameters so that the FTLM result for the optical conductivity is reproduced. It is noteworthy that we can get a very good fit to FTLM data, and that the shape of the high-frequency peak is roughly a log-normal distribution. We then compare the resulting $\chi_{\mathbf{q}}^{\mathrm{mh}}(i\nu)$ and the corresponding $\Lambda^{xx,\mathrm{mh}}$ [obtained via Eq. (10)] to CTINT data. We find solid agreement, as shown in the upper part of Fig. 20.

In the lower part of Fig. 20 we illustrate how fitting the Matsubara data to a hydrodynamic law without the high-frequency peak will yield wrong results for D and Γ, even if a

FIG. 18. Moderate coupling, moderate doping. Full lines: full bubble result [Eq. (48)] for the uniform ($\mathbf{q} = 0$) longitudinal current-current correlation function. Dashed lines: hydrodynamic form (22) fitted at $\nu \to 0$.

proper high-frequency cutoff is used. We do a fully unbiased fit of $\chi_{\mathbf{q}}^{\mathrm{mh}}(i\nu)$ (with $a, b, c = 0$ and β_{art} fixed to 0.3, D, Γ χ_c, C free), to reproduce at the same time χ and Λ CTINT results at five small $\mathbf{q}$ vectors. We get an excellent fit, but we get completely wrong values for D and Γ. The optical conductivity contains two peaks, and fitting with only a single peak will compensate by making this one peak wider and shorter, thus underestimating D and overestimating Γ. Figure 20 nicely illustrates the difficulty of analytical continuation: the fit function on the imaginary axis is almost indistinguishable between the top and bottom rows, yet corresponds to drastically different optical conductivity.

In Fig. 21 we show the $\langle n_{\mathbf{q}}(t) \rangle$ curves, corresponding to χ^{mh} parameters from the upper part of Fig. 20. Comparing to the corresponding pure hydrodynamic law χ^{hyd} [Eq. (21)], we find no visible difference: the inability of the hydrodynamic law to describe high-frequency features of χ are unlikely to have affected the fitting procedure in Ref. [18].

IV. DISCUSSION AND PROSPECTS

Our work builds on the milestone study of charge fluctuations in the Hubbard model by Hafermann *et al.* [23]. In that work, the noninteracting charge-charge correlation function was calculated, but only at half-filling, and with a relatively low resolution: the striking two-linear-modes feature that we observe at finite doping was, therefore, overlooked. More importantly, the Matsubara data were fitted to a law which only allows for a linear mode at long wavelengths, which may not be appropriate. In light of more recent experimental evidence, and on general physical grounds, the emergence of diffusive behavior and a quadratic mode around $\mathbf{q} = 0$ is expected. Furthermore, in the work by Hafermann *et al.*, vertex corrections had unlimited range, but were calculated as a diagrammatic extension of DMFT [40], which introduces
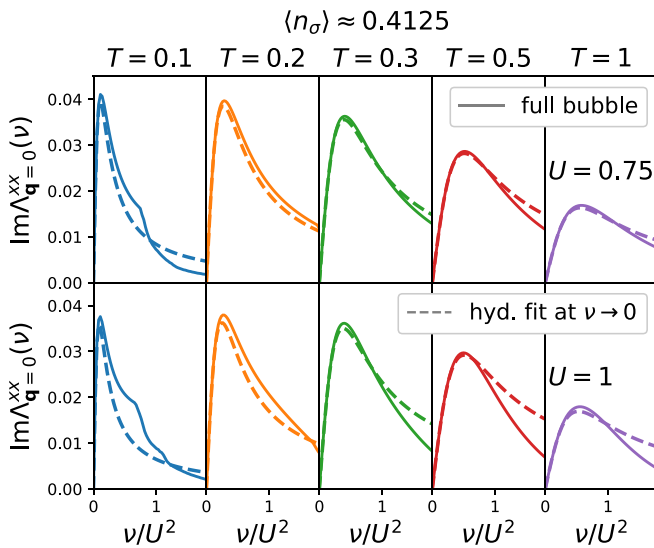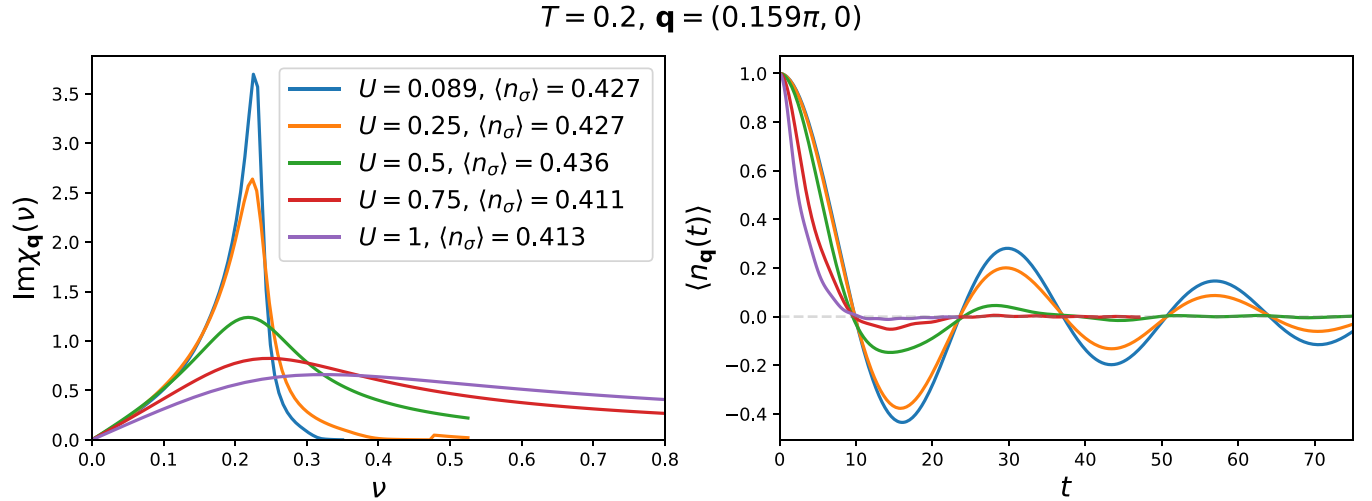
$$T = 0.2, \ \mathbf{q} = (0.159\pi, 0)$$

FIG. 19. Weak to moderate coupling, moderate doping, moderate temperature. Left: full bubble calculation [Eq. (48)] for the charge-charge correlation function at a fixed wave vector at different values of coupling. Right: corresponding CDW amplitude vs time curves [Eq. (13)]. Prediction based on Eq. (56) for this doping and temperature is that $q_D(U = 1) \approx 0.15\pi$, in agreement with the data in the plot on the right.

systematic errors. By using CTINT at 10×10 lattice size, we capture complete vertex corrections up to a medium range, yet the finite-size effects in our theory are unlikely to have introduced significant systematic error. Finally, Hafermann *et al.* have derived numerous useful identities relevant for charge-charge and current-current correlation function. However, the fully general equation (7) may have been overlooked so far.

Our weak-coupling calculation is complementary to the semiclassical Boltzmann equation approach of Kiely and Mueller [16]. It is not clear that either of the two approaches yield exact results, even in the $U \to 0$ limit, thus it is important to cross-check the results and look for robust, shared features. Indeed, our results at low dopings are in excellent qualitative agreement with the Boltzmann equation: we observe linear resistivity at half-filling and an emerging T^2 at low temperature as one dopes away from half-filling. However, there is a significant quantitative difference in the values of $\tilde{\rho}_{dc}$. The Boltzmann equation predicts the high-temperature asymptotic behavior $\tilde{\rho}_{dc} = 0.076(T/t) = 0.304(T/4t)$ while our Kubo bubble theory yields $\tilde{\rho}_{dc} = 13.08(T/4t)$. The difference is nearly two orders of magnitude. Comparing to numerically exact FTLM result at $U = 1.25$, it is clear that our extrapolated $U \to 0$ theory strongly overestimates ρ_{dc} at high temperature (see Fig. 16). However, the coefficient for the linear high-T asymptotics is overestimated by a factor of 2–3, at most. Furthermore, we can compute the bubble result at a finite coupling to obtain much better results, the relative error unlikely being more than 30%–40% in the relevant range of temperature. The Boltzmann theory result extrapolated to $U = 1.25$, on the other hand, would be barely visible on the scale of Fig. 16. Our bubble theory appears to give results in significantly better agreement with the reference FTLM solution. There is also a striking qualitative difference in the $\rho_{dc}(T)$ at large doping. At $\langle n_\sigma \rangle = 0.1$ Kiely and Mueller observe an exponential drop of resistivity at low temperature, in sharp contrast to our observations. Their finding was argued to be due to frustration of umklapp scattering. It is possible

that, in our approach, vertex corrections are needed to observe this phenomenon. Further work is necessary to fully resolve the origin of this discrepancy. Finally, our approach allows us to compute the full optical conductivity, and estimate D and Γ as separate objects, which, to the best of our understanding, could not have been done in their work. To our understanding, Γ was extracted from D, *assuming* the validity of the Boltzmann expression for conductivity [Eq. (31)]. The analysis based on the asymptotic behavior of $\chi_{\mathbf{q} \to 0}(i\nu)$ that shows that the hydrodynamic theory [Eqs. (3) and (4)] is consistent with Eq. (31) may have been previously overlooked.

Our analysis of the equation of motion for the current [Eq. (11)], as well as our numerical results displaying $D\Gamma = 2t^2$ at weak coupling and high temperature (Fig. 15) provide some microscopic evidence for the validity of the hydrodynamic theory proposed in Ref. [18]. Also, our Fig. 19 provides some support for $q_D = \sqrt{\Gamma/4D}$ which is a specific property of the hydrodynamic theory [Eqs. (3) and (4)]. However, the definite answer to the questions raised in this paper will have to come from more sophisticated methods. It is essential to formulate the theory in real frequency and at the same time treat the thermodynamic limit and the vertex corrections. The recently developed real-frequency diagrammatic Monte Carlo (RFDiagMC) [41–45] is a clear candidate, and our Kubo bubble and second-order self-energy theory is the first step in this approach. Very recently, RFDiagMC was used to calculate the charge-charge correlation function in a slightly different model, at very weak coupling [46]. Pushing RFDiagMC to stronger coupling [45,47–50] and higher resolution necessary to investigate the hydrodynamic behavior in the regime relevant for cold-atom experiments is a difficult task that we leave for future work.

Finally, it is important to view our T-linear-resistivity result in the $U \to 0$ limit in light of the very recent work by Xu *et al.* [51]. In this work, a quantum critical line is observed to pass through $U = 0$, $\langle n_\sigma \rangle = 0.5$, separating two distinct ordered phases in the ground-state (δ, U) phase diagram of the Hubbard model. This is in line with our observation that

$U = 1.875,\ T = 0.4,\ \langle n_\sigma \rangle \approx 0.4125,\ D = 0.59,\ \Gamma = 0.29,\ C = 4.00,\ \beta_{\text{art}}^{-1} = 0.30,\ a = 6.50,\ b = 0.70,\ c = 0.48$

$U = 1.875,\ T = 0.4,\ \langle n_\sigma \rangle \approx 0.4125,\ D = 0.24,\ \Gamma = 1.18,\ C = 3.54,\ \beta_{\text{art}}^{-1} = 0.3,\ a, b, c = 0$
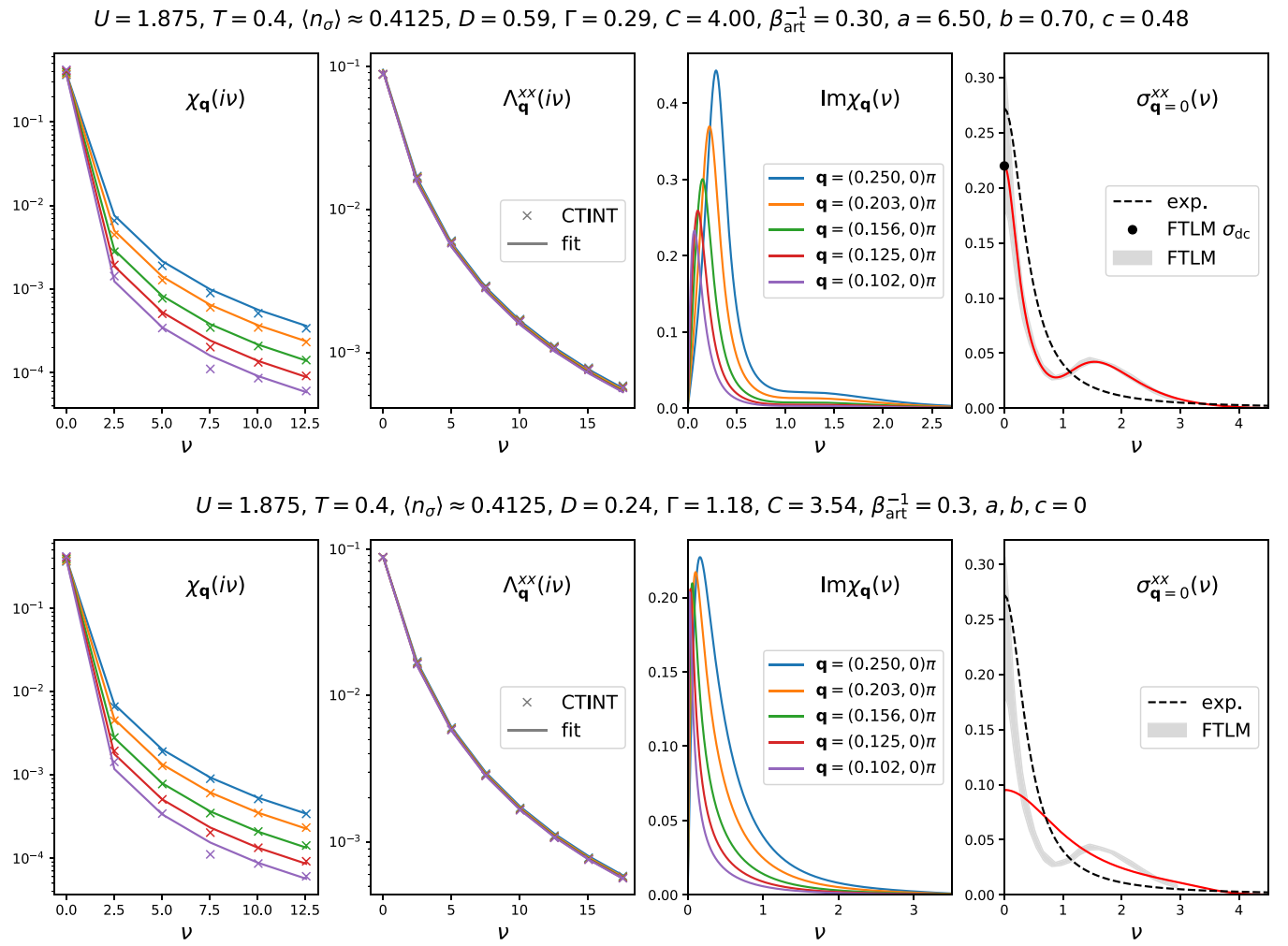

FIG. 20. Strong coupling, moderate doping, and temperature. Upper panels: modified hydrodynamic law with parameters hand-picked to reproduce FTLM result for optical conductivity (rightmost panel, gray stripe, and black dot); two panels on the left: comparison of the modified hydrodynamic law the with corresponding CTINT results for the Matsubara-axis charge-charge and current-current correlation functions; third panel: corresponding real-frequency charge-charge correlation function. Lower panels: unbiased fit of the modified hydrodynamic law without the high-frequency peak to the CTINT charge-charge and current-current correlation functions, simultaneously. The result has a strong bias for the values of D and Γ.
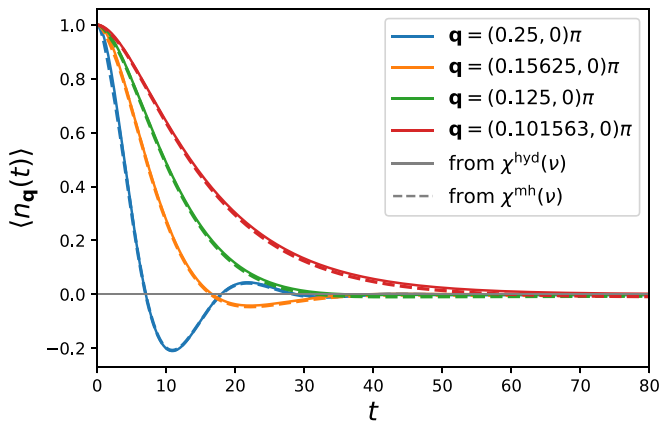

FIG. 21. CDW amplitude vs time curves, corresponding to the modified hydrodynamic law from the upper panels of Fig. 20, compared to the original hydrodynamic law [Eq. (14)] with the same D and Γ.

the charge-charge and spin-spin susceptibilities diverge at $\mathbf{q} = (\pi, \pi)$ as $T \to 0$ at $U = 0$, $\mu = 0$ (see Appendix F). The hypothesis considered in many works [8] is that linear resistivity is expected above quantum critical points. The linear resistivity that we observe may, indeed, be intimately linked to instability towards order, i.e., a degeneracy of the ground state at $U \to 0$ at half-filling. The van Hove singularity at the Fermi level perhaps does not play the essential role here, in contrast to the conclusions in Ref. [17]. Whether resistivity remains linear all the way down to zero temperature when Fermi level is at a van Hove singularity in the density of states, regardless of any ordering instabilities, is currently unclear.

V. CONCLUSIONS

We have studied charge fluctuations and transport in the Hubbard model. In the noninteracting limit, charge fluctuations are anisotropic, and can have multiple linear modes at long wavelengths. Near the empty limit, the charge spectral

function resembles that of the electron. At weak coupling, the self-energy presents several peculiar behaviors, including an abundance of kinks in the frequency dependence. At low temperature we generally find two peaks in $\text{Im}\Sigma_{\mathbf{k}}(\omega)$ at any $\mathbf{k}$. At half-filling and $T \to 0$, we find $\text{Im}\Sigma_{\mathbf{k}=(0,\pi)}(\omega) \sim |\omega|^{4/5}$ and, along the Fermi surface, $\text{Im}\Sigma_{\mathbf{k}=(0,\pi)\leftrightarrow(\pi,0)}(\omega) \sim |\omega|$, the latter being in agreement with previous work [27]. As temperature is raised, a sharp peak in $\text{Im}\Sigma_{\mathbf{k}}(\omega)$ rises at low frequency, splitting the quasiparticle peak in $\text{Im}G_{\mathbf{k}}(\omega)$ at around $\mathbf{k} = (\pi, \pi)$. At high temperature, we find that self-energy has a single peak as a function of frequency at around $\omega = \varepsilon_{\mathbf{k}}$, and it is not smooth. We observe that the dc resistivity is linear at half-filling and at high temperature, in agreement with recent findings [16]. Surprisingly, nonlocal self-energy components are found to have little effect on dc resistivity. Precisely at the band insulator transition, our bubble approximation predicts a finite resistivity at $T \to 0$, coming as a consequence of perfect cancellation of the reducing velocity and scattering rate, both scaling as T. We observe that the hydrodynamic parameters (diffusion constant and momentum relaxation rate) are roughly inversely proportional, in the bubble approximation at weak coupling, as well as in the numerically exact FTLM result at strong coupling. Their product appears to be $D\Gamma \approx 2t^2$, which coincides with one term in the microscopic equation of motion for the current, indicating that other terms might play less of a role. This supports the hydrodynamic theory, for which we show that it must satisfy $D\Gamma = 2t^2$ at weak coupling and high temperature. Finally, we propose a modified hydrodynamic law that has correct behavior at high frequency, and find that it is consistent with both the numerically exact FTLM and the numerically exact CTINT. Our results provide some evidence that the hydrodynamic theory is correct, but further work with better methods is needed to fully resolve this issue.

APPENDIX A: CONTINUITY EQUATION ON THE LATTICE

We start by noting the general expression for the time derivative of a bosonic operator $\mathcal{O}$ in the Heisenberg picture

$$\partial_t \mathcal{O}(t) = \partial_t e^{itH} \mathcal{O} e^{-itH}$$
$$= i[H, \mathcal{O}]. \tag{A1}$$

We will also need the general expression for commutators of the following general form, with $a^\dagger, b, c^\dagger, d$ fermionic creation and annihilation operators

$$[a^\dagger b, c^\dagger d] = \delta_{bc} a^\dagger d - \delta_{ad} c^\dagger b. \tag{A2}$$

This can be proven simply by using $[AB, C] = A[B, C] + [A, C]B$, $[A, BC] = B[A, C] + [A, B]C$, and therefore $[AB, CD] = A(C[B, D] + [B, C]D) + (C[A, D] + [A, C]D)B$.

Using these we can then show

$$\partial_t n_{\mathbf{r}}(t) = i[H_{\text{kin}}, n_{\mathbf{r}}] = -it \left[\sum_{\sigma',\mathbf{r}',s\in\{1,-1\},\eta\in\{x,y\}} c^\dagger_{\sigma',\mathbf{r}'} c_{\sigma',\mathbf{r}'+s\mathbf{e}_\eta}, \sum_\sigma c^\dagger_{\sigma,\mathbf{r}} c_{\sigma,\mathbf{r}} \right]$$

$$= -it \sum_{\sigma,s\in\{1,-1\},\eta\in\{x,y\}} ([c^\dagger_{\sigma,\mathbf{r}} c_{\sigma,\mathbf{r}+s\mathbf{e}_\eta}, c^\dagger_{\sigma,\mathbf{r}} c_{\sigma,\mathbf{r}}] + [c^\dagger_{\sigma,\mathbf{r}-s\mathbf{e}_\eta} c_{\sigma,\mathbf{r}}, c^\dagger_{\sigma,\mathbf{r}} c_{\sigma,\mathbf{r}}])$$

$$= -it \sum_{\sigma,s\in\{1,-1\},\eta\in\{x,y\}} (-c^\dagger_{\sigma,\mathbf{r}} c_{\sigma,\mathbf{r}+s\mathbf{e}_\eta} + c^\dagger_{\sigma,\mathbf{r}-s\mathbf{e}_\eta} c_{\sigma,\mathbf{r}}) = -\sum_{\eta\in\{x,y\}} (j^\eta_{\mathbf{r}} - j^\eta_{\mathbf{r}-\mathbf{e}_\eta}) \tag{A3}$$

with the definition $j^\eta_{\mathbf{r}} = it \sum_\sigma (c^\dagger_{\sigma,\mathbf{r}+\mathbf{e}_\eta} c_{\sigma,\mathbf{r}} - c^\dagger_{\sigma,\mathbf{r}} c_{\sigma,\mathbf{r}+\mathbf{e}_\eta})$. The expression $\sum_{\eta\in\{x,y\}} (j^\eta_{\mathbf{r}} - j^\eta_{\mathbf{r}-\mathbf{e}_\eta})$ is the lattice version of the divergence of current.

We can express the continuity equation in momentum space by Fourier transform of both sides

$$\partial_t n_{\mathbf{q}} = i[H, n_{\mathbf{q}}] = -\sum_{\eta\in\{x,y\}} (1 - e^{iq_\eta}) j^\eta_{\mathbf{q}}, \tag{A4}$$

where $n_{\mathbf{q}} = \sum_{\mathbf{r}} e^{i\mathbf{q}\cdot\mathbf{r}} n_{\mathbf{r}} = \sum_{\mathbf{k}} c^\dagger_{\mathbf{k}+\mathbf{q}} c_{\mathbf{k}}$. Notice that we distinguish between $n_{\mathbf{k}} = c^\dagger_{\mathbf{k}} c_{\mathbf{k}}$ and $n_{\mathbf{q}}$ solely by the choice of the symbol in the subscript.

APPENDIX B: CONNECTION BETWEEN THE CHARGE-CHARGE AND CURRENT-CURRENT CORRELATION FUNCTIONS

Here we make use of the general equation of motion

$$z^2 \langle\langle A; B \rangle\rangle_z = -z \langle [A, B] \rangle - \langle [[A, H], B] \rangle + \langle\langle [A, H]; [H, B] \rangle\rangle_z,$$
(B1)

where we denote with $\langle\langle A; B \rangle\rangle_z$ the correlator of operators A and B as a function of complex frequency z. The full derivation of Eq. (B1) is given in Appendix D.

If we replace $A = n_{\mathbf{q}}$ and $B = n_{-\mathbf{q}}$, and using $[A, H] = -[H, A]$ and $1/i = -i$ we get

$$z^2 \langle\langle n_{\mathbf{q}}; n_{-\mathbf{q}} \rangle\rangle_z = -z \langle [n_{\mathbf{q}}, n_{-\mathbf{q}}] \rangle + i \sum_{\eta \in \{x,y\}} (1 - e^{iq_\eta}) \langle [j_{\mathbf{q}}^\eta, n_{-\mathbf{q}}] \rangle$$

$$+ \sum_{\eta, \eta' \in \{x,y\}} (1 - e^{iq_\eta} - e^{-iq_{\eta'}} + e^{i(q_\eta - q_{\eta'})})$$

$$\times \langle\langle j_{\mathbf{q}}^\eta; j_{-\mathbf{q}}^{\eta'} \rangle\rangle_z.$$
(B2)

Let us work out the two commutators

$$[n_{\mathbf{q}}, n_{-\mathbf{q}}] = \sum_\sigma \left[\sum_{\mathbf{k}} c_{\sigma, \mathbf{k+q}}^\dagger c_{\sigma, \mathbf{k}}, \sum_{\mathbf{k'}} c_{\sigma, \mathbf{k'}}^\dagger c_{\sigma, \mathbf{k'+q}} \right]$$

$$= \sum_\sigma \sum_{\mathbf{k}} [c_{\sigma, \mathbf{k+q}}^\dagger c_{\sigma, \mathbf{k}}, c_{\sigma, \mathbf{k}}^\dagger c_{\sigma, \mathbf{k+q}}]$$

$$= \sum_\sigma \sum_{\mathbf{k}} (n_{\sigma, \mathbf{k+q}} - n_{\sigma, \mathbf{k}})$$

$$= \sum_\sigma (n_{\sigma, \mathbf{r}=0} - n_{\sigma, \mathbf{r}=0})$$

$$= 0.$$
(B3)

Therefore, the first term drops out.

For the second term one gets

$$[j_{\mathbf{q}}^\eta, n_{-\mathbf{q}}] = \left[\sum_{\mathbf{k}} v_{\mathbf{k,q}}^\eta c_{\sigma, \mathbf{k+q}}^\dagger c_{\sigma, \mathbf{k}}, \sum_{\mathbf{k'}} c_{\sigma, \mathbf{k'}}^\dagger c_{\sigma, \mathbf{k'+q}} \right]$$

$$= \sum_\sigma \sum_{\mathbf{k}} v_{\mathbf{k,q}}^\eta (n_{\sigma, \mathbf{k+q}} - n_{\sigma, \mathbf{k}}),$$
(B4)

where $v_{\mathbf{kq}}^\eta = it(e^{-i(k_\eta + q_\eta)} - e^{ik_\eta})$. The overall prefactor is purely real for each $\mathbf{k}$:

$$i^2 t(1 - e^{iq_\eta})(e^{-i(k_\eta + q_\eta)} - e^{ik_\eta})$$

$$= -t(e^{-i(k_\eta + q_\eta)} - e^{ik_\eta} - e^{-ik_\eta} + e^{i(k_\eta + q_\eta)})$$

$$= -2t[\cos(k_\eta + q_\eta) - \cos k_\eta]$$

$$\equiv \Phi_{\mathbf{k,q}}^\eta.$$
(B5)

This leads us to the fully general expression (7), and here we write it separately for the real and imaginary parts:

$$z^2 \text{Re}\chi_{\mathbf{q}}(z)$$
(B6)

$$= \sum_{\eta = \{x,y\}} \sum_{\mathbf{k}} \Phi_{\mathbf{k,q}}^\eta (\langle n_{\mathbf{k+q}} \rangle - \langle n_{\mathbf{k}} \rangle)$$

$$+ \text{Re} \sum_{\eta, \eta' \in \{x,y\}} (1 - e^{iq_\eta} - e^{-iq_{\eta'}} + e^{i(q_\eta - q_{\eta'})}) \Lambda_{\mathbf{q}}^{\eta, \eta'}(z),$$

$$z^2 \text{Im}\chi_{\mathbf{q}}(z)$$

$$= \text{Im} \sum_{\eta, \eta' \in \{x,y\}} (1 - e^{iq_\eta} - e^{-iq_{\eta'}} + e^{i(q_\eta - q_{\eta'})}) \Lambda_{\mathbf{q}}^{\eta, \eta'}(z). \quad (B7)$$

Notice that the constant shift in Eq. (B6) is crucial to allow that both χ and Λ scale as $1/\nu^2$ at high Matsubara frequency, which is expected on grounds of symmetry of these correlators in imaginary time. At large ν we get for the real part $\nu^2 \frac{\text{const}}{\nu^2} = \text{const} + 1/\nu^2$ which reduces to const = const as ν goes to infinity. This expression also reveals the high-frequency scaling which must hold in general:

$$\text{Re}\chi_{\mathbf{q}}(i\nu \to i\infty) = -\frac{1}{\nu^2} \sum_{\eta = \{x,y\}} \sum_{\mathbf{k}} \Phi_{\mathbf{k,q}}^\eta (\langle n_{\mathbf{k+q}} \rangle - \langle n_{\mathbf{k}} \rangle).$$
(B8)

APPENDIX C: CONSTITUTIVE EQUATION

In the following we derive the time derivative of current operator in the Heisenberg picture. The derivation boils down to working out the following commutators:

$$\partial_t j_{\mathbf{r}}^\eta = i[H, j_{\mathbf{r}}^\eta] = i([H_{\text{kin}}, j_{\mathbf{r}}^\eta] + [H_{\text{int}}, j_{\mathbf{r}}^\eta] + [H_{\text{chem}}, j_{\mathbf{r}}^\eta]).$$
(C1)

The commutator with kinetic energy reads as

$$i[H_{\text{kin}}, j_{\mathbf{r}}^\eta] = i\left[-t \sum_{\mathbf{r'}, \sigma', s \in \{1, -1\}, \eta' \in \{x,y\}} c_{\sigma', \mathbf{r'}}^\dagger c_{\sigma', \mathbf{r'} + s\mathbf{e}_{\eta'}}, \quad it \sum_\sigma (c_{\sigma, \mathbf{r} + \mathbf{e}_\eta}^\dagger c_{\sigma, \mathbf{r}} - c_{\sigma, \mathbf{r}}^\dagger c_{\sigma, \mathbf{r} + \mathbf{e}_\eta}) \right]$$

$$= -t^2 \sum_\sigma \left\{ [c_{\sigma, \mathbf{r} + \mathbf{e}_\eta}^\dagger c_{\sigma, \mathbf{r}}, c_{\sigma, \mathbf{r}}^\dagger c_{\sigma, \mathbf{r} + \mathbf{e}_\eta}] - [c_{\sigma, \mathbf{r}}^\dagger c_{\sigma, \mathbf{r} + \mathbf{e}_\eta}, c_{\sigma, \mathbf{r} + \mathbf{e}_\eta}^\dagger c_{\sigma, \mathbf{r}}] \right.$$

$$+ \sum_{\mathbf{u} \in \{-\mathbf{e}_\eta, \mathbf{e}_{\bar{\eta}}, -\mathbf{e}_{\bar{\eta}}\}} ([c_{\sigma, \mathbf{r} + \mathbf{u}}^\dagger c_{\sigma, \mathbf{r}}, c_{\sigma, \mathbf{r}}^\dagger c_{\sigma, \mathbf{r} + \mathbf{e}_\eta}] + [c_{\sigma, \mathbf{r} + \mathbf{e}_\eta}^\dagger c_{\sigma, \mathbf{r} + \mathbf{e}_\eta - \mathbf{u}}, c_{\sigma, \mathbf{r}}^\dagger c_{\sigma, \mathbf{r} + \mathbf{e}_\eta}]$$

$$\left. - [c_{\sigma, \mathbf{r}}^\dagger c_{\sigma, \mathbf{r} + \mathbf{u}}, c_{\sigma, \mathbf{r} + \mathbf{e}_\eta}^\dagger c_{\sigma, \mathbf{r}}] - [c_{\sigma, \mathbf{r} + \mathbf{e}_\eta - \mathbf{u}}^\dagger c_{\sigma, \mathbf{r} + \mathbf{e}_\eta}, c_{\sigma, \mathbf{r} + \mathbf{e}_\eta}^\dagger c_{\sigma, \mathbf{r}}]) \right\}$$

$$= -t^2 \sum_\sigma \left\{ 2c^\dagger_{\sigma,\mathbf{r}+\mathbf{e}_\eta} c_{\sigma,\mathbf{r}+\mathbf{e}_\eta} - 2c^\dagger_{\sigma,\mathbf{r}} c_{\sigma,\mathbf{r}} + \sum_{\mathbf{u}\in\{-\mathbf{e}_\eta,\mathbf{e}_{\bar\eta},-\mathbf{e}_{\bar\eta}\}} (c^\dagger_{\sigma,\mathbf{r}+\mathbf{u}} c_{\sigma,\mathbf{r}+\mathbf{e}_\eta} - c^\dagger_{\sigma,\mathbf{r}} c_{\sigma,\mathbf{r}+\mathbf{e}_\eta -\mathbf{u}} + \text{H.c}) \right\}. \tag{C2}$$

The first two terms comprise the lattice version of the gradient of charge in the direction of current. The other terms are longer-range hoppings.

The commutator of the current with the total number of particles has to be zero, and we leave out the explicit derivation of $[H_{\text{chem}}, j^\eta_{\mathbf{r}}]$. The commutator with the local Hubbard interaction, on the other hand, is nontrivial:

$$i[H_{\text{int}}, j^\eta_{\mathbf{r}}] = i\left[U \sum_{\mathbf{r}'} c^\dagger_{\uparrow,\mathbf{r}'} c_{\uparrow,\mathbf{r}'} c^\dagger_{\downarrow,\mathbf{r}'} c_{\downarrow,\mathbf{r}'}, \quad -it \sum_\sigma (c^\dagger_{\sigma,\mathbf{r}} c_{\sigma,\mathbf{r}+\mathbf{e}_\eta} - c^\dagger_{\sigma,\mathbf{r}+\mathbf{e}_\eta} c_{\sigma,\mathbf{r}}) \right]$$

$$= tU \sum_\sigma \{ n_{\bar\sigma,\mathbf{r}}([c^\dagger_{\sigma,\mathbf{r}} c_{\sigma,\mathbf{r}}, c^\dagger_{\sigma,\mathbf{r}} c_{\sigma,\mathbf{r}+\mathbf{e}_\eta}] - [c^\dagger_{\sigma,\mathbf{r}} c_{\sigma,\mathbf{r}}, c^\dagger_{\sigma,\mathbf{r}+\mathbf{e}_\eta} c_{\sigma,\mathbf{r}}])$$

$$+ n_{\bar\sigma,\mathbf{r}+\mathbf{e}_\eta}([c^\dagger_{\sigma,\mathbf{r}+\mathbf{e}_\eta} c_{\sigma,\mathbf{r}+\mathbf{e}_\eta}, c^\dagger_{\sigma,\mathbf{r}} c_{\sigma,\mathbf{r}+\mathbf{e}_\eta}] - [c^\dagger_{\sigma,\mathbf{r}+\mathbf{e}_\eta} c_{\sigma,\mathbf{r}+\mathbf{e}_\eta}, c^\dagger_{\sigma,\mathbf{r}+\mathbf{e}_\eta} c_{\sigma,\mathbf{r}}]) \}$$

$$= tU \sum_\sigma \{ n_{\bar\sigma,\mathbf{r}}(c^\dagger_{\sigma,\mathbf{r}} c_{\sigma,\mathbf{r}+\mathbf{e}_\eta} + c^\dagger_{\sigma,\mathbf{r}+\mathbf{e}_\eta} c_{\sigma,\mathbf{r}}) - n_{\bar\sigma,\mathbf{r}+\mathbf{e}_\eta}(c^\dagger_{\sigma,\mathbf{r}} c_{\sigma,\mathbf{r}+\mathbf{e}_\eta} + c^\dagger_{\sigma,\mathbf{r}+\mathbf{e}_\eta} c_{\sigma,\mathbf{r}}) \}$$

$$= -tU \sum_\sigma (n_{\bar\sigma,\mathbf{r}+\mathbf{e}_\eta} - n_{\bar\sigma,\mathbf{r}})(c^\dagger_{\sigma,\mathbf{r}} c_{\sigma,\mathbf{r}+\mathbf{e}_\eta} + c^\dagger_{\sigma,\mathbf{r}+\mathbf{e}_\eta} c_{\sigma,\mathbf{r}}). \tag{C3}$$

The terms we get are all assisted hopping terms.

The final expression reads as

$$\partial_t j^\eta_{\mathbf{r}} = -t^2 \sum_\sigma \left\{ 2n_{\sigma,\mathbf{r}+\mathbf{e}_\eta} - 2n_{\sigma,\mathbf{r}} + \sum_{\mathbf{u}\in\{-\mathbf{e}_\eta,\mathbf{e}_{\bar\eta},-\mathbf{e}_{\bar\eta}\}} (c^\dagger_{\sigma,\mathbf{r}+\mathbf{u}} c_{\sigma,\mathbf{r}+\mathbf{e}_\eta} - c^\dagger_{\sigma,\mathbf{r}} c_{\sigma,\mathbf{r}+\mathbf{e}_\eta -\mathbf{u}} + \text{H.c}) \right\}$$

$$-tU \sum_\sigma (n_{\bar\sigma,\mathbf{r}+\mathbf{e}_\eta} - n_{\bar\sigma,\mathbf{r}})(c^\dagger_{\sigma,\mathbf{r}} c_{\sigma,\mathbf{r}+\mathbf{e}_\eta} + c^\dagger_{\sigma,\mathbf{r}+\mathbf{e}_\eta} c_{\sigma,\mathbf{r}}). \tag{C4}$$

A straightforward Fourier transformation of both sides yields

$$\partial_t j^\eta_{\mathbf{q}} = -t^2 \sum_\sigma \left\{ 2(e^{iq_\eta} - 1)n_{\sigma,\mathbf{q}} + \sum_{\mathbf{u}\in\{-\mathbf{e}_\eta,\mathbf{e}_{\bar\eta},-\mathbf{e}_{\bar\eta}\}} \left((e^{-i\mathbf{q}\cdot\mathbf{u}} - 1) \sum_{\mathbf{k}} e^{i\mathbf{k}\cdot(\mathbf{e}_\eta-\mathbf{u})} c^\dagger_{\sigma,\mathbf{k}+\mathbf{q}} c_{\sigma,\mathbf{k}} + \text{H.c.} \right) \right\}$$

$$+ tU \sum_\sigma \sum_{\mathbf{k},\mathbf{q}'} (e^{-ik_\eta} + e^{i(k_\eta+q_\eta-q'_\eta)})(1 - e^{iq'_\eta}) n_{\bar\sigma,\mathbf{q}'} c^\dagger_{\sigma,\mathbf{k}+\mathbf{q}-\mathbf{q}'} c_{\sigma,\mathbf{k}}. \tag{C5}$$

It is interesting to consider the limit $\mathbf{q} = 0$,

$$\partial_t j^\eta_{\mathbf{q}=0} = tU \sum_\sigma \sum_{\mathbf{k},\mathbf{q}'} (e^{-ik_\eta} + e^{i(k_\eta-q'_\eta)})(1 - e^{iq'_\eta}) n_{\bar\sigma,\mathbf{q}'} c^\dagger_{\sigma,\mathbf{k}-\mathbf{q}'} c_{\sigma,\mathbf{k}}$$

$$= iU \sum_\sigma \sum_{\mathbf{k},\mathbf{q}'} (v^\eta_{\mathbf{k}-\mathbf{q}'} - v^\eta_{\mathbf{k}}) n_{\bar\sigma,\mathbf{q}'} c^\dagger_{\sigma,\mathbf{k}-\mathbf{q}'} c_{\sigma,\mathbf{k}}, \tag{C6}$$

which clearly shows that scattering events that do not transfer momentum do not contribute to the decay of current; more precisely, only the scattering events that change the velocity of an electron in the direction of the current contribute to the decay of the current. In principle, this expression can be used to express the optical conductivity via higher-order correlation functions using Eq. (B1).

APPENDIX D: EQUATION OF MOTION

Here we derive Eq. (B1). We start with the standard definition of the correlator in real time

$$\langle\langle A; B \rangle\rangle_t = i\theta(t)\langle [A(t), B(0)] \rangle, \tag{D1}$$

where A and B are bosonic operators, thus we adopt the definition without the minus sign in front.

The equations of motion are obtained by taking time derivatives. The first derivative yields

$$\frac{d}{dt} \langle\langle A; B \rangle\rangle_t = i\theta(t)\langle [\dot{A}(t), B(0)] \rangle + i\delta(t)\langle [A, B] \rangle. \tag{D2}$$

We now perform the Laplace transform with respect to t:

$$\langle\langle A; B \rangle\rangle_z = \int_{0^+}^\infty dt\, e^{izt} \langle\langle A; B \rangle\rangle_t. \tag{D3}$$

Now for $f(t) = \langle\langle A; B \rangle\rangle_t$, we integrate per parts

$$\int_{0^+}^{\infty} dt\, e^{izt} \frac{d}{dt} f(t) = e^{izt} f(t)\big|_{0^+}^{+\infty} - iz \int dt\, e^{izt} f(t)$$
$$= -i\langle [A, B] \rangle - iz\langle\langle A; B \rangle\rangle_z. \quad (D4)$$

Note that the δ is not included in the integration domain. The second term comes directly from the definition of the Laplace transform (D3). Equating this result with the Laplace transform of the right-hand side of Eq. (D8) we get

$$-i\langle [A, B] \rangle - iz\langle\langle A; B \rangle\rangle_z = \langle\langle i[H, A]; B \rangle\rangle_z \quad (D5)$$

which, up to the factor i, is the equation of motion in its usual form.

We will want the second derivative to apply to the operator B, thus, we first perform a time shift

$$\frac{d}{dt}\langle\langle A; B \rangle\rangle_t = i\theta(t)\langle [\dot{A}(0), B(-t)] \rangle + i\delta(t)\langle [A, B] \rangle \quad (D6)$$

and only then apply the second time derivative

$$\frac{d^2}{dt^2}\langle\langle A; B \rangle\rangle_t = i\theta(t)\langle [\dot{A}(0), -\dot{B}(-t)] \rangle$$
$$+ i\delta(t)\langle [\dot{A}, B] \rangle + i\delta'(t)\langle [A, B] \rangle. \quad (D7)$$

For convenience, we shift back in time

$$\frac{d^2}{dt^2}\langle\langle A; B \rangle\rangle_t = -i\theta(t)\langle [\dot{A}(t), \dot{B}(0)] \rangle$$
$$+ i\delta(t)\langle [\dot{A}, B] \rangle + i\delta'(t)\langle [A, B] \rangle. \quad (D8)$$

The integration by parts once more leads to

$$\int_{0^+}^{\infty} dt\, e^{izt} \frac{d^2}{dt^2} f(t)$$
$$= \frac{d}{dt}\big(e^{izt} \dot{f}(t)\big)\big|_{0^+}^{+\infty} - iz \int dt\, e^{izt} \frac{d}{dt}\dot{f}(t)$$
$$= -i\langle [\dot{A}, B] \rangle - iz(-i\langle [A, B] \rangle - iz\langle\langle A; B \rangle\rangle_z)$$
$$= -i\langle [\dot{A}, B] \rangle - z\langle [A, B] \rangle - z^2\langle\langle A; B \rangle\rangle_z, \quad (D9)$$

where the second and third terms come directly from Eq. (D5). Equating this result with the Laplace transform of the right-hand side of Eq. (D8) (there note the minus sign in front of the first term, and note that $\dot{A}\dot{B} = -[H, A][H, B]$):

$$-i\langle [\dot{A}, B] \rangle - z\langle [A, B] \rangle - z^2\langle\langle A; B \rangle\rangle_z = \langle\langle [H, A]; [H, B] \rangle\rangle_z. \quad (D10)$$

We rearrange the result

$$z^2\langle\langle A; B \rangle\rangle_z = -i\langle [\dot{A}, B] \rangle - z\langle [A, B] \rangle - \langle\langle [H, A]; [H, B] \rangle\rangle_z \quad (D11)$$

and finally obtain

$$z^2\langle\langle A; B \rangle\rangle_z$$
$$= -\langle [[A, H], B] \rangle - z\langle [A, B] \rangle + \langle\langle [A, H]; [H, B] \rangle\rangle_z \quad (D12)$$

which is the expression used in the derivation in Appendix B.
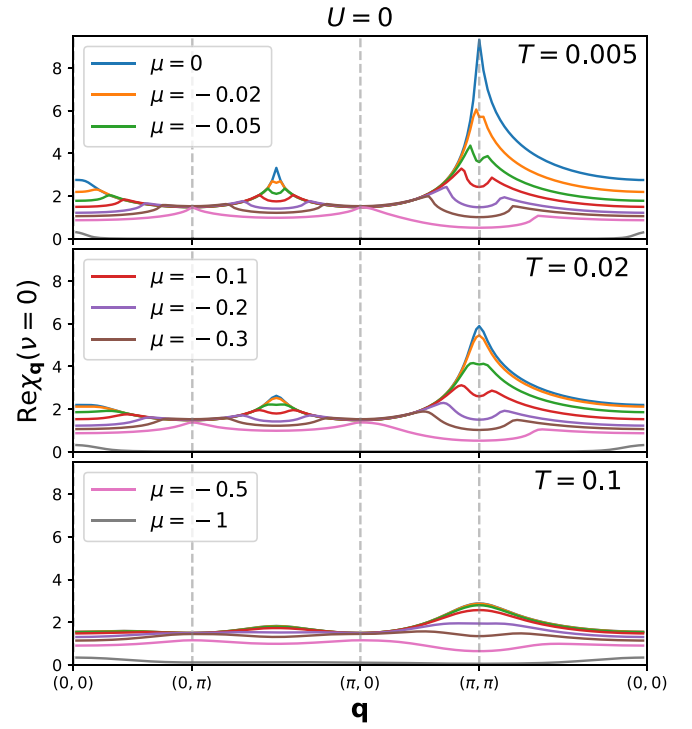
FIG. 22. Static susceptibility in the noninteracting limit as a function of momentum, at different fillings and temperatures.

APPENDIX E: CALCULATION OF SECOND-ORDER SELF-ENERGY

The optimal way to compute the second-order self-energy (46) it is to first evaluate the "triple density of states" by a three-dimensional (3D) histogram on a dense energy grid

$$\rho_{3,\mathbf{k}}(\varepsilon_1, \varepsilon_2, \varepsilon_3) = \frac{1}{N^2 \Delta\omega^3} \sum_{\mathbf{k}', \mathbf{q}} \delta_{\varepsilon_1, \varepsilon_{\mathbf{k}-\mathbf{q}}} \delta_{\varepsilon_2, \varepsilon_{\mathbf{k}'+\mathbf{q}}} \delta_{\varepsilon_3, \varepsilon_{\mathbf{k}'}}, \quad (E1)$$

where $\Delta\omega$ is the step in the energy grid. This calculation only needs to be performed once, for $\mu = 0$, and it does not depend
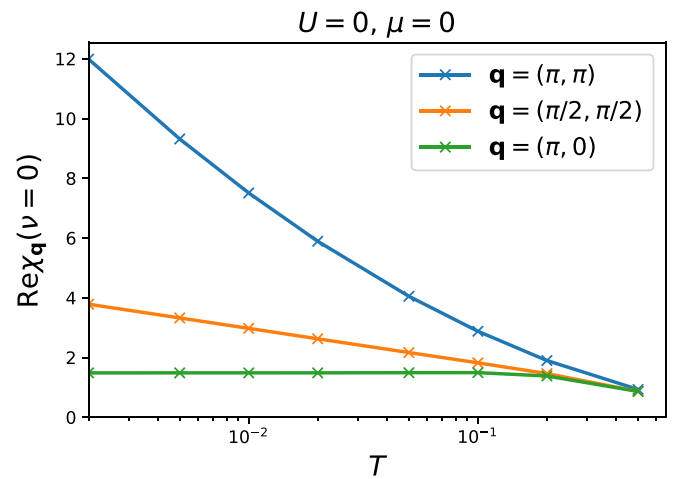
FIG. 23. Static susceptibilities in the noninteracting limit, at half-filling, as a function of temperature. The values at $\mathbf{q} = (\pi, \pi)$ and $\mathbf{q} = (\pi/2, \pi/2)$ appear to diverge as $T \to 0$.

on T. Then for a given (μ, T) we accumulate pole amplitudes for the self-energy on the same energy grid as

$$
\begin{aligned}
&\mathrm{Im}\tilde{\Sigma}_{\mathbf{k}}(\omega) \\
&= -\frac{\pi}{\Delta\omega} \int d\varepsilon_1 d\varepsilon_2 d\varepsilon_3 \; \rho_{3,\mathbf{k}}(\varepsilon_1, \varepsilon_2, \varepsilon_3) \delta_{\omega+\mu-\varepsilon_1-\varepsilon_2+\varepsilon_3} \\
&\quad \times \sum_{s=\pm 1} n_F[s(\varepsilon_1 - \mu)] n_F[s(\varepsilon_2 - \mu)] n_F[-s(\varepsilon_3 - \mu)].
\end{aligned}
$$

$$(E2)$$

The real part of the self-energy can then be obtained via the standard Kramers-Kronig relation.

In our calculations we consider lattices $L \times L$, up to $L = 256$. When calculating histograms, the optimal number of bins is the square root of the number of the data points. Therefore, in Eq. (E1) the number of energy bins per axis should be equal to $\sqrt{N^2}^{1/3} = L^{2/3}$, but for the sake of numerical simplicity, we take the number of energy bins (per axis) to be L. This means that, up to the overhead of evaluating Eq. (E1) once, we have reduced the complexity of the calculation from L^4 [Eq. (46)] to L^3 [Eq. (E2)], which is a huge speedup.

APPENDIX F: DIVERGENCE OF STATIC SUSCEPTIBILITY AT $U = 0$, $T \to 0$

In this Appendix we show results for the static susceptibility $\mathrm{Re}\chi_{\mathbf{q}}(\nu = 0)$, in the noninteracting limit. The results are obtained by setting $\phi, \varphi = 1$, $z = 0$ in Eq. (34) and using a 6000×6000 lattice. In Fig. 22 we observe that there are peaks at $\mathbf{q} = (0, 0)$, $\mathbf{q} = (\pi, \pi)$, and $\mathbf{q} = (\pi/2, \pi/2)$, but the highest peak is at $\mathbf{q} = (\pi, \pi)$. As one dopes away from half-filling, the peaks split. At $\mu = -0.5$, the peaks are at $\mathbf{q} = (0, \pi)$ and the symmetry related $\mathbf{q} = (\pi, 0)$. In the nearly empty limit, the only peak is at $\mathbf{q} = (0, 0)$. As expected, the peaks become less pronounced as one increases temperature. In Fig. 23 we further observe that the value at $\mathbf{q} = (\pi, \pi)$ and $\mathbf{q} = (\pi/2, \pi/2)$ appears to diverge as $T \to 0$, indicating competing instabilities towards charge order. It is important to note that in the noninteracting limit, spin and charge susceptibilities are equal. Therefore, any instability towards charge order is accompanied by instability towards spin order. As soon as interaction is turned on, the degeneracy between charge and spin order is lifted.

[1] B. Keimer, S. A. Kivelson, M. R. Norman, S. Uchida, and J. Zaanen, Nature (London) **518**, 179 (2015).

[2] R. A. Cooper, Y. Wang, B. Vignolle, O. J. Lipscombe, S. M. Hayden, Y. Tanabe, T. Adachi, Y. Koike, M. Nohara, H. Takagi, C. Proust, and N. E. Hussey, Science **323**, 603 (2009).

[3] A. Legros, S. Benhabib, W. Tabis, F. Laliberté, M. Dion, M. Lizaire, B. Vignolle, D. Vignolles, H. Raffy, Z. Z. Li, P. Auban-Senzier, N. Doiron-Leyraud, P. Fournier, D. Colson, L. Taillefer, and C. Proust, Nat. Phys. **15**, 142 (2018).

[4] Y. Cao, D. Chowdhury, D. Rodan-Legrain, O. Rubies-Bigorda, K. Watanabe, T. Taniguchi, T. Senthil, and P. Jarillo-Herrero, Phys. Rev. Lett. **124**, 076801 (2020).

[5] J. Ayres, M. Berben, M. Čulo, Y.-T. Hsu, E. van Heumen, Y. Huang, J. Zaanen, T. Kondo, T. Takeuchi, J. R. Cooper, C. Putzke, S. Friedemann, A. Carrington, and N. E. Hussey, Nature (London) **595**, 661 (2021).

[6] S. A. Grigera, R. S. Perry, A. J. Schofield, M. Chiao, S. R. Julian, G. G. Lonzarich, S. I. Ikeda, Y. Maeno, A. J. Millis, and A. P. Mackenzie, Science **294**, 329 (2001).

[7] S. Licciardello, J. Buhot, J. Lu, J. Ayres, S. Kasahara, Y. Matsuda, T. Shibauchi, and N. E. Hussey, Nature (London) **567**, 213 (2019).

[8] P. Cha, N. Wentzell, O. Parcollet, A. Georges, and E.-A. Kim, Proc. Natl. Acad. Sci. USA **117**, 18341 (2020).

[9] X. Deng, J. Mravlje, R. Žitko, M. Ferrero, G. Kotliar, and A. Georges, Phys. Rev. Lett. **110**, 086401 (2013).

[10] J. Vučičević, D. Tanasković, M. J. Rozenberg, and V. Dobrosavljević, Phys. Rev. Lett. **114**, 246402 (2015).

[11] E. Perepelitsky, A. Galatas, J. Mravlje, R. Žitko, E. Khatami, B. S. Shastry, and A. Georges, Phys. Rev. B **94**, 235115 (2016).

[12] J. Kokalj, Phys. Rev. B **95**, 041110(R) (2017).

[13] E. W. Huang, R. Sheppard, B. Moritz, and T. P. Devereaux, Science **366**, 987 (2019).

[14] J. Vučičević, J. Kokalj, R. Žitko, N. Wentzell, D. Tanasković, and J. Mravlje, Phys. Rev. Lett. **123**, 036601 (2019).

[15] A. Vranić, J. Vučičević, J. Kokalj, J. Skolimowski, R. Žitko, J. Mravlje, and D. Tanasković, Phys. Rev. B **102**, 115142 (2020).

[16] T. G. Kiely and E. J. Mueller, Phys. Rev. B **104**, 165143 (2021).

[17] F. Herman, J. Buhmann, M. H. Fischer, and M. Sigrist, Phys. Rev. B **99**, 184107 (2019).

[18] P. T. Brown, D. Mitra, E. Guardado-Sanchez, R. Nourafkan, A. Reymbaut, C.-D. Hébert, S. Bergeron, A.-M. S. Tremblay, J. Kokalj, D. A. Huse, P. Schauß, and W. S. Bakr, Science **363**, 379 (2019).

[19] J. Jaklič and P. Prelovšek, Adv. Phys. **49**, 1 (2000).

[20] J. Kokalj and R. H. McKenzie, Phys. Rev. Lett. **110**, 206402 (2013).

[21] A. N. Rubtsov, V. V. Savkin, and A. I. Lichtenstein, Phys. Rev. B **72**, 035122 (2005).

[22] E. Gull, A. J. Millis, A. I. Lichtenstein, A. N. Rubtsov, M. Troyer, and P. Werner, Rev. Mod. Phys. **83**, 349 (2011).

[23] H. Hafermann, E. G. C. P. van Loon, M. I. Katsnelson, A. I. Lichtenstein, and O. Parcollet, Phys. Rev. B **90**, 235105 (2014).

[24] D. Forster, *Hydrodynamic Fluctuations, Broken Symmetry, and Correlation Functions* (CRC Press, Boca Raton, FL, 2018).

[25] P. Coleman, *Introduction to Many-body Physics* (Cambridge University Press, Cambridge, England, 2015).

[26] H. Aoki, N. Tsuji, M. Eckstein, M. Kollar, T. Oka, and P. Werner, Rev. Mod. Phys. **86**, 779 (2014).

[27] D. Rohe and C. Honerkamp, SciPost Phys. **9**, 084 (2020).

[28] F. Šimkovic, J. P. F. LeBlanc, A. J. Kim, Y. Deng, N. V. Prokof'ev, B. V. Svistunov, and E. Kozik, Phys. Rev. Lett. **124**, 017003 (2020).

[29] A. J. Kim, F. Simkovic, and E. Kozik, Phys. Rev. Lett. **124**, 117602 (2020).

[30] M. Klett, N. Wentzell, T. Schäfer, F. Simkovic, O. Parcollet, S. Andergassen, and P. Hansmann, Phys. Rev. Res. **2**, 033476 (2020).

[31] T. Schäfer, N. Wentzell, F. Šimkovic, Y.-Y. He, C. Hille, M. Klett, C. J. Eckhardt, B. Arzhang, V. Harkov, F.-M. Le Régent,

A. Kirsch, Y. Wang, A. J. Kim, E. Kozik, E. A. Stepanov, A. Kauch, S. Andergassen, P. Hansmann, D. Rohe, Y. M. Vilk *et al.* Phys. Rev. X **11**, 011058 (2021).

[32] J. Vučičević and R. Žitko, Phys. Rev. B **104**, 205101 (2021).

[33] J. Vučičević, H. Terletska, D. Tanasković, and V. Dobrosavljević, Phys. Rev. B **88**, 075143 (2013).

[34] A. Georges, G. Kotliar, W. Krauth, and M. J. Rozenberg, Rev. Mod. Phys. **68**, 13 (1996).

[35] K. G. Wilson, Rev. Mod. Phys. **47**, 773 (1975).

[36] H. R. Krishna-murthy, J. W. Wilkins, and K. G. Wilson, Phys. Rev. B **21**, 1003 (1980).

[37] R. Bulla, T. A. Costi, and T. Pruschke, Rev. Mod. Phys. **80**, 395 (2008).

[38] R. Žitko and T. Pruschke, Phys. Rev. B **79**, 085106 (2009).

[39] F. Šimkovic IV, R. Rossi, and M. Ferrero, Phys. Rev. Res. **4**, 043201 (2022).

[40] G. Rohringer, H. Hafermann, A. Toschi, A. A. Katanin, A. E. Antipov, M. I. Katsnelson, A. I. Lichtenstein, A. N. Rubtsov, and K. Held, Rev. Mod. Phys. **90**, 025003 (2018).

[41] A. Taheridehkordi, S. H. Curnoe, and J. P. F. LeBlanc, Phys. Rev. B **99**, 035120 (2019).

[42] J. Vučičević and M. Ferrero, Phys. Rev. B **101**, 075113 (2020).

[43] A. Taheridehkordi, S. H. Curnoe, and J. P. F. LeBlanc, Phys. Rev. B **101**, 125109 (2020).

[44] A. Taheridehkordi, S. H. Curnoe, and J. P. F. LeBlanc, Phys. Rev. B **102**, 045115 (2020).

[45] J. Vučičević, P. Stipsić, and M. Ferrero, Phys. Rev. Res. **3**, 023082 (2021).

[46] B. D. E. McNiven, H. Terletska, G. T. Andrews, and J. P. F. LeBlanc, Phys. Rev. B **106**, 035145 (2022).

[47] W. Wu, M. Ferrero, A. Georges, and E. Kozik, Phys. Rev. B **96**, 041105(R) (2017).

[48] F. Šimkovic and E. Kozik, Phys. Rev. B **100**, 121102(R) (2019).

[49] R. Rossi, F. Šimkovic, and M. Ferrero, Europhys. Lett. **132**, 11001 (2020).

[50] A. J. Kim, N. V. Prokof'ev, B. V. Svistunov, and E. Kozik, Phys. Rev. Lett. **126**, 257001 (2021).

[51] H. Xu, H. Shi, E. Vitali, M. Qin, and S. Zhang, Phys. Rev. Res. **4**, 013239 (2022).

[52] O. Parcollet, M. Ferrero, T. Ayral, H. Hafermann, I. Krivenko, L. Messio, and P. Seth, Comput. Phys. Commun. **196**, 398 (2015).

Microscopic derivation of Dirac composite fermion theory:
Aspects of noncommutativity and pairing instabilities

Dragoljub Gočanin ,[1] Sonja Predin ,[2] Marija Dimitrijević Ćirić,[1] Voja Radovanović,[1] and Milica Milovanović [3,*]

[1]*Faculty of Physics, University of Belgrade, Studentski Trg 12-16, 11000 Belgrade, Serbia*
[2]*Institute of Information Systems, Alfons-Goppel-Platz 1, 95030 Hof, Germany*
[3]*Scientific Computing Laboratory, Center for the Study of Complex Systems, Institute of Physics Belgrade,*
University of Belgrade, Pregrevica 118, 11080 Belgrade, Serbia

Building on previous work [N. Read, Phys. Rev. B **58**, 16262 (1998); Z. Dong and T. Senthil, Phys. Rev. B **102**, 205126 (2020)] on the system of bosons at filling factor $\nu = 1$, we derive the Dirac composite fermion theory for a half-filled Landau level from first principles and apply the Hartree-Fock approach in a preferred representation. On the basis of the microscopic formulation, in the long-wavelength limit, we propose a noncommutative field-theoretical description, which in a commutative limit reproduces the Son's theory, with additional terms that may be expected on physical grounds. The microscopic representation of the problem is also used to discuss pairing instabilities of composite fermions. We find that a presence of a particle-hole symmetry breaking leads to a weak (BCS) coupling *p*-wave pairing in the lowest Landau level, and strong coupling *p*-wave pairing in the second Landau level that occurs in a band with nearly flat dispersion, a third power function of momentum.

I. INTRODUCTION

The fractional quantum Hall effect (FQHE) can be explained by focusing on a strongly correlated problem of particles (electrons) in two dimensions when there is a commensuration between the number of particles and the number of flux quanta of the applied, orthogonal to the two-dimensional plane magnetic field. Many phenomenological questions can be answered by assuming that the most important physics takes place in a fixed Landau level (LL) with the precise commensuration of the number of particles and the number of orbitals in a fixed LL (and other LLs are inert). That is why a mathematical, idealized problem of an isolated LL is so useful and relevant for the understanding of the FQHE.

Some of the most interesting experimental phenomena occur at filling factors (ratio of the number of electrons and the number of flux quanta) $\nu = \frac{1}{2}$ and $\frac{5}{2}$, even-denominator fractions. The gapless system at $\nu = \frac{1}{2}$ is believed to be in a Fermi-liquid state of underlying quasiparticles [composite fermions (CFs)], as proposed and described in [1] early on, while it is believed that incompressible (gapped) FQHE at $\nu = \frac{5}{2}$ can be associated with some kind of *p*-wave pairing of CFs in the second LL (sLL), as proposed in [2]. To understand more closely these systems, one may start by focusing on an isolated half-filled LL, the lowest LL (LLL) at $\nu = \frac{1}{2}$ in the case of the CF liquid (CFL), and sLL at $\nu = \frac{5}{2}$ in the case of the gapped system.

One of the most interesting theoretical developments associated with the physics in an isolated, half-filled LL is the proposal in [3] for the description of the CFL state that is based on an assumption that the underlying quasiparticles: CFs can be effectively described as Dirac CFs, using an effective Dirac theory in two dimensions. This can be of general interest: a system of interacting fermions on a noncommutative (NC) space of an isolated LL, in which they fill half of the allowed, countable states, can be described by an effective Dirac theory.

The proposed Dirac CF theory is a phenomenological theory, based on the assumption that an effective theory of an isolated, half-filled LL must be manifestly invariant under the particle- (electron-) hole transformation. Certainly, there is a need for a microscopic derivation of the Dirac CF theory, which can serve as a base for further understanding of this strongly correlated system. In this paper we develop a microscopic support for the Dirac CF theory, and provide a framework for a more detailed investigations.

To describe the physics of an isolated half-filled LL, we generalize the approach to bosons in an isolated LL at filling factor one, of Pasquier and Haldane [4], and later developed by Read [5], and more recently by Dong and Senthil [6]. This approach introduces additional, vortex degrees of freedom to efficiently capture Laughlin-Jastrow correlations. In the case of bosons, the vortex (holelike, unphysical) degrees of freedom are fermionic, and combine with elementary bosons to make quasiparticles of the problem, CFs. Due to their fermionic nature, the vortex degrees of freedom are uniformly distributed in the LL and make a uniform background. (This feature also guarantees a necessary independence of physics under transformations in the unphysical sector.) We generalize this description to the case of the half-filled LL of electrons, by assuming a uniform distribution of two kinds of unphysical degrees of freedom: holelike and electronlike. There are hole-like vortices as many as particlelike (electronlike) vortices,

*Corresponding author: milica.milovanovic@ipb.ac.rs

and they behave as hard-core bosons among themselves, making a uniform background. To ensure the uniform background we need to introduce constraints in the description. Because of two kinds of unphysical degrees of freedom, the holelike vortices combine with electrons to make CFs, and the particlelike vortices combine with holes to make composite holes (CHs). We can choose either electrons or holes as physical degrees of freedom of the half-filled LL, but if we want to capture particle-hole (PH) symmetry (i.e., the symmetry under exchange of particles and holes), we should treat them on an equal footing. Thus, we need to include additional constraints that will preclude the simultaneous presence of a hole and an electron in an orbital of the fixed LL, and therefore describe them as dependent (not two independent) degrees of freedom. The requirement of the PH symmetry also justifies our assumption on the manner in which unphysical (vortexlike) degrees of freedom enter the description. In this way, on the basis of two sets of constraints, we are able to formulate the problem of the half-filled LL, that is explicitly invariant under exchange of particles and holes. Furthermore, within this framework, which explicitly includes the additional vortex degrees of freedom, we are able to consider the "preferred (form of) Hamiltonian" in the language of CFs and CHs, natural quasiparticles that, on the level of Hartree-Fock treatment, can effectively capture the physics of the system. Thus, a two-component fermion description, with the CF and CH fields, necessarily and naturally appears as a consequence of the demand for the PH symmetry, and we show that the description is of the Dirac type (when the constraints are taken into account). This provides a microscopic derivation of the Dirac description and explains the Dirac nature of the fermionic quasiparticle excitations of the low-energy physics.

On the basis of this microscopic formulation, in the long-wavelength limit, we propose a noncommutative field-theoretical description, which in a commutative limit reproduces the Son's theory, with additional terms that may be expected on physical grounds. We also discuss pairing instabilities within the developed microscopic framework, and provide a physical understanding of the p-wave pairing instability in the LLL, and in the sLL. The pairing in the LLL is of the BCS, weak coupling kind, and this may explain the scarcity of the pairing phenomena in the LLL. On the other hand, the pairing in the sLL is of the strong coupling (weak pairing) kind as proposed and discussed in [7], though we find that the Dirac CF band dispersion $\epsilon(k)$ is flatter: it obeys a third-power law, i.e., $\epsilon(k) \sim k^3$.

The section that follows is a review of the bosonic problem at $\nu = 1$, in which we also introduce a point of view of the formalism developed in [4,5], that will be useful for the half-filled problem of electrons. Sections III and IV consider a (simpler) system, closely related to the one of the half-filled LL, a special-bilayer system with two kinds of particles, parallel to the existence of electrons and holes in the half-filled LL. A transformation into holes of just one kind of particles in the special-bilayer system enables a formulation of the half-filled LL problem in Sec. V, with all necessary constraints. Following the usual approach [8] to a formulation with constraints [that enables a Hartree-Fock (HF) treatment] we discuss a "preferred" form of the Hamiltonian in Sec. VI, and in Sec. VII a Dirac form of the Hamiltonian

in the HF approximation. In Sec. VIII we describe how in the long-wavelength limit of the microscopic formulation we can reach a field-theoretical description with gauge fields next to the Dirac composite fermions. In Secs. IX and X we discuss the description of possible pairing instabilities. The structure of the proposed NC field theory is described in Appendix A, while Appendix B concerns some specific aspects of the relevant covariant derivatives. Conclusions are summarized in Sec. XI.

II. REVIEW OF THE $\nu = 1$ BOSON SYSTEM AND INTRODUCTORY REMARKS

A CF is a composite object, a bound state of an underlying elementary particle with a whole number of vortices; a vortex represents an excitation of the FQHE system due to an insertion of one flux quantum that induces a depletion of charge. At filling factors $\nu = 1/q$, where q is an integer, a composite fermion is a neutral object; a composite of an electron (fermion) and a hole (more precisely a depletion of charge) associated with q flux quanta, when q is even, and a composite of a boson and a hole associated with q flux quanta, when q is odd. To simplify the terminology, we will always call the excitation with q flux quanta a vortex. These introductory remarks serve just to remind the reader of the physical picture of the CF, and for an elaborate introduction to the CF formulation the reader may consult [5]. We conclude that it may be expected and natural that an operator describing annihilation or creation of CF will carry two indices, one for the state of the elementary particle and the other for the state of the hole in an orthonormal basis. In the following we will introduce the two-index formalism that was first proposed in [4] and further elaborated in [5] and [6].

We start from an enlarged space with (composite) fermion $c_{mn}^\dagger$ with two indices, each corresponding to an orbital in the LLL (fixed LL): $m, n = 1, \ldots, N_\phi \equiv N$ such that

$$\{c_{nm}, c_{m'n'}^\dagger\} = \delta_{n,n'} \delta_{m,m'}. \tag{1}$$

Each c_{nm} fermion represents a composite object. We define physical subspace of bosonic states in the LLL by

$$|n_1, \ldots, n_N\rangle = \sum_{m_1, \ldots, m_N}^{N_\phi} \varepsilon^{m_1 \cdots m_N} c_{m_1 n_1}^\dagger \cdots c_{m_N n_N}^\dagger |0\rangle, \tag{2}$$

where $\varepsilon^{m_1 \cdots m_N}$ is the Levi-Civita symbol. In this way, bosonic physical states have a property, defined by

$$\rho_{mm'}^R = \sum_n c_{mn}^\dagger c_{nm'}, \tag{3}$$

that

$$\rho_{mm}^R |n_1, \ldots, n_N\rangle = 1 \ |n_1, \ldots, n_N\rangle, \tag{4}$$

expressing a single occupancy of each unphysical orbital m. The physical states are defined by this property so that unphysical orbitals make a uniformly occupied background. They furnish a spin-singlet representation of SU(N) group,

$$m \neq m', \quad \rho_{mm'}^R |n_1, \ldots, n_N\rangle = 0, \tag{5}$$

which is in agreement with the requirement that the physics should not depend on the choice of basis in the unphysical sector R.

But, we may reformulate this requirement by demanding that (1) $\rho_{mm}^R = 1$ and that (2) "unphysical" particles (objects), which are uniformly distributed in the LLL, are fermions. This will automatically lead to (5). In other words, introducing a certain type of statistics in the unphysical sector is a way of specifying physical states together with the demand for $\rho_{mm}^R = 1$. In the following we would like to further this view and introduce an approach, which will make a basis for our description of the $\nu = \frac{1}{2}$ problem, and contrast it with respect to the previous construction of the bosonic $\nu = 1$ state.

First, we will recapitulate the Pasquier-Haldane construction, and the way vortex statistics enters the description. The Pasquier-Haldane enlarged space consists of states

$$c_{m_1 n_1}^\dagger \ldots c_{m_N n_N}^\dagger |0\rangle, \qquad (6)$$

which describe the presence of N composite objects. To each object we associate two single-particle LL states, the state n_i of the elementary, physical particle, boson, and state m_i of vortex. By exchanging states $n_i \leftrightarrow n_j$ or $m_i \leftrightarrow m_j$, we do not get the same state up to a sign, i.e., we cannot speak about definite statistics. But if we trace out one of the (two) degrees of freedom, like by tracing out in an antisymmetric way vortices in (2), we can speak about definite statistics; we have to do an ordinary (symmetric) trace in all n indices to get a state with definite statistics in the unphysical sector, a single Slater (Vandermonde) determinant of fermionic vortices in this $\nu = 1$ case.

This motivates our approach: we consider an enlarged space (a subspace of the Pasquier-Haldane space) in which all m's (in the unphysical sector) are different (i.e., $m_i \neq m_j$ for $i \neq j$; $i, j = 1, \ldots, N$). Physically, we may understand this as a modeling of a uniformly distributed vortex background. The SU(N) invariance in the R sector is present, and acts trivially, because each generator (3) with $m \neq m'$ will map out of this restricted space, and thus effectively (considering the necessary projection) annihilate state in the restricted space. If we further require that the states of the restricted space have definite (fermionic) statistics of vortices we will have a unique realization of the SU(N) symmetry, given by (2). Thus, we do not constrain the unphysical degrees of freedom by a single symmetry requirement (as in the approach to the bosonic $\nu = 1$ in [6], and which is possible, allowed in that system), but primarily by a physical requirement of the uniform vortex (unphysical degrees of freedom) density. Thus, we consider a description with an (additional but necessary) constraint in the unphysical sector, which is present automatically in the bosonic $\nu = 1$ case, because of the fermionic statistics of the unphysical degrees of freedom. The constraint of the uniform vortex density is a way to introduce bosonic vortices into a theory, and still maintain the SU(N) invariance in the unphysical (vortex) sector, i.e., invariance of the physics under change of basis (transformations) in the unphysical sector. We will consider examples of this at the end of this section and in the following section when we discuss a special bilayer problem as a preparation for the half-filled LL problem. Furthermore, we will see that in the half-filled LL problem, unphysical degrees of freedom are associated with both L and R sectors,

and thus we see that in that case also, the requirement of the uniform density of the unphysical degrees of freedom is the most natural to constrain these degrees of freedom, and maintain the invariance under change of basis [not by a spin-singlet realization of SU(N) symmetry in one (R) sector]. Therefore, we can specify physical states by demanding the uniform distribution of unphysical degrees of freedom in the states that enter description of the physical states. These states form a space that is effectively invariant under SU(N) transformations. The demand for a definite statistics of unphysical degrees of freedom in these states leads to physical states.

Thus, in principle, we can discuss a possible physical sector (system) in an enlarged theory for which $\rho_{mm}^R = 1$, but with the unphysical particles being ("hard-core") bosons, and the physical sector being a $\nu = 1$ fermionic system. The old requirement (5) would be fulfilled effectively (= under the necessary projection) in a restricted space for which $\rho_{mm}^R = 1$, i.e., space defined by *hard-core* vortex configurations (of N of vortices). The physical space is defined by a hard-core configuration of vortices that correlate as bosons. In this case

$$|n_1, \ldots, n_N\rangle_f = \sum_{m_1,\ldots,m_N}^{N_\phi} s^{m_1 \ldots m_N} c_{m_1 n_1}^\dagger \ldots c_{m_N n_N}^\dagger |0\rangle, \qquad (7)$$

where $s^{m_1 \ldots m_N} = 1$ only if no index is equal to any other index, but otherwise zero. But as we know, this would not lead to a plausible Hartree-Fock description, i.e., a good representation in which the Hartree-Fock approach to the system of composite fermions c_{nm} would make a good starting point for more refined descriptions.

Therefore, in principle, we can consider both bosonic and fermionic realizations of the SU(N) group (that works in the unphysical sector), by considering the theory with CFs as building blocks of the effective description, at a particular fraction, and only one will realize as a physical theory. [We should choose composite bosons (CBs) in the system in which the CF realization fails.] The single occupancy in the unphysical sector will lead to definite statistics (fermionic or bosonic) in the unphysical sector because the algebra of the density operators (that the theory is built on), in a LL basis, is

$$\left[\rho_{mm'}^R, \rho_{ll'}^R \right] = \rho_{ml'}^R \delta_{m',l} - \rho_{lm'}^R \delta_{m,l'}, \qquad (8)$$

i.e., the algebra of SU(N) generators that can be realized either by fermions or bosons. The constant density and demand for fermionic statistics will coincide with a simple SU(N) invariance: the group action will map the state in (2) into itself. The constant density requirement and demand for bosonic statistics will coincide with a special SU(N) invariance (a maintenance of the symmetry under the projection to the constant density): the group action will map the state in (7) into the same state up to a number (a coefficient because of the projection) and only the symmetric group S_n, for $n = N$, a subgroup of SU(N), represented by signed permutation matrices, will map the state into itself, up to a sign. Thus, by fixing the density, we will have either fermionic or bosonic realization in the unphysical sector, and in the following we will emphasize which realization (statistics) we choose.

III. TOWARDS $\nu = \frac{1}{2}$ FERMIONS: A SPECIAL BILAYER SYSTEM

As a preparation for a setup of the $\nu = \frac{1}{2}$ (i.e., the half-filled LL) problem in the language of composite quasiparticles, we will discuss a setup for a special quantum Hall bilayer system. The special bilayer is characterized by two layers of electrons, each at filling factor $\nu = \frac{1}{2}$ of a fixed LL, but what is special is that an electron in one layer cannot be in the same (LL) orbital with an electron from the other layer. Thus, we may speak about two kinds of composite objects, composite fermions c and d, which are overall neutral objects consisting of elementary particle electron of a given layer, and unphysical (vortex) object of opposite charge. Therefore, we consider two CFs, $c_{mn}^{\dagger}$ and $d_{mn}^{\dagger}$, for the two layers, and an enlarged space with states

$$c_{m_1 n_1}^{\dagger} \dots c_{m_{N/2} n_{N/2}}^{\dagger} d_{m_1' n_1'}^{\dagger} \dots d_{m_{N/2}' n_{N/2}'}^{\dagger} |0\rangle, \tag{9}$$

i.e., always there are $N/2$ c fermions and $N/2$ d fermions, where N, as before, is the number of available orbitals in the LL.

The density of the unphysical objects, vortices (of the opposite charge with respect to electrons), may be expressed in the analogous way as in the previous section:

$$\rho_{mm'}^{R(c)} = \sum_n c_{mn}^{\dagger} c_{nm'} \tag{10}$$

and

$$\rho_{mm'}^{R(d)} = \sum_n d_{mn}^{\dagger} d_{nm'}. \tag{11}$$

Following the discussion in the previous section, we require

$$\rho_{mm}^{R(c)} + \rho_{mm}^{R(d)} = 1, \tag{12}$$

i.e., we uniformly distribute particles in the unphysical sector. Furthermore, we choose them to be bosons and mutual bosons. The requirement (12) may be associated with special (identical for both c fermions and d fermions) transformations of the LL basis in the unphysical sector, which we denote by $SU_c^R(N)$ (where c stands for charge), a transformation that is realized identically on both c fermions and d fermions by affecting their unphysical index. These transformations would leave the physical states unchanged if we work in the restricted subspace with (unphysical) hard-core bosons

$$m \neq m', \quad (\rho_{mm'}^{R(c)} + \rho_{mm'}^{R(d)})|n_1, \dots, n_{N/2} n_1', \dots, n_{N/2}'\rangle = 0, \tag{13}$$

where the equality is the result of the projection to the restricted state, and thus by assuming (12) and bosonic correlations in the unphysical sector, we have that

$$|n_1, \dots, n_{N/2}, n_1', \dots, n_{N/2}'\rangle$$
$$= \sum_{m_1, \dots, m_{N/2}, m_1', \dots, m_{N/2}'}^{N} s^{m_1 \dots m_{N/2} m_1', \dots, m_{N/2}'}$$
$$\times c_{m_1 n_1}^{\dagger} \dots c_{m_{N/2} n_{N/2}}^{\dagger} d_{m_1' n_1'}^{\dagger} \dots d_{m_{N/2}' n_{N/2}'}^{\dagger} |0\rangle, \tag{14}$$

where $s^{m_1 \dots m_{N/2} m_1', \dots, m_{N/2}'}$ is nonzero, equal to one only if no index is equal to any other index.

In (14) we have not only required that the unphysical bosonic degrees of freedom are uniformly distributed (12), but that they correlate mutually in a symmetric way. Thus, we chose a sector of definite statistics in the enlarged space.

If $N = 2$, we have the following candidates for physical states:

$$|n, n'\rangle = (c_{1n}^{\dagger} d_{2n'}^{\dagger} + c_{2n}^{\dagger} d_{1n'}^{\dagger})|0\rangle, \tag{15}$$

where $n, n' = 1, 2$. Additionally, as a part of the definition, we require that in the special bilayer system, i.e., two half-filled LL system, LL orbitals in the physical states cannot be doubly occupied. Thus, what is needed is to suppress the unwanted states [those with $(n, n') = (1, 1)$ or $(2, 2)$ in the $N = 2$ example] of double occupancy (with an eye on the half-filled problem). Therefore, we need also

$$\rho_{nn}^{L(c)} + \rho_{nn}^{L(d)} = 1. \tag{16}$$

This leads to $|\text{phy}\rangle$, physical states for which

$$n \neq n', \quad (\rho_{nn'}^{L(c)} \pm \rho_{nn'}^{L(d)})|\text{phy}\rangle = 0. \tag{17}$$

We may associate the plus combination with $SU_c^L(N)$, and the minus combination with $SU_s^L(N)$ "spin" transformations which are inverse in the d sector with respect to the ones in the c sector. Together, (16) and (17) with the plus sign lead to conclusion that $|\text{phy}\rangle$ states are spin singlet(s) under $SU_c^L(N)$. On the other hand, in the physical states, the generators of $SU_s^L(N)$ transformations

$$\rho_{nn}^{L(c)} - \rho_{nn}^{L(d)} \tag{18}$$

may have expectation values from the interval $[-1, 1]$. At the beginning, before the requirement (16), operator sets $\{\rho_{nn'}^{L(c)}\}$ and $\{\rho_{nn'}^{L(d)}\}$, with the constraints $\sum \rho_{nn}^{L(c)} = \sum \rho_{nn}^{L(d)} = N/2$, furnished two adjoint representations of $SU(N)$ group. However, with the hard-core constraint (16), we have only one nontrivial representation of $SU(N)$ group, $SU_s^L(N)$. The physical states are invariant under global $U_s(1)$ transformation because

$$\sum_n \rho_{nn}^{L(c)} = \sum_n \rho_{nn}^{L(d)} = N/2, \tag{19}$$

and so are the unphysical (R-sector) states

$$\sum_n \rho_{nn}^{R(c)} = \sum_n \rho_{nn}^{R(d)} = N/2, \tag{20}$$

by definition.

This completes a constraint [(12), (16), (19), (20)] plus statistics setup for the description in an enlarged space of the problem that concerns a special bilayer at $\nu_{\text{tot}} = 1$ with two kinds of electrons, i.e., composite c fermions and d fermions, which cannot occupy the same orbital in the restricted space of a fixed LL.

IV. SPECIAL BILAYER SYSTEM AND ITS TRANSFORMATION INTO THE HALF-FILLED SYSTEM

We may consider the previous formulation of the special bilayer as a starting point for the formulation of the half-filled problem. To reach the half-filled problem, one kind of electron (in one of the layers) should transform, i.e., become (elementary, physical) holes. If we consider a layer with composite

d fermion, under the special electrons into holes transformation, what was the density of "physical" electrons $\rho^{L(d)}$ should become the description of the density of unphysical vortices, quasielectrons, and be a part of the constraints and description in the unphysical sector, i.e., $\rho^{R(d)} \to \rho^{L(d)}$. And similarly, what was the density of unphysical vortices (with charge opposite to the one of electron) $\rho^{R(d)}$ should become the description of the density of "physical" holes, and be a part of constraints and description in the physical sector, i.e., $\rho^{L(d)} \to \rho^{R(d)}$.

Thus, by making a PH transformation, i.e., charge conjugation in one of the layers, described by composite object d, it is appropriate to call this object *composite hole* because now the physical degree of freedom is a hole.

We may make this discussion more concrete by considering the special bilayer description in the inverse space and fixing the notation that will be in place also for the half-filled case. Also, we will discuss possible particle-hole transformations in the special bilayer case and derive again the necessary transformations that transform the special bilayer problem into the one of the half-filled LL.

We consider a representation of c and d composite fermions of the special bilayer in the inverse (momentum) space. Following the previous studies on the $\nu = 1$ bosonic problem, we introduce the following decompositions:

$$c_{nm} = \int \frac{d\mathbf{k}}{(2\pi)^{\frac{3}{2}}} \langle n|\tau_{\mathbf{k}}|m\rangle c_{\mathbf{k}} \qquad (21)$$

and

$$d_{nm} = \int \frac{d\mathbf{k}}{(2\pi)^{\frac{3}{2}}} \langle n|\tau_{\mathbf{k}}|m\rangle d_{\mathbf{k}}, \qquad (22)$$

with $\tau_{\mathbf{k}} = \exp(i\mathbf{k} \cdot \mathbf{R})$, where $\mathbf{R}$ is a guiding-center coordinate of a single particle in the external magnetic field,

$$[R_x, R_y] = -i, \qquad (23)$$

we took l_B (magnetic length) $= 1$, and $\{|n\rangle\}$ are single-particle states (orbitals) in a fixed LL.

With these decompositions we find that

$$\rho_{nn'}^{L(c)} = \sum_m c_{mn}^\dagger c_{n'm} = \int \frac{d\mathbf{q}}{2\pi} \langle n'|\tau_{\mathbf{q}}|n\rangle \rho_{\mathbf{q}}^{L(c)}, \qquad (24)$$

where

$$\rho_{\mathbf{q}}^{L(c)} = \int \frac{d\mathbf{k}}{(2\pi)^2} c_{\mathbf{k}-\mathbf{q}}^\dagger c_{\mathbf{k}} \exp\left(i\frac{\mathbf{k} \times \mathbf{q}}{2}\right), \qquad (25)$$

and similarly for $\rho_{nn'}^{L(d)}$,

$$\rho_{nn'}^{L(d)} = \sum_m d_{mn}^\dagger d_{n'm} = \int \frac{d\mathbf{q}}{2\pi} \langle n'|\tau_{\mathbf{q}}|n\rangle \rho_{\mathbf{q}}^{L(d)}, \qquad (26)$$

where

$$\rho_{\mathbf{q}}^{L(d)} = \int \frac{d\mathbf{k}}{(2\pi)^2} d_{\mathbf{k}-\mathbf{q}}^\dagger d_{\mathbf{k}} \exp\left(i\frac{\mathbf{k} \times \mathbf{q}}{2}\right). \qquad (27)$$

Note the inverse order of indices n and n', on the left- and right-hand sides of (24) and (26). Similarly,

$$\rho_{mm'}^{R(c)} = \sum_n c_{mn}^\dagger c_{nm'} = \int \frac{d\mathbf{q}}{2\pi} \langle m|\tau_{\mathbf{q}}|m'\rangle \rho_{\mathbf{q}}^{R(c)}, \qquad (28)$$

where

$$\rho_{\mathbf{q}}^{R(c)} = \int \frac{d\mathbf{k}}{(2\pi)^2} c_{\mathbf{k}-\mathbf{q}}^\dagger c_{\mathbf{k}} \exp\left(-i\frac{\mathbf{k} \times \mathbf{q}}{2}\right), \qquad (29)$$

and analogously for $\rho_{nn'}^{R(d)}$,

$$\rho_{mm'}^{R(d)} = \sum_n d_{mn}^\dagger d_{nm'} = \int \frac{d\mathbf{q}}{2\pi} \langle m|\tau_{\mathbf{q}}|m'\rangle \rho_{\mathbf{q}}^{R(d)}, \qquad (30)$$

where

$$\rho_{\mathbf{q}}^{R(d)} = \int \frac{d\mathbf{k}}{(2\pi)^2} d_{\mathbf{k}-\mathbf{q}}^\dagger d_{\mathbf{k}} \exp\left(-i\frac{\mathbf{k} \times \mathbf{q}}{2}\right). \qquad (31)$$

Note the positions of indices m and m' on the left- and right-hand sides of (28) and (30).

We have

$$[\rho_{\mathbf{q}}^L, \rho_{\mathbf{q}'}^L] = 2i \sin\left(\frac{\mathbf{q} \times \mathbf{q}'}{2}\right) \rho_{\mathbf{q}+\mathbf{q}'}^L \qquad (32)$$

and

$$[\rho_{\mathbf{q}}^R, \rho_{\mathbf{q}'}^R] = -2i \sin\left(\frac{\mathbf{q} \times \mathbf{q}'}{2}\right) \rho_{\mathbf{q}+\mathbf{q}'}^R, \qquad (33)$$

i.e., Girvin-MacDonald-Plazmann (GMP) algebra for two kinds of particles, particles with opposite electric charge.

We may introduce a particle-hole transformation in the d sector by taking

$$d_{\mathbf{k}} \to d_{-\mathbf{k}}^\dagger \quad (d_{\mathbf{k}}^\dagger \to d_{-\mathbf{k}}). \qquad (34)$$

This implies

$$d_{mn} \to d_{mn}^\dagger \quad (d_{mn}^\dagger \to d_{mn}), \qquad (35)$$

and also for

$$\rho_{nn'}^{L(d)} = \sum_m d_{mn}^\dagger d_{n'm}, \quad n \neq n' \qquad (36)$$

we have

$$\rho_{nn'}^{L(d)} \to \sum_m d_{mn} d_{n'm}^\dagger = -\sum_m d_{n'm}^\dagger d_{mn} = -\rho_{n'n}^{R(d)}. \qquad (37)$$

In the inverse space this implies

$$\rho^{L(d)}(\mathbf{q}) \to -\rho^{R(d)}(\mathbf{q}), \qquad (38)$$

which is consistent with our expectation of what a particle-hole transformation should imply on the physical density in the d sector; it should induce a density of particles of opposite charge in the magnetic field ($L \to R$) (and a minus sign that is always accompanied with such a transformation). We can reach the same result by considering $\rho^{L(d)}(\mathbf{q})$ for $\mathbf{q} \neq 0$,

$$\rho^{L(d)}(\mathbf{q}) = \int \frac{d\mathbf{k}}{(2\pi)^2} d_{\mathbf{k}-\mathbf{q}}^\dagger d_{\mathbf{q}} \exp\left(i\frac{\mathbf{k} \times \mathbf{q}}{2}\right), \qquad (39)$$

and applying the transformation $d_{\mathbf{k}} \to d_{-\mathbf{k}}^\dagger$ ($d_{\mathbf{k}}^\dagger \to d_{-\mathbf{k}}$).

Therefore, this transformation may be identified to be the one that corresponds (in the enlarged space) to the particle-hole transformation on the elementary (fundamental) degrees of freedom e_d, the second kind of electrons in the special bilayer: $e_d \to h_d^\dagger, e_d^\dagger \to h_d$ (where $e_d, e_d^\dagger, h_d, h_d^\dagger$ are annihilation and creation operators).

Above we introduced the effect of the particle-hole transformation (on electrons e_d) in the d sector on composite

fermion operators, while putting aside the question of the diagonal terms $\rho_{nn}^{L(d)}$ and the necessary existence of a constant term, equal to N, due to the anticommutation relation of d_{mn}'s. This would imply an additional delta-function contribution $[\sim \delta^2(\boldsymbol{q})]$ in the inverse space for the particle-hole transformation of $\rho^{L(d)}(\boldsymbol{q})$.

To comply with the restrictions of physical spaces in the enlarged spaces of composite fermion operators d_{nm} and c_{nm} of the half-filled and special bilayer problem, we expect

$$\rho_{nn}^{L(d)} \rightarrow 1 - \rho_{nn}^{R(d)} \tag{40}$$

because the summation on n on both sides, and the restrictions

$$\sum_n \rho_{nn}^{L(d)} = \sum_n \rho_{nn}^{R(d)} = \frac{N}{2} \tag{41}$$

would be consistent with the particle-hole (single-layer) symmetry of the physical system and restrictions on the special bilayer system.

Thus, in order to project the transformation $d_{mn} \rightarrow d_{mn}^\dagger$ on the physical spaces of half-filled and special bilayer problems we demand

$$\rho_{nn}^{L(d)} \rightarrow 1 - \rho_{nn}^{R(d)}, \tag{42}$$

which requires an additional subtraction of a constant term $(N - 1)$ after the $d_{mn} \rightarrow d_{mn}^\dagger$ ($d_{mn}^\dagger \rightarrow d_{mn}$) transformation, in order to project out the unphysical degrees of freedom. In the inverse space this affects the delta-function contribution; thus, for $\boldsymbol{q} \neq 0$ we still have $\rho^{L(d)}(\boldsymbol{q}) \rightarrow -\rho^{R(d)}(\boldsymbol{q})$.

In the following we would like to examine how this particle-hole transformation affects the constraints imposed on the bilayer system in order to see how they look like in the (enlarged) space of the special bilayer system. The two "hard-core" constraints $\rho_{nn}^{R(c)} + \rho_{nn}^{R(d)} = 1$ in (12) and $\rho_{nn}^{L(c)} + \rho_{nn}^{L(d)} = 1$ in (16) become

$$\rho_{nn}^{R(c)} = \rho_{nn}^{L(d)} \tag{43}$$

and

$$\rho_{nn}^{L(c)} = \rho_{nn}^{R(d)}, \tag{44}$$

respectively, which is consistent with the view that now the d sector is described by hole degrees of freedom. On the other hand, the operator $\rho_{nn}^{L(c)} - \rho_{nn}^{L(d)}$ transforms into $\rho_{nn}^{L(c)} + \rho_{nn}^{R(d)} - 1$, i.e., $\rho_{nn}^{L(c)} + \rho_{nn}^{R(d)}$ acquires expectation values in the physical states ranging from 0 to 2. Thus, we introduced the hole view in the d sector and this increased the allowed occupancy of c particles and d holes of a single site to 2. *But, we want to introduce a description in terms of holes not in the*
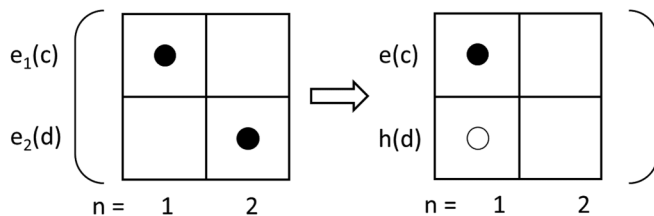
FIG. 1. An illustration of the particle-hole transformation in the special bilayer problem. The transformation is done in the layer with particles (electrons) 2 and thus also on the associated composite d fermion.
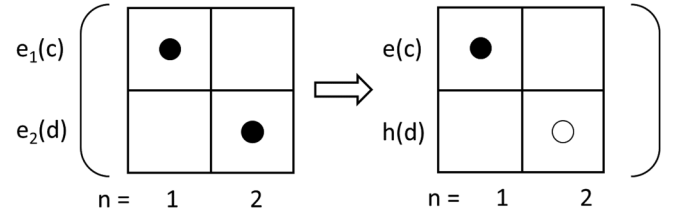
FIG. 2. An illustration of the "active" particle-hole transformation, i.e., the particle-hole conjugation on particles (electrons) 2 which become holes. In this way the special bilayer problem is transformed into the half-filled LL problem.

way of change of variables but in the way of a real change in the d sector: where there are particles there should be holes and vice versa. Thus, $\rho^{L(d)} \rightarrow \rho^{R(d)}$ and $\rho^{R(d)} \rightarrow \rho^{L(d)}$ in accordance with the discussion at the beginning of this section. In this way the operator $\rho_{nn}^{L(c)} - \rho_{nn}^{L(d)}$ becomes $\rho_{nn}^{L(c)} - \rho_{nn}^{R(d)}$ and describes fluctuating charge of the half-filled LL. Also, the following action on operators d_{mn} and $d_{mn}^\dagger$ is implied:

$$d_{mn} \rightarrow d_{nm} \quad (d_{mn}^\dagger \rightarrow d_{nm}^\dagger) \tag{45}$$

[compare the definitions of the density operators in (26) and (30), in L and R sectors]. Figures 1 and 2 illustrate the difference between the particle-hole transformation as a change of variables, and one that is an active transformation that transforms the special bilayer problem into the one of the half-filled LL.

V. FORMULATION OF THE HALF-FILLED PROBLEM

On the basis of the discussion in the previous section, we can conclude that the charge fluctuations around mean density $\frac{1}{2}(\frac{1}{2\pi l_B^2})$, where l_B is the magnetic length, can be expressed by $(\rho_{nn}^{L(c)} - \rho_{nn}^{R(d)})/2$. Thus, the Hamiltonian that can be considered together with the hard-core constraints $\rho_{nn}^{R(c)} + \rho_{nn}^{L(d)} = 1$ and $\rho_{nn}^{L(c)} + \rho_{nn}^{R(d)} = 1$ is

$$\mathcal{H} = \frac{1}{2} \int d\boldsymbol{q} \, V(|\boldsymbol{q}|)$$
$$\times \frac{\rho^{L(c)}(\boldsymbol{q}) - \rho^{R(d)}(\boldsymbol{q})}{2} \frac{\rho^{L(c)}(-\boldsymbol{q}) - \rho^{R(d)}(-\boldsymbol{q})}{2}. \tag{46}$$

The charge operator $[\rho^{L(c)}(\boldsymbol{q}) - \rho^{R(d)}(\boldsymbol{q})]/2$ does not satisfy the GMP algebra because of the doubling of the degrees of freedom (extra 2 in the GMP algebra). But together with the constraint $\rho^{L(c)}(\boldsymbol{q}) + \rho^{R(d)}(\boldsymbol{q}) = 0$ it does because $[\rho^{L(c)}(\boldsymbol{q}) - \rho^{R(d)}(\boldsymbol{q})]/2$ becomes $\rho^{L(c)}(\boldsymbol{q})$ [or $-\rho^{R(d)}(\boldsymbol{q})$ due to the PH symmetry] with the constraint, and represents the physical charge that satisfies the GMP algebra, expressed as a change of the electron density $\rho^{L(c)}(\boldsymbol{q})$ or a negative change in the hole density $-\rho^{R(d)}(\boldsymbol{q})$.

In the form of the Hamiltonian in (46) we incorporated the PH symmetry, by including both particles and holes with equal weights (on an equal footing) in the description of the change of the physical (electric) charge from the mean value. The Hamiltonian is manifestly invariant under the transformation $\rho^{L(c)} \rightarrow \rho^{R(d)}$ and $\rho^{R(d)} \rightarrow \rho^{L(c)}$, which represents an effective PH transformation. It consists of a charge conjugation, which transforms CFs, i.e., c's into CHs, i.e., d's,

and vice versa, and an antiunitary, i.e., time-reversal transformation that transforms phases into complex-conjugated ones ($R \to L$ and $R \to L$). Also, the transformation incorporates the reversal of momenta $\boldsymbol{k} \to -\boldsymbol{k}$ that can be associated with the time reversal, and thus $\rho^{L(c)}(\boldsymbol{q}) \to \rho^{R(d)}(-\boldsymbol{q})$ and $\rho^{R(d)}(\boldsymbol{q}) \to \rho^{L(c)}(-\boldsymbol{q})$. The charge conjugation and time reversal constitute the usual definition of the PH transformation in the presence of the magnetic field, under which the physics should be invariant. We should note that the charge conjugation in our case is not uniquely defined on c's and d's and we get the same transformations of $\rho^{L(c)}$ and $\rho^{R(d)}$ by considering $c_{\boldsymbol{k}} \to \alpha d_{-\boldsymbol{k}}$ and $d_{\boldsymbol{k}} \to \beta c_{-\boldsymbol{k}}$, where α and β are constants, and $|\alpha| = |\beta| = 1$.

We will recapitulate the necessary constraints in the formulation of the half-filled LL problem. We summarize that

$$\rho_{nn}^{R(c)} + \rho_{nn}^{L(d)} = 1, \tag{47}$$

together with the definite statistics requirement in the unphysical sector, and

$$\rho_{nn}^{L(c)} + \rho_{nn}^{R(d)} = 1, \tag{48}$$

with global constraints

$$\sum_n \rho_{nn}^{L(c)} = \sum_n \rho_{nn}^{R(d)} = N/2 \tag{49}$$

and

$$\sum_n \rho_{nn}^{R(c)} = \sum_n \rho_{nn}^{L(d)} = N/2 \tag{50}$$

form a set of constraints that define the half-filled LL problem.

In this case physical states are

$$|n_1, \dots, n_{N/2}, n_1', \dots, n_{N/2}'\rangle$$

$$= \sum_{m_1, \dots, m_{N/2}, m_1', \dots, m_{N/2}'}^{N} s^{m_1 \dots m_{N/2} m_1', \dots, m_{N/2}'}$$

$$\times c_{m_1 n_1}^\dagger \dots c_{m_{N/2} n_{N/2}}^\dagger d_{n_1' m_1'}^\dagger \dots d_{n_{N/2}' m_{N/2}'}^\dagger |0\rangle, \tag{51}$$

where $s^{m_1 \dots m_{N/2} m_1', \dots, m_{N/2}'}$ is nonzero, equal to one only if no index is equal to any other index. Compare with (14), and the discussion and (45) at the end of the previous section. Also, in (51), $n_i \neq n_j'$ for any $i, j = 1, \dots, N/2$.

VI. PREFERRED FORM OF THE HAMILTONIAN

The most natural binding in $\mathcal{H}$ is the Cooper pair binding $\langle c_{\boldsymbol{k}} d_{-\boldsymbol{k}} \rangle \neq 0$ in the s-wave channel. In a Hartree-Fock treatment, the mean-field description would have kinetic terms with quadratic dispersions, for c and d degrees of freedom, but this description of these objects does not conform to our expectation that they are dipoles, distinct dipole objects that pair, and that their dispersion comes from the polarization energy due to their dipole moments in a Hartree contribution as emphasized in [6]. In this way, we see a reason why the so-called PH Pfaffian, connected with s-wave pairing, is absent in a fixed LL [9–12].

As in the $\nu = 1$ bosonic case we may wonder whether there exists a "preferred" form of the Hamiltonian, i.e., the Hamiltonian with some of constraints included in its formulation but with the same description (and action) as the original one in

the physical space. The "preferred" form should capture the basic physics in the most efficient way, enabling the description of the basic physics in a Hartree-Fock treatment.

It is not hard to see that a unique low-momentum possibility for a kinetic (nonpairing) term can be reached by an addition of the following term:

$$\mathcal{H} \to \mathcal{H} + \frac{1}{2} \int d\boldsymbol{q} \, V(|\boldsymbol{q}|)$$

$$\times \frac{\rho^{R(c)}(\boldsymbol{q}) + \rho^{L(d)}(\boldsymbol{q})}{2} \frac{\rho^{R(c)}(-\boldsymbol{q}) + \rho^{L(d)}(-\boldsymbol{q})}{2}, \tag{52}$$

which uses the following constraint,

$$\rho^{R(c)}(\boldsymbol{q}) + \rho^{L(d)}(\boldsymbol{q}) = 0, \tag{53}$$

in the physical sector for the unphysical degrees of freedom that directly follows from the requirement (47).

In this way, we removed the cause for the s-wave Cooper pairing and modified the relevant term from

$$\sim \int d\boldsymbol{q} [-\rho^{L(c)}(\boldsymbol{q})\rho^{R(d)}(-\boldsymbol{q})]V(|\boldsymbol{q}|) \tag{54}$$

to

$$\sim \int d\boldsymbol{q} [-\rho^{L(c)}(\boldsymbol{q})\rho^{R(d)}(-\boldsymbol{q}) + \rho^{R(c)}(\boldsymbol{q})\rho^{L(d)}(-\boldsymbol{q})]V(|\boldsymbol{q}|)$$

$$\sim \int d\boldsymbol{q} \int d\boldsymbol{k}_1 \int d\boldsymbol{k}_2 \, c_{\boldsymbol{k}_1-\boldsymbol{q}}^\dagger c_{\boldsymbol{k}_1} d_{\boldsymbol{k}_2+\boldsymbol{q}}^\dagger d_{\boldsymbol{k}_2}$$

$$\times [i(\boldsymbol{k}_1 + \boldsymbol{k}_2) \times \boldsymbol{q}]V(|\boldsymbol{q}|). \tag{55}$$

Clearly, this term in the Hartree-Fock treatment can lead only to a $\langle c_{\boldsymbol{k}}^\dagger d_{\boldsymbol{k}} \rangle \neq 0$ instability and a Dirac-type description of the low-momentum physics.

VII. DIRAC THEORY FROM THE MEAN FIELD

Thus, we apply the Hartree-Fock approach to the relevant part of the Hamiltonian (we neglect the quadratic contributions from the other terms)

$$\mathcal{H}_D = \int \frac{d\boldsymbol{q}}{4} V(|\boldsymbol{q}|)[-\rho^{L(c)}(\boldsymbol{q})\rho^{R(d)}(-\boldsymbol{q}) + \rho^{R(c)}(\boldsymbol{q})\rho^{L(d)}(-\boldsymbol{q})]$$

$$\approx \int d\boldsymbol{q} \int d\boldsymbol{k}_1 \int d\boldsymbol{k}_2 \, \frac{V(|\boldsymbol{q}|)}{4(2\pi)^4}[i(\boldsymbol{k}_1 + \boldsymbol{k}_2) \times \boldsymbol{q}]$$

$$\times \left[\langle c_{\boldsymbol{k}_1-\boldsymbol{q}}^\dagger d_{\boldsymbol{k}_2} \rangle d_{\boldsymbol{k}_2+\boldsymbol{q}}^\dagger c_{\boldsymbol{k}_1} \right.$$

$$\left. + c_{\boldsymbol{k}_1-\boldsymbol{q}}^\dagger d_{\boldsymbol{k}_2} \langle d_{\boldsymbol{k}_2+\boldsymbol{q}}^\dagger c_{\boldsymbol{k}_1} \rangle - \langle c_{\boldsymbol{k}_1-\boldsymbol{q}}^\dagger d_{\boldsymbol{k}_2} \rangle \langle d_{\boldsymbol{k}_2+\boldsymbol{q}}^\dagger c_{\boldsymbol{k}_1} \rangle \right]$$

$$= \int \frac{d\boldsymbol{k}}{(2\pi)^2} (\Delta_{\boldsymbol{k}}^* d_{\boldsymbol{k}}^\dagger c_{\boldsymbol{k}} + \Delta_{\boldsymbol{k}} c_{\boldsymbol{k}}^\dagger d_{\boldsymbol{k}}) + \mathcal{C}, \tag{56}$$

where $\mathcal{C}$ is a constant and

$$\Delta_{\boldsymbol{k}} = |\boldsymbol{k}| \int d\boldsymbol{q} \, \frac{V(|\boldsymbol{q}|)}{2(2\pi)^2}(i\hat{\boldsymbol{k}} \times \boldsymbol{q})\langle d_{\boldsymbol{k}+\boldsymbol{q}}^\dagger c_{\boldsymbol{k}+\boldsymbol{q}} \rangle. \tag{57}$$

We diagonalize $\mathcal{H}_D$ by introducing $\alpha_{\boldsymbol{k}}$ and $\beta_{\boldsymbol{k}}$ operators

$$\begin{bmatrix} c_{\boldsymbol{k}} \\ d_{\boldsymbol{k}} \end{bmatrix} = \frac{1}{\sqrt{2}} \begin{bmatrix} 1 & -\exp\{-i\delta_{\boldsymbol{k}}\} \\ \exp\{i\delta_{\boldsymbol{k}}\} & 1 \end{bmatrix} \begin{bmatrix} \alpha_{\boldsymbol{k}} \\ \beta_{\boldsymbol{k}} \end{bmatrix}, \tag{58}$$

where $\delta_{\boldsymbol{k}}$ is defined by $\Delta_{\boldsymbol{k}} = |\Delta_{\boldsymbol{k}}| \exp\{-i\delta_{\boldsymbol{k}}\}$.

The very important question is how we choose the occupation of the momentum $\boldsymbol{k}$ states in the ground state that is

subjected to the constraints

$$\rho_{nn'}^{R(c)} + \rho_{n'n}^{L(d)} = \delta_{nn'} \qquad (59)$$

and

$$\rho_{nn'}^{L(c)} + \rho_{n'n}^{R(d)} = \delta_{nn'}. \qquad (60)$$

In a mean-field treatment we expect that at least the global constraints

$$\int \frac{d\boldsymbol{k}}{(2\pi)^2} c_{\boldsymbol{k}}^\dagger c_{\boldsymbol{k}} = \int \frac{d\boldsymbol{k}}{(2\pi)^2} d_{\boldsymbol{k}}^\dagger d_{\boldsymbol{k}} = \bar{\rho}_e = \frac{1}{2} \frac{1}{2\pi l_B^2} \qquad (61)$$

will be satisfied.

In the $\alpha_{\boldsymbol{k}}$, $\beta_{\boldsymbol{k}}$ language this implies

$$\int d\boldsymbol{k} (e^{-i\delta_{\boldsymbol{k}}} \alpha_{\boldsymbol{k}}^\dagger \beta_{\boldsymbol{k}} + e^{i\delta_{\boldsymbol{k}}} \beta_{\boldsymbol{k}}^\dagger \alpha_{\boldsymbol{k}}) = 0. \qquad (62)$$

This is a complex constraint and we may try to satisfy the requirement on α's and β's, by demanding that also the number of α's and β's is conserved. We might expect

$$\int \frac{d\boldsymbol{k}}{(2\pi)^2} \alpha_{\boldsymbol{k}}^\dagger \alpha_{\boldsymbol{k}} = \int \frac{d\boldsymbol{k}}{(2\pi)^2} \beta_{\boldsymbol{k}}^\dagger \beta_{\boldsymbol{k}} = \bar{\rho}_e. \qquad (63)$$

This seems a very crude "translation" of (62), but it incorporates the basic idea of our approach: to treat the particles and holes in an equal way, with their dynamics not independent but constrained, and in this way duplicated in a theory. The constraint implies two sectors, α and β, in the ground-state configuration: half-filled α sector and half-empty β sector. In this we implicitly assumed the finiteness of the available volume of $\boldsymbol{k}$: the number of available $\boldsymbol{k}$'s is N, the number of orbitals in the fixed LL. We expect that the description is duplicated by treating particles and holes in an equal way and, in the first (mean-field) approximation, the dynamics of α and β are separate and independent, and we may consider one or the other sector as a description of the problem.

Thus, for $\Delta_{\boldsymbol{k}}$ we get, by self-consistency,

$$\Delta_{\boldsymbol{k}} = |\boldsymbol{k}| e^{-i\phi_{\boldsymbol{k}}} \int_{|\boldsymbol{q}| \leqslant q_F} d\boldsymbol{q} \frac{V(|\boldsymbol{q}|)}{4(2\pi)^2} (i\hat{\boldsymbol{k}} \times \boldsymbol{q}) e^{-i\phi_{\boldsymbol{k}+\boldsymbol{q}}+i\phi_{\boldsymbol{k}}}, \qquad (64)$$

where $q_F = 1/l_B(=1)$. In this expression for $\Delta_{\boldsymbol{k}}$, because of the Gaussian in $V(|\boldsymbol{q}|)$, and the long-wavelength $|\boldsymbol{k}| \sim 0$ approximation, the contribution of the α sector is taken into account and we neglected the contribution from the β sector. We choose $\delta_{\boldsymbol{k}}$ to describe a definite momentum state $\delta_{\boldsymbol{k}} = \phi_{\boldsymbol{k}}$, where $\phi_{\boldsymbol{k}}$ is the phase of the complex variable $k = k_x + ik_y$. It follows that

$$|\Delta_{\boldsymbol{k}}| = |\boldsymbol{k}| \frac{\pi}{4(2\pi)^2} \int_0^{q_F} dq \, q^2 V(q). \qquad (65)$$

The strength of the amplitude is zero for higher angular momenta (other than angular momentum one).

Thus, by applying the Hartree-Fock approach to the preferred form of the Hamiltonian (53), we reached a low-energy description of the problem in terms of

$$\mathcal{H}_D = \int \frac{d\boldsymbol{k}}{(2\pi)^2} (\Delta_{\boldsymbol{k}}^* d_{\boldsymbol{k}}^\dagger c_{\boldsymbol{k}} + \Delta_{\boldsymbol{k}} c_{\boldsymbol{k}}^\dagger d_{\boldsymbol{k}}), \qquad (66)$$

where $\Delta_{\boldsymbol{k}} = (k_x - ik_y)\Delta$ with $\Delta = \frac{\pi}{4(2\pi)^2} \int_0^{q_F} dq \, q^2 V(q)$, at the finite density of the Dirac system.

The system that is described by the Dirac Hamiltonian, at finite density, represents a Fermi liquid. The time reversal in this system transforms a state at momentum $\boldsymbol{k}$ into a one with momentum $-\boldsymbol{k}$. Concretely, the state with momentum $\boldsymbol{k}$,

$$\frac{1}{\sqrt{2}} \begin{bmatrix} \exp\{-i\phi_{\boldsymbol{k}}\} \\ 1 \end{bmatrix}, \qquad (67)$$

where $\phi_{\boldsymbol{k}}$ is the phase of $k_+ = k_x + ik_y$, is transformed under the time-reversal transformation $U = -i\sigma_y K$, where σ_y is the Pauli matrix, and K denotes the complex conjugation, into

$$\frac{1}{\sqrt{2}} \begin{bmatrix} -1 \\ \exp\{i\phi_{\boldsymbol{k}}\} \end{bmatrix}, \qquad (68)$$

i.e., the state of the same energy but opposite momentum $-\boldsymbol{k}$. In the language of the basic PH transformation on the system (that acts on elementary particles, electrons, and holes), more precisely its realization on the particular description of the problem that we introduced, the time-reversal transformation, in the Dirac description, corresponds to the following transformation on c's and d's: $c_{\boldsymbol{k}} \to -d_{-\boldsymbol{k}}$ and $d_{\boldsymbol{k}} \to c_{-\boldsymbol{k}}$ (or $c_{\boldsymbol{k}} \to d_{-\boldsymbol{k}}$ and $d_{\boldsymbol{k}} \to -c_{-\boldsymbol{k}}$, compare with the description in Sec. V).

VIII. INCLUSION OF THE GAUGE INVARIANCE IN THE EFFECTIVE DIRAC THEORY

The original SU(N) gauge invariance (i.e., invariance under a change of basis in the fixed LL) is broken down [6] to U(1) in the mean-field (Hartree-Fock, averaged) description in (66). As we already detailed, in the microscopic approach the SU(N) gauge invariance is realized by the following two constraints,

$$\rho_{nn}^{R(c)} + \rho_{nn}^{L(d)} = 1, \qquad (69)$$

i.e., equal charge distribution of unphysical degrees of freedom, and

$$\rho_{nn}^{L(c)} + \rho_{nn}^{R(d)} = 1, \qquad (70)$$

i.e., the exclusion of the double occupancy between particles and holes (extra unphysical degrees of freedom).

To include fluctuations beyond the Hartree-Fock (mean-field) level in the long-wavelength domain, Dong and Senthil reinstated the SU(N) invariance in the description of the boson problem in terms of CFs by introducing composite fermion fields on noncommutative (deformed) space,

$$c(\boldsymbol{R}, \tau) = \int \frac{d^2\boldsymbol{k}}{(2\pi)^{\frac{3}{2}}} \exp(i\boldsymbol{k} \cdot \boldsymbol{R}) c_{\boldsymbol{k},\tau}, \qquad (71)$$

where $\boldsymbol{R}$ is the noncommutative (guiding center) coordinate, and τ is imaginary time. The connection with the microscopic description is the following:

$$c_{nm} = \langle n|c(\boldsymbol{R}, \tau)|m\rangle = \int \frac{d^2\boldsymbol{k}}{(2\pi)^{\frac{3}{2}}} \langle n|\tau_{\boldsymbol{k}}|m\rangle c_{\boldsymbol{k},\tau}. \qquad (72)$$

Physically, the state of the CF with vortex orbital m and electron orbital n can be described by a superposition of the (commutative) momentum $\boldsymbol{k}$ states, the weights of which depend on the effective distance between orbitals (the size of the dipole), $|\boldsymbol{k}_{\text{eff}}|$, because $\tau_{\boldsymbol{k}} = \exp(i\boldsymbol{k} \cdot \boldsymbol{R})$ is the translation

operator. For more details see [6]. In this way, the L and R transformations on c_{nm},

$$c_{nm} \rightarrow U^L_{n'n} c_{nm} U^R_{mm'}, \qquad (73)$$

can be represented by noncommutative Moyal-Weyl star product of fields on ordinary commutative space,

$$c(\boldsymbol{x}, \tau) \rightarrow U^L(\boldsymbol{x}, \tau) \star c(\boldsymbol{x}, \tau) \star U^R(\boldsymbol{x}, \tau), \qquad (74)$$

the star product being defined by

$$a(\boldsymbol{x}, \tau) \star b(\boldsymbol{y}, \tau) = e^{-\frac{i}{2} l_B^2 \epsilon^{ij} \frac{\partial}{\partial x^i} \frac{\partial}{\partial y^j}} a(\boldsymbol{x}, \tau) b(\boldsymbol{y}, \tau)|_{\boldsymbol{y} \rightarrow \boldsymbol{x}}. \qquad (75)$$

Two-dimensional Levi-Civita ($i, j = 1, 2$) is defined by $\epsilon^{12} = -\epsilon^{21} = 1$. See Appendix A for a more elaborate account.

The two constraints in our problem, (69) and (70), imply, in the effective description, simultaneous SU(N) transformations in L and R sectors to which we may associate gauge fields $a^{(1)}_\mu$ and $a^{(2)}_\mu$. We may also consider a (background) field A_μ that is associated with physical degrees of freedom (particles and holes) $\rho^{L(c)}_{nn} - \rho^{R(d)}_{nn}$.

Thus, we expect the corresponding covariant derivatives of the following form:

$$D_\mu c = \partial_\mu c - i\big(a^{(1)}_\mu + A_\mu\big) \star c - ic \star a^{(2)}_\mu, \qquad (76)$$

$$D_\mu d = \partial_\mu d - ia^{(2)}_\mu \star d - id \star \big(a^{(1)}_\mu - A_\mu\big) \qquad (77)$$

in the noncommutative description of the low-energy physics, following the considerations in [6] for the $\nu = 1$ system of bosons.

But, there is a problem with this proposal for a noncommutative description: the structure of these derivatives is not consistent with unitarity of gauge transformations (see Appendix B for details).

We have to step back to understand why this problem occurs. The formulation of the half-filled LL with constraints (69) and (70) is different from the case of bosons at $\nu = 1$ filling, in which there is a clear distinction between L and R, physical and unphysical sector, The formulation of the half-filled LL system is more intricate since it includes an exchange of L and R sectors, which complicates the distinction between them.

Having this in mind, we may reconsider the question of constraints and gauge invariance in an effective, long-wavelength theory that we are looking for, a theory that will nevertheless include some noncommutative aspects of the physical system. In order to get a gauge-invariant description, we will also apply the long-wavelength limit on the constraints (not just in the derivation of the Hamiltonian). In the ensuing long-wavelength description there is no distinction between physical (particles or holes) and unphysical (quantum of flux excitation) degrees of freedom, constraints (69) and (70) become one [compare (25) and (29) in the small-q limit, etc.]. We may also expect that A_μ (background field) couples symmetrically to the unphysical and physical sector. Thus, we may define covariant derivatives $D_\mu c$ and $D_\mu d$ in a way that ensures gauge invariance of the theory:

$$D_\mu c = \partial_\mu c - iA_\mu \star c - ic \star (a_\mu - A_\mu), \qquad (78)$$

$$D_\mu d = \partial_\mu d - iA_\mu \star d - id \star (a_\mu - A_\mu). \qquad (79)$$

The R gauge field is introduced in a decomposed way $a_\mu - A_\mu$, that will be natural in the commutative limit.

The change that we introduced by going from (76) and (77) to (78) and (79) is certainly drastic; the change is a departure from the microscopic description that we found based on the view of quasiparticles as neutral composites. In the case of bosons at filling factor one, Dong and Senthil showed that, on the basis of the Hartree-Fock description that is modified to include the SU(N) invariance, in the manner of noncommutative field theory, an approximate commutative field theory description can be reached (via Seiberg-Witten map) in the form of Halperin-Lee-Read (HLR) [1] description with a Chern-Simons term. This description cannot be viewed as a HLR theory (although of the same form), but as one that is based on the neutral composites (CFs) and limited to a LL, a description that is analogous to the description by composite bosons of the Laughlin case in [13]. In the case of electrons, in the half-filled LL, for which the Son's theory is relevant, one expects that, due to the requirement for the PH symmetry, a microscopic description will not generate a Chern-Simons term in an effective description. We encountered difficulties in the application of the program proposed by Dong and Senthil to maintain the gauge invariance we consider constraints in the long-wavelength limit, which certainly implies changes in the microscopic physics, i.e., ultraviolet domain. We will find that the ensuing field theory will have a Chern-Simons term, but one may argue that now Pauli-Villars type of regularization is associated with the field theory, i.e., we have to treat the high-energy physics in a different way as opposed to the version of the Son's theory that was first proposed by Son, and assumes the dimensional regularization. Therefore, although we have done a drastic change in the microscopic domain, the theory may still make sense as a theory based on another kind of quasiparticle [12,14] and give a version of the Son's theory described in [15–17].

The covariant derivatives (78) and (79) can define an NC description, and it should be checked whether in the commutative limit via Seiberg-Witten map we can recover the Son's theory to the linear order in the small parameter $\theta = -l_B^2$. Because of the simultaneous presence of small-θ and long-wavelength expansions, we will seek an effective description by considering only lowest-order terms. To find the first correction to the commutative limit we start with the (Euclidean) NC action of the form

$$S_{\text{NC}} = \int d\tau \, d^2\boldsymbol{x} \, (c^\dagger \star D_\tau c + d^\dagger \star D_\tau d + c^\dagger \star (iD_x + D_y)d$$
$$+ d^\dagger \star (iD_x - D_y)c + i(a_0 - A_0)\bar{\rho}_e). \qquad (80)$$

In S_{NC} we have a constraint term, linear in NC field $a_0 - A_0$, that fixes the total number of c and d fermions. Recall that our description is for $0 \leqslant |\boldsymbol{k}|$ in the upper half of Fig. 3, and thus we have

$$\int \frac{d^2\boldsymbol{k}}{(2\pi)^2} (c^\dagger_{\boldsymbol{k}} c_{\boldsymbol{k}} + d^\dagger_{\boldsymbol{k}} d_{\boldsymbol{k}})|_{\text{upper half}} = \bar{\rho}_e. \qquad (81)$$

In Appendix A we detail the small-θ expansion in terms of commutative fields $\hat{c}, \hat{d}, \hat{a}_\mu, \hat{A}_\mu$ (denoted by a hat symbol). We find $S_{\text{NC}} = S^{(0)} + S^{(1)} + \cdots$, where the classical limit ($\theta = 0$)
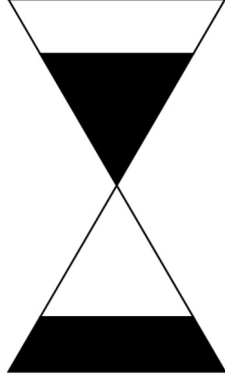
FIG. 3. A schematic illustration of the implementation of the global constraint in (61) via (63), i.e., half-filled positive-energy sector and half-empty negative-energy sector.

is simply

$$S^{(0)} = \int d\tau \, d^2\mathbf{x} \, (\hat{c}^\dagger D_\tau \hat{c} + \hat{d}^\dagger D_\tau \hat{d}$$
$$+ \hat{c}^\dagger (iD_x + D_y)\hat{d} + \hat{d}^\dagger (iD_x - D_y)\hat{c} + i(\hat{a}_0 - \hat{A}_0)\bar{\rho}_e),$$
(82)

and the linear NC correction reads as (see Appendix A for details)

$$S^{(1)} = \frac{i\bar{\rho}_e\theta}{2}\epsilon^{\alpha\beta\gamma}\int d\tau \, d^2\mathbf{x} \, (\hat{a}_\alpha - \hat{A}_\alpha)\partial_\beta(\hat{a}_\gamma - \hat{A}_\gamma)$$
$$+ \theta \int d\tau \, d^2\mathbf{x}\left[\hat{c}^\dagger\left(\frac{1}{2}\hat{f}_{12} - \hat{F}_{12}\right)D_\tau \hat{c}\right.$$
$$\left. - \hat{c}^\dagger\left(\frac{1}{2}\hat{f}_{10} - \hat{F}_{10}\right)D_y \hat{c} + \hat{c}^\dagger\left(\frac{1}{2}\hat{f}_{20} - \hat{F}_{20}\right)D_x \hat{c}\right]$$
$$+ \theta \int d\tau \, d^2\mathbf{x}\left[\hat{d}^\dagger\left(\frac{1}{2}\hat{f}_{12} - \hat{F}_{12}\right)D_\tau \hat{d}\right.$$
$$\left. - \hat{d}^\dagger\left(\frac{1}{2}\hat{f}_{10} - \hat{F}_{10}\right)D_y \hat{d} + \hat{d}^\dagger\left(\frac{1}{2}\hat{f}_{20} - \hat{F}_{20}\right)D_x \hat{d}\right],$$
(83)

where we introduced classical (commutative) gauge field strengths

$$\hat{F}_{\mu\nu} = \partial_\mu \hat{A}_\nu - \partial_\nu \hat{A}_\mu,$$
(84)

$$\hat{f}_{\mu\nu} = \partial_\mu \hat{a}_\nu - \partial_\nu \hat{a}_\mu,$$
(85)

and $\varepsilon^{\alpha\beta\gamma}$ is the Levi-Civita symbol.

The classical action $S^{(0)}$ and the Chern-Simons term in $S^{(1)}$ give the description of a version of the Son's theory [3] of the Dirac composite fermion [15–17] that assumes the Pauli-Villars type of regularization [12,14] because of the presence of the Chern-Simons term for field a_μ. Note that

the CS term has the correct coefficient $\frac{1}{8\pi}$. Also, in the linear NC correction $S^{(1)}$ the Dirac momentum density couples to the external electric field as expected from the Galilean invariance [4,18]. On the other hand, the presence of a coupling to the internal electric field $\hat{a}_\mu$ is quite natural and expected given the influence of other particles on a selected one. Also, we find that the presence of internal and external (i.e., departure from the uniform) magnetic field induces a change in the coefficient of the kinetic terms $\hat{c}^\dagger\partial_\tau\hat{c}$ and $\hat{d}^\dagger\partial_\tau\hat{d}$. Thus, we can conclude that the NC formulation, up to the first order in θ, recovers known results but also systematically adds terms that we may expect on physical grounds.

Although we reproduced the version of the Son's theory from a conjectured NC field theory that is partially based on the microscopic approach, we may wonder whether there is a formulation of an NC field theory that can reproduce, via the Seiberg-Witten map, the original version of the Son's theory. In that case, there would be no terms that are not invariant under the PH transformation, like the CS term for gauge field a_μ, and we would not have to assume that their effect will be erased or canceled by a particular way of regularization.

With the experience of the previous derivation that resulted in Eqs. (78) and (79) for covariant derivatives [and action (80)], we may ask ourselves how Eqs. (76) and (77) can be modified in a way that they still express the microscopic constraints, but represent valid covariant derivatives. A way to do that is by including a symmetry between physical and unphysical sectors by assuming that the background field A_μ couples to both sectors.

Thus, we consider

$$D_\mu c = \partial_\mu c - i(a_\mu^{(1)} + A_\mu) \star c - ic \star (a_\mu^{(2)} - A_\mu), \quad (86)$$

$$D_\mu d = \partial_\mu d - i(a_\mu^{(2)} + A_\mu) \star d - id \star (a_\mu^{(1)} - A_\mu). \quad (87)$$

Note that, as before, in the course of the implementing microscopic constraints (69) and (70), where each one constrains densities both in R and L sectors, the implied gauge fields connect, i.e., transform, at the same time, in the R and L sectors of fields c and d. We warn the reader that, as it stands, in the proposed covariant derivatives, only fields $b_{\mu,\pm}^{(1)} \equiv a_\mu^{(1)} \pm A_\mu$ and $b_{\mu,\pm}^{(2)} \equiv a_\mu^{(2)} \pm A_\mu$ are assumed to transform canonically (see Appendix B for details), and fields $a_\mu^{(1)}$, $a_\mu^{(2)}$, and A_μ, that enter their decompositions (as they refer both to R and L sectors) do not. The complete setup of the new NC theory is given in terms of $b_{\mu,\pm}^{(1)}$ and $b_{\mu,\pm}^{(2)}$ only. In Appendix B we explain why necessarily $b_{\mu,\pm}^{(1)} = b_{\mu,\pm}^{(2)} = b_{\mu,\pm}$, i.e., $a_\mu^{(1)} = a_\mu^{(2)}$, and we have an emerging symmetry between the unphysical and physical sectors. The fields $a_\mu = b_{\mu,+} + b_{\mu,-}$ and $A_\mu = (b_{\mu,+} - b_{\mu,-})/2$ will assume their expected U(1) gauge field roles in the commutative limit of the new theory in which we get the original version of the Son's theory that incorporates the PH symmetry (CP or CT in [3]). The resulting NC action up to first order is given by

$$S_{\text{NC}} = \int d\tau \, d^2\mathbf{x}(\hat{c}^\dagger D_\tau \hat{c} + \hat{d}^\dagger D_\tau \hat{d} + \hat{c}^\dagger(iD_x + D_y)\hat{d} + \hat{d}^\dagger(iD_x - D_y)\hat{c} + i\hat{a}_0\bar{\rho}_e) + \frac{i}{4\pi}\varepsilon^{\alpha\beta\gamma}\int d\tau \, d^2\mathbf{x} \, A_\alpha\partial_\beta a_\gamma$$
$$+ \theta \int d\tau \, d^2\mathbf{x}(\hat{c}^\dagger \hat{F}_{12}D_\tau \hat{c} - \hat{c}^\dagger \hat{F}_{10}D_y \hat{c} + \hat{c}^\dagger \hat{F}_{20}D_x \hat{c} + \hat{d}^\dagger \hat{F}_{12}D_\tau \hat{d} - \hat{d}^\dagger \hat{F}_{10}D_y \hat{d} + \hat{d}^\dagger \hat{F}_{20}D_x \hat{d}). \quad (88)$$

Thus, we obtained an effective (long-wavelength) NC field theory that consistently reproduces the Son's theory in the commutative limit. The introduced formalism and NC setup can be used to systematically generate corrections in small parameter θ. The achieved NC descriptions need further understanding and analysis especially concerning the questions of regularization and scaling of gauge fields [3,17,19]. At first glance, it seems that our approach does not have the scaling problem.

IX. INCLUSION OF PAIRING

We have eliminated unphysical degrees of freedom in a way of constraint (47), although in the case of the half-filled Landau level we also had to impose additional bosonic correlations of the unphysical degrees of freedom to fix a unique subspace of physical states: we called it spin-singlet sector of the SU(N) gauge symmetry of unphysical degrees of freedom. [Subsequently, we also had to impose (48) to eliminate hole degrees of freedom.]

We may search for another such state for unphysical degrees of freedom by imposing other constraint(s), such as

$$\rho_{nn'}^{R(c)} = \rho_{n'n}^{L(d)}. \tag{89}$$

In the inverse space this corresponds to

$$\rho^{R(c)}(\boldsymbol{q}) - \rho^{L(d)}(\boldsymbol{q}) = 0. \tag{90}$$

This choice seems natural as a requirement that will equalize and uniformly distribute the electric charge of the unphysical degrees of freedom (similarly to the special bilayer system).

The Hamiltonian that we can consider now is

$$\mathcal{H}_p = \mathcal{H} - \frac{1}{2} \int d^2\boldsymbol{q}\, V(|\boldsymbol{q}|)$$
$$\times \frac{\rho^{R(c)}(\boldsymbol{q}) - \rho^{L(d)}(\boldsymbol{q})}{2} \frac{\rho^{R(c)}(-\boldsymbol{q}) - \rho^{L(d)}(-\boldsymbol{q})}{2}, \tag{91}$$

which contains the same relevant two-body part for the Dirac physics as in the previous inclusion of constraints (53), but now we have the diagonal terms in the c and d sectors, like

$$\sim \int d^2\boldsymbol{q} \big[\rho^{L(c)}(\boldsymbol{q})\rho^{L(c)}(-\boldsymbol{q}) - \rho^{R(c)}(\boldsymbol{q})\rho^{R(c)}(-\boldsymbol{q})\big] V(|\boldsymbol{q}|)$$
$$\sim \int d^2\boldsymbol{q} \int d^2\boldsymbol{k}_1 \int d^2\boldsymbol{k}_2\, c_{\boldsymbol{k}_1-\boldsymbol{q}}^\dagger c_{\boldsymbol{k}_1} c_{\boldsymbol{k}_2+\boldsymbol{q}}^\dagger c_{\boldsymbol{k}_2}$$
$$\times i[(\boldsymbol{k}_1 - \boldsymbol{k}_2) \times \boldsymbol{q}] V(|\boldsymbol{q}|), \tag{92}$$

in the c sector, that can lead to p-wave (Pfaffian in the c sector and anti-Pfaffian in the d sector) instabilities.

We will assume a PH symmetry breaking and an effective Hartree-Fock-BCS Hamiltonian of the following form:

$$\mathcal{H}_{\mathrm{BCS}} = \int \frac{d^2\boldsymbol{k}}{(2\pi)^2}(\Delta_{\boldsymbol{k}}^* d_{\boldsymbol{k}}^\dagger c_{\boldsymbol{k}} + \Delta_{\boldsymbol{k}} c_{\boldsymbol{k}}^\dagger d_{\boldsymbol{k}})$$
$$+ \int \frac{d^2\boldsymbol{k}}{(2\pi)^2}(\tilde{\Delta}_{\boldsymbol{k}}^* c_{-\boldsymbol{k}} c_{\boldsymbol{k}} + \tilde{\Delta}_{\boldsymbol{k}} c_{\boldsymbol{k}}^\dagger c_{-\boldsymbol{k}}^\dagger). \tag{93}$$

Here, $\Delta_{\boldsymbol{k}}$ is defined in (57) and

$$\tilde{\Delta}_{\boldsymbol{k}}^* = |\boldsymbol{k}| \int d^2\boldsymbol{q}\, \frac{V(|\boldsymbol{q}|)}{4(2\pi)^2}(i\hat{\boldsymbol{k}} \times \boldsymbol{q})\langle c_{\boldsymbol{k}-\boldsymbol{q}}^\dagger c_{-\boldsymbol{k}+\boldsymbol{q}}^\dagger\rangle. \tag{94}$$

We project to the α sector by taking

$$c_{\boldsymbol{k}} \to \frac{1}{\sqrt{2}}\, \alpha_{\boldsymbol{k}} \tag{95}$$

and

$$d_{\boldsymbol{k}} \to \frac{1}{\sqrt{2}} e^{i\phi_{\boldsymbol{k}}} \alpha_{\boldsymbol{k}}. \tag{96}$$

Thus,

$$\mathcal{H}_{\mathrm{BCS}}^\alpha = \int \frac{d^2\boldsymbol{k}}{(2\pi)^2}\left[|\Delta_{\boldsymbol{k}}|\alpha_{\boldsymbol{k}}^\dagger \alpha_{\boldsymbol{k}} + \left(\frac{\tilde{\Delta}_{\boldsymbol{k}}^*}{2}\alpha_{-\boldsymbol{k}}\alpha_{\boldsymbol{k}} + \mathrm{H.c.}\right)\right]. \tag{97}$$

Equations [7] that follow and need to be solved self-consistently are

$$|\Delta_{\boldsymbol{k}}| = |\boldsymbol{k}| \int d^2\boldsymbol{q}\, \frac{V(|\boldsymbol{q}|)}{8(2\pi)^2}|\boldsymbol{q}| \sin^2(\phi_{\boldsymbol{q}})\left(1 - \frac{|\Delta_{\boldsymbol{k}+\boldsymbol{q}}| - |\Delta_{q_F}|}{E_{\boldsymbol{k}+\boldsymbol{q}}}\right) \tag{98}$$

and

$$|\tilde{\Delta}_{\boldsymbol{k}}| = |\boldsymbol{k}| \int d^2\boldsymbol{q}\, \frac{V(|\boldsymbol{q}|)}{16(2\pi)^2}|\boldsymbol{q}| \sin^2(\phi_{\boldsymbol{q}})\frac{|\tilde{\Delta}_{\boldsymbol{k}+\boldsymbol{q}}|}{E_{\boldsymbol{k}+\boldsymbol{q}}}, \tag{99}$$

where $E_{\boldsymbol{q}}^2 = (|\Delta_{\boldsymbol{q}}| - |\Delta_{q_F}|)^2 + |\tilde{\Delta}_{\boldsymbol{q}}|^2$. In this way, by specifying $V(|\boldsymbol{q}|)$ that will include factors due to the projection to a fixed Landau level, we can find amplitudes in $\tilde{\Delta}_{\boldsymbol{k}} = |\tilde{\Delta}_{\boldsymbol{k}}|\exp\{-i\phi_{\boldsymbol{k}}\}$ and $\Delta_{\boldsymbol{k}} = |\Delta_{\boldsymbol{k}}|\exp\{-i\phi_{\boldsymbol{k}}\}$.

X. PAIRING SOLUTIONS

The effective interaction in a fixed LL, $m = 0, 1, 2, \ldots$, is given by the following expression:

$$V(|\boldsymbol{q}|) = V_c(|\boldsymbol{q}|)e^{-\frac{|\boldsymbol{q}|^2}{2}}\left[L_m\left(\frac{|\boldsymbol{q}|^2}{2}\right)\right]^2, \tag{100}$$

where

$$V_c(|\boldsymbol{q}|) = \frac{V_0}{|\boldsymbol{q}|} \tag{101}$$

represents the Coulomb interaction $l_B = 1$, and L_m denotes the Laguerre polynomial associated with a fixed LL with the quantum number m.

In the LLL, Eqs. (98) and (99) lead to self-consistent solutions with the following amplitudes in the kinetic part $|\Delta_{\boldsymbol{k}}| = \Delta|\boldsymbol{k}|$ where $\Delta \approx 0.017\,086\, V_0$, and in the pairing part $|\tilde{\Delta}_{\boldsymbol{k}}| = \tilde{\Delta}|\boldsymbol{k}|$ where $\tilde{\Delta} \approx 0.001\,414\, V_0$. The self-consistent solution is numerically obtained using *Mathematica* with error estimation to 5×10^{-7}. Obviously, this represents a weak coupling case in which the kinetic part dominates. In Fig. 4 is illustrated solutions of Eqs. (98) and (99) with corresponding self-consistent solution.

In the sLL, we found that Eqs. (98) and (99) do not support a coexistence of (nonzero) kinetic and pairing amplitudes, and thus if only pairing is present it leads to a gapless (critical) p-wave state at this level of approximation. We considered the question of coexistence when a cubic term is generated in the expansion (56), in the kinetic part. The resulting equations are slightly modified equations (98) and (99) ($V \to \frac{V}{3!}$, etc.), and lead to a solution that describes a coexistence of pairing
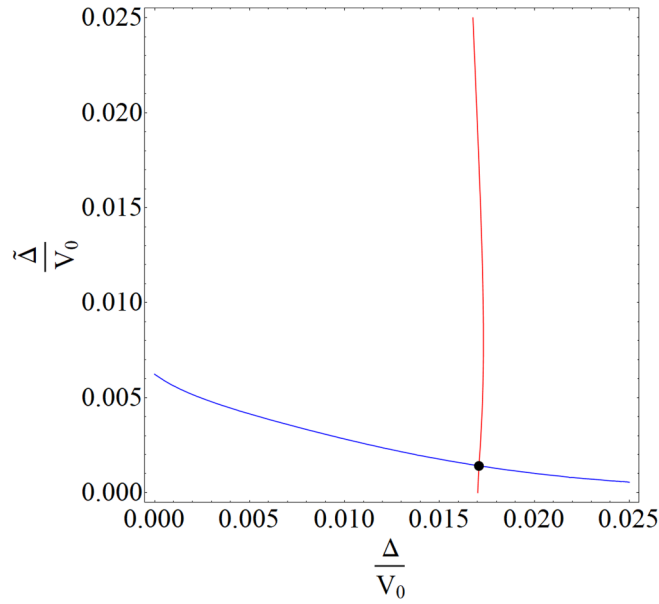
FIG. 4. The red line and the blue line represent solutions of Eqs. (98) and (99), respectively. The black dot marks the corresponding self-consistent solution.

$|\tilde{\Delta}_{\boldsymbol{k}}| = \tilde{\Delta}|\boldsymbol{k}|$ where $\tilde{\Delta} \approx 0.002\,337\,V_0$, and now $|\Delta_{\boldsymbol{k}}| = \Delta|\boldsymbol{k}|^3$ where $\Delta \approx 0.000\,591\,V_0$ ($l_B = 1$). The numerically obtained solution using *Mathematica* is shown in Fig. 5. The error is estimated to 1×10^{-6}. Thus, this is a strong coupling, weak pairing case that can be identified with the usual Pfaffian-state case in which all composite fermions are paired in the same way of a *p* wave.
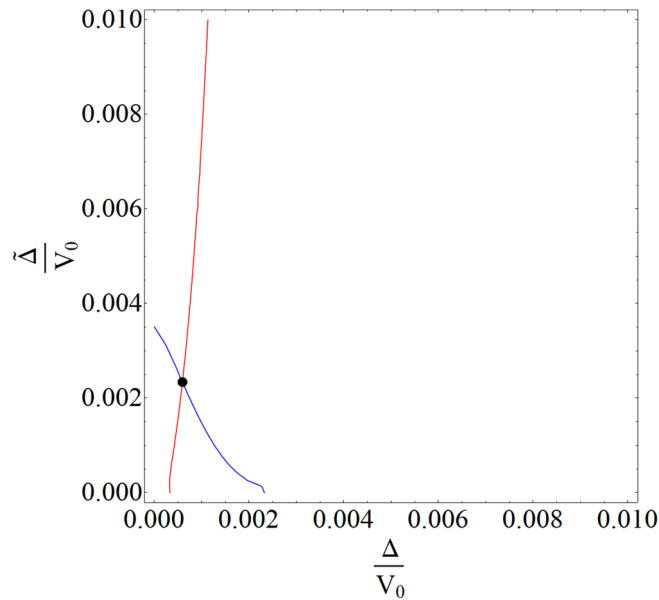

FIG. 5. The red line and the blue line illustrate solutions of modified equations (98) (with $V \to \frac{V}{3!}$, etc.) and (99), respectively. The black dot shows the corresponding self-consistent solution with pairing $|\tilde{\Delta}_{\boldsymbol{k}}| = \tilde{\Delta}|\boldsymbol{k}|$, and $|\Delta_{\boldsymbol{k}}| = \Delta|\boldsymbol{k}|^3$.

XI. CONCLUSIONS

To conclude, we presented a microscopic derivation of the Dirac CF theory and proposed an effective (long-wavelength) noncommutative field-theoretical description. The developed formalism can serve as a base for a deeper understanding of the strongly correlated physics of the half-filled LL. The microscopic formulation is used to describe (in a mean-field approach) pairing instabilities of the half-filled LL. The description is consistent with the known experimental and numerical phenomenology and provides further insights into the nature of pairing instabilities.

APPENDIX A: BASIC STRUCTURE OF NONCOMMUTATIVE GAUGE FIELD THEORY

Noncommutative (NC) spaces are geometric structures for which the notion of a point loses its meaning. They arise naturally in physics, the most famous example being the "quantum" phase space of generalized coordinates and momenta, understood as mutually noncommuting (incompatible) observables that satisfy Heisenberg's uncertainty relations $[q^i, p_j] = i\hbar\delta^i_j$. Another important example of NC space is realized by a single particle moving in the LLL; the guiding center coordinates of such a particle satisfy the following nontrivial commutation relation $[R_x, R_y] = -il_B^2$. Finally, in the context of quantum gravity, the idea of NC geometry is applied to the structure of space-time itself. In this case, the degree to which space-time coordinates fail to commute is usually taken to be proportional to the square of the Planck length. For a more comprehensive review see, for example, [20].

Here we give a short review of the basic structure of a non-commutative gauge field theory based on the Seiberg-Witten (SW) construction, first presented in the context of string theory [21]. An NC field theory is a field theory defined on a noncommutative space-time, i.e., a space-time described by mutually noncommuting coordinates $[x^\mu, x^\nu] \neq 0$. One way to implement this NC structure is to deform the algebra of functions (fields) on ordinary (commutative) space-time by introducing an NC star product, the simplest of which is the Moyal-Weyl star product

$$f(x) \star g(y) = e^{\frac{i}{2}\theta^{\mu\nu}\frac{\partial}{\partial x^\mu}\frac{\partial}{\partial y^\nu}} f(x)g(y)|_{y \to x}. \qquad (A1)$$

The deformation parameters $\theta^{\mu\nu}$ make a constant antisymmetric matrix (hence the term *constant noncommutativity*). Note that the first term in the expansion (in powers of θ) is just the ordinary commutative product of functions; higher-order terms represent NC corrections. When applied to coordinate functions themselves, the above formula gives us

$$[x^\mu, x^\nu] = x^\mu \star x^\nu - x^\nu \star x^\mu = i\theta^{\mu\nu}, \qquad (A2)$$

which is the simplest form of noncommutativity. Other types of noncommutativity are related to different star products (see [22]), but we will be working only with the Moyal-Weyl star product. A more comprehensive account on various aspects of NC geometry and NC gauge field theory can be found in [23].

Let $\{T_A\}$ be a set of generators of a gauge group $\mathcal{G}$. Infinitesimal SW gauge variation (NC gauge transformation) of an NC field Φ transforming in the fundamental representation of the

gauge group (e.g., a matter field) is defined by

$$\delta_\Lambda^{\text{SW}} \Phi = i\Lambda \star \Phi, \tag{A3}$$

where Λ stands for an NC gauge parameter. This transformation rule is analogous to the familiar one in ordinary, commutative gauge field theory, except for the noncommutative Moyal-Weyl star product.

There is a notorious problem concerning the closure axiom for SW gauge transformations. Namely, assuming that NC gauge parameter is Lie algebra valued, $\Lambda = \Lambda^A T_A$, the commutator of two SW transformations is given by

$$\begin{aligned}
\left[\delta_1^{\text{SW}} \overset{\star}{,} \delta_2^{\text{SW}}\right]\Phi &= (\Lambda_1 \star \Lambda_2 - \Lambda_2 \star \Lambda_1) \star \Phi \\
&= \tfrac{1}{2}\big(\big[\Lambda_1^A \overset{\star}{,} \Lambda_2^B\big]\{T_A, T_B\} + \big\{\Lambda_1^A \overset{\star}{,} \Lambda_2^B\big\}[T_A, T_B]\big) \star \Phi.
\end{aligned} \tag{A4}$$

Due to the appearance of anticommutator $\{T_A, T_B\}$, infinitesimal SW transformations do not in general close in the Lie algebra of a gauge group. A way to surmount this difficulty is to assume that NC gauge parameter Λ belongs to the universal enveloping algebra (UEA), which is always infinite dimensional [24]. This, however, leads to an infinite tower of new degrees of freedom (new fields), which is not a preferable property. To see this, consider a SW variation of the covariant derivative

$$\delta_\Lambda^{\text{SW}} D_\mu \Phi = i\Lambda \star D_\mu \Phi, \tag{A5}$$

with $D_\mu \Phi = \partial_\mu \Phi - iV_\mu \star \Phi$ (here we only consider "left" gauge field; the case of "right" gauge field is treated in a similar manner). This implies the following transformation rule for the NC gauge potential

$$\delta_\Lambda^{\text{SW}} V_\mu = \partial_\mu \Lambda + i[\Lambda \overset{\star}{,} V_\mu], \tag{A6}$$

meaning that it is also an UEA-valued object, which leaves us with an infinite number of new fields in the theory (one for each basis element of UEA).

SW map resolves this issue by demanding that NC fields can be expressed in terms of the NC parameter $\theta^{\mu\nu}$, commutative gauge parameter $\lambda = \lambda^A T_A$, commutative gauge potential $v_\mu = v_\mu^A T_A$, and their derivatives,

$$\Lambda = \Lambda(\theta, \lambda, v_\mu; \partial\lambda_\mu, \partial v_\mu, \dots), \tag{A7}$$

$$V_\mu = V_\mu(\theta, v_\mu, \partial v_\mu, \dots), \tag{A8}$$

where the ellipses stand for higher derivatives. In this way, NC theory is defined by the corresponding commutative one. There are no new degrees of freedom, just new interaction terms in the NC action.

NC gauge transformations are now induced by the corresponding commutative ones,

$$\delta_\lambda^{\text{SW}} \Lambda = \Lambda(v_\mu + \delta_\lambda v_\mu) - \Lambda(v_\mu), \tag{A9}$$

$$\delta_\lambda^{\text{SW}} V_\mu = V_\mu(v_\mu + \delta_\lambda v_\mu) - V_\mu(v_\mu), \tag{A10}$$

with $\delta_\lambda v_\mu = \partial_\mu \lambda + i[\lambda, v_\mu]$.

From (A4) and (A7) follows a consistency condition for NC gauge parameter,

$$\Lambda_1 \star \Lambda_2 - \Lambda_2 \star \Lambda_1 + i\big(\delta_1^{\text{SW}} \Lambda_2 - \delta_2^{\text{SW}} \Lambda_1\big) = i\Lambda_{-i[\lambda_1, \lambda_2]}, \tag{A11}$$

which can be solved perturbatively (this makes sense because the star product is also defined perturbatively). To this end, we represent the NC gauge parameter as an expansion in powers of the NC parameter θ, with coefficients built out of fields from the commutative theory,

$$\Lambda = \lambda + \Lambda^{(1)} + \Lambda^{(2)} + \cdots. \tag{A12}$$

The first term in the expansion (zeroth order in θ) is the commutative gauge parameter $\lambda = \lambda^A T_A$.

An NC gauge parameter, up to first order in $\theta^{\alpha\beta}$, is given by

$$\Lambda = \lambda - \tfrac{1}{2}\theta^{\alpha\beta} v_\alpha \partial_\beta \lambda + O(\theta^2), \tag{A13}$$

where $\theta^{\alpha\beta}$ ($\alpha, \beta = 0, 1, 2$) is a constant antisymmetric matrix of deformation parameters. In our case, $\theta^{\alpha\beta} = \theta\epsilon^{\alpha\beta}$ where $\theta = -l_B^2$ and $\epsilon^{\alpha\beta}$ is defined by $\epsilon^{0i} = 0$ ($i = 1, 2$) and $\epsilon^{12} = -\epsilon^{21} = 1$. Note that we work in $2 + 1$ dimensions and that the definition of $\epsilon^{\alpha\beta}$ implies that noncommutativity is realized only between spatial coordinates; it does not involve the time coordinate. Generalization to an arbitrary number of dimensions is straightforward.

Using the expansion (A13) and the transformation rule (A3) we readily obtain

$$\Phi = \phi - \frac{\theta^{\alpha\beta}}{2} v_\alpha \partial_\beta \phi + \frac{i\theta^{\alpha\beta}}{4} v_\alpha v_\beta \phi + O(\theta^2). \tag{A14}$$

Also, from (A6) follows the transformation law for the NC gauge field:

$$V_\mu = v_\mu - \frac{\theta^{\alpha\beta}}{2} v_\alpha (\partial_\beta v_\mu + F_{\beta\mu}). \tag{A15}$$

In connection to our model, with left (L) and right (R) NC U(1) gauge transformations acting on NC CF fields c and d, it is convenient to combine the two CFs into a two-component spinor,

$$\Psi = \begin{pmatrix} c \\ d \end{pmatrix}. \tag{A16}$$

Under an NC gauge transformation it changes as

$$\Psi \to \Psi' = U_L \star \Psi \star U_R, \tag{A17}$$

where $U_{L/R} = e^{i\Lambda_{L/R}}$. The NC gauge parameters $\Lambda_{L/R}$ have a special form given by

$$\Lambda_{L/R} = \begin{pmatrix} \Lambda_{L/R}^c & 0 \\ 0 & \Lambda_{L/R}^d \end{pmatrix}. \tag{A18}$$

Infinitesimally, we get

$$\delta\Psi = i(\Lambda_L \star \Psi + \Psi \star \Lambda_R). \tag{A19}$$

Covariant derivative of Ψ is defined by

$$D_\mu \Psi = \partial_\mu \Psi - iV_\mu^L \star \Psi - i\Psi \star V_\mu^R, \tag{A20}$$

where we introduced left V_μ^L and right V_μ^R NC gauge potential. One can show that $D_\mu \Psi$ transforms covariantly,

$$(D_\mu \Psi)' = U_L \star (D_\mu \Psi) \star U_R, \tag{A21}$$

provided that NC gauge potentials V_μ^L and V_μ^R transform in the following way:

$$\left(V_\mu^L\right)' = U_L \star V_\mu^L \star U_L^\dagger - i\partial_\mu U_L \star U_L^\dagger,$$
$$\left(V_\mu^R\right)' = U_R^\dagger \star V_\mu^R \star U_R - iU_R^\dagger \star \partial_\mu U_R. \quad (A22)$$

The NC action (in Euclidean signature) reads as

$$S_{\text{NC}} = \int d\tau\, d^2\boldsymbol{x}\left[\Psi^\dagger \star \tau^\mu D_\mu \Psi + i(V_0^L + V_0^R)\bar{\rho}_e\right], \quad (A23)$$

where we have

$$\tau^0 = \begin{pmatrix} 1 & 0 \\ 0 & 1 \end{pmatrix}, \quad \tau^1 = \begin{pmatrix} 0 & i \\ i & 0 \end{pmatrix}, \quad \tau^2 = \begin{pmatrix} 0 & 1 \\ -1 & 0 \end{pmatrix}. \quad (A24)$$

In terms of components, the action is

$$S_{\text{NC}} = \int d\tau\, d^2\boldsymbol{x}\left(c^\dagger \star D_\tau c + d^\dagger \star D_\tau d \right.$$
$$+ c^\dagger \star (iD_x + D_y)d + d^\dagger \star (iD_x - D_y)c$$
$$\left. + i(V_0^L + V_0^R)\bar{\rho}_e\right). \quad (A25)$$

The SW map allows us to represent NC fields in terms of ordinary fields from the corresponding commutative theory; these commutative fields will be denoted by a hat symbol. NC fields are organized as perturbation series in powers of the deformation parameter, and they reduce to ordinary fields in the $\theta = 0$ limit.

SW expansions of NC gauge parameters $\Lambda_{L/R}$ (up to first order) are (note the sign difference) given by

$$\Lambda_L = \hat{\Lambda}_L - \frac{\theta}{2}\epsilon^{\alpha\beta}\hat{V}_\alpha^L \partial_\beta \hat{\Lambda}_L,$$
$$\Lambda_R = \hat{\Lambda}_R + \frac{\theta}{2}\epsilon^{\alpha\beta}V_\alpha^R \partial_\beta \hat{\Lambda}_R. \quad (A26)$$

Likewise, SW expansions of L and R NC gauge potentials are (again, note the sign difference)

$$V_\mu^L = \hat{V}_\mu^L - \frac{\theta}{2}\epsilon^{\alpha\beta}\hat{V}_\alpha^L(\partial_\beta \hat{V}_\mu^L + \hat{F}_{\beta\mu}^L), \quad (A27)$$

$$V_\mu^R = \hat{V}_\alpha^R + \frac{\theta}{2}\epsilon^{\alpha\beta}\hat{V}_\alpha^R(\partial_\beta \hat{V}_\mu^R + \hat{F}_{\beta\mu}^R), \quad (A28)$$

with (commutative) gauge field strengths

$$\hat{F}_{\alpha\beta}^L = \partial_\alpha \hat{V}_\beta^L - \partial_\beta \hat{V}_\alpha^L,$$
$$\hat{F}_{\alpha\beta}^R = \partial_\alpha \hat{V}_\beta^R - \partial_\beta \hat{V}_\alpha^R. \quad (A29)$$

Finally, the SW expansion of the NC matter field reads as

$$\Psi = \hat{\Psi} - \frac{\theta}{2}\epsilon^{\alpha\beta}\left((\hat{V}_\alpha^L - \hat{V}_\alpha^R)\partial_\beta \hat{\Psi} - i\hat{V}_\alpha^L \hat{V}_\beta^R \hat{\Psi}\right). \quad (A30)$$

In particular, if we take $V_\mu^L = A_\mu$ and $V_\mu^R = a_\mu - A_\mu$ (both $V_\mu^{L/R}$ act as scalars), we get covariant derivatives (78) and (79), and the previous equation becomes

$$\Psi = \hat{\Psi} + \frac{\theta}{2}\epsilon^{\alpha\beta}((\hat{a}_\alpha - 2\hat{A}_\alpha)\partial_\beta \hat{\Psi} - i\hat{a}_\alpha \hat{A}_\beta \hat{\Psi}). \quad (A31)$$

In general, to compute a first-order NC correction for a product of two NC fields, we apply the following formula:

$$(A \star B)^{(1)} = A^{(1)}\hat{B} + \hat{A}B^{(1)} + \frac{i}{2}\theta^{\alpha\beta}\partial_\alpha\hat{A}\partial_\beta\hat{B}, \quad (A32)$$

where $A^{(1)}$ and $B^{(1)}$ are first-order NC corrections of A and B, respectively.

Thus, we can readily compute the NC covariant derivative

$$D_\mu\Psi = \partial_\mu\Psi - iV_\mu^L \star \Psi - i\Psi \star V_\mu^R$$
$$= D_\mu\hat{\Psi} + \frac{\theta}{2}\epsilon^{\alpha\beta}[(\hat{a}_\alpha - 2\hat{A}_\alpha)\partial_\beta D_\mu\hat{\Psi}$$
$$- i\hat{a}_\alpha\hat{A}_\beta D_\mu\hat{\Psi} - (\hat{f}_{\alpha\mu} - 2\hat{F}_{\alpha\mu})D_\beta\hat{\Psi}], \quad (A33)$$

with commutative field strengths $\hat{f}_{\mu\nu} = \partial_\mu\hat{a}_\nu - \partial_\nu\hat{a}_\mu$ and $\hat{F}_{\mu\nu} = \partial_\mu\hat{A}_\nu - \partial_\nu\hat{A}_\mu$. Commutative covariant derivative is simply $D_\mu\hat{\Psi} = \partial_\mu\hat{\Psi} - i\hat{a}_\mu\hat{\Psi}$.

Inserting (A27), (A28), (A31), and (A33) into the NC action (A23) and applying the rule (A32), we obtain the commutative action (82) and its first-order (in θ) NC correction (83).

In a similar fashion, if we consider covariant derivatives (86) and (87), i.e.,

$$D_\mu c = \partial_\mu c - i\left(a_\mu^{(1)} + A_\mu\right) \star c - ic \star \left(a_\mu^{(2)} - A_\mu\right), \quad (A34)$$

$$D_\mu d = \partial_\mu d - i\left(a_\mu^{(2)} + A_\mu\right) \star d - id \star \left(a_\mu^{(1)} - A_\mu\right), \quad (A35)$$

and require $a_\mu^{(1)} = a_\mu^{(2)} = \frac{1}{2}a_\mu$ (a full symmetry between physical and unphysical sectors), by the same procedure we obtain action (88) that reproduces the Son's theory at the commutative level.

APPENDIX B: STRUCTURE OF NC COVARIANT DERIVATIVES

Let us assume that the structure of NC covariant derivatives is given by Eqs. (76) and (77), i.e.,

$$D_\mu c = \partial_\mu c - i\left(a_\mu^{(1)} + A_\mu\right) \star c - ic \star a_\mu^{(2)}, \quad (B1)$$

$$D_\mu d = \partial_\mu d - ia_\mu^{(2)} \star d - id \star \left(a_\mu^{(1)} - A_\mu\right), \quad (B2)$$

as consistent with the microscopic constraints.

If we want both (B1) and (B2) to transform covariantly, i.e.,

$$D_\mu c \to U_L^c \star D_\mu c \star U_R^c, \quad (B3)$$

$$D_\mu d \to U_L^d \star D_\mu d \star U_R^d, \quad (B4)$$

we get two separate transformation laws for the gauge field $a_\mu^{(2)}$ (in the c case it acts from the right and in the d case from the left):

$$a_\mu^{(2)} \to U_R^{c\dagger} \star a_\mu^{(2)} \star U_R^c - iU_R^{c\dagger} \star \partial_\mu U_R^c, \quad (B5)$$

$$a_\mu^{(2)} \to U_L^d \star a_\mu^{(2)} \star U_L^{d\dagger} - i\partial_\mu U_L^d \star U_L^{d\dagger}. \quad (B6)$$

Consistency of the two demands the following constraints:

$$U_L^d = U_R^{c\dagger}, \quad (B7)$$

$$U_R^{c\dagger} \star \partial_\mu U_R^c = U_L^d \star \partial_\mu U_L^{d\dagger} = \partial_\mu U_L^d \star U_L^{d\dagger}. \quad (B8)$$

The second equation implies that $(\partial_\mu U_L^d) \star U_L^{d\dagger} - U_L^d \star (\partial_\mu U_L^{d\dagger}) = 0$, which is not consistent with U_L^d being unitary. Thus, we must change the structure of the derivatives.

Now consider the case when two covariant derivatives have the same structure,

$$D_\mu c = \partial_\mu c - iA_\mu \star c - ic \star b_\mu, \tag{B9}$$

$$D_\mu d = \partial_\mu d - iA_\mu \star d - id \star b_\mu, \tag{B10}$$

with two gauge fields: the external background field A_μ (which is L gauge field for both fields c and d) and $b_\mu = a_\mu - A_\mu$ (which is R gauge field for both fields c and d). They transform under gauge transformations in the following way:

$$A_\mu \rightarrow U_L \star A_\mu \star U_L^\dagger - i(\partial_\mu U_L) \star U_L^\dagger, \tag{B11}$$

$$b_\mu \rightarrow U_R^\dagger \star b_\mu \star U_R - iU_R^\dagger \star (\partial_\mu U_R). \tag{B12}$$

In the commutative limit, these become simple U(1) gauge transformations

$$A_\mu \rightarrow A_\mu + \partial_\mu \varphi_A, \tag{B13}$$

$$b_\mu \rightarrow b_\mu + \partial_\mu \varphi_b. \tag{B14}$$

The relevant field $a_\mu = b_\mu + A_\mu$ represents an independent U(1) gauge field with respect to A_μ.

In the setup implied by (86) and (87), i.e.,

$$D_\mu c = \partial_\mu c - i\left(a_\mu^{(1)} + A_\mu\right) \star c - ic \star \left(a_\mu^{(2)} - A_\mu\right), \tag{B15}$$

$$D_\mu d = \partial_\mu d - i\left(a_\mu^{(2)} + A_\mu\right) \star d - id \star \left(a_\mu^{(1)} - A_\mu\right), \tag{B16}$$

we have to consider four different gauge fields $b_{\mu,\pm}^{(1)} \equiv a_\mu^{(1)} \pm A_\mu$ and $b_{\mu,\pm}^{(2)} \equiv a_\mu^{(2)} \pm A_\mu$. Their transformation laws are given by

$$b_{\mu+}^{(1)} \rightarrow U_L^c \star b_{\mu+}^{(1)} \star U_L^{c\dagger} - i\partial_\mu U_L^c \star U_L^{c\dagger}, \tag{B17}$$

$$b_{\mu-}^{(1)} \rightarrow U_R^{d\dagger} \star b_{\mu-}^{(1)} \star U_R^d - iU_R^{d\dagger} \star \partial_\mu U_R^d, \tag{B18}$$

$$b_{\mu+}^{(2)} \rightarrow U_L^d \star b_{\mu+}^{(2)} \star U_L^{d\dagger} - i\partial_\mu U_L^d \star U_L^{d\dagger}, \tag{B19}$$

$$b_{\mu-}^{(2)} \rightarrow U_R^{c\dagger} \star b_{\mu-}^{(2)} \star U_R^c - iU_R^{c\dagger} \star \partial_\mu U_R^c. \tag{B20}$$

However, these four fields are not mutually independent, $b_{\mu,+}^{(1)} - b_{\mu,-}^{(1)} = b_{\mu,+}^{(2)} - b_{\mu,-}^{(2)}$, because aside from the external field, the theory can have only two more independent gauge fields, connected with two kinds of constraints. If we require that the difference of gauge fields transforms as a gauge field, we will have $U_L^c = U_R^{d\dagger}$ and $U_{L/R}^c = U_{L/R}^d$, i.e., possibilities for independent gauge transformations, independent gauge fields, will be reduced to just one, but this would contradict our beginning setup. That is why we need to take $a_\mu^{(1)} = a_\mu^{(2)}$, and have two independent gauge transformations and fields $a_\mu = 2a_\mu^{(1)} = 2a_\mu^{(2)}$ and A_μ in the commutative limit.

[1] B. I. Halperin, P. A. Lee, and N. Read, Phys. Rev. B **47**, 7312 (1993).

[2] G. Moore and N. Read, Nucl. Phys. B **360**, 362 (1991).

[3] D. T. Son, Phys. Rev. X **5**, 031027 (2015).

[4] V. Pasquier and F. D. M. Haldane, Nucl. Phys. B **516**, 719 (1998).

[5] N. Read, Phys. Rev. B **58**, 16262 (1998).

[6] Z. Dong and T. Senthil, Phys. Rev. B **102**, 205126 (2020).

[7] N. Read and D. Green, Phys. Rev. B **61**, 10267 (2000).

[8] G. Murthy and R. Shankar, Rev. Mod. Phys. **75**, 1101 (2003).

[9] A. C. Balram, M. Barkeshli, and M. S. Rudner, Phys. Rev. B **98**, 035127 (2018).

[10] R. V. Mishmash, D. F. Mross, J. Alicea, and O. I. Motrunich, Phys. Rev. B **98**, 081107(R) (2018).

[11] M. Yutushui and D. F. Mross, Phys. Rev. B **102**, 195153 (2020).

[12] L. Antonić, J. Vučičević, and M. V. Milovanović, Phys. Rev. B **98**, 115107 (2018).

[13] N. Read, Phys. Rev. Lett. **62**, 86 (1989).

[14] M. V. Milovanović, S. Djurdjević, J. Vučičević, and L. Antonić, Mod. Phys. Lett. B **34**, 2030004 (2020).

[15] A. C. Potter, M. Serbyn, and A. Vishwanath, Phys. Rev. X **6**, 031026 (2016).

[16] C. Wang, N. R. Cooper, B. I. Halperin, and A. Stern, Phys. Rev. X **7**, 031029 (2017).

[17] N. Seiberg, T. Senthil, C. Wang, and E. Witten, Ann. Phys. **374**, 395 (2016).

[18] K. Prabhu and M. M. Roberts, arXiv:1709.02814.

[19] D. Karabali, V. P. Nair, and A. P. Polychronakos, Nucl. Phys. B **627**, 565 (2002).

[20] R. J. Szabo, Phys. Rep. **378**, 207 (2003).

[21] N. Seiberg and E. Witten, J. High Energy Phys. 09 (1999) 032.

[22] P. Aschieri, L. Castellani, and M. Dimitrijević, Phys. Rev. D **87**, 024017 (2013).

[23] P. Aschieri, M. Dimitrijević, P. Kulish, F. Lizzi, and J. Wess, *Noncommutative Spacetimes: Symmetries in Noncommutative Geometry and Field Theory* (Springer, New York, 2009), Vol. 774.

[24] B. Jurčo, S. Schraml, P. Schupp, and J. Wess, Eur. Phys. J. C **17**, 521 (2000).

Pairing Instabilities and Critical States in Graphene Quantum Hall Systems

Sonja Predin

Scientific Computing Laboratory, Center for the Study of Complex Systems,Institute of Physics Belgrade, University of Belgrade, Pregrevica 118, 11080 Belgrade, Serbia

Abstract. The even-denominator fractional quantum Hall effect (FQHE) in graphene, observed in the fourth Landau level ($\mathcal{N} = 3$) [1], motivates our study of pairing and ground state properties in this system. Composite fermions, formed by electrons binding magnetic flux quanta, provide a key framework for understanding FQHE in conventional systems at half-filled Landau levels. Using the dipole representation of composite fermions [2], we derive an effective Hamiltonian for half-filled Landau levels, emphasizing particle-hole symmetry. At the Fermi level, the interplay of topology and symmetry drives the system toward a critical state. While we explore the possibility of paired states with well-defined solutions, our results show that the energetically favored state is a regularized, boost-invariant configuration without pairing instabilities [3]. This finding holds for the half-filled fourth Landau level ($\mathcal{N} = 3$) in graphene. We discuss the consistency of our results with experiments and simulations, highlighting the need for further research into alternative configurations in quantum Hall systems.

REFERENCES

1. Y. Kim, A. C. Balram, T. Taniguchi, K. Watanabe, J. K. Jain, and J. H. Smet, *Even denominator fractional quantum Hall states in higher Landau levels of graphene*, Nature Phys. **15**, 154 (2019).
2. S. Predin, A. Knežević, and M. V. Milovanović, *Dipole representation of half-filled Landau level*, Phys. Rev. B **107**, 155132 (2023).
3. Sonja Predin, *Dipole representation of composite fermions in graphene quantum Hall systems*, Phys. Rev. B **111**, 045132 (2025).

TT 31: Topology: Quantum Hall Systems

Time: Wednesday 15:00–16:45   Location: H31

Invited Talk   TT 31.1   Wed 15:00   H31
Quantum Skyrmion Hall Effect — •Ashley Cook — MPI-PKS, Dresden, Germany

Motivated by recent discovery of additional topologically non-trivial phases of matter in lattice models beyond established classification schemes, we generalise the framework of the quantum Hall effect (QHE) to that of the quantum skyrmion Hall effect (QSkHE). This involves one key generalisation: considering particles on a two-sphere, which see a $U(1)$ monopole, one can project to the lowest Landau level (LLL). Upon performing such a projection, the position coordinates become proportional to $SU(2)$ generators by quenching of kinetic energy. An almost point-like LLL corresponds to matrix representation size for the $SU(2)$ generators of N by N, with N small. The key generalisation is that such an almost point-like LLL with small orbital degeneracy can still host an intrinsically 2+1 dimensional topologically non-trivial many-body state. Equivalently, in regimes in which spin has previously been treated as a label (small N), spin encodes some finite number of spatial dimensions, in general. This many-body state can play the role, in the QSkHE, that a charged particle plays in the QHE.

TT 31.2   Wed 15:30   H31
Electric Field Induced Second-Order Anomalous Hall Transport in an Unconventional Rashba System — •Ankita Bhattacharya and Annica Black-Schaffer — Uppsala University, Sweden

Nonlinear responses in transport experiments may unveil information and generate new phenomena in materials that are not accessible at linear order due to symmetry constraints. While the linear anomalous Hall response strictly requires the absence of time-reversal symmetry, the second order, thus nonlinear, Hall response needs broken inversion symmetry. Recently, much effort has been made to obtain a second-order Hall voltage in response to a longitudinal ac driving current, both to obtain information about band geometric quantities and for its useful technological applications in rectification and frequency doubling. Typically, additional material engineering is required in noncentrosymmetric systems to obtain second-order responses since it obeys a stringent crystallographic symmetry constraint. To circumvent this, an alternative route is to apply a dc electric field. In our work, we uncover an electric field induced second-order anomalous Hall effect in an inversion-broken system possessing unconventional Rashba bands. We establish that the quantum metric, a geometrical feature of electronic wave functions providing information on non-trivial structure of Bloch bands, is responsible for providing the nonlinear Hall response. We are able to find a highly tunable electric field induced second-order anomalous Hall transport in probably the simplest system in 2D, which should be uncomplicated to verify experimentally due to multiple materials already being proposed.

TT 31.3   Wed 15:45   H31
Topological Thermal Hall Effect in the Geometrically Frustrated Magnet Gd_2PdSi_3 — •Parisa Mokhtari[1,2], Daiki Yamaguchi[1], Rinsuke Yamada[1], Akiko Kikkawa[3], Philipp Gegenwart[2], Yasujiro Taguchi[3], Yoshinori Tokura[1,3], and Max Hirschberger[1,3] — [1]Department of Applied Physics and Quantum-Phase Electronics Center, The University of Tokyo, Bunkyo-ku, Tokyo 113-8656, Japan — [2]Experimental Physics VI, Center for Electronic Correlations and Magnetism, University of Augsburg, 86135 Augsburg, Germany — [3]RIKEN Center for Emergent Matter Science, Wako, Saitama 351-0198, Japan

Geometrical frustrated Skyrmion lattices exemplify nontrivial topological states with non-zero scalar spin chirality and a finite Berry curvature in real space. In 2019, T. Kurumaji *et al.* reported a large topological Hall effect in the skyrmion phase in Gd_2PdSi_3 related to the spin chirality of the ground state [1].

In this talk, I will present the thermal Hall conductivity of the frustrated triangular-lattice magnet Gd_2PdSi_3. By entering the skyrmion lattice ground state, the field-dependent thermal Hall effect sharply increases against the adjacent incommensurate phases, similar to the electric Hall conductivity behaviour. Eventually, I will investigate the

relationship of Hall entropy to the charge current and discuss the non-dissipativity of topological quantum transport in the geometrically frustrated magnet Gd_2PdSi_3.
[1] T. Kurumaji *et al.*, Science **365**, 914 (2019).

TT 31.4   Wed 16:00   H31
Orbital Magnetization of Dirac Electrons on Curved Surfaces — •Maximilian Fürst — Universität Regensburg

Orbital magnetic response of 2D, (almost) free electrons has extensively been studied in the past, starting from the discovery of Landau levels of Schrödinger [1]/(massless) Dirac [2] electrons with a linear/squareroot dispersion in the field strength B. Apart from Landau diamagnetism, this leads to De-Haas-van-Alphen type oscillations of the susceptibility, that are periodic in $1/B$ [3]. Confining (massless) Dirac electrons on a curved surface predominantly leads to unusual oscillations of the susceptibility with periodicity in B. We discuss three example surfaces (Sphere, Cone, Pseudosphere) in a coaxial magnetic field.
[1] L. Landau, Z. Phys. A 64, 629 (1930).
[2] J. W. McClure, Phys. Rev. 104, 666 (1956).
[3] L. Heße, K. Richter, Phys. Rev. B 90, 205424 (2014).

TT 31.5   Wed 16:15   H31
Probing Fractional Statistics through Aharonov-Bohm Oscillations in Hanbury-Brown-Twiss Geometry — •Felix Puster, Matthias Thamm, and Bernd Rosenow — Institut für Theoretische Physik, Universität Leipzig, Brüderstraße 16, 04103 Leipzig, Germany

Since the theoretical prediction of anyonic excitations in the fractional quantum Hall effect, experimental evidence for their fractional statistics has been highly sought. In recent years, experiments have determined fractional braiding phases, providing clear evidence for fractional exchange phases. However, the braiding phase fixes the exchange phase of the particles only up to modulo Pi, leaving ambiguity in its exact value. Therefore, experiments capable of determining the exchange phase unambiguously are desired. To this end, we revisit the Hanbury-Brown-Twiss (HBT) geometry in the fractional quantum Hall regime. Our calculations extend previous theoretical work by incorporating an Aharonov-Bohm (AB) phase, finite temperature, and a finite distance between the tunneling points. We compute the current and current-current correlation functions and find that the anyonic exchange phase enters the AB oscillations in both quantities as an additive shift. While this shift is expected for the current-current correlations due to two-particle interference, for the current we interpret it as another example of time domain braiding of anyons – a phenomenon previously reported in geometries with tunneling of anyons across a quantum point contact.

TT 31.6   Wed 16:30   H31
Dipole Representation of Composite Fermions in Graphene's Quantum Hall Systems — •Sonja Predin — Scientific Computing Laboratory, Institute of Physics Belgrade, University of Belgrade, Pregrevica 118, 11080 Belgrade, Serbia

The even-denominator fractional quantum Hall effect has been observed in graphene's fourth Landau level (N = 3) [1]. Motivated by recent studies [2] on pairing and the nature of the ground state in this system, we extend the dipole representation of composite fermions to adapt it to graphene's quantum Hall systems, focusing on half-filled Landau levels. We derive an effective Hamiltonian incorporating particle-hole symmetry. At the Fermi level, the energetic instability of the dipole state is driven by the interplay between topology and symmetry, pushing the system towards a critical state. While paired states are considered, our findings demonstrate that a boost-invariant state lacking well-defined pairing instabilities is energetically favorable stable state, suggesting the absence of pairing instabilities in this system.
[1] Y.Kim,A.C.Balram,T.Taniguchi,K.Watanabe,J.K.Jain, J.H.Smet, Nat. Phys. 15, 154 (2019).
[2] A.Sharma, S.Pu, A.C.Balram, J.K.Jain, PRL 130, 126201 (2023).
[3] S.Predin, A.Knežević, M.V.Milovanović, PRB 107, 155132 (2023).
[4] S. Predin, arXiv:2408.10375.

Agent Based Modelling for Sustainable Public Transport Planning

Sonja Predin[1,2] and Richard Göbel[1]

[1]Institute of Information Systems, Hof University, Alfons-Goppel-Platz 1, 95030 Hof, Germany
[2]Scientific Computing Laboratory, Center for the Study of Complex Systems, Institute of Physics Belgrade, University of Belgrade, Pregrevica 118, 11080 Belgrade, Serbia, sonja@ipb.ac.rs

Abstract. Peripheral regions in Germany are facing significant negative demographic changes, including aging and population decline due to negative natural growth and relocation to industrial centers. Planning urban transport in peripheral regions is a challenging task, as the costs for municipal authorities are high, and despite these costs, users face infrequent and limited departures, long waiting times, and indirect routes. The aim of the Mobidig project, which was financed by the German Ministry of Transport and Digitalization, was to improve transport in these regions. We used demand forecasts and simulations to record and study the mobility needs of the people in the region. Using machine learning and statistical methods we analyzed data on topics such as population distribution, destinations, movements of vehicles and mobile devices, use of means of transport, and basic geodata, and created a virtual image of the region. Based on these analyses, we developed traffic simulation of the city of Hof, which allows us to predict the use of buses under various conditions. This simulation, as a digital twin of traffic, has shown very good alignment with the data used in real traffic. These project results already form the basis for further projects outside and within the region to create an economical and comprehensive public transport system in rural regions.

Keywords: Agent-oriented simulation, Demand generation, MATSim, Neural network, Probability method

Fractional Quantum Anomalous Hall Effect and Fractional Chern Insulators

Posters will be presented in two poster sessions - **Monday, 5th February, 17:30 - 18:30** (focus on odd poster numbers) and **Tuesday, 6th February, 19:00 - 20:00** (focus on even poster numbers) **- the poster numbers.**

For each poster contribution there will be one poster wall (width: 97 cm, height: 250 cm) available. Please do not feel obliged to fill the whole space. Posters can be put up for the full duration of the event.

POSTER

Entanglement smectic and stripe order
Chakraborty, Nilotpal

Spontaneous symmetry breaking and more recently entanglement are two cornerstones of quantum matter. We introduce the notion of anisotropic entanglement ordered phases, where the spatial profile of spin-pseudospin entanglement spontaneously lowers the four-fold rotational symmetry of the underlying crystal to a two-fold one, while the charge density retains the full symmetry. The resulting phases, which we term entanglement smectic and entanglement stripe, exhibit a rich Goldstone mode spectrum and set of phase transitions as a function of underlying anisotropies. We discuss experimental consequences of such anisotropic entanglement phases distinguishing them from more conventional charge or spin stripes. Our discussion of this interplay between entanglement and spontaneous symmetry breaking focuses on multicomponent quantum Hall systems realizing textured Wigner crystals, as may occur in graphene or possibly also in moire systems, highlighting the rich landscape and properties of possible entanglement ordered phases.

+

The Landscape of Tight-Binding models
Dagnino, Andrea Kouta

Tight-binding models are ubiquitous in condensed matter physics. Fundamental properties of many materials can be understood from simple toy models of electrons hopping between orbitals on a lattice. In particular, crystallographic symmetries are crucial in determining the degeneracies of band structures at high symmetry points in the Brillouin zone. These degeneracies fundamentally affect the properties of the material that is being modelled, ranging from the allowed optical

transitions to symmetry-indicated topological invariants. Getting a full list of crystal symmetries of a material is therefore crucial when trying to predict or understand its physical properties. In this poster, we systematically study the symmetries of lattices in 3 dimensions and their implications for the corresponding tight-binding models. We uncover a landscape of tight-binding models related by crystal symmetries, and apply these findings to understand the recently uncovered altermagnetic nature of RuO_2 and MnTe.

+

Higher Chern number ideal bands of helical twisted trilayer graphene in magnetic fields

Datta, Anushree

Helical twisted trilayer graphene (HTTG), characterized by three layers of graphene with same successive twists, is an unique tunable platform for realizing a variety of correlated and topological phases. It exhibits a supermoire with domains centered around stacking points ABA or BAB, where two well separated low energy bands appear with Chern numbers +/-(2, -1) forming a Chern mosaic. When the twists are tuned to a 'magic-angle', these bands flatten perfectly at the chiral limit, with large degeneracies at the zero energy. We show that HTTG retains such precise flatness of the low energy bands in the chiral limit even when a perpendicular magnetic field is applied. By a mapping of the zero-energy wavefunctions with those of the lowest Landau level, we identify the analytical forms of the zero-modes at finite magnetic fields. Furthermore, we find topological phase transitions involving gap closings and openings, at fields corresponding to unit and half-flux per unit cell, leading to higher Chern number bands. Such transitions happen at the supermoire scale which alter with each other when the direction of the field is reversed. Due to large moire length scale, these transitions at strong flux limit can become experimentally accessible.

+

E-T Duality of type-II Composite Fermion Wigner Solid in Two Dimensional Hole Gas

Dong, Yu-Jiang

Two-dimensional hole gas (2DHG) system exists the competition of quantum Hall effect (QHE) liquid and Wigner solid (WS) solid under high magnetic field (B) and low temperature (T). We report non-linear differential conductance around $v=1$ and $nu=1/3$ states in GaAs/AlGaAs quantum well (QW) 2DHGs, which in accord with the feature of type-II CFWS. Particularly, the applied electric field affects the magnetoconductance diagram in a way similar to the temperature, which is known as "E-T duality". According to our analysis, this "E-T duality" is consistent with the Berezinskii-Kosterlitz-Thouless (BKT) theory, which is well-known in two-dimensional phase transitions.

+

Continuum Hamiltonians for non-abelian spin liquids

Feuerpfeil, Andreas

The bosonic fractional Chern insulator is intricately connected to quantum spin liquids. Thus, we investigate the Read-Rezayi fractional quantum Hall states for $k = 2$ (Moore-Read) and $k = 3$. The non-abelian excitations of the $k = 3$-state are Fibonacci anyons and thus provide a platform for universal quantum computing. Following the analogy of the Calogero-Sutherland model, we construct parent continuum

Hamiltonians for these states. Based on the identification of fractional quantum Hall states with correlation functions of CFTs, we use the Belavin–Polyakov–Zamolodchikov equation for the corresponding primary fields to find destruction operators with the ground state in their kernels and combine them to form parent Hamiltonians.

+

Strain-induced pseudo-magnetic field beyond graphene

Guo, Huaiming

Quantum Monte Carlo simulations are applied to study quantum antiferromagnets on a hexagonal lattice under three-axis stress. We consider the triangular geometry, where strain induces dimerization of the exchange couplings around the three corners of the triangle, thereby disrupting the antiferromagnetic order. The antiferromagnetic regions continuously shrink with increasing strain, and for the same strain intensity, the precise numerical results yield much smaller antiferromagnetic regions than predicted by linear spin-wave theory. We also extract the local magnetization using numerical analytical continuation for the Heisenberg case and find no evidence of pseudo-Landau levels. However, it is currently unclear whether the absence of pseudo-Landau levels is a consequence of the numerical analytical continuation itself. Therefore, the existence of pseudo-Landau levels for magnons generated by three-axis strain in the Heisenberg Hamiltonian remains an open question. Our theoretical results are closely related to two-dimensional van der Waals antiferromagnets and hold promise for experimental realization.

+

Fractional Chern Insulator in Twisted Bilayer MoTe2

He, Yuchi

A recent experiment has reported the first observation of a zero-field fractional Chern insulator (FCI) phase in twisted bilayer MoTe2 moiré superlattices. The experimental observation is at an unexpected large twist angle 3.7∘ and calls for a better understanding of the FCI in real materials. In this work, we perform large-scale density functional theory calculation for the twisted bilayer MoTe2, and find that lattice reconstruction is crucial for the appearance of an isolated flat Chern band. The existence of the FCI state at ???? $= -2/3$ is confirmed by exact diagonalization. We establish phase diagrams with respect to the twist angle and electron interaction, which reveal an optimal twist angle of 3.5∘ for the observation of FCI. We further demonstrate that an external electric field can destroy the FCI state by changing band geometry and show evidence of the ???? $= -3/5$ FCI state in this system. Our research highlights the importance of accurate single particle band structure in the quest for strong correlated electronic states and provides insights into engineering fractional Chern insulator in moiré superlattices.

+

Laughlin topology in fractal lattices without area law

Jha, Mani Chandra

Laughlin states have recently been constructed on fractal lattices, and the charge and braiding statistics of the quasiholes were used to confirm that these states have Laughlin-type topology. Here we investigate density, correlation, and entanglement properties of the states on a fractal lattice derived from a Sierpinski triangle with the purpose of identifying similarities and differences compared to two-dimensional

systems and with the purpose of investigating whether various probes of topology work for fractal lattices. Similarly to two-dimensional systems, we find that the connected particle-particle correlation function decays roughly exponentially with the distance between the lattice sites measured in the two-dimensional plane, but the values also depend on the local environment. Contrary to two-dimensional systems, we find that the entanglement entropy does not follow the area law if one defines the area to be the number of nearest-neighbor bonds that cross the edge of the selected subsystem. Considering bipartitions with two bonds crossing the edge, we find a close to logarithmic scaling of the entanglement entropy with the number of sites in the subsystem. This also means that the topological entanglement entropy cannot be extracted using the Kitaev-Preskill or the Levin-Wen methods. Studying the entanglement spectrum for different bipartitions, we find that the number of states below the entanglement gap is robust and the same as for Laughlin states on two-dimensional lattices. Reference: PHYSICAL REVIEW B 105, 085152 (2022)

+

Nagaoka ferromagnetism and spin-hole fractionalization in hole-doped Kitaev spin liquids

Kadow, Wilhelm

The dynamical response of a quantum spin liquid upon injecting a hole is a pertinent open question. In experiments, the hole spectral function, measured momentum-resolved in angle-resolved photoemission spectroscopy (ARPES) or locally in scanning tunneling microscopy (STM), can be used to identify spin liquid materials. In this study, we employ tensor network methods to simulate the time evolution of a single hole doped into the Kitaev spin-liquid ground state and reveal two fundamentally different scenarios. For ferromagnetic spin couplings, the spin liquid is highly susceptible to hole doping: a Nagaoka ferromagnet forms dynamically around the doped hole, even at weak coupling. By contrast, in the case of antiferromagnetic spin couplings, the hole spectrum demonstrates an intricate interplay between charge, spin, and flux degrees of freedom, best described by a parton mean-field ansatz of fractionalized holons and spinons. Moreover, we find a good agreement of our numerical results to the analytically solvable case of slow holes. Our results demonstrate that dynamical hole spectral functions provide rich information on the structure of fractionalized quantum spin liquids.

+

D2 or dDsC van der Waals corrections for twisted MoTe2 Comparison of many-body phase diagrams

Li, Jiangxu

We investigate the global many-body phase diagram in twisted bilayer MoTe2, using continuum model multiband exact diagonalization. From previous large-scale first-principles calculations, two groups of continuum model parameters have been proposed from D2 and dDsC corrections, respectively. Compared to the experimental phase diagram, we note the dDsC continuum model well captures the $\upsilon=1$ integer, $\upsilon=-2/3$ fractional quantum anomalous Hall states, and $\upsilon=-1/3$ charge density wave states simultaneously. While for the continuum model from D2 correction, we observe a Mott ferroelectric state at $\upsilon=1$ for dielectric constant $\epsilon<10$ at experimental twist angles 〖3.0〗 ^∘$<\theta<$ 〖4.0〗 ^∘. More importantly, in the D2 continuum model, $\upsilon=-1/3$ and $\upsilon=-2/3$ are both fractional quantum anomalous Hall states at $\epsilon=10$, and charge density wave states at $\epsilon=5$.

+

Broken Symmetry in Ideal Chern Bands

Liu, Hui

Recent observations of the fractional anomalous quantum Hall effect in moir\'e materials have reignited the interest in fractional Chern insulators (FCIs). The chiral limit in which analytic Landau level-like single particle states form an "ideal" Chern band and local interactions lead to Laughlin-like FCIs at 1/3 filling, has been very useful for understanding these systems by relating them to continuum Landau levels. We show, however, that, even in the idealized chiral limit, a fluctuating quantum geometry leads to strongly broken symmetries and a phenomenology very different from that of Landau levels. In particular, particle-hole symmetry is strongly violated and e.g. at 2/3 filling an emergent interaction driven Fermi liquid state with no Landau level counterpart is energetically favoured.

+

Lattice relaxation, electronic structure and continuum model for twisted bilayer MoTe2

Mao, Ning

Our study delves into the effect of lattice relaxation on the moiré band structures of twisted bilayer MoTe2 , implemented by large-scale first-principles calculations and transfer learning neural network. Throughout our study, we have incorporated two van der Waals correction methods: the Grimme D2 method and a density-dependent energy correction. Notably, the latter method demonstrates a continuous evolution of bandwidth with respect to twist angles. Our findings reveal the critical role of in-plane lattice displacements, which generate substantial pseudomagnetic fields, reaching up to 250 T. Building on these insights, we have developed a comprehensive continuum model with a single set of parameters for a wide range of twist angles, providing a useful starting point for many-body simulation.

+

Kagome chiral spin liquid in transition metal dichalcogenide moiré bilayers

Motruk, Johannes

While electronic topological phases in moiré heterostructures of transition metal dichalcogenides (TMDs) have been confirmed experimentally, exotic magnetic orders have not been reported so far. In this work, we investigate TMD moiré bilayers at n = 3/4 filling of the moiré flat band, where they can develop a kagome charge order. We derive an effective spin model for the resulting localized spins and find that its further neighbor spin interactions can be much less suppressed than the corresponding electron hopping strength. Using density matrix renormalization group simulations, we study its phase diagram and, for realistic model parameters relevant for WSe_2/WS_2, we show that this material can realize the exotic chiral spin liquid phase and the highly debated kagome spin liquid. Our work thus demonstrates that the frustration and strong interactions present in TMD heterobilayers provide an exciting platform to study spin liquid physics.

+

Fractional quantum Hall effect on fractals

Nielsen, Anne

The Laughlin and Moore-Read states can be formulated as infinite-dimensional-matrix product states. The construction allows us to generalize the Laughlin and Moore-Read states to arbitrary lattices embedded in two dimensions and to find few-body, non-local, exact parent Hamiltonians for the states. We numerically and analytically study the properties of the Laughlin state on fractal lattices with different Hausdorff dimensions. We find that the states support anyons with fractional statistics as expected for the Laughlin state, but the states do not necessarily follow the area law. Finally, we optimize local Hamiltonians to have maximal ground state overlap with the Laughlin state. References: Phys. Rev. Research 2, 023401 (2020) Phys. Rev. B 105, 085152 (2022) J. Stat. Mech. 2023, 053103 (2023) Phys. Rev. A 107, 063315 (2023)

+

Braiding Laughlin quasi-holes in ultracold atoms using Ramsey interferometry

Palm, Felix

Braiding non-Abelian anyons in topologically ordered systems has been proposed as a possible route towards topologically protected quantum computing. While recent experiments based on various platforms have made significant progress towards this goal, coherent control over individual anyonic excitations has still not been achieved today. At the same time, progress in cold-atom quantum simulators resulted in the realization of a two-boson $v = 1/2$-Laughlin state, a paradigmatic fractional quantum Hall state hosting Abelian anyonic quasi-holes. Here we show that cold atoms in quantum gas microscopes are a suitable platform to create and manipulate these quasi-holes. First, we show that a Laughlin state of eight bosons can be realized by connecting small patches accessible in experiments. Next, we demonstrate that two cross-shaped pinning potentials are sufficient to create two quasi-holes in this Laughlin state. Starting with these two quasi-holes we numerically perform an adiabatic exchange procedure, and reveal their semionic braiding statistics for various exchange paths, thus clarifying the topological nature of these excitations. Finally, we propose an experimentally feasible interferometry protocol to probe the braiding phase in quantum gas microscopes, using a two-level impurity immersed in the fractional quantum Hall fluid. We conclude that braiding experiments of Abelian anyons are now within reach in cold-atom quantum simulators, providing a crucial step towards the long-standing goal of non-Abelian anyon braiding with local coherent control.

+

Probing chirality in Weyl and Dirac semimetals with a non-linear Hall response

Peshcherenko, Nikolai

We suggest a simple chirality probe in TR invariant Weyl and Dirac semimetals by nonlinear Hall response. Chiral anomaly effect arising in parallel electric and magnetic fields causes Weyl cones of different chirality to become shifted in energy space with respect to each other which leads to chirally asymmetric intranode relaxation times. Due to this asymmetry, electrical currents excited by external electric field do not perfectly compensate each other. We predict that this effect could be also observed in circular dichroism measurements.

+

Floquet engineering of the toric-code Hamiltonian

Petiziol, Francesco

We present a hybrid Floquet-Trotter approach for the quantum simulation of Kitaev's toric-code Hamiltonian, implementable in superconducting circuits. Our method exploits the commutativity of different terms in Kitaev's Hamiltonian and achieves the required four-spin interactions in a nonperturbative way. Building on this result, we further present protocols for preparing topologically ordered ground states with high fidelity and to simulate the transition into the spin liquid phase. We discuss opportunities to use periodic driving to mimic non-Abelian behaviour in the Abelian model.

+

Dipole representation of half-filled Landau level: quantum Hall and its bilayers

Predin, Sonja

The formalism for composite fermions, initially developed for bosons at filling factor $v = 1$ [1, 2], has been a cornerstone in understanding the fractional quantum Hall effect (FQHE). We derive the Dirac composite fermion theory for a half-filled Landau level from first principles [3]. In this talk, we introduce a variant of dipole representation for composite fermions in a half-filled Landau level, taking into account the symmetry under exchange of particles and holes. This is implemented by a special constraint on composite fermion and composite hole degree of freedom (of an enlarged space), that makes the resulting composite particle, dipole, a symmetric object. Our investigation focuses on an effective Hamiltonian that commutes with the constraint in physical space while preserving boost invariance at the Fermi level. Our calculations [4] of the Fermi liquid parameter F2 demonstrate remarkable agreement with previous numerical investigations [5]. Furthermore, the quantum Hall bilayer at filling factor $v=1$ represents a competition of Bose-Einstein condensation (BEC) at small distances between layers and fermionic condensation, which influence grows with distance and results in two separate Fermi liquid states of underlying quasiparticles at very large (infinite) distance. The most intriguing question is whether at intermediate distances between layers a special, distinct phase exists, or a single transition occurs, with possibility that this happens at infinite distance. Here, using a dipole representation of fermionic quasiparticles, we find a support for the latter scenario: for a large, relevant interval BEC condensation, identified as a Cooper s-wave pairing of dipole quasiparticles, wins over Cooper p-wave pairing and s−wave excitonic pairing of the same quasiparticles [6]. [1] N. Read, Phys. Rev. B 58, 16262 (1998). [2] Z. Dong and T. Senthil, Phys. Rev. B 102, 205126 (2020). [3] D. Gočanin, S. Predin, M. D. Ćirić, V. Radovanović, and M. Milovanović, Phys. Rev. B 104, 115150 (2021). [4] S. Predin, A. Knežević, and M. V. Milovanović, Phys. Rev. B 107, 155132 (2023). [5] K. Lee, J. Shao, E.-A. Kim, F. D. M. Haldane, and E. H. Rezayi, Phys. Rev. Lett. 121, 147601 (2018). [6] S. Predin, and M. Milovanovic, S. Predin and M. V. Milovanovic, Phys. Rev. B 108, 155129, (2023).

Rashba spin-orbital coupling enhanced excitonic topological order in InAs/GaSb bilayer system

Qiao, Weiliang

In the last few decades, the coupling between layers in two-dimensional correlated electronic system has been one of the most interesting topics in the field of condensed matter physics [1-3]. InAs/GaSb quantum well (QW) is one of the most interesting layer-layer correlated systems. Thanks to the unique inverted band structure, InAs/GaSb bilayer systems can simultaneously hosts spatially closed 2DEG and 2DHG in InAs and GaSb QW, respectively. In recent years, many exotic quantum

phases have been observed in this system [4-6]. Particularly, excitonic topological order found in InAs/GaSb system is of great interest, since the excitons carry 1/2 fractional topological charge similar to composite fermion in fractional quantum Hall system [6]. The moat band dispersion of exciton is a prerequisite for excitonic topological order. Besides imbalanced carrier density of electrons and holes [6], theoretical analysis found that Rashba spin-orbital coupling can also help to form moat band of excitons [7]. In this work, we show some preliminary experiment results that the Rashba spin-orbital coupling can stabilize excitonic topological order in InAs/GaSb bilayer system. References: [1] J. Eisenstein and A. MacDonald, Nature 432, 691 (2004). [2] X. Liu, K. Watanabe, T. Taniguchi, B. I. Halperin, and P. Kim, Nature Physics 13, 746 (2017). [3] Y. Cao, V. Fatemi, S. Fang, K. Watanabe, T. Taniguchi, E. Kaxiras, and P. Jarillo-Herrero, Nature 556, 43 (2018). [4] L. Du, I. Knez, G. Sullivan, and R.-R. Du, Physical Review Letters 114, 096802 (2015). [5] L. Du, X. Li, W. Lou, G. Sullivan, K. Chang, J. Kono, and R.-R. Du, Nature Communications 8, 1971 (2017). [6] R. Wang, T. A. Sedrakyan, B. Wang, L. Du, and R.-R. Du, Nature 619, 57 (2023). [7] C. Wu, Modern Physics Letters B, 23, 1 (2009)

+

Topological protection of transport in fast Thouless pumps in the presence of disorder

Sidorenko, Anna

Quantized dynamics is essential for natural processes and technological applications alike. It has been shown that quantized particle transport in Thouless pumps is not restricted to the limit of slow driving in non-Hermitian Floquet systems [1]. The degree of topological protection provided by non-Hermiticity in such systems is of great interest. Here we conduct a comparative study of the robustness of directional transport in the presence of static random disorder in two periodically driven systems – quantum ratchet [2] and fast Thouless pumps [1]. In the case of the ratchet, quantized transport relies on a resonant effect that requires fine-tuning of driving parameters. On the contrary, directional transport in Thouless pumping is of a topological origin and observed for a range of driving frequencies considering the closed cycle in parameter space. Our experimental implementation of the models is realized by evanescently coupled dielectric-loaded surface-plasmon polariton waveguide arrays based on the mathematical identity between the coupled mode theory equations and the discrete Schrödinger equation in the tight-binding approximation. In the present joint experimental and theoretical study, we analyzed the effect of topological protection on directional transport by gradually introducing identical on-site disorder distribution to both systems. We demonstrated that topologically protected directional transport in the case of a Thouless pump is able to sustain static disorder while in the case of a quantum ratchet, the high-strength disorder results in a complete directionality breakdown. References [1] Z. Fedorova, H. Qiu, S. Linden, J. Kroha, Observation of topological transport quantization by dissipation in fast Thouless pumps, Nat Commun 11, 3758 (2020). [2] Z. Fedorova, C. Dauer, A. Sidorenko, S. Eggert, J. Kroha, S. Linden, Dissipation engineered directional filter for quantum ratchets, Phys. Rev. Research 3(1), 013260 (2021).

+

Topological multipoles probed by magnetic fields

Tada, Yasuhiro

Multipoles are fundamental quantities in the context of (higher order) topological insulators. However, it is known that definitions of bulk multipoles have some difficulties in general dimensions. Indeed, the well-known Resta formula for dipoles

gives vanishing dipole moments in higher dimensions. Also, a similar formula for quadrupoles does not work for thermodynamically large systems even in two dimensions. In this study, we propose new many-body multipole indices which have several advantages over the previously proposed ones [1]. Our argument is based on an introduction of appropriate magnetic fields and point group symmetries. The magnetic fields can twist the spatial symmetries and thus probe anomalous responses to point group operations, which leads to the multipole indices in interacting systems. With the new indices, we can prove the bulk-boundary correspondence (or the filling anomaly) in presence of interactions. These analytical discussions are fully supported by numerical calculations. [1] Yasuhiro Tada and Masaki Oshikawa, "Many-body multipole index and bulk-boundary correspondence", arXiv:2302.00800, to be published in Phys. Rev. B.

+

Non-universal Behaviours of Thermal Hall Conductance in Fractional Quantum Hall States

Tan, Fei

The fractional quantum Hall (FQH) effect has become one of the most studied phenomena in condensed matter physics for the past 40 years. One classic approach studying these systems is to compute their thermal Hall conductance (THC) since it can be a quantized quantity for certain FQH states and they do not depends on the details of the system. The quantized value of THC, which is an integer or fractional value in units of K_0 ($K_0 = \frac{\pi^2 k_B^2}{3h}$), can be used to determine whether the FQH states is Abelian or non-Abelian states. This quantization however can only be robust if the edge of the system is modelled by using the chiral Luttinger liquid (χLL) under the linear dispersion. In experiments, this model may break down due to the nonlinearity of the confinement potential and the finite temperature effect. In this work, we analytically derive the THC of FQH states (i) with finite-size/low-temperature correction and (ii) under general dispersion relation. This can be accomplished by proper mathematical tools including integer partition generating function, Mellin transformation and asymptotic expansion. We conjectured that the THC can only be a universal quantity if the system is under linear dispersion. The non-universal corrections can provide guidance for a reasonable error range of THC measurements in realistic experiments.

+

Deformed Fredkin model for the $\nu = 5/2$ Moore-Read state on thin cylinders

Voinea, Cristian

We propose a frustration-free model for the Moore-Read quantum Hall state on sufficiently thin cylinders with circumferences $\lesssim 7$ magnetic lengths. While the Moore-Read Hamiltonian involves complicated long-range interactions between triplets of electrons in a Landau level, our effective model is a simpler one-dimensional chain of qubits with deformed Fredkin gates. We show that the ground state of the Fredkin model has high overlap with the Moore-Read wave function and accurately reproduces the latter's entanglement properties. Moreover, we demonstrate that the model captures the dynamical response of the Moore-Read state to a geometric quench, induced by suddenly changing the anisotropy of the system. We elucidate the underlying mechanism of the quench dynamics and show that it coincides with the linearized bimetric field theory. The minimal model introduced here can be directly implemented as a first step towards quantum

simulation of the Moore-Read state, as we demonstrate by deriving an efficient circuit approximation to the ground state and implementing it on IBM quantum processor.

+

The MT Protected Topological States and Local Symmetry in 2D Antiferromagnetic SrMn2Bi2

Wang, Hao

Antiferromagnetic topological insulators (AFMTIs) with gapless edge states represent a novel class of topological states for spintronics applications. Understanding principles behind symmetry protection and exploring AFMTIs with desirable properties, manipulable by external stimuli, are crucial. In this study, through first-principles calculations and symmetry analysis, we investigate the topological properties of monolayer SrMn2Bi2, demonstrating their sensitivity to the magnetic configuration. When the system is an out-of-plane antiferromagnetic ground state, we observe a gapless helical edge state protected by the mirror plane combined with time reversal symmetry. In the ferromagnetic state, the system resides in the quantum anomalous Hall phase, and the topology is trivial for the in-plane magnetization. We show that the topological properties can be efficiently manipulated by strain. Additionally, we emphasize that constructing proper Wannier functions which obey symmetry constraints in key for avoiding the prediction of spurious states in the surface spectra. Our work not only provides an ideal candidate for AFMTIs, but also guides the symmetry analysis of magnetic topological materials using Wannier functions.

+

Thermal transport of excitonic topological state in InAs/GaSb heterojunctions

Wang, Xinghao

Recently, a new time-reversal-symmetry breaking excitonic ground state with long-range quantum entanglement called ETO state has been discovered in shallow inverted InAs/GaSb electron-hole bilayer systems. It is attributed to frustration induced by imbalance of electron/hole density or spin polarization and a bosonic moat band with exotic topological order at zero magnetic field. Theoretically, moat band structure is likely to result in (fractional) quantum anomalous Hall effect (FQAH) or the so-called fractional Chern insulators, which is very encouraging in this field. After thorough low-temperature electrical transport experiment of this new state, we suggest that only thermal transport can distinguish this FQAH state from other topological order because excitons do not carrier charges but carry energy. Its thermal conductance is predicted to be the same as that of $1/2$ bosonic FQH state. Our future experiment is going to explore the thermal transport nature of ETO state.

+

Graviton modes in Fractional Quantum Hall Fluid

Wang, Yuzhu

Neutral excitations in a fractional quantum Hall droplet define the incompressibility gap of the topological phase. In this project, we derived a set of analytical results for the energy gap of the graviton modes with two-body and three-body Hamiltonians in both the long-wavelength and the thermodynamic limit. These allow us to construct model Hamiltonians for the graviton modes in different FQH phases and to elucidate a hierarchical structure of conformal Hilbert spaces (null spaces of

model Hamiltonians) with respect to the graviton modes and their corresponding ground states. Numerical results of the Laughlin $v = 1/5$ and the Gaffnian $v = 2/5$ phases confirm that for gapped phases, low-lying neutral excitations can undergo a "phase transition" even when the ground state is invariant. The compressibility of the Gaffnian phase, the possibility of multiple graviton modes, the transition from the graviton modes to the "hollow-core" modes, and the chirality of graviton modes are discussed in detail, as well as their experimental consequences.

+

Maximally Localized Wannier Orbitals, Interaction Models and Fractional Quantum Anomalous Hall Effect in Twisted Bilayer MoTe2

Xu, Cheng

We investigate the moir\'e band structures and the strong correlation effects in twisted bilayer $MoTe_2$ for a wide range of twist angles, employing a combination of various techniques. Using large-scale first principles calculations, we pinpoint realistic continuum modeling parameters, subsequently deriving the maximally localized Wannier functions for the top three moir\'e bands. Simplifying our model with reasonable assumptions, we obtain a minimal two-band model, encompassing Coulomb repulsion, correlated hopping, and spin exchange. Our minimal interaction models pave the way for further exploration of the rich many-body physics in twisted $MoTe_2$. Furthermore, we explore the phase diagrams of the system through Hartree-Fock approximation and exact diagonalization. Our two-band exact diagonalization analysis underscores significant band-mixing effects in this system, which enlarge the optimal twist angle for fractional quantum anomalous Hall states.

+

Quantum geometry, particle-hole asymmetry and their application in Moire materials

Yang, Kang

Topological bands with a flat dispersion host strongly correlated states with or without intrinsic topological orders. The kinetic part of the system is trivial and the system is dominated by the interaction. At a first glance, electrons do not have any preference to occupy in the Brillouin zone. Despite the featureless kinetic dispersion, topological bands are usually equipped with nontrivial band geometry. We show that the nonuniform band geometry gives rise to emergent Fermi surfaces and it leads to a general particle-hole asymmetry. The electrons tend to fill regions in the Brillouin zone where their quantum distance is shorter. The emergent Fermi surface transforms the strongly interacting problem to a weakly interacting one. This dictates the low-energy physics and serves as a guiding principle for potential symmetry-breaking states. We show that in moiré materials, the quantum distance can be well approximated by a local quantity called the quantum metric. From this simple quantity, we can deduce what phases are favoured in different moiré systems at fractional fillings.

+

Quantum quenches and emergent hydrodynamics in a Landau Level

Zerba, Caterina

Fractional quantum Hall states are stabilized in two-dimensional systems with applied magnetic field. They are promising platforms for realizing kinetically constrained dynamics. Particles restricted to one Landau level behave as if they were on a one-dimensional lattice with effective dipole-conserving interactions. In this work, we investigate the rich quantum dynamics of this system on a torus. We find that in the thick torus limit, the system relaxes with hydrodynamic tails governed by subdiffusive fracton hydrodynamics. When decreasing the thickness of the torus, the dynamics slow down and display long prethermalization behaviors. We propose to use these signatures to characterize the dynamics of fractional quantum Hall states in quantum simulators of ultra-cold atoms. A key experimental signature of their hydrodynamics behavior can be found in the fluctuations of the number of particles in a subregion of the system. Furthermore, we provide a connection with experiments, by studying the full (non-projected) evolution in the basic constituent of our model. Our analysis shows that quantum dynamics of fractional quantum Hall states is particularly rich due to an effective dipole conservation, entailing Hilbert space fragmentation and fracton hydrodynamics.

+

Gate-Tunable Fractional Chern Insulators in Twisted Double Bilayer Graphene

Zhou, Yi Han

Fractional Chern insulators (FCIs) generalize the conventional fractional quantum Hall effect from continuum two-dimensional electron gases to lattice setups. We propose twisted double bilayer graphene (TDBG) as a versatile platform for the realization of FCIs without the need of a magnetic field. The conduction band of TDBG can carry Chern number $C = 1$ and $C = 2$, which is readily controlled by tuning the vertical gate potential and the twist angle. By extensive exact diagonalization, we explore the many-body phase diagram of the system at band filling $v = 1/3, 2/5$, and $1/5$. Remarkably, we find compelling numerical evidence of various FCIs in different regions of band Chern number, including spin-valley polarized states and spin singlet Halperin states. We try to understand the stability of these states by considering the energetics and quantum geometry of the topological flat band.

+

Dipole representation of half-filled Landau level: quantum Hall and its bilayers

Sonja Predin

Center for the Study of Complex Systems Belgrade

The formalism for composite fermions, initially developed for bosons at filling factor v = 1 [1, 2], has been a cornerstone in understanding the fractional quantum Hall effect (FQHE). We derive the Dirac composite fermion theory for a half-filled Landau level from first principles [3]. In this talk, we present novel insights into this phenomenon by employing a dipole representation for composite fermions that incorporates the symmetry under particle-hole exchange. By imposing a unique constraint on the degrees of freedom of composite fermions and composite holes within an enlarged space, we ensure that the resulting composite particles, known as dipoles, possess symmetric characteristics. Our investigation focuses on an effective Hamiltonian that commutes with the constraint in physical space while preserving boost invariance at the Fermi level. Remarkably, our calculations [4] of the Fermi liquid parameter F2 demonstrate remarkable agreement with previous numerical investigations [5]. Furthermore, we investigate the phase diagram of the quantum Hall bilayer (QHB) system at total filling factor v = 1, where physics at small interlayer distances is understood in terms of Bose-Einstein condensation (BEC), while at large distances, physics is mostly understood in terms of fermionic condensation. We have now shown that composite fermions offer an accurate description of the system for all distances [6].

References
[1] N. Read, Phys. Rev. B 58, 16262 (1998).
[2] Z. Dong and T. Senthil, Phys. Rev. B 102, 205126 (2020).
[3] D. Gočanin, S. Predin, M. D. Ćirić, V. Radovanović, and M. Milovanović, Phys. Rev. B 104, 115150 (2021).
[4] S. Predin, A. Knežević , and M. V. Milovanović, Phys. Rev. B 107, 155132 (2023).
[5] K. Lee, J. Shao, E.-A. Kim, F. D. M. Haldane, and E. H. Rezayi, Phys. Rev. Lett. 121, 147601 (2018).
[6] S. Predin, and M. Milovanovic, to be appeared.

Dipole representation of half-filled Landau level

M. V. Milovanović[a], S. Predin[a] and A. Knežević[b]

[a] *Scientific Computing Laboratory, Center for the Study of Complex Systems, Institute of Physics Belgrade, University of Belgrade, Pregrevica 118, 11080 Belgrade, Serbia*
[b] *Faculty of Physics, University of Belgrade, Studentski Trg 12-16, 11000 Belgrade, Serbia*

Abstract. The fractional quantum Hall effect is a phenomenon of strongly correlated electrons that is amenable to quasiparticle pictures and modeling. The presence of a strong magnetic field very often leads to the dominance of the physics inside a Landau level (LL) and it justifies approaches that assume that the description of the problem can be confined to an isolated LL. We will introduce a variant of a dipole representation for composite fermions in a half-filled LL, which takes into account the symmetry under an exchange of particles (electrons) and holes. This is implemented by a special constraint on a composite fermion and a composite hole degree of freedom (of an enlarged space), which makes the resulting composite particle (dipole) a symmetric object. We will analyze an effective Hamiltonian that commutes with the constraint on the physical space and fulfills the requirement for boost invariance on the Fermi level. The calculated Fermi liquid parameter F_2 is in good agreement with numerical investigations in K. Lee et al., which predicted Pomeranchuk instabilities in higher LLs.
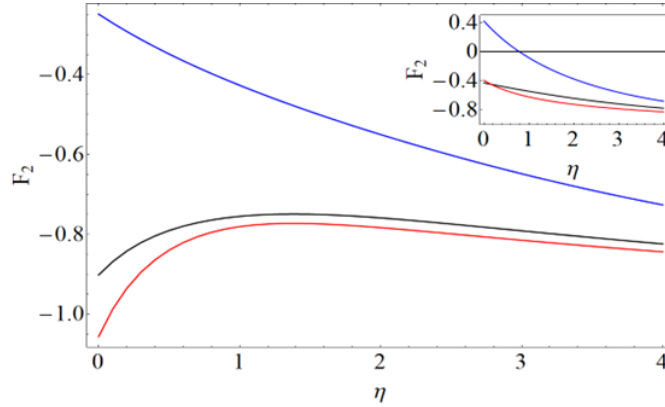
FIGURE The calculated Fermi liquid parameter F_2 for a generalized Coulomb interaction, $e^{-\eta r}/r$: the lowest LL - blue, the second LL- black, and the third LL – red. The Pomeranchuk instability is expected for $F_2 < -1$. **Inset:** F_2 with an incomplete account of the boost invariance. From S. Predin et al.

REFERENCES

1. Lee, K., Shao, J., Kim, E.-A., Haldane, F. D. M., Reyazi, E. H., *Phys. Rev. Lett.* **121**, 147601 (2018).
2. Predin, S., Knežević, A., Milovanović, M. V., *Phys. Rev. B* **107**, 155132 (2023).